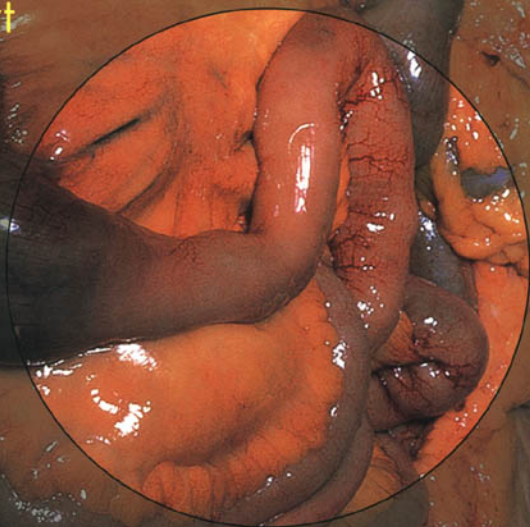


THIRD EDITION

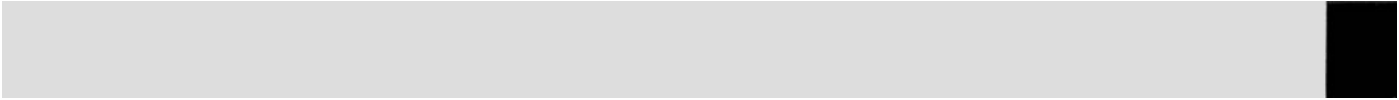
COLOUR ATLAS OF
**ANATOMICAL
PATHOLOGY**

Robin A. Cooke
Brian Stewart

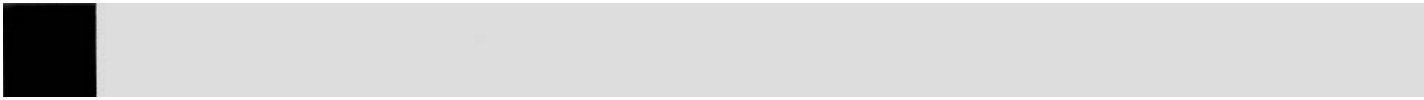
Foreword by
Juan Rosai



 CHURCHILL
LIVINGSTONE



COLOUR ATLAS OF
**ANATOMICAL
PATHOLOGY**



Commissioning Editor: Timothy Horne
Project Development Manager: Clive Hewat
Project Manager: Frances Affleck
Designer: Erik Bigland

COLOUR ATLAS OF **ANATOMICAL PATHOLOGY**

Robin A. Cooke OBE OAM MD DCP FRCPA FRCPath FACTM

Professor, University of Queensland, Graduate School of Medicine, Brisbane, Australia
Senior Visiting Pathologist, Queensland Health Pathology Service and Mater Health Services,
Brisbane, Australia
Emeritus Consultant, Royal Brisbane Hospital, Brisbane, Australia
Visiting Professor and External Consultant, University of Papua New Guinea, Papua New Guinea

Brian Stewart

Medical Illustrator, Formerly Senior Photographer, Royal Brisbane Hospital, Brisbane, Australia
Medical Photographer, The Wesley Hospital, Brisbane, Australia

THIRD EDITION

Foreword by
Juan Rosai MD
Chairman, Department of Pathology, National Cancer Institute, Milan, Italy



EDINBURGH LONDON NEW YORK OXFORD PHILADELPHIA ST LOUIS SYDNEY
TORONTO 2004

CHURCHILL LIVINGSTONE
An imprint of Elsevier Science Limited

© Text: Elsevier 2004
© Illustrations: Robin A. Cooke 2004

The right of Robin Cooke and Brian Stewart to be identified as authors of this work has been asserted by them in accordance with the Copyright, Designs and Patents Act 1988.

No part of this publication may be reproduced, stored in a retrieval system, or transmitted in any form or by any means, electronic, mechanical, photocopying, recording or otherwise, without either the prior permission of the publishers or a licence permitting restricted copying in the United Kingdom issued by the Copyright Licensing Agency, 90 Tottenham Court Road, London W1T 4LP. Permissions may be sought directly from Elsevier's Health Sciences Rights Department in Philadelphia, USA: phone: (+1) 215 238 7869, fax: (+1) 215 238 2239, e-mail: healthpermissions@elsevier.com. You may also complete your request on-line via the Elsevier Science homepage (<http://www.elsevier.com>), by selecting 'Customer Support' and then 'Obtaining Permissions'.

First edition 1987
Second edition 1995
Reprinted 1999
Third edition 2004

ISBN 0443073600

British Library Cataloguing in Publication Data

A catalogue record for this book is available from the British Library

Library of Congress Cataloging in Publication Data

A catalog record for this book is available from the Library of Congress



your source for books,
journals and multimedia
in the health sciences

www.elsevierhealth.com

The
publisher's
policy is to use
paper manufactured
from sustainable forests

Printed in China

FOREWORD TO THE THIRD EDITION

It has often been stated that pathology is primarily a visual discipline. The observation, not always meant as a compliment, has a component of truth, in the sense that a large segment of pathology practice consists in the interpretation of images of one type or another. The magnification range of the images that the pathologist has been asked to evaluate has increased exponentially over the years, from the gross to the microscopic, down to the ultrastructural and cytogenetic; but the basic purpose has remained the same: to extract from the visible structural features all the necessary information in an attempt to ascertain the nature and mechanism of formation of the abnormalities present.

In its beginning, the imagery of pathology was exclusively of a macroscopic nature, and the expertise of the pathologists was once judged on the basis of their acumen in predicting the histology on the basis of the gross appearance of the specimens. Legends were built around this prowess, like the story of Karl Rokitansky looking at a cross-section of a pneumonia and being able to indicate which foci were composed of neutrophils and of histiocytes. A good measure of the importance given at one time to gross pathology is the fact that an integral component of every major department of pathology was the museum, in which a formally appointed curator (none more famous than Thomas Hodgkin) supervised all the activities leading to the selection, processing, identification and displaying of selected specimens.¹

A related activity, which has progressively replaced the actual museums, has been the production and publication of atlases of gross pathology. Some of these were based on the museum pieces and others on fresh specimens, the latter having the obvious advantage of rendering a more faithful representation of the appearance of the 'live' lesion. The importance of this material in the teaching of anatomic pathology at both the undergraduate and postgraduate level cannot be overemphasized, particularly at a time when the attitude is gradually taking hold that the examination of a gross specimen is simply the technical step required for the acquisition of the microscopic slides. Nothing can be further from the truth, either in surgical pathology or autopsy pathology. As stated in an editorial appropriately titled 'In praise of the gross examination', it is the gross aspect of the specimen that shows the size, form and nature of the process so that it can be understood both in a structural sense and in a clinical context.² For some specimens, a careful gross examination is infinitely superior to the examination of random microscopic sections taken from that specimen. Therefore, books and atlases that display in an optimal fashion the features of these specimens are crucial to the specialty, and I dare say they will remain so long after the genetic background of all human diseases has been determined. Alas, it is not easy to produce such a work. First of all, it takes a place that handles a wide range of specimens in order to select those that are most representative of the conditions being depicted. Secondly, it needs a prosecutor who handles those specimens, as Arthur Hertig once put it, 'with loving care'. Thirdly, it takes a photographer who is not only technically skilled but who also has an aesthetic feeling for those specimens. Unfortunately, these desiderata are rarely found together. Regarding the latter aspect, it has been stated in frustration that '[gross] photographs are often not taken, or, when taken, they are [often] not useful because of underexposure, overexposure, inappropriate lighting, poor selection of background, or blood-stained or blood-smearred backgrounds'.³ I have learned the truth of this statement the hard way when searching the photography archives of one pathology department or another for good pictures for my Surgical Pathology book, only to discard nine out of ten of those pictures because of those very reasons.

It was therefore with great pleasure, admiration and a touch of envy that I looked at the remarkable collection of photographs that Dr Robin Cooke has been able to assemble in this Atlas. The

specimens are superb, the pictures are technically excellent, the range of diseases they depict is all-encompassing, and the accompanying text is informative while refreshingly succinct.

This opus should be of great utility to anybody interested in the pathology of human diseases, whether as companion of a standard textbook or as a stand-alone publication.

Juan Rosai MD
Milan
2004

REFERENCES

1. Gonzalez-Crussi F. Suspended animation. Six essays on the preservation of bodily parts. San Diego: Harcourt Brace; 1995.
2. Smith C. In praise of the gross examination. *Hum Pathol* 1974; 5: 505–506.
3. Barker NJ. Photography. In: Westra W et al, eds. *Surgical pathology dissection. An illustrated guide*. 2nd edn. New York: Springer; 2003: 26.

PREFACE

Since the publication of the second edition of this Atlas there has been, in many countries, a rapid escalation in the closure of pathology museums, as well as a steep decline in the number of autopsies being performed. This means that students, both undergraduate and postgraduate, are even more deprived of access to the teaching of gross pathology than they were in 1995. It is hoped that this Atlas will help to fill the void thus created in this important aspect of medical education.

New technologies for the identification of gross pathology in living patients are constantly being introduced. To acknowledge these developments we have included a number of examples of radiological imaging, and in Chapter 4, The Alimentary System, we have included some endoscopic views of gastrointestinal pathology. We always intended that this Atlas should be useful for teachers preparing material for problem-based learning exercises. In this third edition we have taken the opportunity to expand some of the topics to improve its usefulness in this regard.

We believe that medicine should be studied in its broadest connotations. This includes having knowledge of medical history, so that the practice of medicine today can be put into proper perspective. To this end, we have included a few historical specimens from some of the older medical museums in Europe. Medicine is a universal profession, and represents a continuum of experience as one generation of doctors benefits from the knowledge of previous generations.

We hope the readers enjoy this book as much as the authors have enjoyed compiling it.

Robin A. Cooke
Brian Stewart
Brisbane
2004

ACKNOWLEDGEMENTS

Professor Sir Peter Morris, President of the Royal College of Surgeons of England, and Ms Stella Mason, Keeper of the College Collections, kindly gave permission for publication of photographs of specimens from the Hunterian Museum.

Professor Sir Colin Berry, Professor of Pathology, the Royal London Hospital and St Bartholomew's Hospital, kindly gave permission for publication of photographs of specimens from St Bartholomew's Hospital Museum.

Professor Sebastian Lucas, Professor of Pathology, Guy's and St Thomas's Hospital, and Mr William Edwards, Curator of the Gordon Museum, Guy's Hospital, kindly gave permission for publication of photographs of specimens from the Gordon Museum.

Professor Hugh Kunze, Director of Queensland Health Pathology Service, kindly gave permission for access to the records of the Teaching Hospitals in Brisbane.

Individual photographs are published with the kind permission of Drs John Sampson, Jane Mc Rohon, Cherrell Hirst, Don Perry Keene, Barry Appleton, John Tyrer, Frank Carmody, Edwina Duhig, Michael Aldred, Ken Miles, and John Sullivan.

Miss Kathy Bevin patiently typed the manuscript, as she did for the Second Edition.

CONTENTS

1	Cardiovascular system	1
2	Lymph nodes and spleen	31
3	Respiratory system	35
4	Alimentary system	59
5	Pancreas, biliary system and liver	107
6	Renal system	131
7	Male genital system	145
8	Breast and female genital system	153
9	Endocrine system	183
10	Bones, joints and connective tissue	205
11	Nervous system	229
	Index	283

CARDIOVASCULAR SYSTEM



Fig. 1.1

Fig. 1.1 Atherosclerosis. M/51. Atheromatous plaques are present on the intimal surface of the abdominal aorta. 'Complicated plaques' are present in the distal aorta and common iliac arteries.

Fig. 1.2 The same case as Figure 1.1. Complicated plaques showing ulceration, calcification, haemorrhage and, at the origin of the left common iliac artery, thrombus formation.

Fig. 1.3 Atherosclerosis in the pulmonary arteries. F/32. This patient had primary pulmonary hypertension. Significant amounts of atherosclerosis occur in the pulmonary arteries only in pulmonary hypertension.



Fig. 1.2



Fig. 1.3



Fig. 1.4 0 cm 5

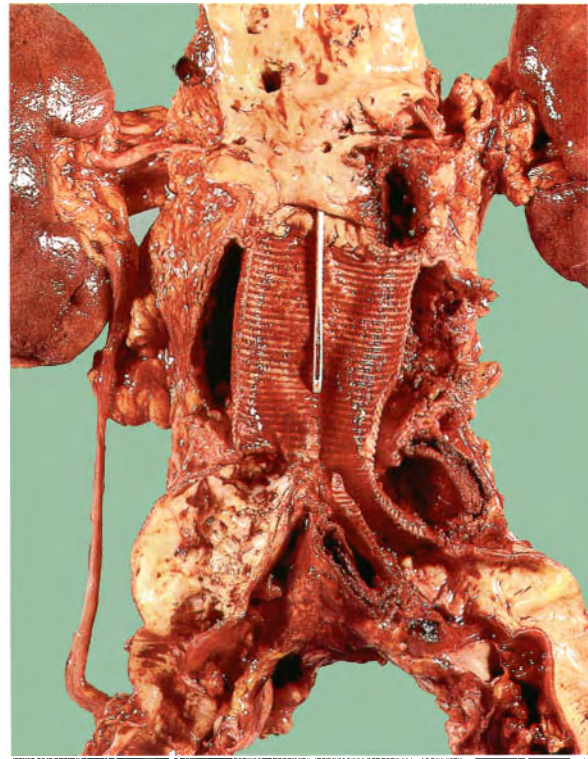


Fig. 1.5



Fig. 1.6

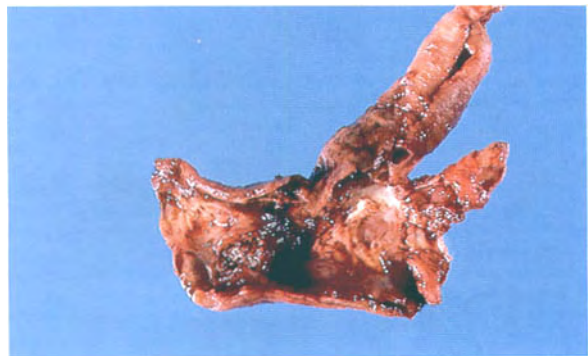


Fig. 1.7 0 cm 1

Fig. 1.4 Aneurysm of the abdominal aorta. M/80. The aneurysm is filled with thrombus and death occurred from rupture. The aorta has been opened posteriorly.

Fig. 1.5 Repaired abdominal aortic aneurysm. M/70. The aneurysm has been repaired by removing its anterior surface (that is, deroofing it) and inserting a Dacron graft. The suture lines are all intact. The aorta and the common iliac arteries show severe atherosclerosis. The patient died from a myocardial infarction some days after surgery.

Fig. 1.6 Severe ischaemia of the left foot. M/73. This resulted from thrombotic occlusion of the popliteal artery. The foot was cold and painful. Femoropopliteal bypass graft was not successful and the lower leg was amputated.

Fig. 1.7 Endarterectomy specimen. M/73. This area of atherosclerosis has been reamed out of the right common carotid artery at its bifurcation. Endarterectomy is often effective in treating atheromatous occlusions.



Fig. 1.8



Fig. 1.9

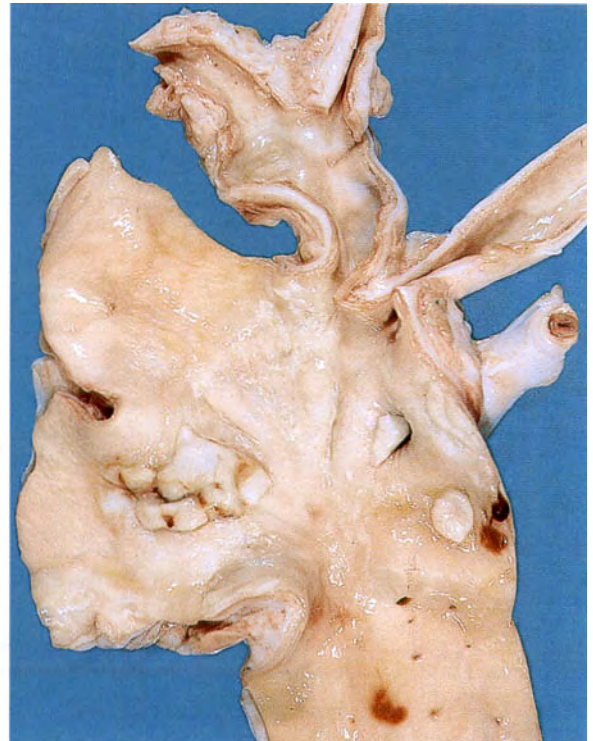


Fig. 1.10

0 cm 5

Fig. 1.8 Syphilitic aneurysm of the arch of the aorta. F/73. The aortic wall is thickened and there are numerous wrinkled, whitish plaques on the intimal surface. The aneurysm is filled with a blood clot. Syphilitic aneurysm of the aorta was first defined as an entity in the 18th century. One of the features noted about these aneurysms was that they enlarged anteriorly and eroded through the anterior chest wall, producing a pulsatile swelling. Death occurred when the aneurysm ruptured.

Fig. 1.9 Syphilitic aneurysm of the arch of the aorta. M/55. This British soldier had pain in his chest for about 2 years. The aneurysm then appeared on his anterior chest wall and continued to grow until it ruptured 1 year later. This specimen was prepared by John Hunter in about 1770 and is displayed in the Museum of the Royal College of Surgeons in London. This was a well recognized complication of syphilitic aortitis.

Fig. 1.10 Takayasu's arteritis. M/26. A patient from Papua New Guinea, where this condition is relatively common, but not as common as in Japan and other parts of southeast Asia. The aortic wall is thickened, and there are thick yellow plaques on the intima. The walls of the innominate and both common carotid arteries are thickened and their lumina are narrowed. The left subclavian artery is almost completely occluded. The consequences of these occlusions give rise to the name for this condition: 'pulseless disease'. The gross and microscopic appearances of this condition are identical to those of syphilis, but it is not caused by spirochaetal infection. It occurs mainly in young adults, but its exact aetiology is not known.

Fig. 1.11 Arteriovenous aneurysm. M/22. This man developed a bulging, red, pulsating right eye following a head injury while fighting. The condition developed because of communication between the carotid artery and the cavernous sinus as a result of the trauma.

Fig. 1.12 Saphena varix. F/42. The specimen consists of a 2 cm diameter aneurysm of the long saphenous vein. This lesion presented as a lump in the groin and the differential diagnosis was a femoral hernia.

Fig. 1.13 Traumatic aneurysm of the left superficial temporal artery. M/25. This was treated by local excision of the affected segment of artery.



Fig. 1.11

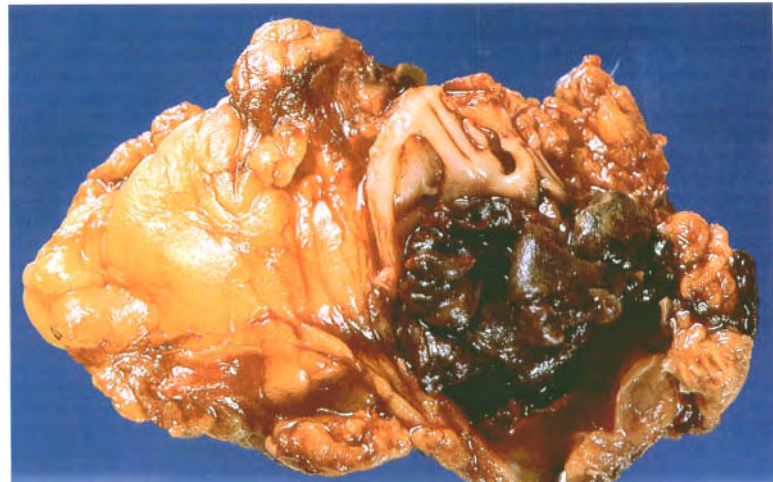


Fig. 1.12

0 cm 1

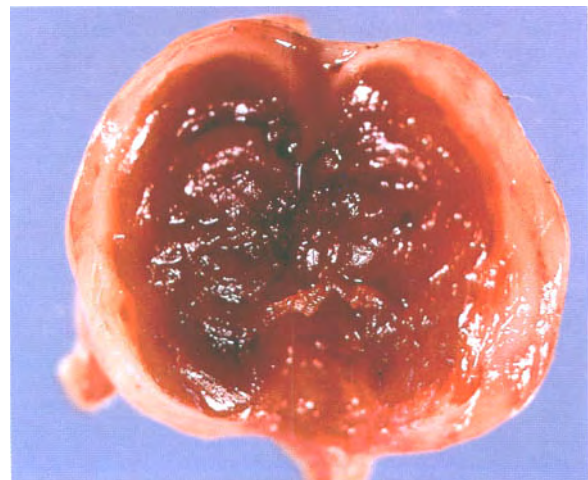


Fig. 1.13

0 cm 1

Fig. 1.14 Dissecting aneurysm of the thoracic aorta.

F/73. The wall of the arch of the aorta has split longitudinally and blood fills the false channel. This can be seen in the top and bottom of the picture. There is a transverse tear in the intima (arrow). This connects with the longitudinal split in the wall of the aorta. The dissection is extending into the innominate and left common carotid arteries.

Fig. 1.15 Dissecting aneurysm of the abdominal aorta.

M/67. The blood has been removed from the false channel (long arrow). The extension of the dissection along the left renal artery can be seen (short arrow).



Fig. 1.14

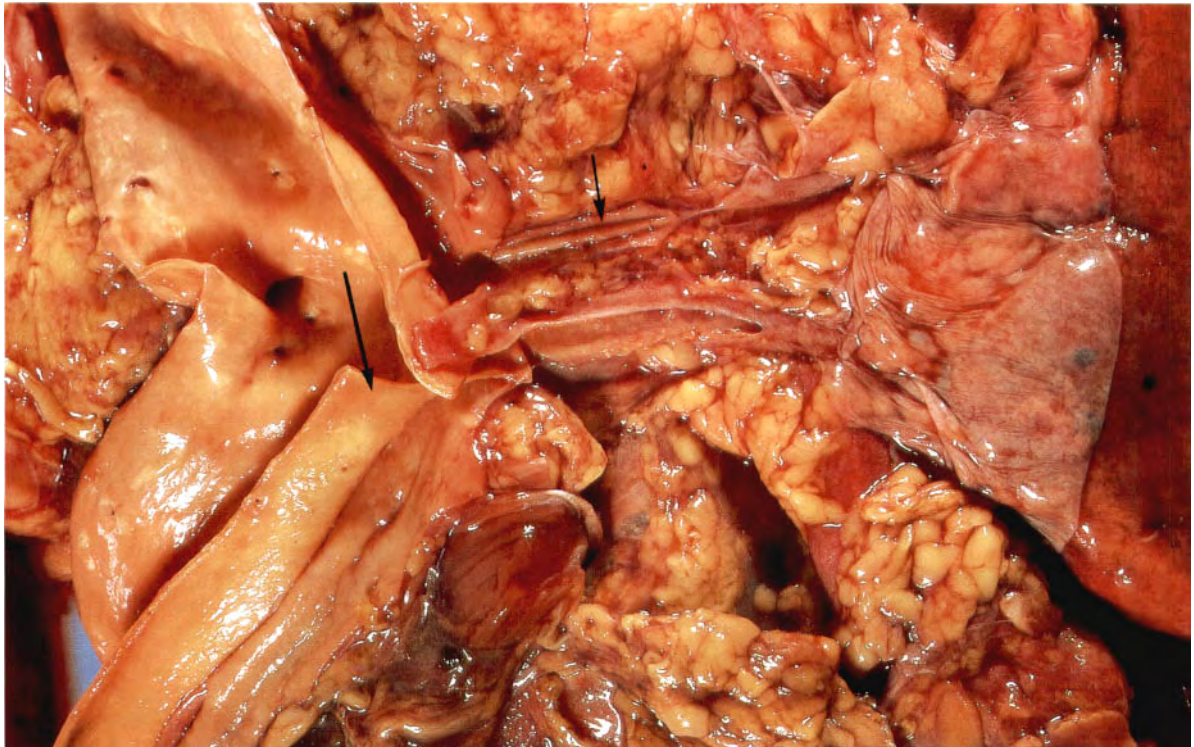


Fig. 1.15



Fig. 1.16



Fig. 1.17

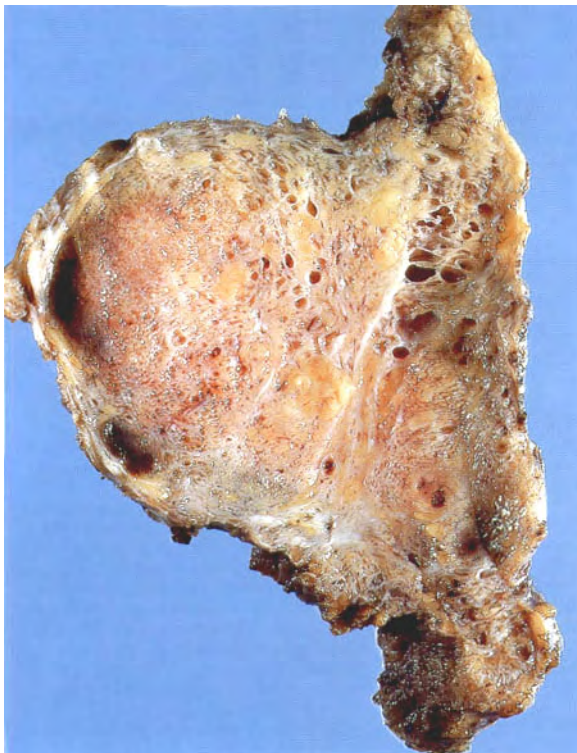


Fig. 1.18

Fig. 1.16 Cutaneous haemangioma. F/3 months.

Fig. 1.17 Lymphangioma (cystic hygroma). M/6 months.

Fig. 1.18 Lymphangioma removed surgically from the left axilla. F/2½. The cut surface shows the spongy appearance of the lymph channels.

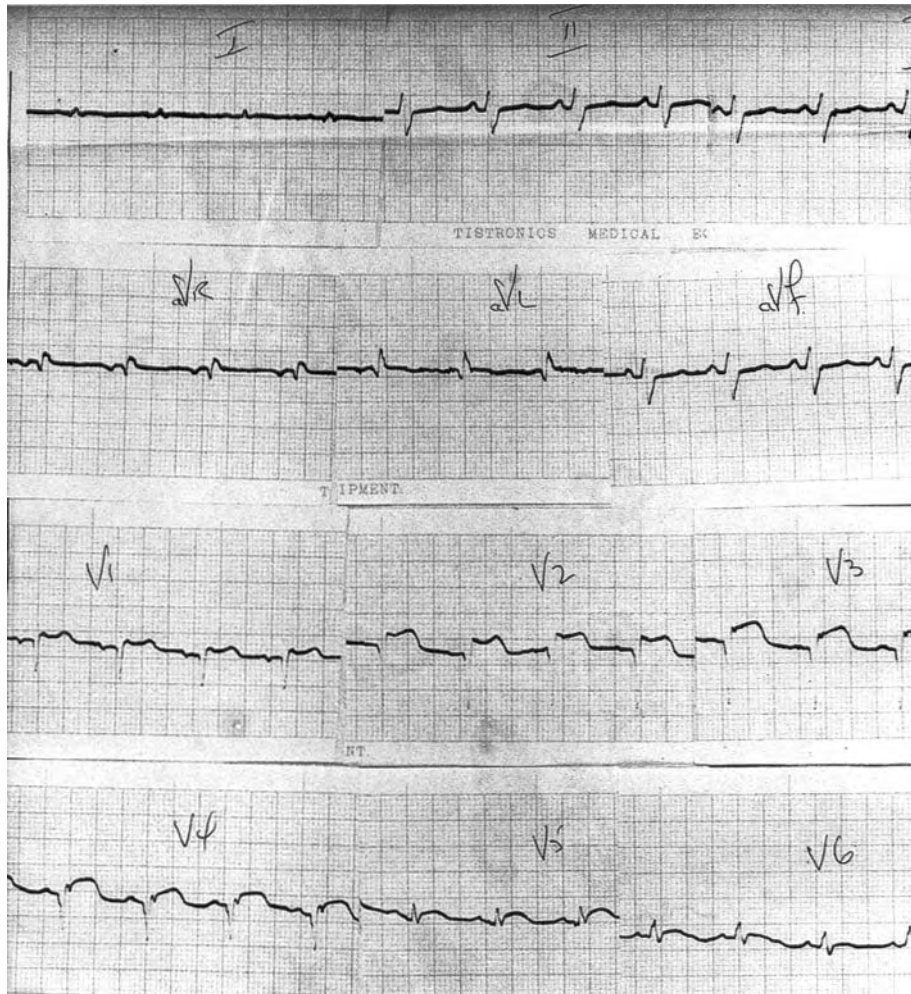


Fig. 1.19

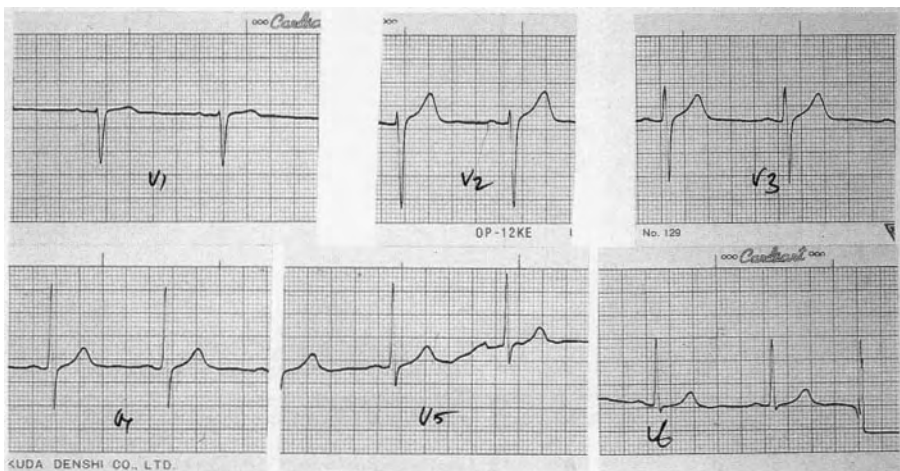


Fig. 1.20

Fig. 1.19 Anterior myocardial infarction. Electrocardiogram (ECG or EKG) of a male, aged 42 years, who complained of a sudden onset of severe chest pain. The ECG shows changes of an acute anterior myocardial infarction, i.e. Q waves and elevated ST segments in the anterior chest leads V2–V5. He died 3 days later.

Fig. 1.20 Electrocardiogram M/60. Normal for comparison.

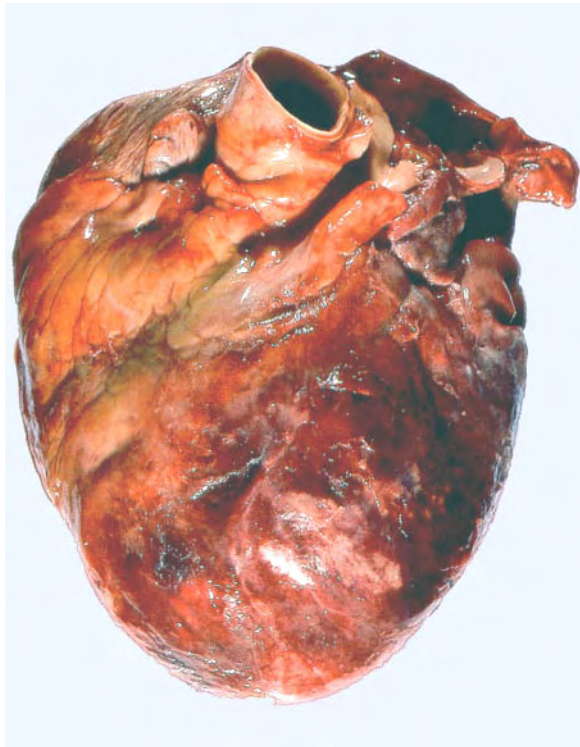


Fig. 1.21

Fig. 1.21 Recent anterior myocardial infarction caused by thrombosis of the anterior descending branch of the left coronary artery. This is the heart from the patient in Figure 1.19. The upper surface of the heart (anterior surface) shows blotchy reddening of the epicardium. This is covered by a fine, fibrinous exudate.

Fig. 1.22 Transverse section through the left ventricle near the apex of the heart illustrated in Figure 1.21. It shows some thinning and softening of the ventricle wall, with the formation of thrombus on the endocardial surface.

Fig. 1.23 The next transverse section through the left ventricle. It follows the section demonstrated in Figure 1.22.



Fig. 1.22



Fig. 1.23

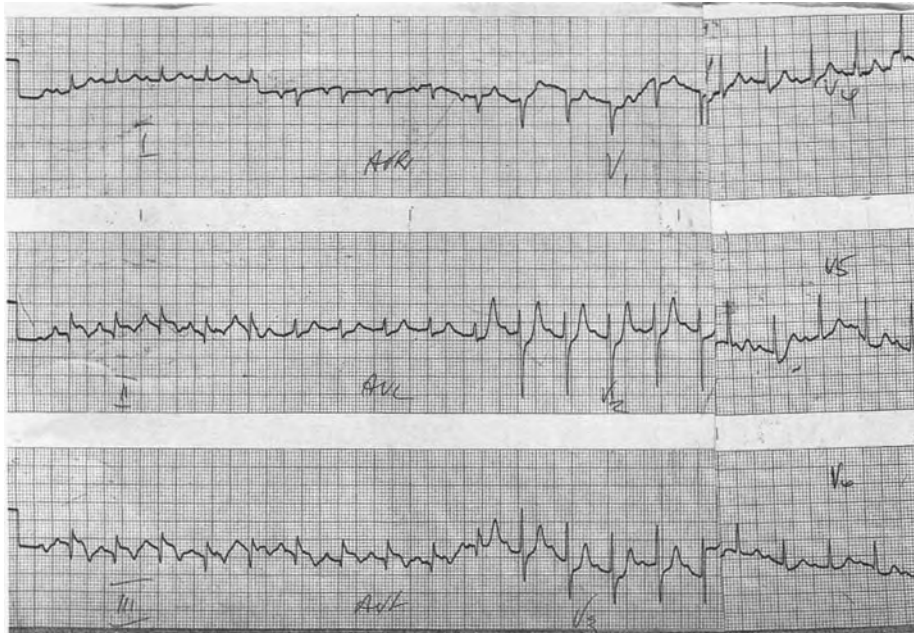


Fig. 1.24

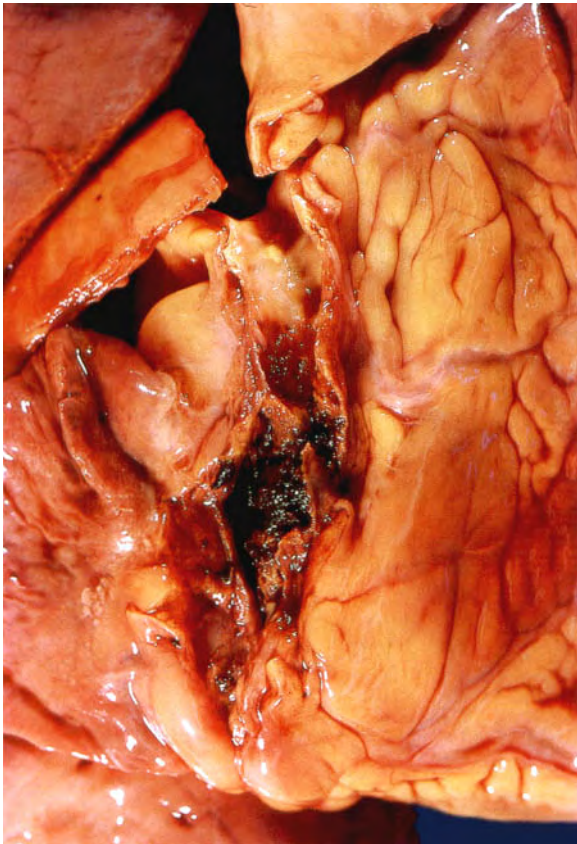


Fig. 1.25

Fig. 1.24 Electrocardiogram. M/75. Posterior myocardial infarction. The patient presented with severe chest pain. The ECG shows Q waves and elevated ST segments in leads II, III and AVF. Reciprocal changes are present in the anterior chest leads V2–V6.

Fig. 1.25 Recent thrombosis of the right coronary artery causing complete occlusion of the vessel. M/40. Occlusion of this artery causes a posterior myocardial infarction. The coronary artery shows severe atherosclerosis. This specimen is from another case.

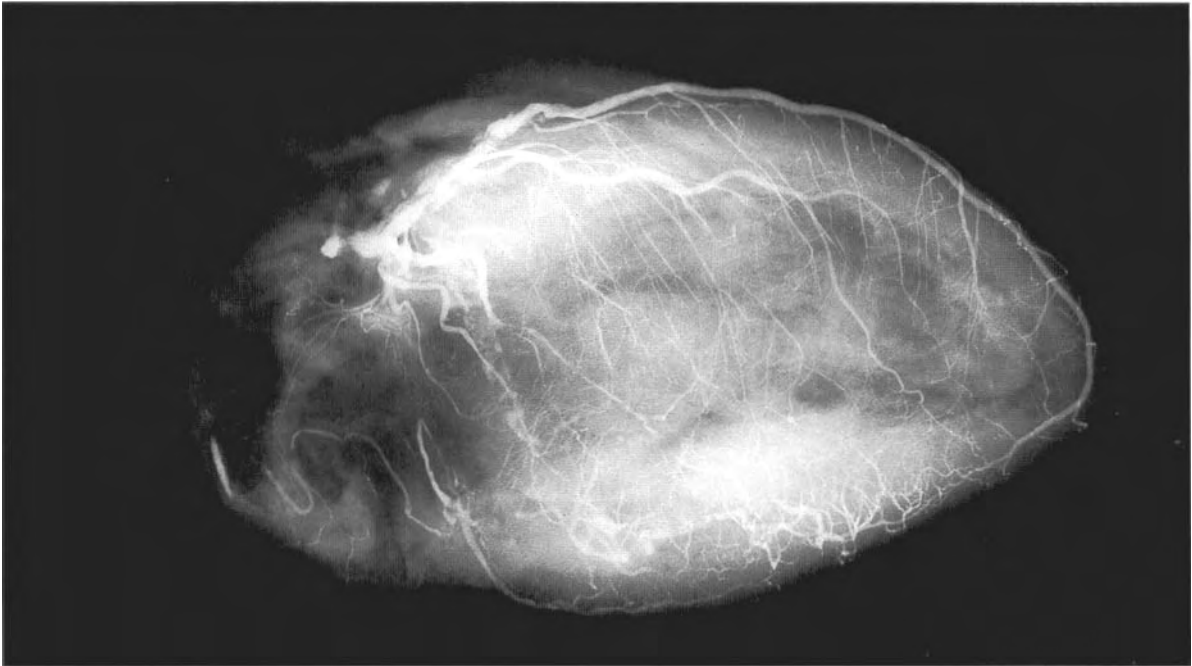


Fig. 1.26



Fig. 1.27

Fig. 1.26 Posterior myocardial infarction. The patient from Figure 1.24 died 6 days after the onset of chest pain. A postmortem angiogram was performed by injecting radio-opaque dye into the left and right coronary arteries before the heart was opened. The left coronary artery and its anterior descending branch have filled with dye. There are two partial obstructions in the proximal portion of this artery. The right coronary artery has failed to fill. This results in virtually no blood going to the inferior (posterior) surface of the left ventricle.

Fig. 1.27 Posterior myocardial infarction with rupture of the ventricle. M/75. This is the heart of the patient indicated in Figure 1.24. The undersurface of the left ventricle shows the features of recent infarction. It is a blotchy red colour, and when examined in the fresh state this portion of the ventricle felt soft. At the apex there is a tear resulting from spontaneous rupture of the infarct (arrow). This usually occurs about 7 days after the acute infarction. Blood escapes into the pericardial cavity causing haemopericardium and death from cardiac tamponade.

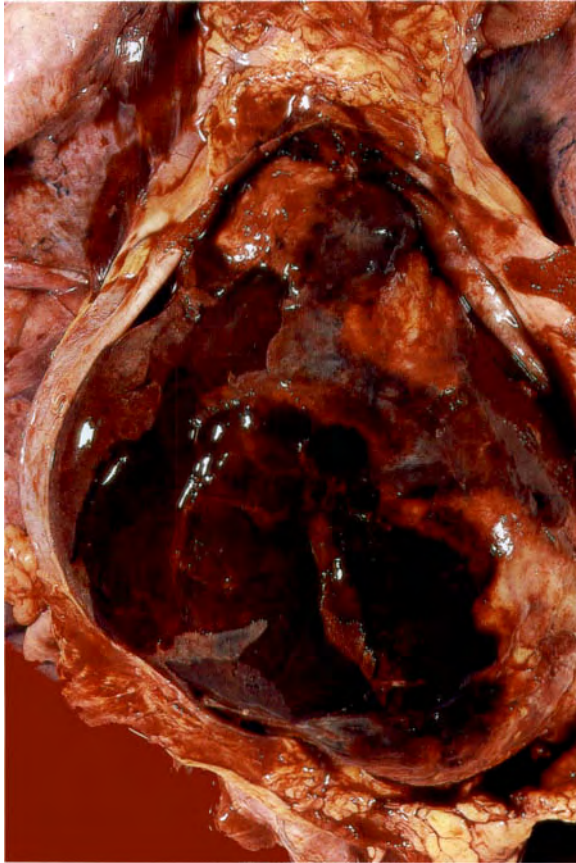


Fig. 1.28

Fig. 1.28 Haemopericardium. F/60. This resulted from rupture of an anterolateral myocardial infarction 7 days after the onset of chest pain.



Fig. 1.29

Fig. 1.29 Posterior myocardial infarction. Slices of the ventricles from just distal to the mitral valve from the heart of the patient in Figure 1.27. The pale area of myocardial infarction can be seen involving the inferior (posterior) portion of the left ventricle. The muscle is necrotic, as can be seen from its appearance. The adjacent portion of the interventricular septum has also been involved in the infarction.

Fig. 1.30 Posterior myocardial infarction. This is a closer view of the middle slice from Figure 1.29. It shows the features of the acute infarction and a site of perforation through the myocardium. The posterior papillary muscle, to which the chordae tendineae of the posterior leaflet of the mitral valve are attached, is included in the infarction. When this occurs the posterior leaflet no longer functions and mitral incompetence occurs.

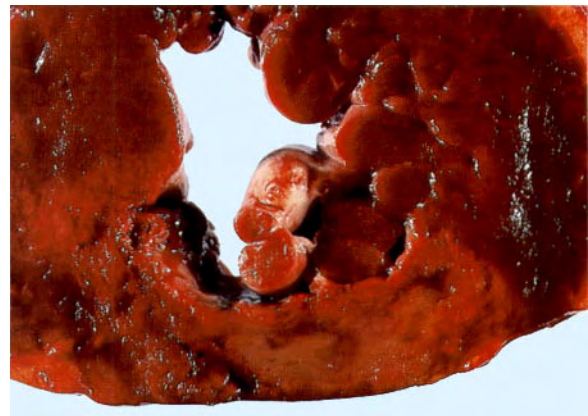


Fig. 1.30



Fig. 1.31

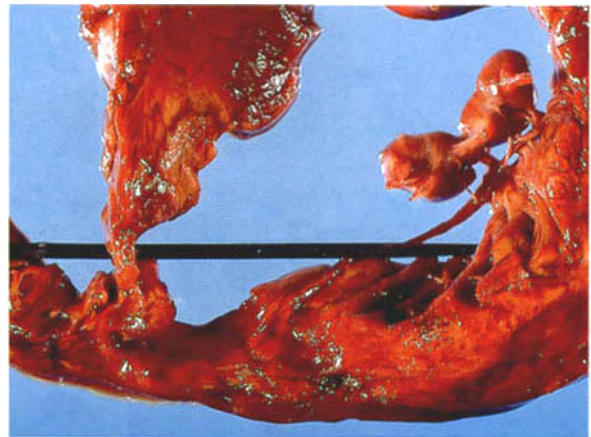


Fig. 1.32



Fig. 1.33

Fig. 1.31 Posterior myocardial infarction. F/72. The heart is sliced from just distal to the mitral valve moving towards the apex. This shows another complication of posterior myocardial infarction, i.e. infarction and rupture of the interventricular septum.

Fig. 1.32 A closer view of the uppermost slice of the ventricles demonstrated in Figure 1.31. The septum is thinned and ruptured.

Fig. 1.33 Posterior myocardial infarction. The middle slice demonstrates the infarction of the ventricle and the interventricular septum, and also the posterior papillary muscle.

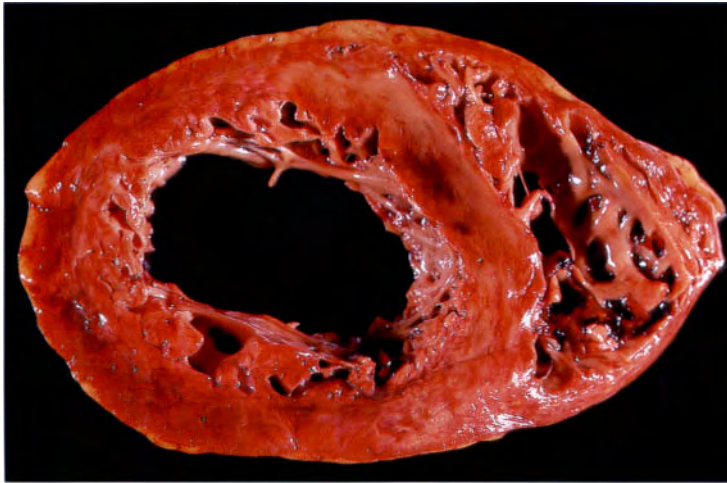


Fig. 1.34



Fig. 1.35

Fig. 1.34 Acute circumferential infarction of the left ventricle. This would have resulted from occlusion of both the right coronary artery and the anterior descending branch of the left coronary artery. This slice from near the apex is viewed from the mitral valve aspect of the heart.

Fig. 1.35 Old posterior myocardial infarction plus a recent lateral infarction. Posterior view of a slice through the ventricles of the heart. The inferior portion of the left ventricle is thinned and fibrotic as a result of healing of a previous posterior infarction. The lateral wall of the ventricle shows reddening of the myocardium, with a yellow area of necrotic muscle in the middle. This is a more recent infarction, probably a few days old.

Fig. 1.36 Old myocardial infarction with mural thrombosis. M/59. The left ventricle is partially filled with thrombus attached to the endocardial surface over the site of a healed myocardial infarction. The patient died from a further acute infarction.



Fig. 1.36

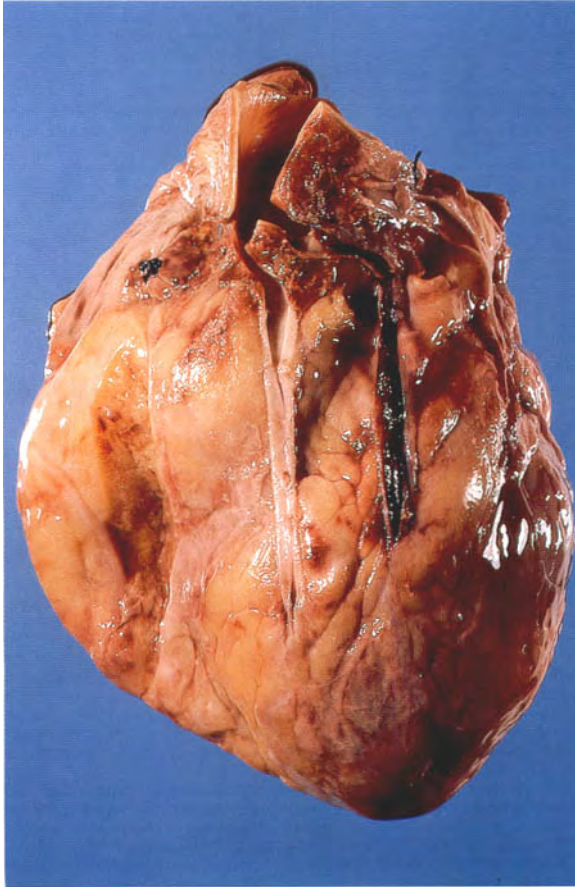


Fig. 1.37

Fig. 1.37 Coronary artery bypass. M/72. Patients with myocardial infarctions have a coronary angiogram performed soon after admission to a coronary care unit. The sites of arterial obstruction are identified. They may be relieved by the passage of a balloon through a cardiac catheter, which is introduced via the subclavian artery into the coronary arteries. The atherosclerotic plaques are then disrupted by inflation of the balloon at the tip of the catheter. If the patient is judged not suitable for this procedure, coronary artery bypass surgery is performed. Vein grafts are inserted into the coronary arteries to bypass the areas of obstruction. This specimen shows the presence of a bypass vein on the epicardial surface of the heart. The vein has thrombosed. Death occurred from a further acute myocardial infarction.

Fig. 1.38 Magnetic resonance image after the administration of gadolinium contrast. This investigation gives a moving image of the heart which shows the blood flow, the functional capability of the myocardium, and, as in this image, areas of myocardial infarction. This view shows all four chambers of the heart. The infarcted myocardium is white and the healthy myocardium is black. There is extensive subendocardial infarction of the septum and the apex of the left ventricle – anterior myocardial infarction.

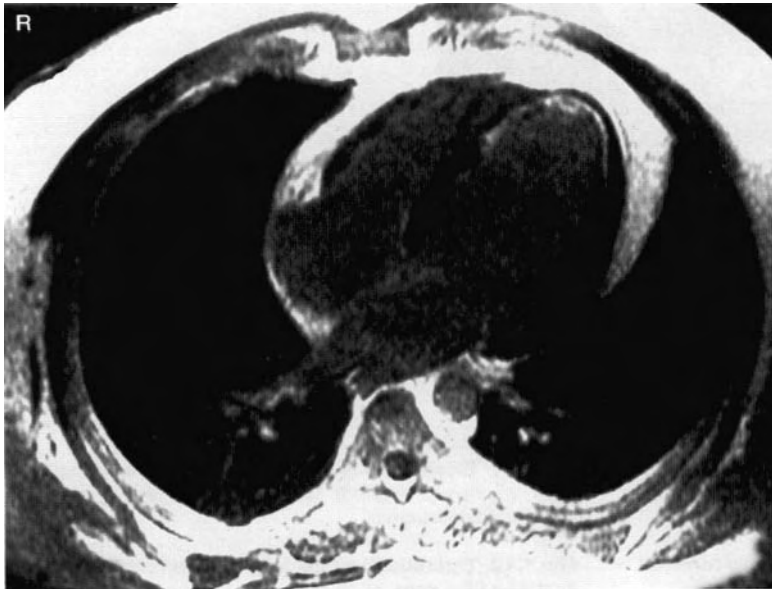


Fig. 1.38

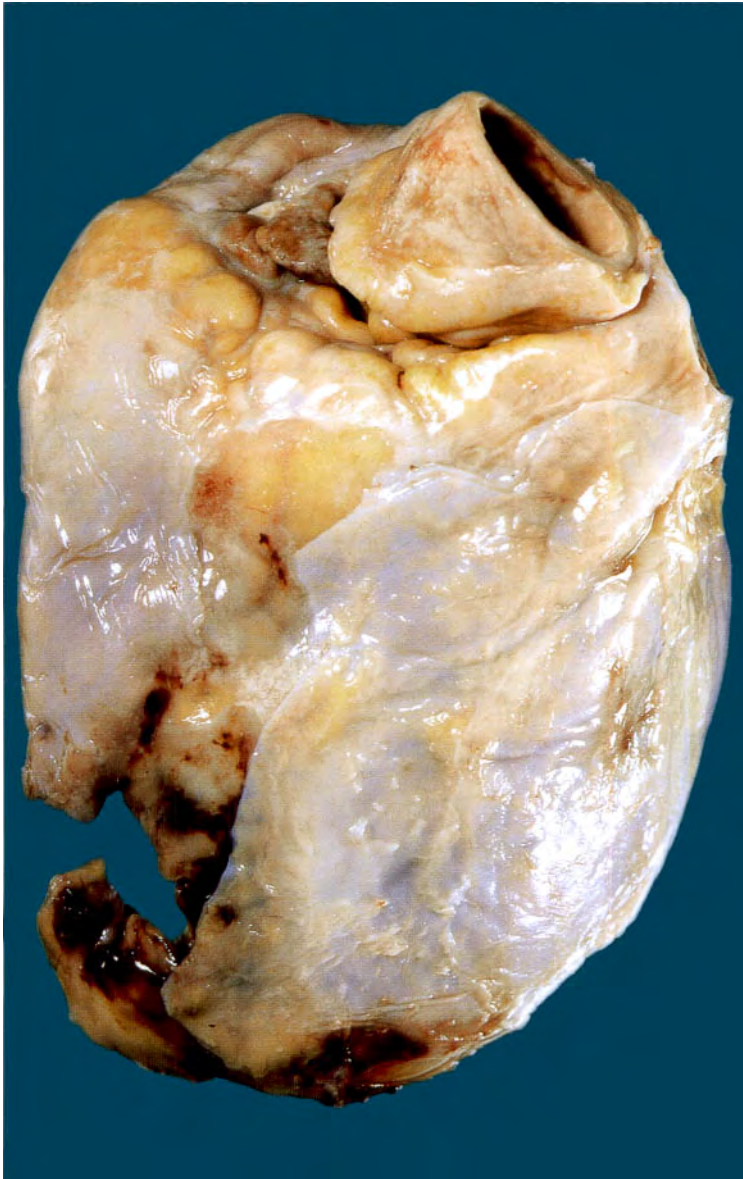


Fig. 1.39

Fig. 1.39 Traumatic rupture of the heart—gunshot wound. M/30. The apex of the heart has been torn away by the bullet. The shooting was suicidal and the muzzle of the gun was held against the chest wall.

Fig. 1.40 Elephantiasis of both legs. F/76. This condition resulted from long-standing obstruction to the lymphatic drainage from the legs.

Fig. 1.41 Elephantiasis due to infection with the parasitic worm *Wuchereria bancrofti*. M/20 from Papua New Guinea, suffering from filariasis.

Fig. 1.42 Thrombosis of the inferior vena cava and left common iliac vein. F/70. This too is a cause of gross oedema of the legs.



Fig. 1.40



Fig. 1.41



Fig. 1.42

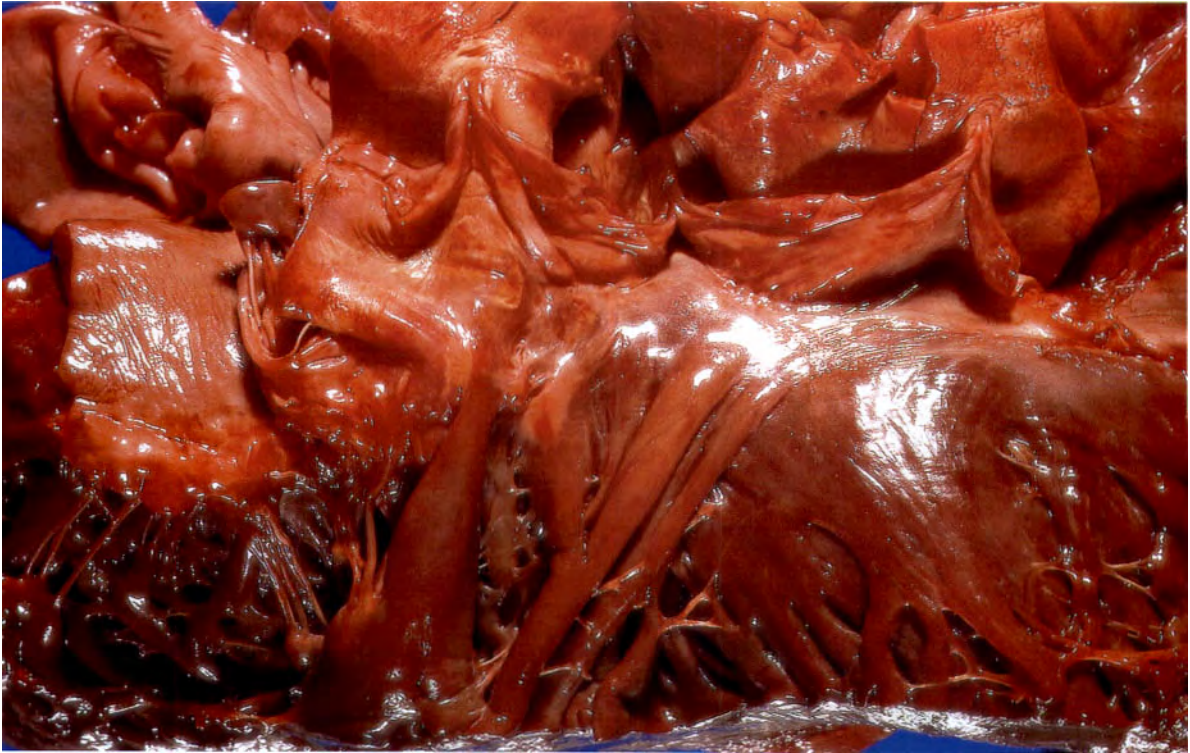


Fig. 1.43

Fig. 1.43 Hypertrophic cardiomyopathy. M/46. The heart has been cut to demonstrate the gross hypertrophy of the left ventricle in the outflow tract. The hypertrophied ventricle bulges into the cardiac chamber below the aortic valve, causing a functional aortic stenosis.

Fig. 1.44 Right ventricular hypertrophy. F/32. The heart has been sliced to show the right ventricular myocardium at the outflow tract, with the pulmonary valve on the top right. The right ventricle is two to three times normal thickness. Right ventricular hypertrophy indicates the presence of pulmonary hypertension.

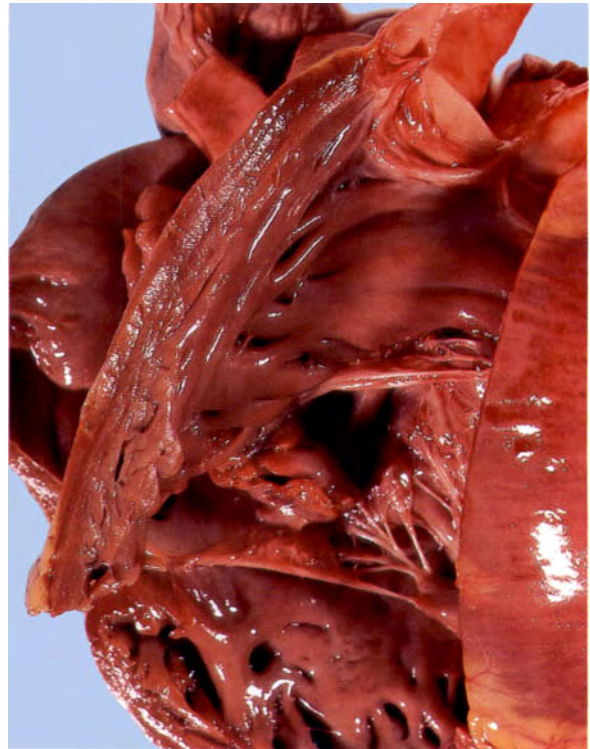


Fig. 1.44

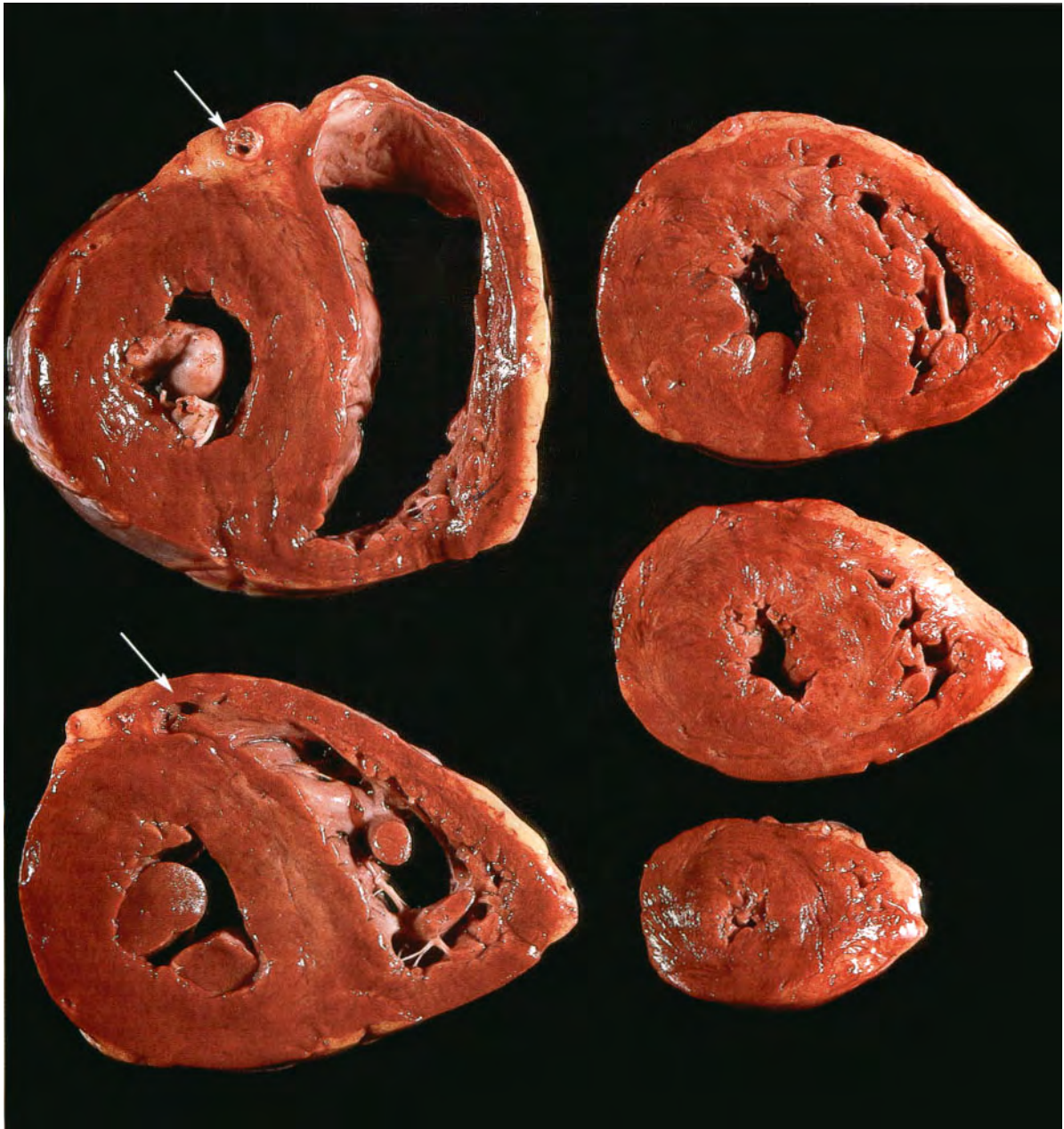


Fig. 1.45

Fig. 1.45 Left ventricular hypertrophy. M/48. The heart has been sliced from the AV valves to the apex and viewed from the posterior aspect. The myocardium is grossly thickened. The hypertrophy resulted from essential hypertension. Note the almost complete occlusion of the anterior descending branch of the left coronary artery in slices top left and bottom left (arrows).

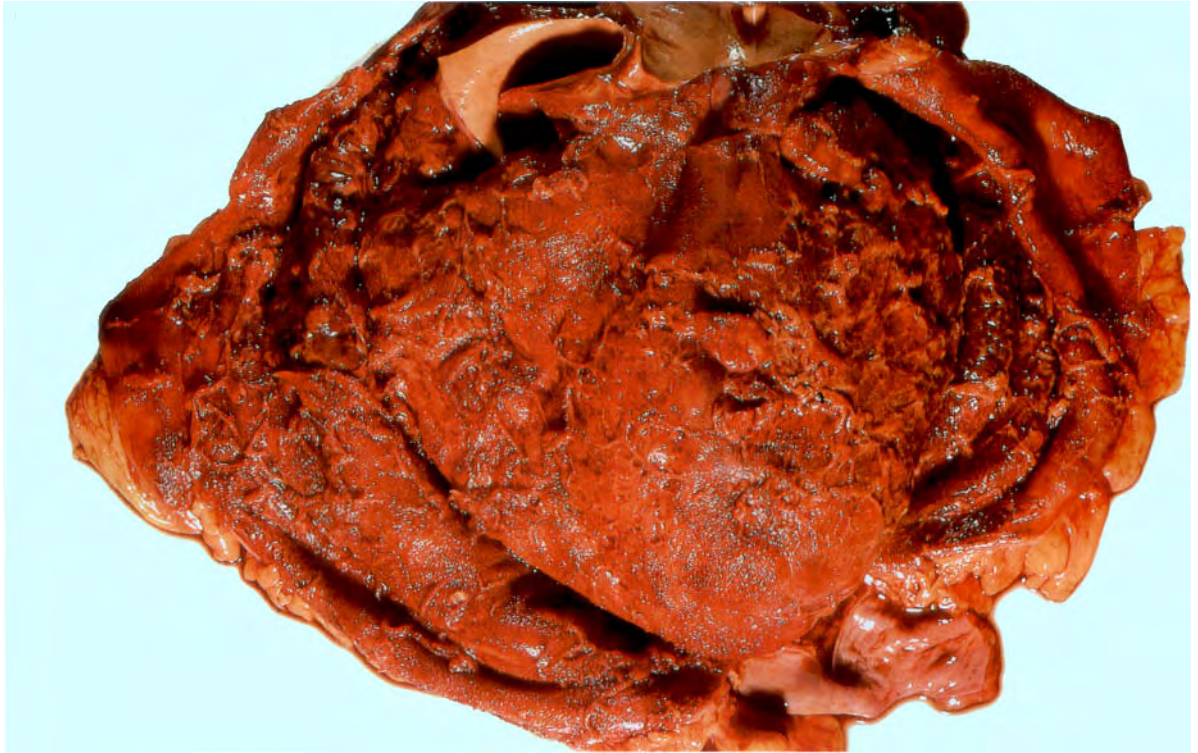


Fig. 1.46

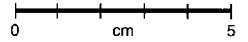


Fig. 1.47

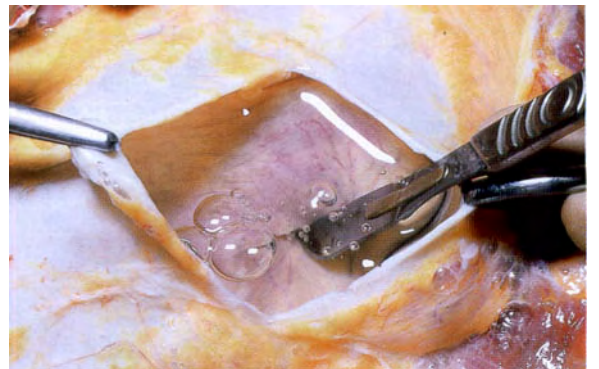


Fig. 1.48



Fig. 1.49

0 cm 1

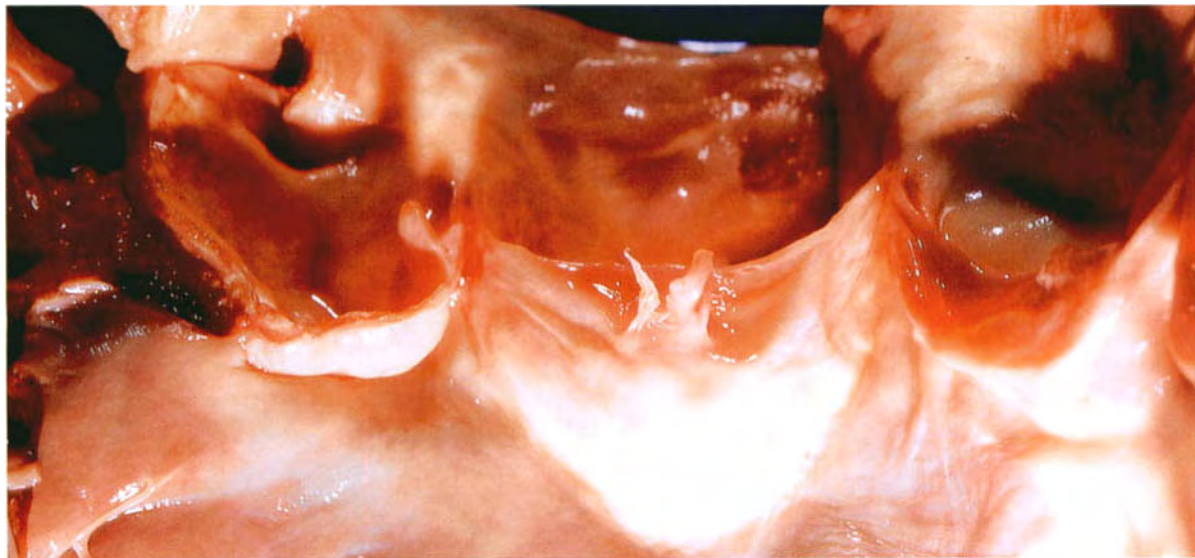


Fig. 1.50

Fig. 1.46 Organizing fibrinous pericarditis. M/56. The parietal layer of the pericardium has been separated from the visceral layer with some difficulty. The surfaces of both layers are covered by shaggy, organizing fibrinous pericarditis which made the two layers adherent to one another.

Fig. 1.47 Pericarditis resulting from deposits of secondary cancer in the pericardium and myocardium. M/60. Lung cancer is the one most likely to invade the pericardium (see Figure. 3.61).

Fig. 1.48 Air embolus. M/39. The patient died suddenly when a large amount of air was accidentally introduced during complicated intravenous therapy. The presence of the air embolus was demonstrated by filling the pericardium with water and making an incision through the water into the ventricular cavity. Bubbles of air then escaped.

Fig. 1.49 Acute rheumatic vegetations on the aortic valve cusps. F/11. The patient died from acute rheumatic carditis.

Fig. 1.50 A Lambl's excrescence on the aortic valve. M/74. These are aggregations of fibrin covered by endothelium. They must be distinguished from true vegetations.

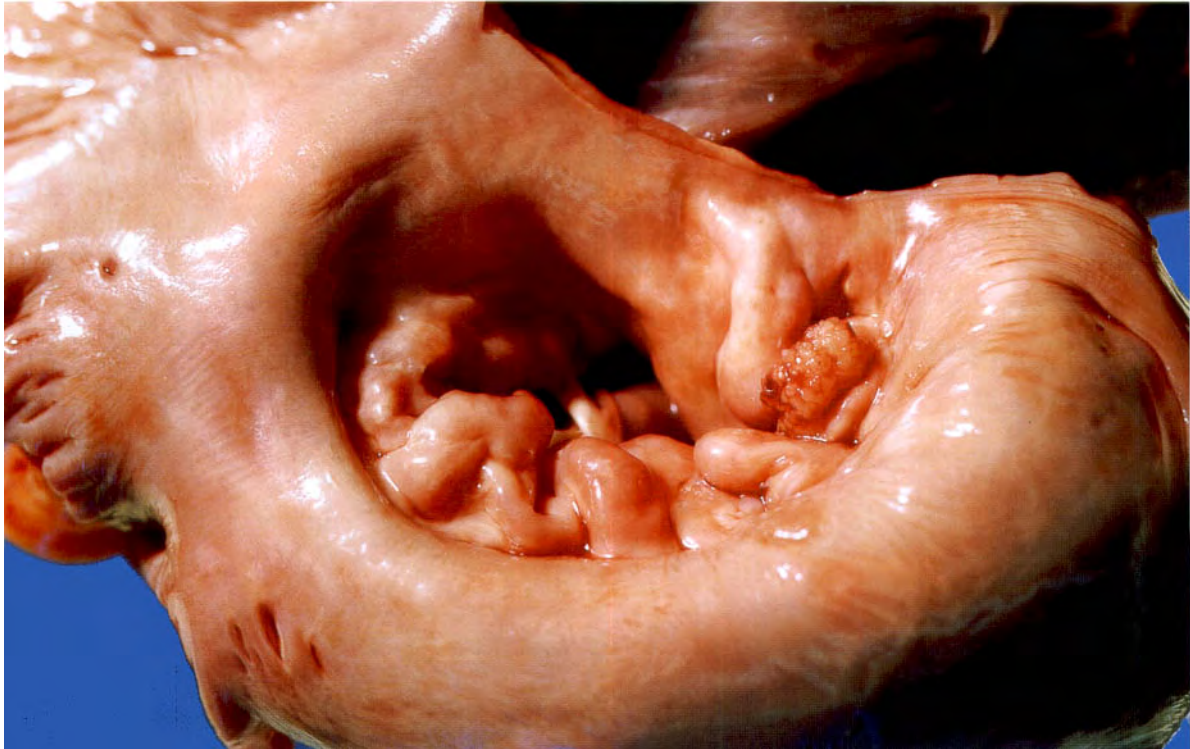


Fig. 1.51

Fig. 1.51 Mitral valve stenosis. F/67. The valve is viewed from the grossly dilated left atrium. The cusps are thickened and adherent, and the orifice is greatly reduced in diameter. The patient had had acute rheumatic fever in childhood. This was a common, late complication of acute rheumatic fever before the introduction of penicillin to treat tonsillitis and other infections caused by the β -haemolytic streptococcus. Mitral valvotomy (splitting the stenosed valve cusps with a blade attached to a surgeon's index finger) was one of the first intracardiac operations performed by cardiac surgeons in the 1950s.

Fig. 1.52 Aortic stenosis. M/76. The valve cusps are thickened, adherent and calcified. This is a slightly less common long-term complication of acute rheumatic fever than mitral stenosis, but in this case there was no history of previous rheumatic fever.

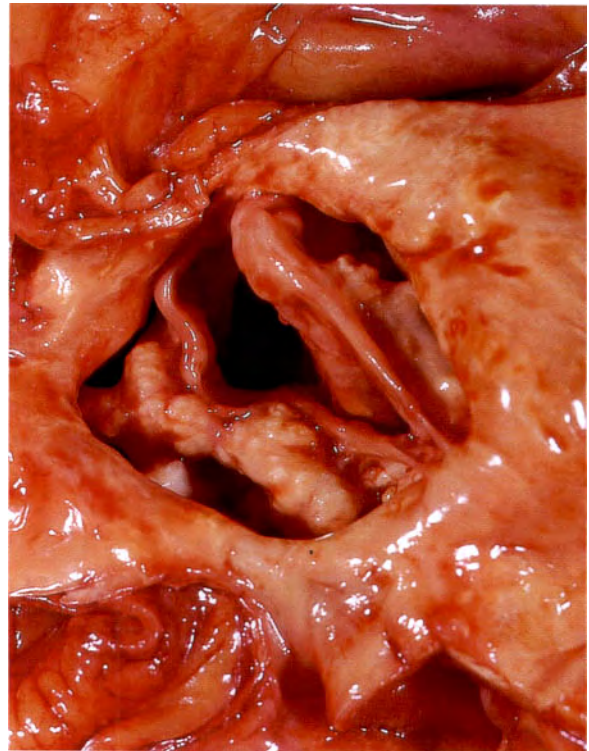


Fig. 1.52

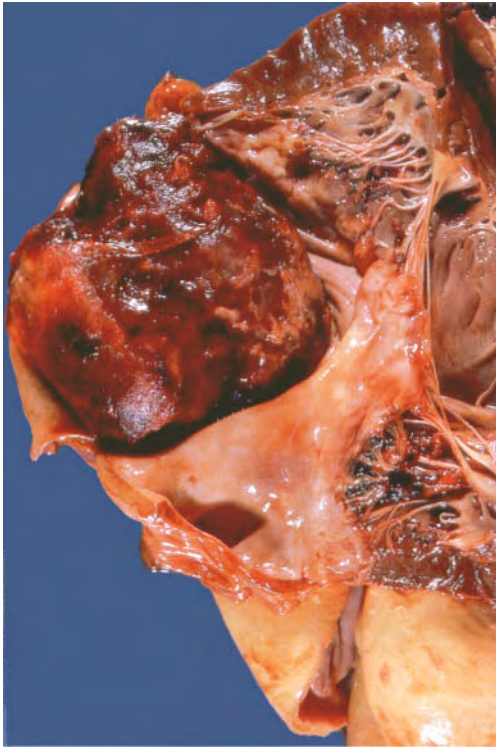


Fig. 1.53

Fig. 1.53 Ball thrombus in the left atrium. M/66. This is a complication of mitral stenosis and auricular fibrillation, and a source of peripheral emboli; however, in this case there appears to be very little abnormality of the mitral valve.

Fig. 1.54 Thrombus in the left auricular appendage. F/85. Thrombus at this site is a complication of auricular fibrillation, and may be a source of peripheral emboli.

Fig. 1.55 Vegetations on the mitral valve in subacute bacterial endocarditis. M/41. These are also a source of peripheral emboli.

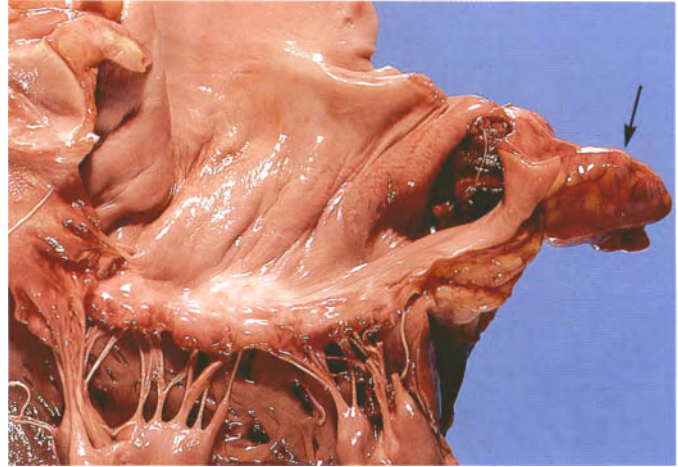


Fig. 1.54

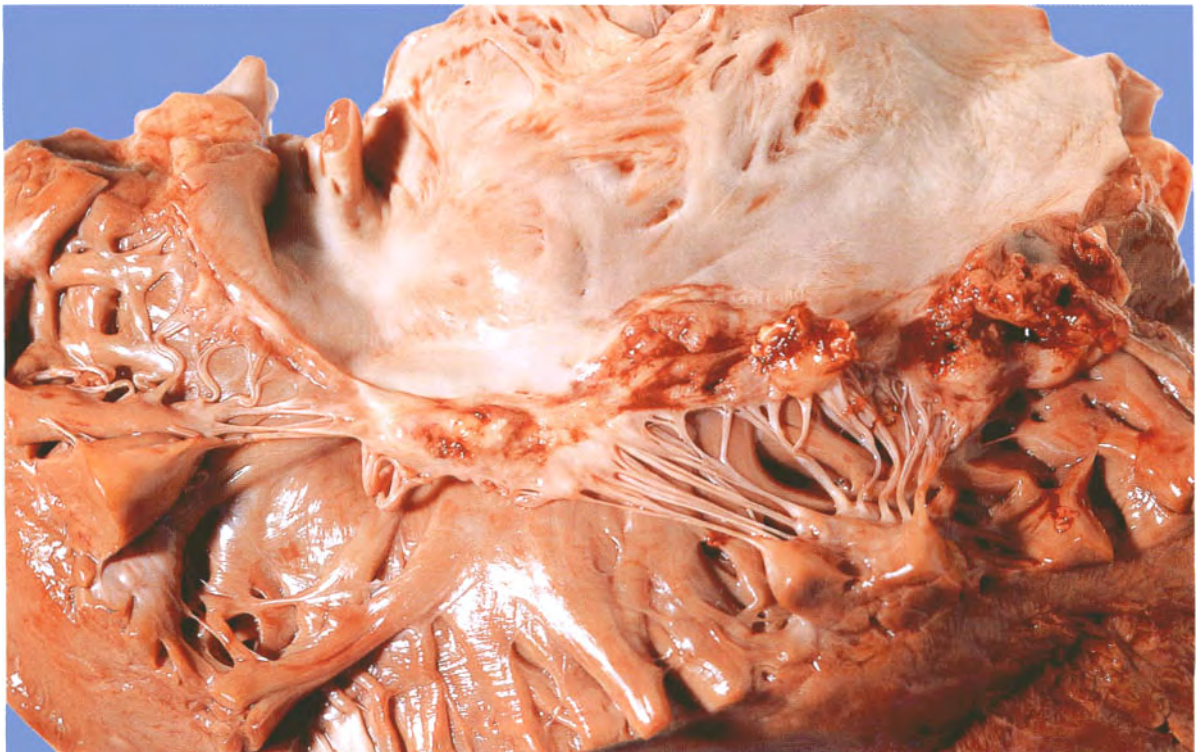


Fig. 1.55

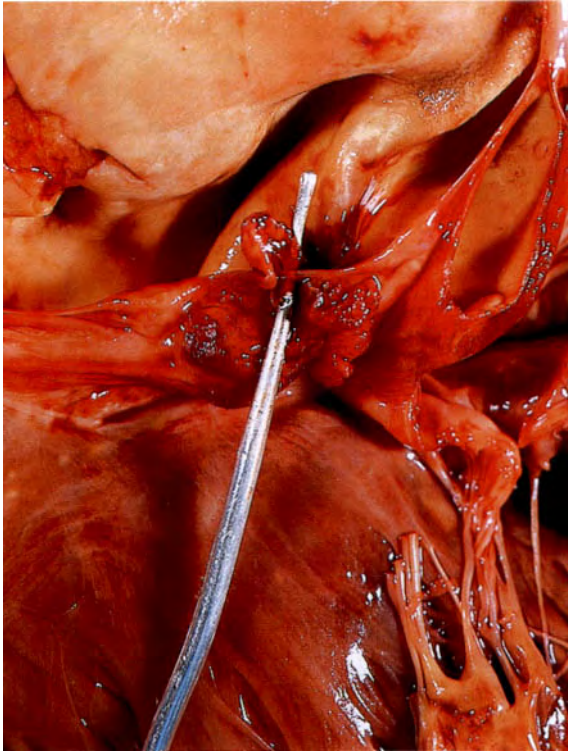


Fig. 1.56



Fig. 1.58

Fig. 1.56 Bacterial endocarditis. Rupture of an aortic valve cusp. M/60.

Fig. 1.57 Recent renal infarct from a septic embolus in bacterial endocarditis. M/56.

Fig. 1.58 Petechial haemorrhages in the conjunctiva from septic emboli in bacterial endocarditis. Note also the linear haemorrhage at the junction between the conjunctiva and the sclera. This is another feature of peripheral embolization.

Fig. 1.59 Fundal photograph showing petechial haemorrhages from septic emboli in bacterial endocarditis.

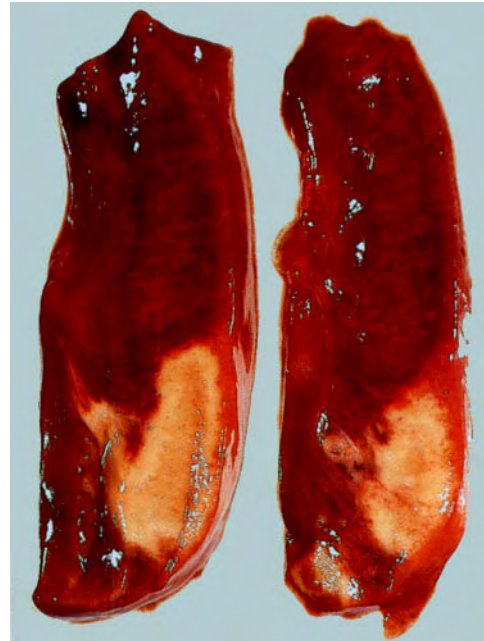


Fig. 1.57

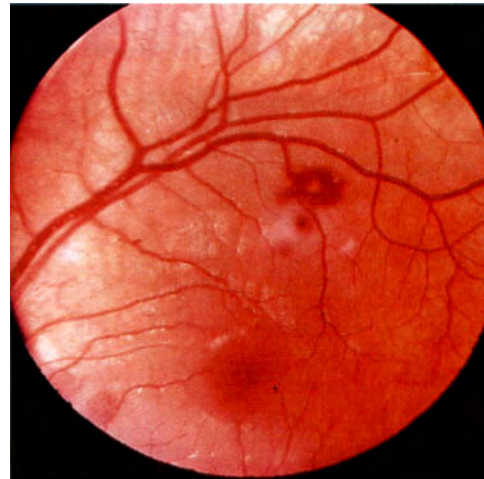
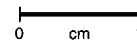


Fig. 1.59

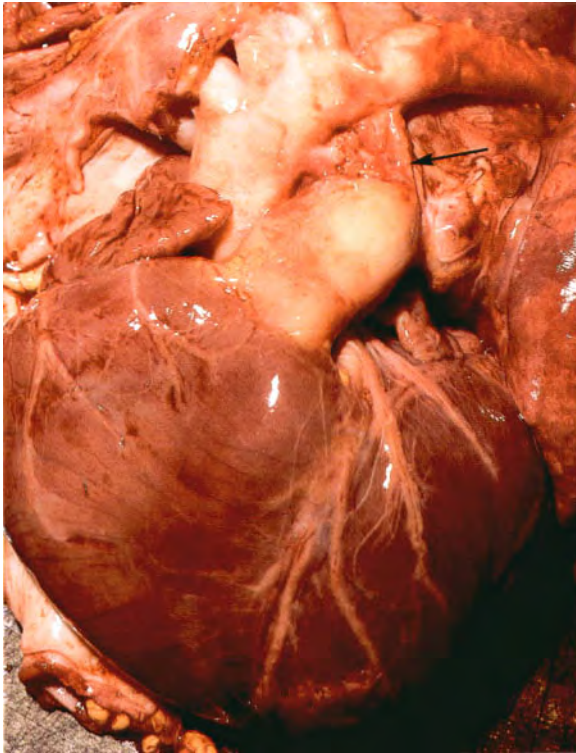


Fig. 1.60

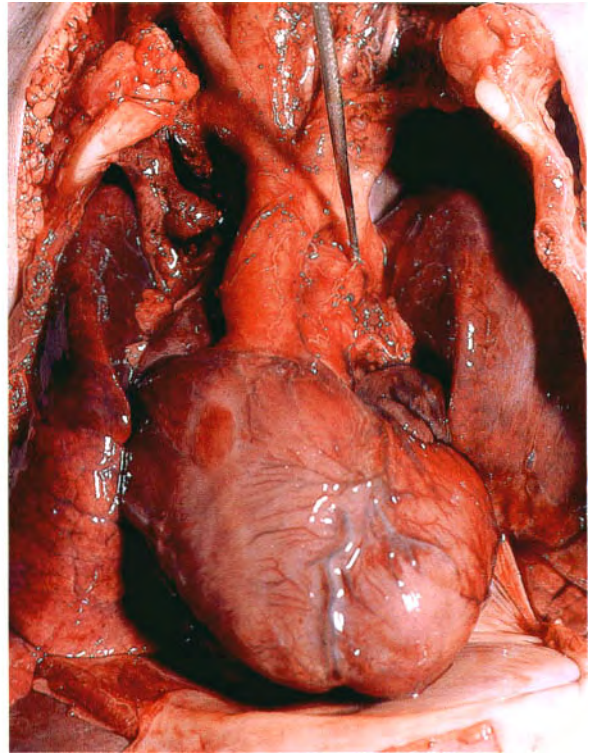


Fig. 1.61

Fig. 1.60 Patent ductus arteriosus. F/3. Joining the pulmonary artery to the aorta (arrow).

Fig. 1.61 Transposition of the great vessels. Neonatal death. The aorta arises from the right ventricle and the pulmonary artery from the left ventricle. The pointer is on the ductus arteriosus.

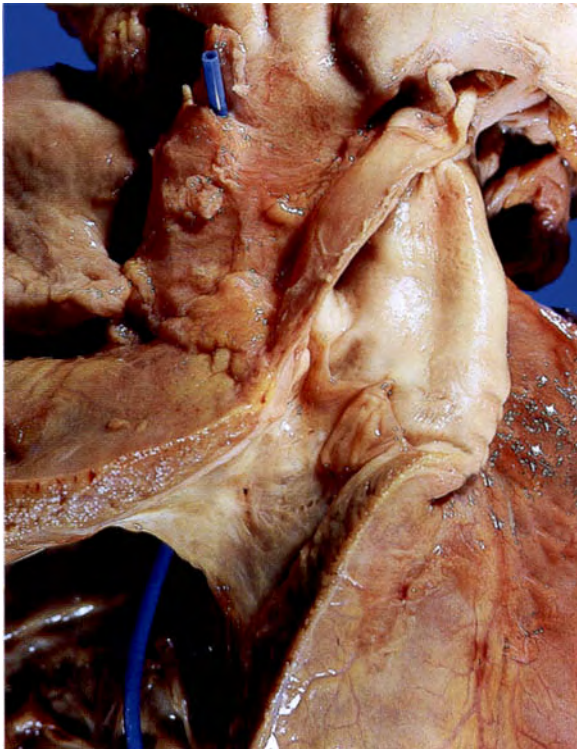


Fig. 1.62

Fig. 1.62 Fallot's tetralogy. M/3. The outflow tract of the right ventricle is viewed in this specimen. There is pulmonary valve stenosis with dilatation of the pulmonary artery beyond this. The right ventricle is hypertrophied and the blue pointer passes from the cavity of the right ventricle into the aorta. This demonstrates the presence of a ventricular septal defect and the fact that the aorta is overriding both ventricles.



Fig. 1.63

Fig. 1.63 Fallot's tetralogy. F/13. This patient was photographed in 1961 when cardiac surgery was in its infancy. She demonstrates the marked cyanosis and clubbing of the fingers that were hallmarks of this disease before the introduction of corrective surgery in infancy. These children were colloquially called 'blue babies'.

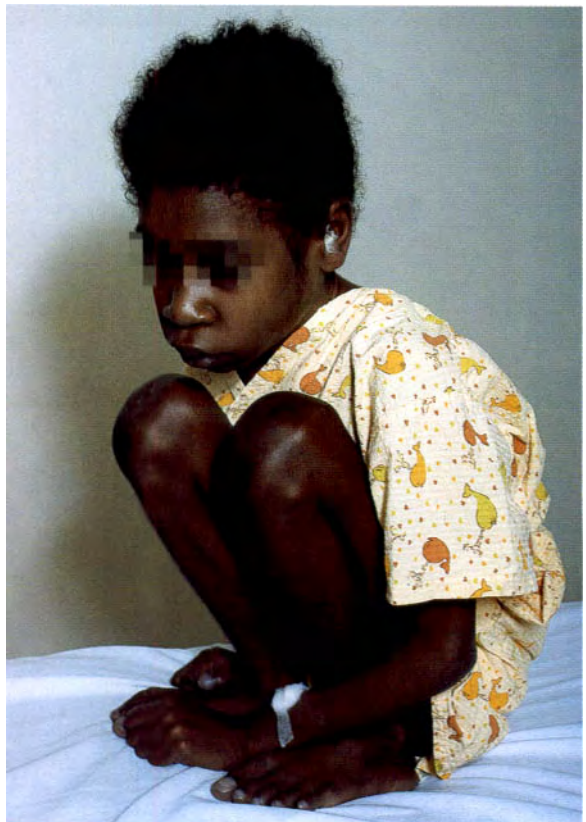


Fig. 1.64

Fig. 1.64 Fallot's tetralogy. M/10. This child from Papua New Guinea was admitted to an Australian hospital for correction of the defect. He is adopting the squatting position, which was very characteristic of patients with untreated Fallot's tetralogy.



Fig. 1.65

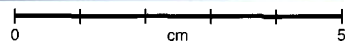


Fig. 1.65 Ventricular septal defect viewed from the left ventricle. M/9.

Fig. 1.66 Probe-patent foramen ovale viewed from the right atrium. M/70. The foramen ovale is probe patent in a small percentage of normal people.

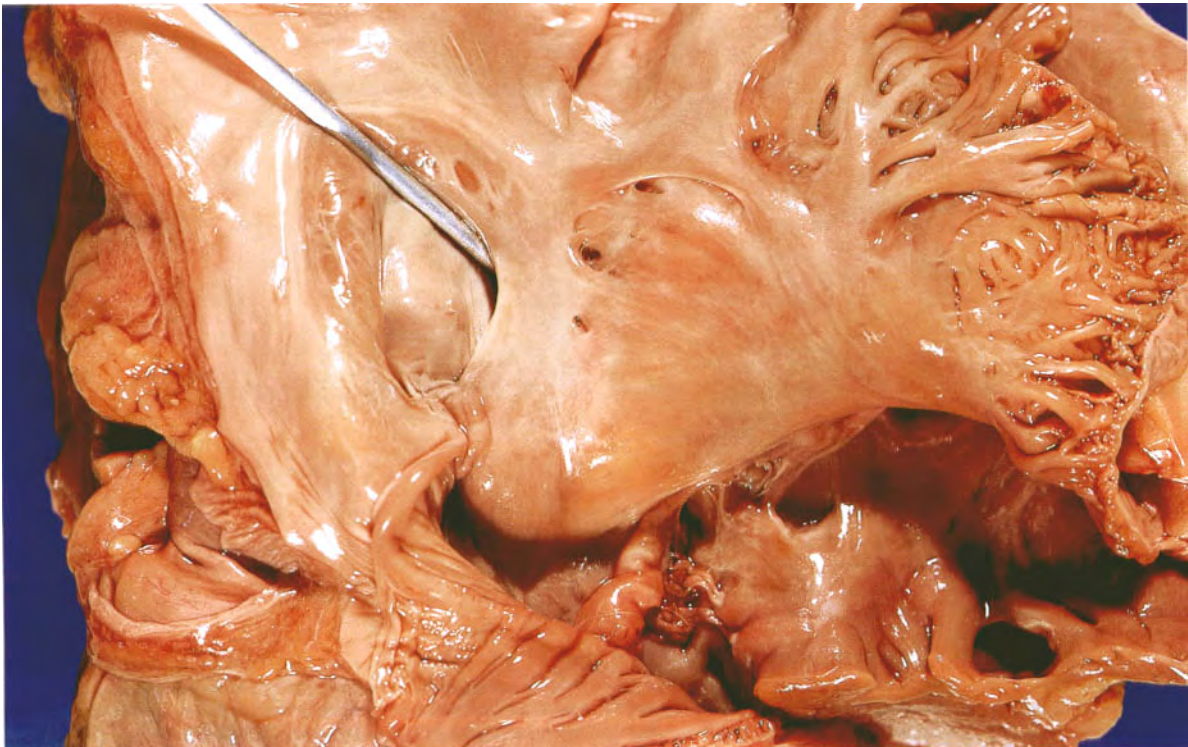


Fig. 1.66

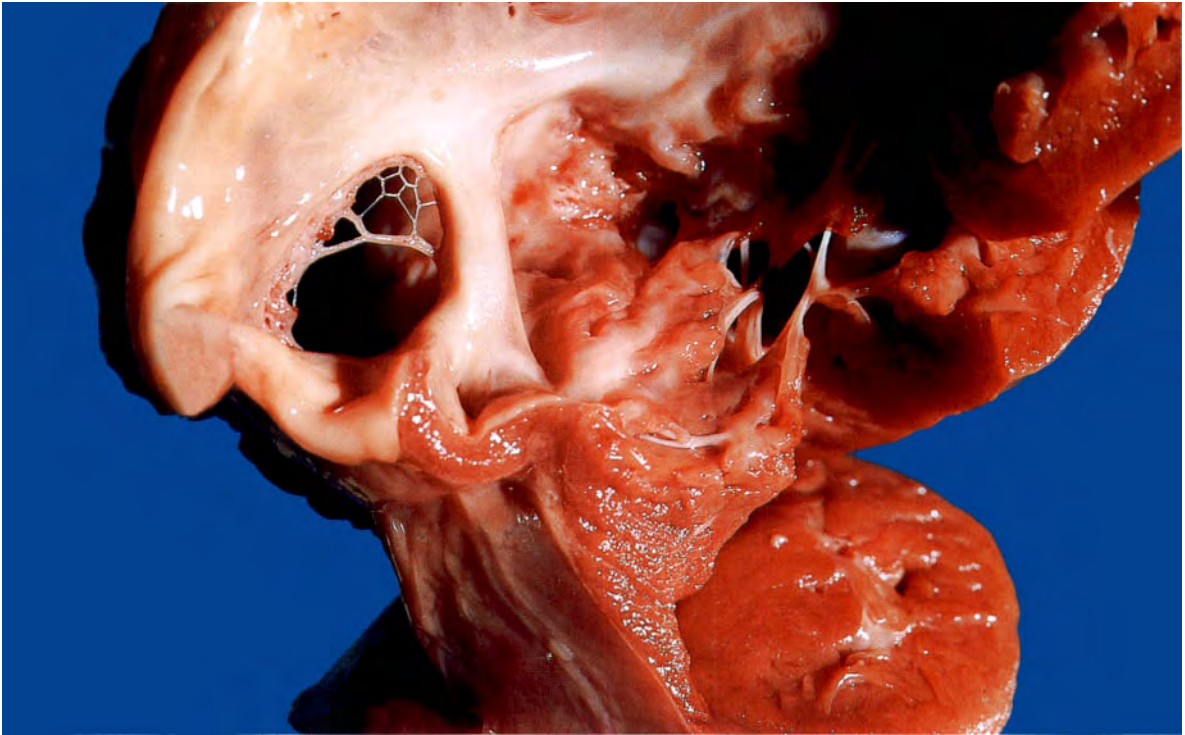


Fig. 1.67

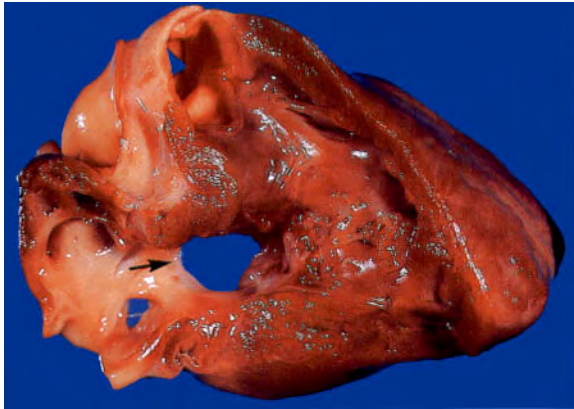


Fig. 1.68

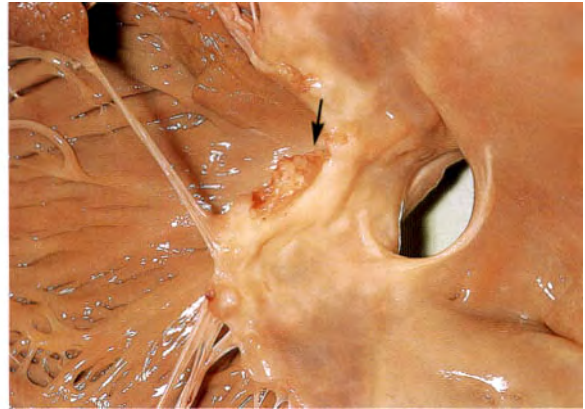


Fig. 1.69

Fig. 1.67 Patent foramen ovale viewed from the right atrium. Stillborn Down's syndrome. All that remains of the septum secundum is a web. Atrial septal defect is frequently encountered in patients with Down's syndrome.

Fig. 1.68 Septum primum atrial septal defect viewed from the right atrium. F/4 months. A septum primum defect involves both the atrial septum and the atrioventricular valve ring, so the membranous portion of the interventricular septum is involved as well.

Fig. 1.69 Septum primum atrial septal defect plus a cleft in the anterior cusp of the mitral valve. F/50. This mitral valve defect is often associated with this type of ASD because of the associated defect in the AV ring. There is a small vegetation on the abnormal mitral valve.

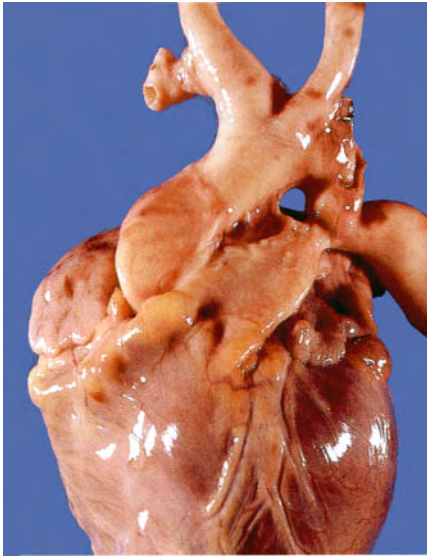


Fig. 1.70



Fig. 1.71

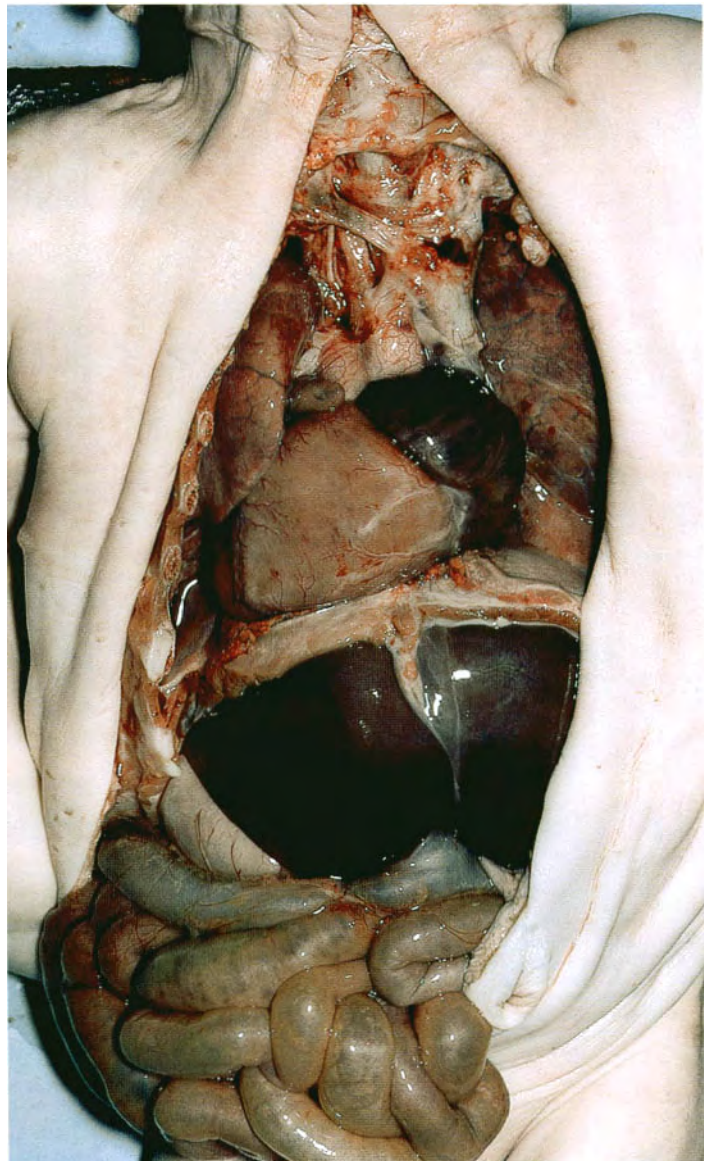


Fig. 1.72

Fig. 1.70 Coarctation of the aorta. F/4. The coarctation is present just distal to the origin of the left subclavian artery, which has been cut off very close to the aorta. The child died from other pathology.

Fig. 1.71 Coarctation of the aorta. The same case as Figure 1.70. The thoracic aorta has been opened from behind to display the coarctation more clearly.

Fig. 1.72 Situs inversus. Neonatal death from respiratory distress. The superior vena cava is on the left, the cardiac apex on the right; the stomach is on the right and the liver on the left.

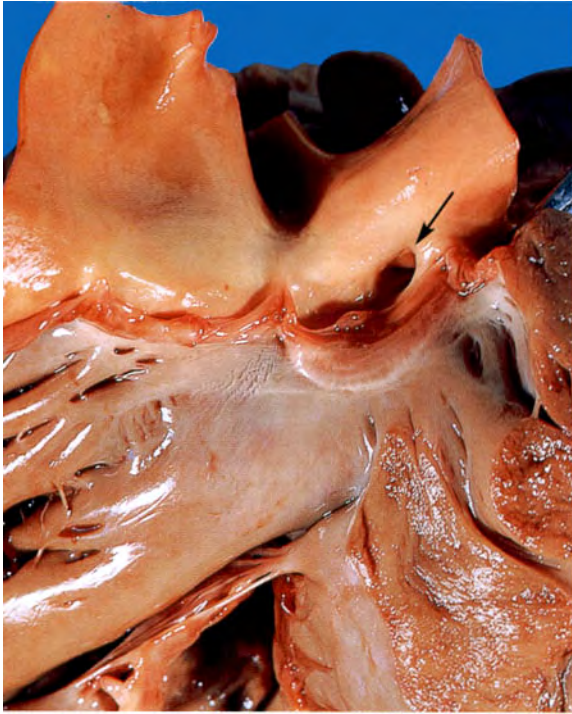


Fig. 1.73

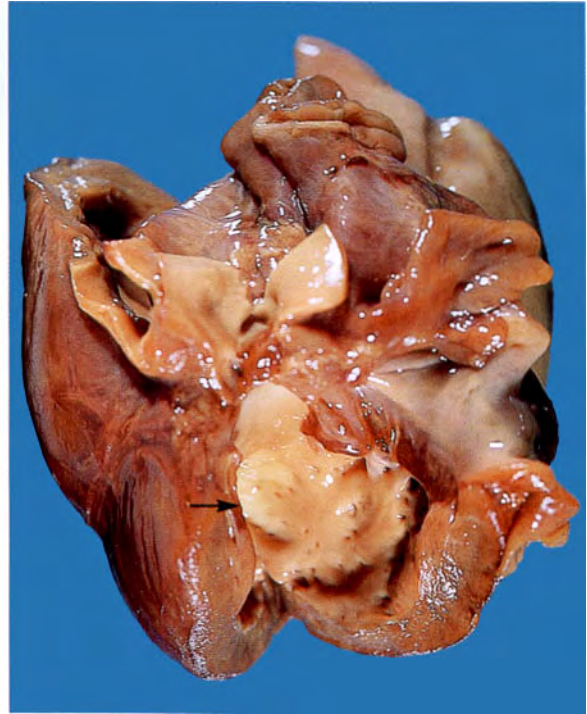


Fig. 1.74

0 cm 1

Fig. 1.73 Left coronary artery arising from the pulmonary trunk. F/7. The orifice of the coronary artery can be seen arising from the sinus above the pulmonary artery cusp on the right (arrow). This is the commonest congenital abnormality of the coronary arteries. Death resulted from myocardial infarction caused by perfusion of the left ventricle by poorly oxygenated blood.

Fig. 1.74 Fibroelastosis of the left ventricle. M/3 weeks. Death from cardiac failure. The endocardial surface of the left ventricle is lined by a thick layer of white tissue.

Fig. 1.75 Left atrial myxoma removed surgically. M/68. The patient presented with symptoms of left heart failure and signs of mitral stenosis. The tumour was identified during clinical workup. This is the commonest primary tumour of the heart.

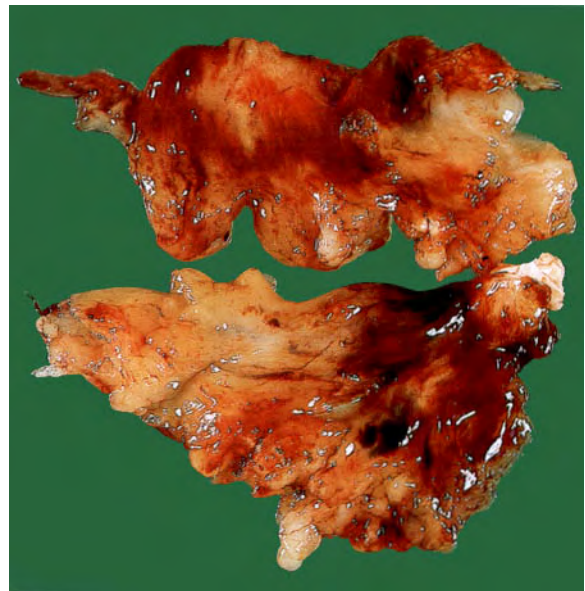


Fig. 1.75

0 cm 5

**LYMPH NODES
AND SPLEEN**

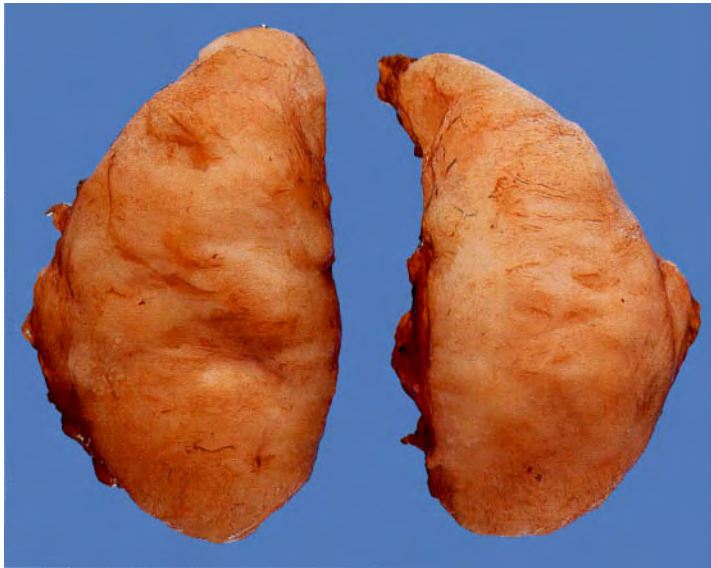


Fig. 2.1



Fig. 2.2



Fig. 2.3



Fig. 2.4

Fig. 2.1 Diffuse malignant lymphoma. M/73. This inguinal lymph node shows complete obliteration of its normal architecture by fleshy, homogeneous tumour tissue.

Fig. 2.2 Nodular malignant lymphoma. F/33. This axillary lymph node has its normal architecture replaced by tumour tissue showing a nodular pattern. The exact diagnosis of malignant lymphomas must be made by microscopic examination.

Fig. 2.3 Burkitt's lymphoma. M/8 from Papua New Guinea. This lymphoma is a common tumour in children in Central Africa and in children in Papua New Guinea, where it is associated with the presence of Epstein-Barr virus in tissue culture of the tumour cells. It occurs less frequently in other parts of the world, and then it is not associated with the presence of Epstein-Barr virus.

Fig. 2.4 Secondary tumour in a lymph node. F/43. The node is replaced by black tumour tissue. Diagnosis of the type of secondary tumour depends on microscopic examination, but when the tumour is black it is very likely to be a secondary melanoma, as this one was.

0 cm 1

0 cm 1

0 cm 1

Fig. 2.5 Spleen in malignant lymphoma. F/70. The normal architecture of the spleen has been replaced by a homogeneous infiltration. The normal malpighian follicles cannot be seen. This appearance is identical for both malignant lymphoma and leukaemia.

Fig. 2.6 Multiple infarcts in a spleen greatly enlarged by malignant lymphoma. F/61. The multiple areas of infarction are well demarcated.

Fig. 2.7 Spleen in Hodgkin's disease. M/34. This spleen was removed during a laparotomy for staging of Hodgkin's disease. One rounded deposit was found. The splenic deposits of Hodgkin's disease tend to be discrete and round, rather than a diffuse infiltration as is seen in non-Hodgkin's lymphomas.

Fig. 2.8 Spleen in Hodgkin's disease. A more advanced Hodgkin's disease than that in Figure 2.7. F/55. There are multiple rounded, creamy, nodular deposits.

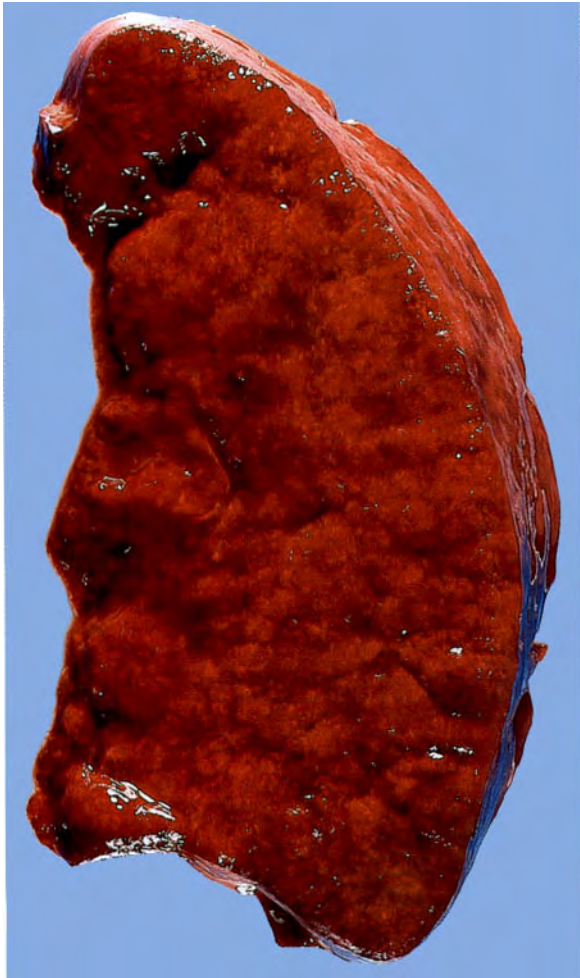


Fig. 2.5



Fig. 2.6

0 cm 5



Fig. 2.7

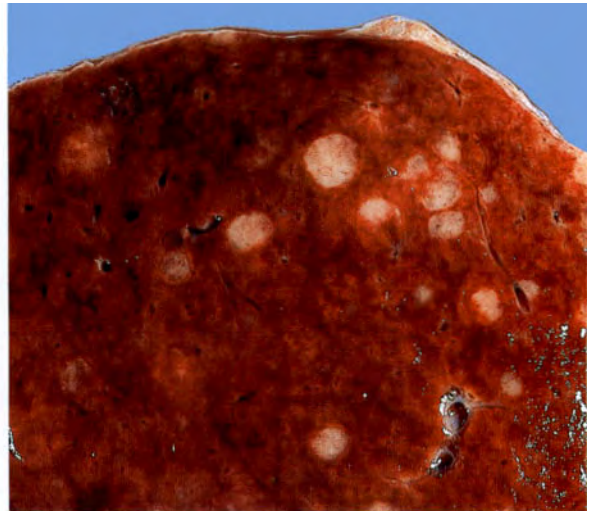


Fig. 2.8



Fig. 2.9 0 cm 5



Fig. 2.10 0 cm 5

Fig. 2.9 Ruptured spleen. F/16. This was a result of a motor traffic accident. There are multiple tears in the spleen, which was removed to stop the haemorrhage. Rupture of a spleen of normal size requires considerable force, as in this case. In countries where malaria is endemic, splenomegaly (often very gross enlargement) is common. These spleens are not protected by the ribcage and rupture occurs with relatively little trauma to the abdomen. Spleens enlarged as a result of infectious mononucleosis and leukaemia also rupture as a result of minor trauma.

Fig. 2.10 Simple cysts in the spleen. F/61. These multiple benign cysts were an incidental postmortem finding and caused no clinical symptoms.

Fig. 2.11 Perisplenitis. M/71. The splenic capsule is covered by thick, white, fibrous plaques. This is a fairly frequent incidental postmortem finding. Its cause is not known.



Fig. 2.11 0 cm 5

RESPIRATORY SYSTEM



Fig. 3.1



Fig. 3.3

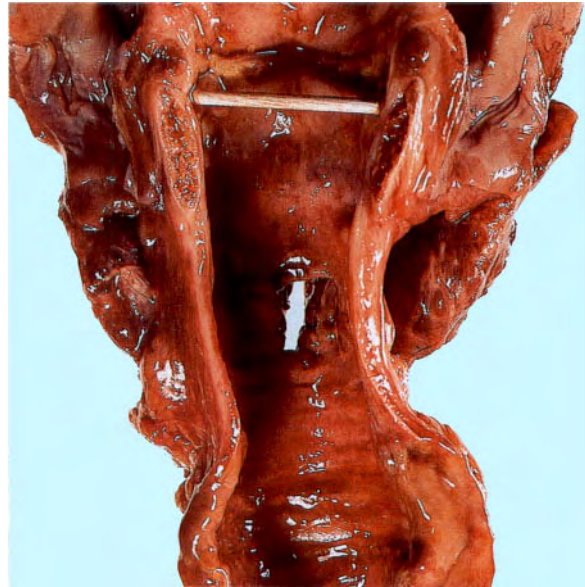


Fig. 3.2

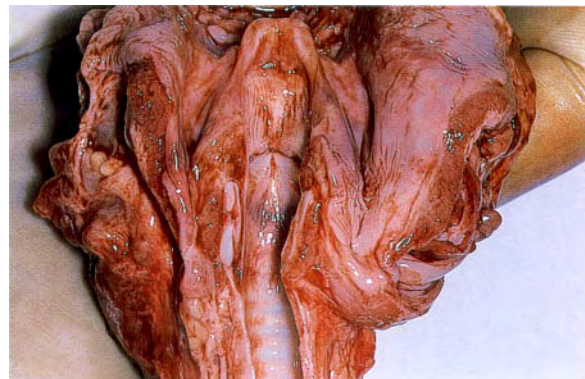


Fig. 3.4

Fig. 3.1 Acute tracheobronchitis. M/68. The mucosa of the trachea is reddened and streaked with pus. The patient died from the respiratory infection.

Fig. 3.2 Acute tracheitis associated with the presence of a tracheostomy tube. F/56. The tracheal mucosa is reddened and there is mucosal ulceration adjacent to the vertical tracheostomy opening. The ulceration was caused by irritation from the inflated bulb of the tracheostomy tube.

Fig. 3.3 Candidiasis of the epiglottis. M/19. The epiglottis is reddened from the acute inflammation and at its tip there is a green membrane, which consisted of purulent exudate plus the hyphal forms of *Candida*. The patient died from acute leukaemia.

Fig. 3.4 Acute epiglottitis. M/4. This child had a sudden onset of stridor leading quickly to respiratory obstruction and death. The epiglottis is acutely inflamed and swollen, but no other abnormality was found at postmortem. This condition probably has a viral aetiology.



Fig. 3.5



Fig. 3.6



Fig. 3.7

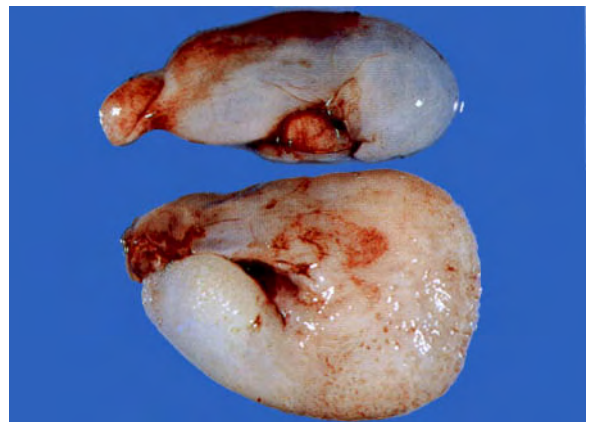


Fig. 3.8

0 cm 1

Fig. 3.5 Rhinoscleroma. M/30. Patient from Papua New Guinea. An inflammatory tumour mass caused by *Klebsiella rhinoscleromatis* is protruding from the left nostril. The nose is expanded by the tumour, which also filled the nasopharynx.

Fig. 3.6 Acute pulmonary oedema. M/21. The trachea is filled with frothy oedema fluid. Both lungs were heavy, and similar fluid could be squeezed from their cut surfaces.

Fig. 3.7 Tracheopathia osteoplastica. M/70. There are multiple hard nodules on the mucosal surface of the trachea. Microscopically, these consisted of cartilage.

Fig. 3.8 Nasal polyps. F/10. These two polyps were removed from the left nasal cavity. Such polyps are fairly common at all ages and are inflammatory in origin.

Fig. 3.9 Squamous cell carcinoma of the hypopharynx. F/65.

Fig. 3.10 Squamous cell carcinoma of the larynx. M/71. The subglottic tumour can be seen in the laryngectomy specimen. The patient presented with hoarseness.

Fig. 3.11 Squamous cell carcinoma of the larynx. M/64. This was primarily an extrinsic carcinoma of the larynx arising in the hypopharynx and compressing the larynx. There is a patch of leukoplakia adjacent to the tumour. Laryngectomy specimen.

Fig. 3.12 Pseudosarcoma of the larynx. M/44. This large, polypoid tumour with a smooth surface is almost completely obstructing the larynx.



Fig. 3.9

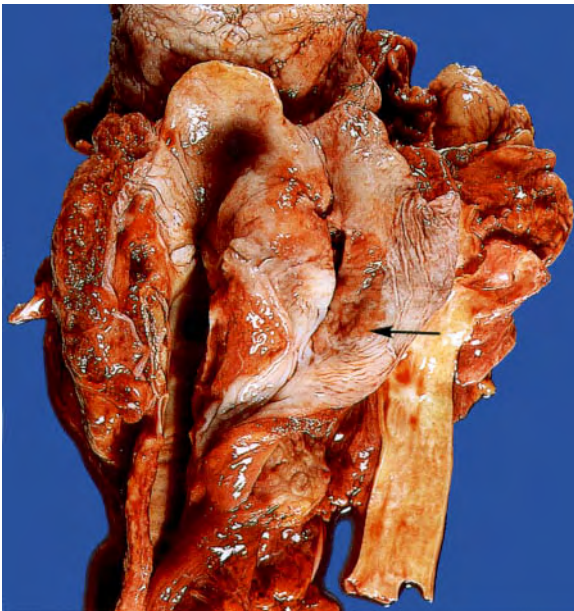


Fig. 3.11

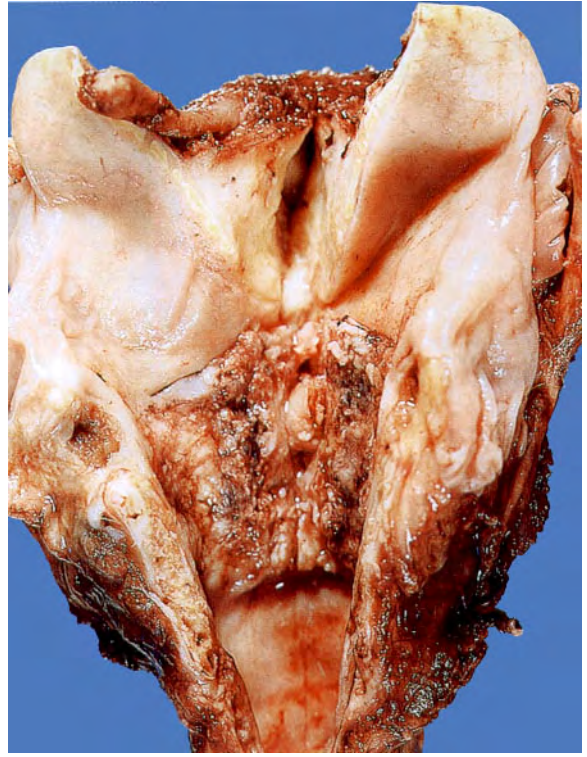


Fig. 3.10

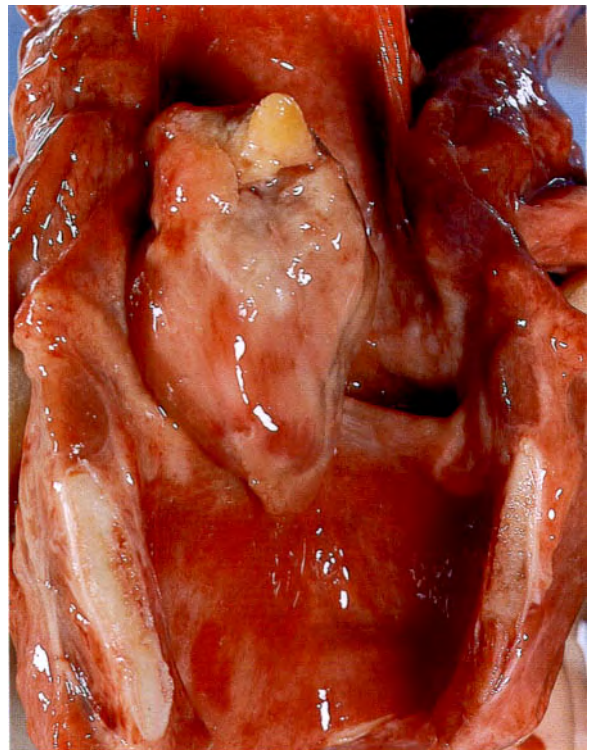


Fig. 3.12



Fig. 3.13



Fig. 3.14

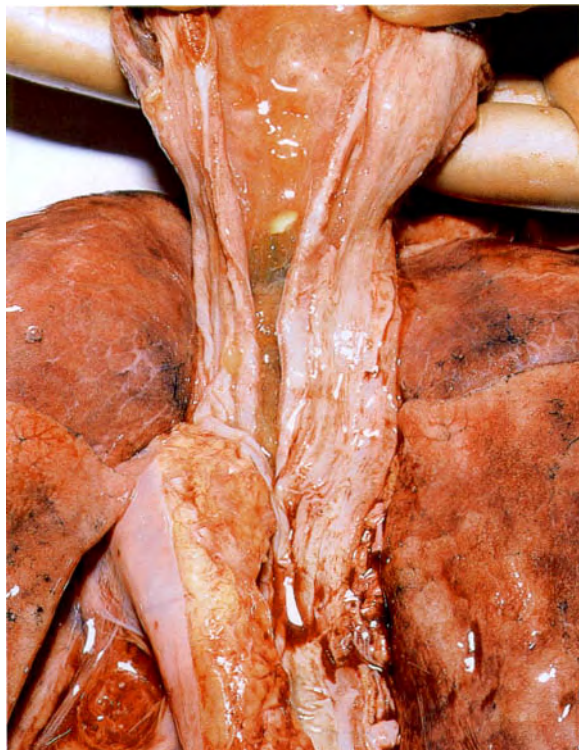


Fig. 3.15

Fig. 3.13 Foreign body (tablet) lodged in the hilum of the right lung, obstructing the middle and lower lobe bronchi. M/84. This is the commonest site for an inhaled foreign body to become impacted because of the anatomy of the bronchial tree. Inhaled foreign bodies are most frequently encountered in children about the age of 2 years.

Fig. 3.14 Unusual inhaled foreign body. M/2. This child was found by his parents covered in his mother's talcum powder. Within a few hours he developed acute respiratory difficulty and died 3 hours later. The whole of the bronchial tree was filled with thick, semisolid material which could be squeezed out as demonstrated. The powder contained silica, and the irritant effect of this must have stimulated the secretion of mucus which in turn mixed with the powder to cause complete blockage of the airways. This gross appearance is similar to that seen in chronic bronchitis (Figure 3.27) and asthma (Figure 3.28).

Fig. 3.15 Inhalation of vomitus. M/70. The trachea and bronchial tubes are filled with vomitus. This was the final cause of death in a debilitated old man.

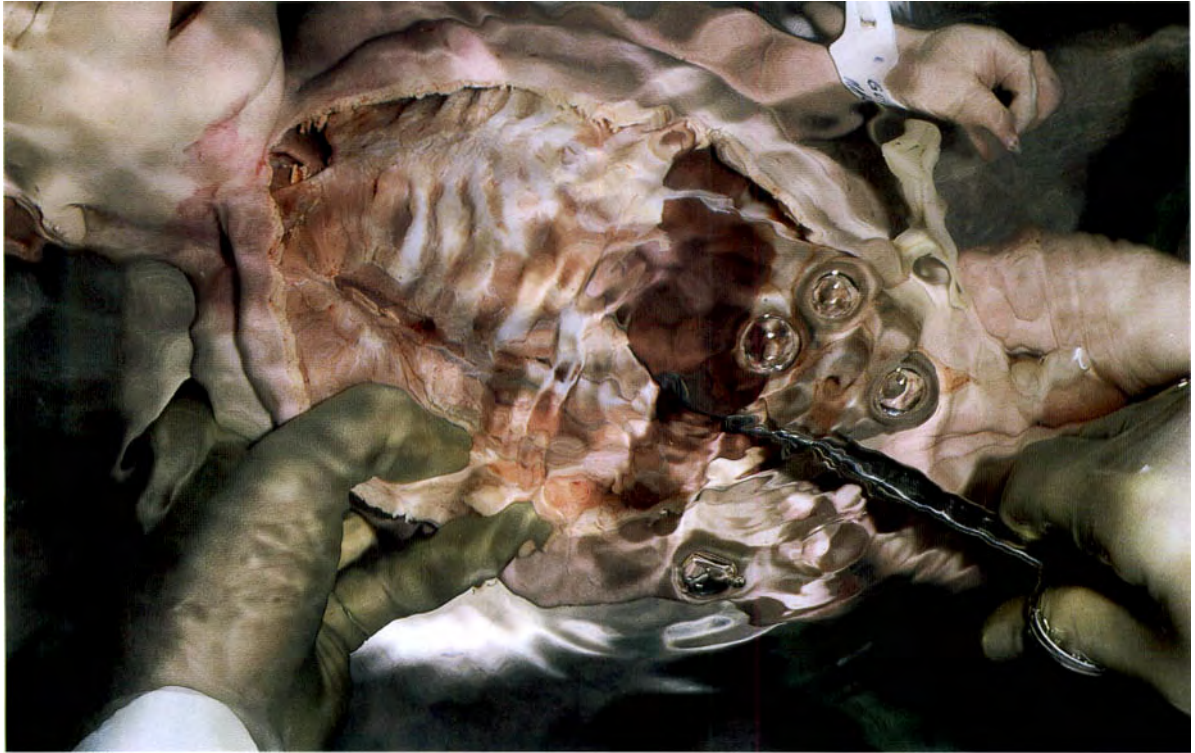


Fig. 3.16

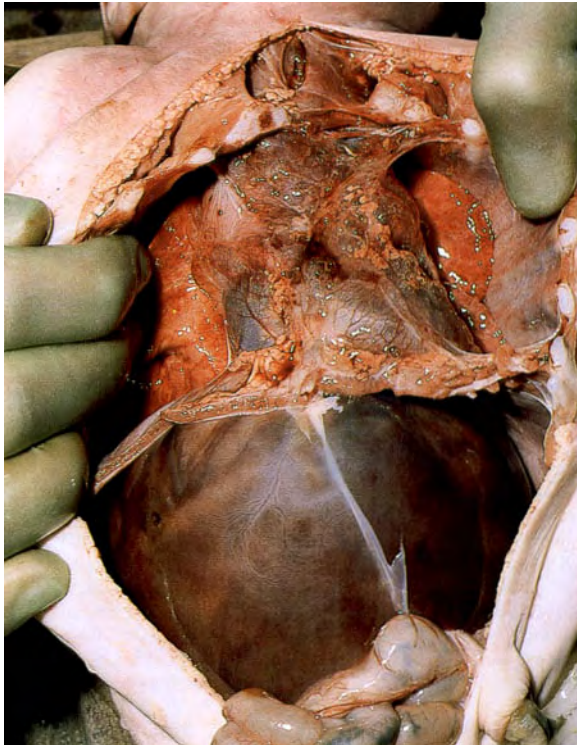


Fig. 3.17



Fig. 3.18

0 cm 1

Fig. 3.16 Tension pneumothorax. M/2 days. This resulted from attempts at resuscitation following delivery. The thoracic cavity was opened under water and the escaping air produced bubbles.

Fig. 3.17 Pneumomediastinum. Gas bubbles in the mediastinum of the patient shown in Figure 3.16.

Fig. 3.18 Interstitial emphysema. F/4 days. This was caused by overenthusiastic resuscitation following delivery. Rupture of bullae such as these resulted in the pathology illustrated in Figures 3.16 and 3.17.

Fig. 3.19 Congenital bronchogenic cyst. F/1 month. The child was investigated for respiratory difficulty present since birth; this abnormal cystic area was identified on chest X-ray and was surgically removed from the left lower lobe.

Fig. 3.20 Congenital lymphectasia of the lung. M/10 hours. The lungs felt spongy. Their cut surfaces show cystic spaces which vary in size, some being quite large (arrow).

Fig. 3.21 Hypoplastic lungs (viewed from behind). F/neonate. Both lungs are hypoplastic, the left (arrowed) more so than the right. The baby had a left diaphragmatic hernia, an anomaly which is usually accompanied by hypoplastic lungs (see Figure 4.31).



Fig. 3.19

0 cm 1



Fig. 3.20



Fig. 3.21

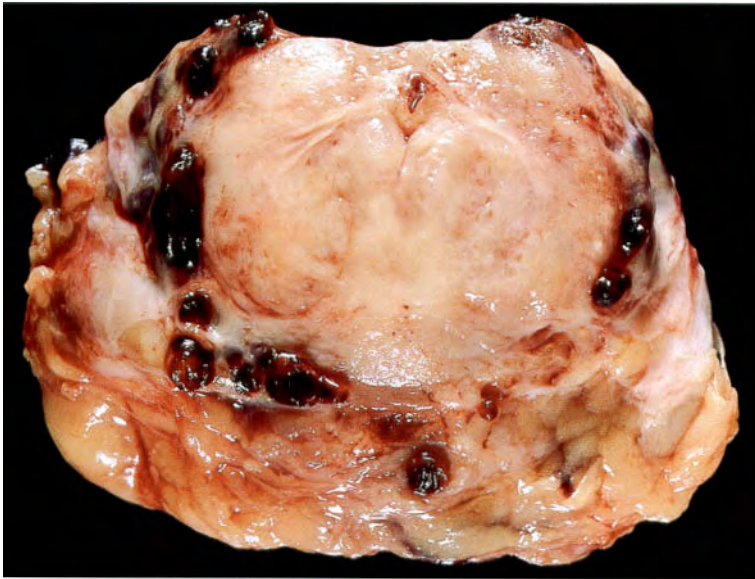


Fig. 3.22

Fig. 3.22 Thrombi in prostatic veins. M/74. Transverse section of the prostate. This patient had congestive cardiac failure which resulted in the formation of these thrombi.

Fig. 3.23 Pulmonary infarction in the patient shown in Figure 3.22. This resulted when fragments of the thrombi broke off, passed through the venous system and became lodged in a pulmonary artery. Note the wedge-shaped haemorrhagic area on the pleural surface of the lung. It is hard, and elevated above the adjacent lung surface.

Fig. 3.24 Pulmonary embolus. Cut surface of a pulmonary infarct showing the embolus in the supplying artery at the apex of the pyramid-shaped infarct.

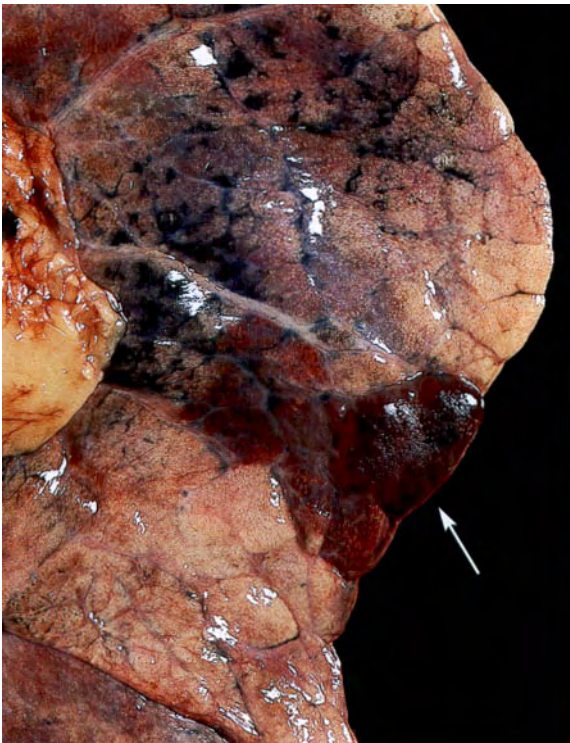


Fig. 3.23

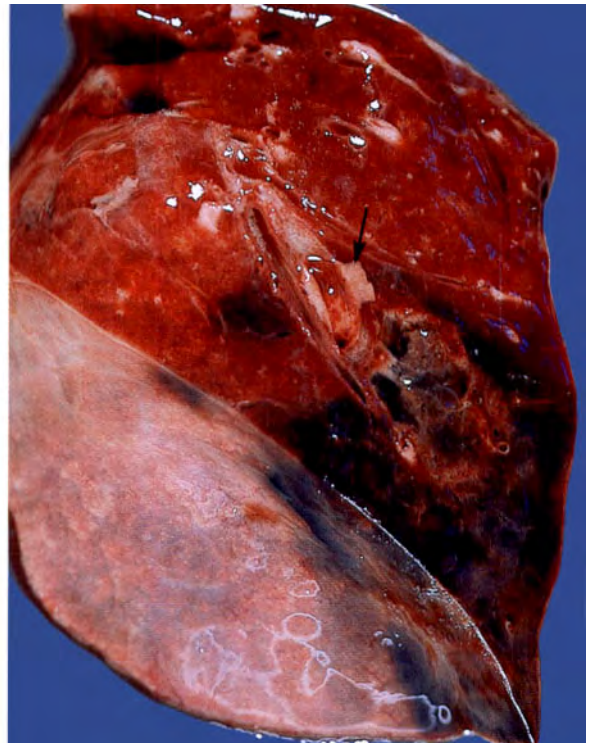


Fig. 3.24



Fig. 3.25

Fig. 3.25 Pan-acinar destructive emphysema – severe emphysema. M/76. The ‘substance’ of the lung has been almost completely lost. When such lungs are removed from the body they are soft and can often be squeezed into a small ball. The pathology can be demonstrated by inflating the intact lung by running formalin into the main bronchus, allowing it to float in formalin for 48 hours for fixation, then slicing it with a long, sharp knife. As the lung is cut, the formalin runs out of the emphysematous spaces but the holey organ can be examined by immersing the slices in water, as was done for this photograph.

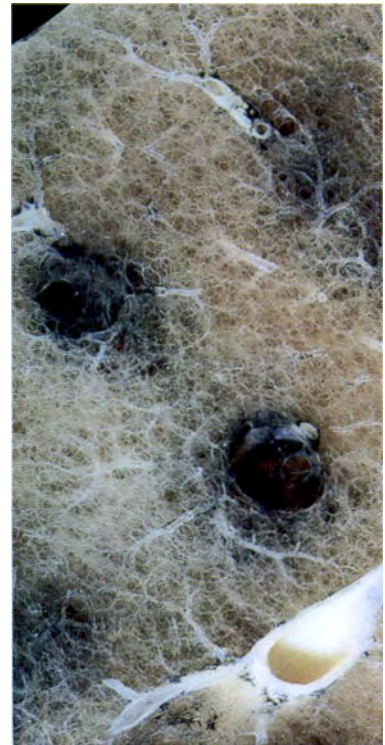


Fig. 3.26

Fig. 3.26 Centrilobular destructive emphysema – mild emphysema. M/70. The respiratory bronchioles and some of the alveolar ducts in the middle of the pulmonary lobules are destroyed. This results in holes being formed – emphysematous spaces. These areas are black because of the accumulation of carbon pigment in the peribronchial lymphatics.



Fig. 3.27

Fig. 3.27 Chronic bronchitis. M/69. This man had suffered from chronic obstructive airways disease for many years. Death was due to plugging of his respiratory passages by thick, tenacious mucus, shown filling the left main bronchus. The lung itself showed minimal emphysema.

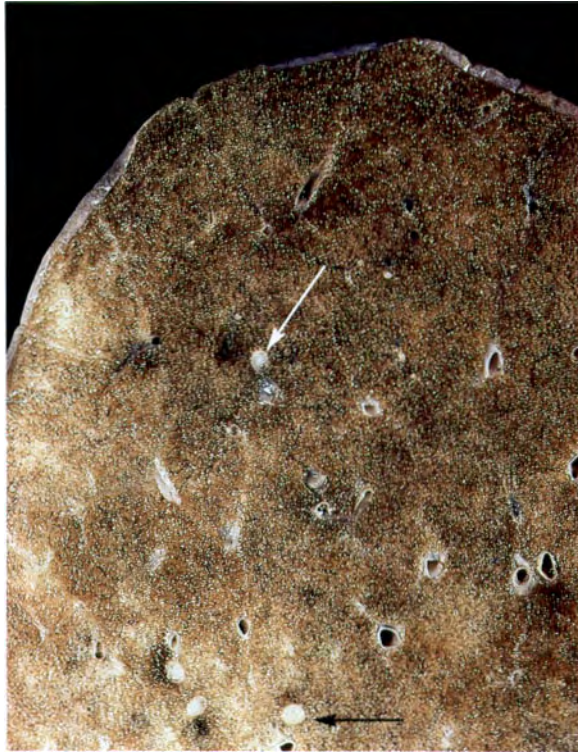


Fig. 3.28

Fig. 3.28 Lung in acute asthma. F/46. The respiratory passages throughout both lungs were completely occluded by thick, tenacious mucus. This woman had suffered from asthma for many years and one day she had an acute attack and died. This sequence of events is well known in asthma, and postmortem examination of the lungs shows the features demonstrated here.

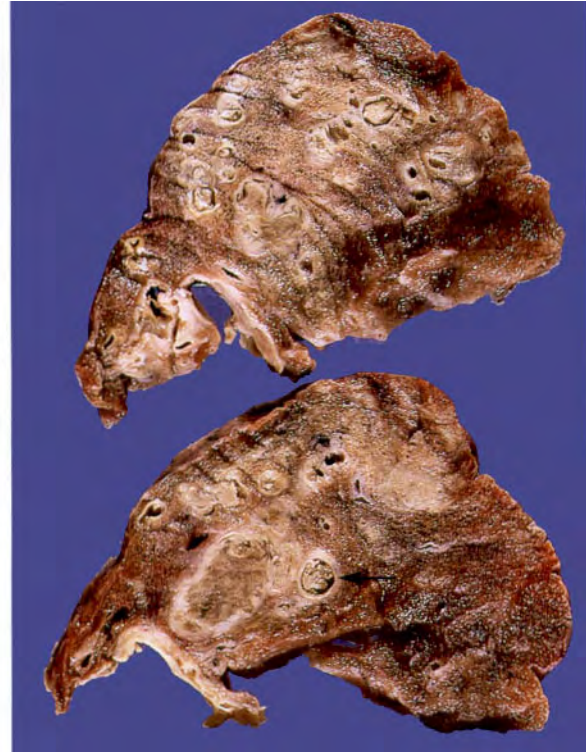


Fig. 3.29

0 cm 1

Fig. 3.29 Localized area of bronchiectasis caused by impaction of a mucus plug. F/49. The patient suffered from asthma and the mucus plug was obstructing the posterior segmental bronchus of the right upper lobe. Microscopic examination showed that the plug consisted of a ball of *Aspergillus* mycelia. Mucus plugs associated with *Aspergillus* are a recognized complication of asthma.

Fig. 3.30 Bronchiectasis. M/17. Left lower lobectomy was performed for chronic bronchiectasis. This patient had had recurrent attacks of pneumonia since his first year of life. The bronchial tubes are extremely dilated. Their walls are thickened and fibrotic, and 'ribbing' can be seen along the mucosal surface of some of them. The adjacent lung has been almost completely destroyed. Surgical treatment of bronchiectasis is only useful when the condition is localized to one segment of the lung. Bronchiectasis of this severity was also seen in patients with mucoviscidosis (see Figures 5.7 to 5.9). It can be prevented by aggressive medical and physiotherapy treatment of pneumonia in children.



Fig. 3.30

0 cm 1

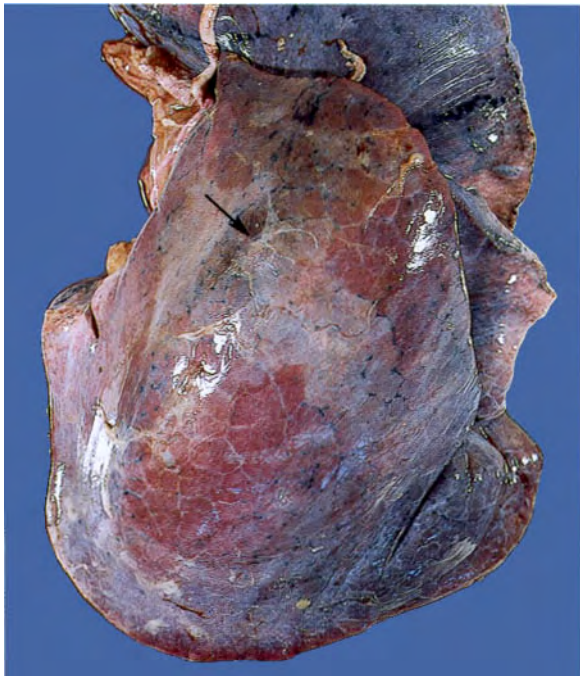


Fig. 3.31



Fig. 3.32

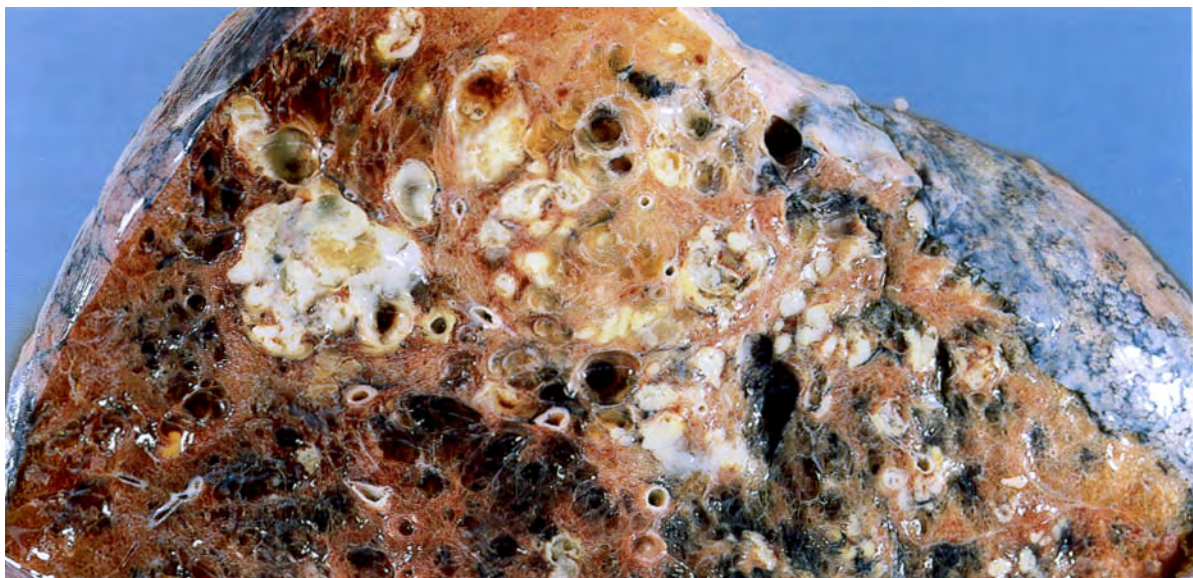


Fig. 3.33

Fig. 3.31 Lobar pneumonia. F/38. One lobe of the lung is consolidated and its pleural surface is covered with a fibrinous pleurisy. The remainder of the lung is relatively unaffected. Patients with lobar pneumonia have less dyspnoea than those with bronchopneumonia, but because of the pleuritic reaction they have chest pain during respiration and with coughing.

Fig. 3.32 Cut surface of lobar pneumonia. M/71. This lung is from another patient but shows that the consolidation is localized to one lobe.

Fig. 3.33 Confluent bronchopneumonia. F/69. As distinct from lobar pneumonia, bronchopneumonia is focal and involves many areas of the lung. The focal collections of pus may become confluent, giving rise to abscesses as demonstrated here. There is no pleural reaction associated with this type of pneumonia. The lung itself is emphysematous.

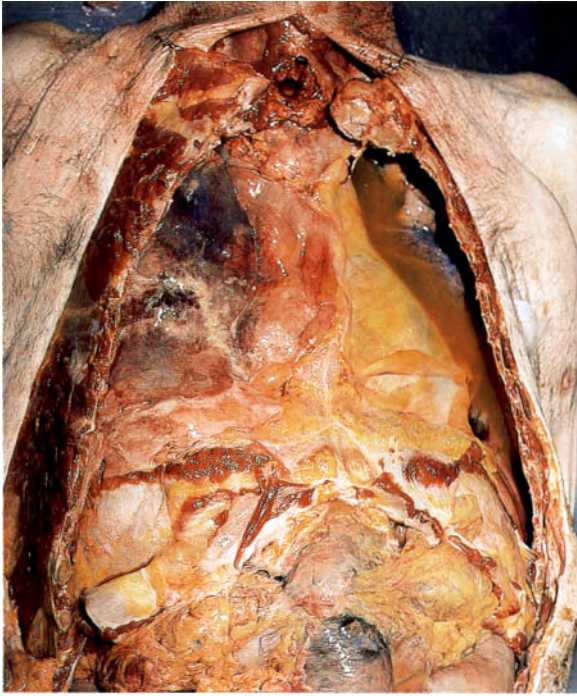


Fig. 3.34

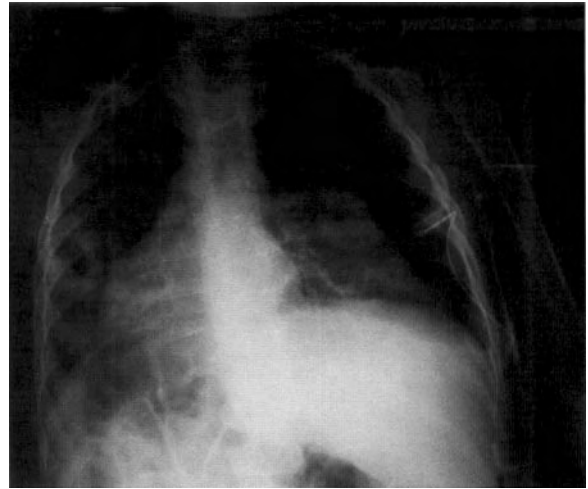


Fig. 3.35a

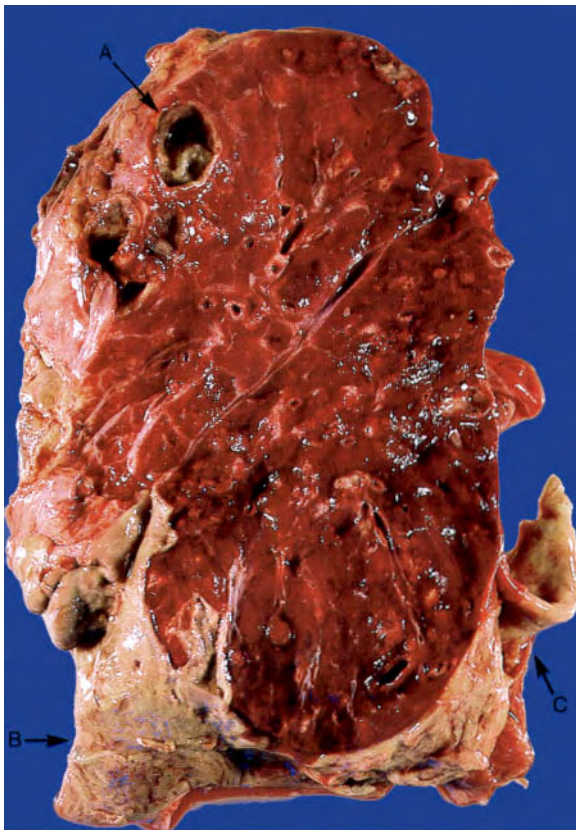


Fig. 3.35

Fig. 3.34 Right-sided empyema and left-sided pleural effusion. M/68. The cream-coloured pus can be seen on the anterior surface of the right lung. The fluid in the left pleural cavity is blood tinged.

Fig. 3.35 Left lung empyema and lung abscesses. M/11. This was a complication of staphylococcal pneumonia. Abscesses are present in the upper lobe (arrow A). There is a large amount of pus covering the surface of the lower lobe (arrow B). The visceral pleura is thickened and, posteriorly, some thickened parietal pleura is adherent to it (arrow C).

Fig. 3.35a Chest X-ray. F/3. Staphylococcal pneumonia with multiple abscesses. An abscess in the left lung has ruptured, causing a pneumothorax and collapse of the lung. Empyema usually results from contamination of the pleural cavity. The pleural surface of the collapsed lung is clearly seen.

Fig. 3.36 Toruloma (cryptococcal infection causing a mass lesion). M/47. Lobectomy specimen. The lobectomy was performed because an asymptomatic opacity was found on a routine chest X-ray. The cut surface of the lesion is grey in colour and has a rather mucoid appearance. This fungal (yeast) infection may occur in patients who have no immunological deficiency, as well as in those who do.

Fig. 3.37 Miliary torulosis of the lung. F/45. Multiple, yellowish nodules were present throughout both lungs.

Fig. 3.38 Aspergilloma. M/52. The upper lobe of the lung is replaced by a mass of grey tissue. *Aspergillus* may cause pneumonia which has no distinguishing macroscopic features, but when it forms a large mass like this it is usually referred to as an aspergilloma. The *Aspergillus* fungus often colonizes lung cavities, forming 'fungal balls' within them.

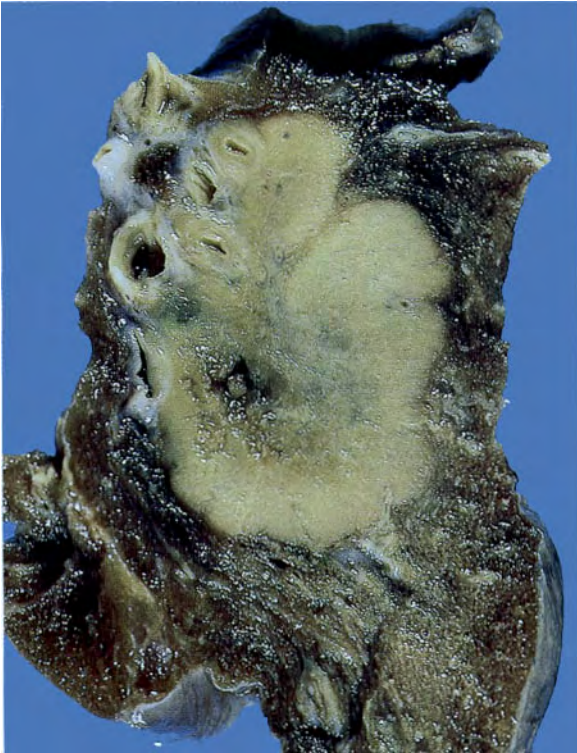


Fig. 3.36



Fig. 3.37



Fig. 3.38



Fig. 3.39

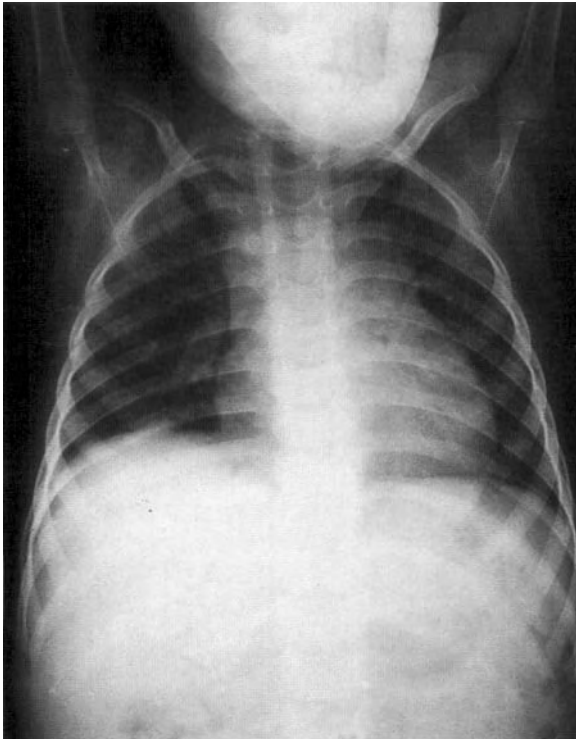


Fig. 3.40



Fig. 3.41



Fig. 3.42

Fig. 3.39 Miliary tuberculosis of the lung with involvement of the mediastinal lymph nodes. F/6. The miliary tubercles appear as yellow subpleural spots. The enlarged mediastinal lymph nodes show the typical caseous necrosis of tuberculous lymphadenopathy.

Fig. 3.40 Chest X-ray of the patient from Figure 3.39, showing a widened mediastinum caused by the tuberculous lymphadenopathy.

Fig. 3.41 Vertical section of the left lung and mediastinum from Figure 3.39. This shows multiple creamy nodules – the miliary tubercles – which were present throughout both lungs. There is also a large, round white focus of tuberculous granulation tissue in the left upper lobe, just beneath the pleura. This has the appearance of what is called a Ghon focus of primary tuberculosis. The child was moribund on admission and died soon afterwards.

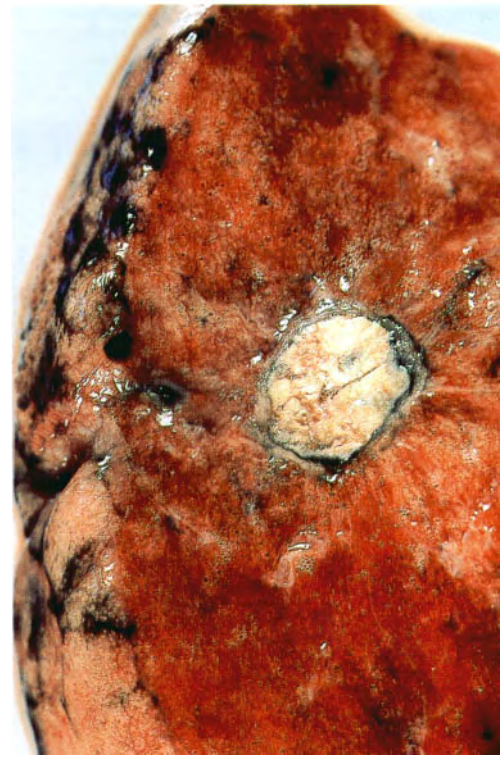


Fig. 3.43

Fig. 3.42 Pulmonary tuberculosis. M/72. The pathology is almost entirely confined to the upper lobe, particularly the apex. There is pneumonic consolidation, together with cavity formation. There is also a minor degree of emphysema present. This is the so-called active type of pulmonary tuberculosis. In many countries tuberculosis has been virtually eradicated by public health measures and effective treatment. However, its prevalence is increasing in countries which cannot afford these measures.

Fig. 3.43 Old, healed, calcified tuberculous lesion in the lung. F/70. This patient had been followed for many years with serial chest X-rays. The lesion had not changed in size, and repeated sputum examinations were negative for acid-fast bacilli.



Fig. 3.44



Fig. 3.45



Fig. 3.46



Fig. 3.47

Fig. 3.44 Miliary tuberculosis. Liver from the patient in Figure 3.39, showing miliary tubercles throughout both lobes. These appear as tiny yellow spots beneath the capsule.

Fig. 3.45 Tuberculous ascites. M/2. In communities in which tuberculosis is common, ascites is a common presentation.

Fig. 3.46 Tuberculous lymphadenopathy. M/14. The boy is emaciated, as is usual with patients with disseminated

tuberculosis. Some of the cervical lymph nodes are enlarged and one of them is discharging through the skin. Cervical lymphadenopathy is a common presentation in communities with a high incidence of tuberculosis.

Fig. 3.47 Tuberculous lymph node. M/24. The cut surface of the node shows that its enlargement is due to the presence of many areas of caseous necrosis.



Fig. 3.48



Fig. 3.49

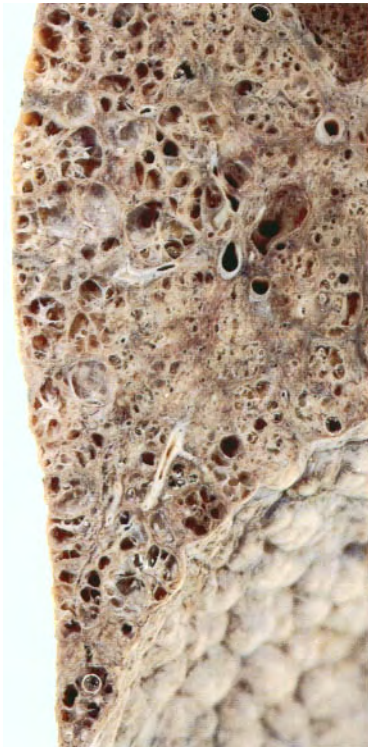


Fig. 3.50



Fig. 3.51

Fig. 3.48 Paraffinoma in the right lower lobe. M/81. There is a wedge-shaped solid black mass in the posterior basal segment of the right lower lobe. Large amounts of oil can be seen glistening on its cut surface. The patient was in the habit of taking a dose of paraffin oil each evening as a laxative. The paraffinoma resulted from small amounts of oil being regurgitated and inhaled during sleep.

Fig. 3.49 Hydatid cyst of the right lung. M/8. The white, laminated membrane of the parasite is present within the capsule of granulation tissue formed by the host as a response to the hydatid cyst – a foreign body reaction. This child came from a sheep-raising part of Australia.

Fig. 3.50 Honeycomb lung. M/63. The patient had interstitial pulmonary fibrosis, the exact cause of which was not determined.

Fig. 3.51 Subpleural rheumatoid nodule in the lung. M/78. The patient had rheumatoid arthritis for many years and the lung showed diffuse interstitial fibrosis.



Fig. 3.52

0 cm 5



Fig. 3.53

Fig. 3.52 Anthracosis – coal miner's lung. M/70. The lung shows extensive deposition of black carbon pigment. In the midportion the lung has become a solid, black shrunken mass. This condition is sometimes referred to as progressive massive fibrosis. The patient had been an underground coal miner for most of his life.

Fig. 3.53 Mixed pneumoconiosis. M/77. There is a thick, white pleural plaque attached to the posterior visceral pleura. This indicates exposure to asbestos. The lung shows a heavy deposition of carbon pigment, together with some emphysema. This man had worked in an electric power station shovelling coal for about 20 years. In that occupation he would have been exposed to asbestos lagging of pipes, as well as to the coal dust.

Fig. 3.54 Silicosis. M/69. Multiple silicotic nodules can be seen under the pleura. This man had worked as a miner for most of his life.



Fig. 3.54



Fig. 3.55

Fig 3.55 Malignant thymoma. F/1. The mediastinum is filled by a lobulated, irregular mass of creamy tissue. It has extended over the pericardium and caused some compression of the left lung.



Fig. 3.56

0 cm 1

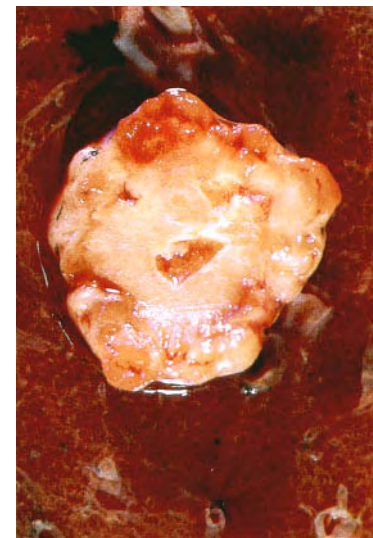


Fig. 3.57

Fig 3.56 Carcinoid tumour of the lung. M/50. Lobectomy specimen. The cream-coloured, well circumscribed carcinoid tumour (arrow) has arisen within the bronchus and caused obstruction distally. The extent of the bronchiectasis caused by the tumour indicates its slow rate of growth.

Fig. 3.57 Benign hamartoma of the lung (adenochondroma). F/61. There is a well circumscribed, lobulated and hard nodule in the lung. An incidental postmortem finding. These lesions are often excised surgically as treatment of a 'coin' lesion discovered by chest X-ray.



Fig. 3.58

Fig 3.58 Bronchogenic carcinoma. M/45. Right lung viewed from behind. The tumour has arisen from the right main bronchus and there are secondaries in the mediastinal lymph nodes and the pleura. In the middle and lower lobes there is tumour spreading along the peribronchial lymphatics (arrow), giving a cream 'worm-like' appearance.



Fig. 3.59

Fig. 3.59 Obstruction of the superior vena cava by a primary lung cancer. M/51. This caused gross swelling of the neck, resulting in respiratory obstruction. The patient was having radiotherapy at the time this photograph was taken, but died a few days later.

Fig. 3.60 Postmortem examination on the patient in Figure 3.59 shows the lung cancer obstructing the superior vena cava and causing dilatation of the veins draining into it (arrow).

Fig. 3.61 Malignant pericarditis. The vascular congestion of the neck was exacerbated by the presence of secondary tumour in the myocardium and pericardium. Same patient as in Figure 3.59.



Fig. 3.60



Fig. 3.61

Fig. 3.62 Left-sided pleural mesothelioma. M/50. The left lung is encased in thick, white, hard tumour tissue and there is secondary tumour in the right lung and in the liver. The patient had been working in an open-cut asbestos mine.

Fig. 3.63 Mesothelioma causing constrictive pericarditis. M/59. The heart has been cut across to show that the pericardial cavity has been completely obliterated by dense, white tissue which was part of a pleural mesothelioma. The patient had worked in an asbestos mine.



Fig. 3.62

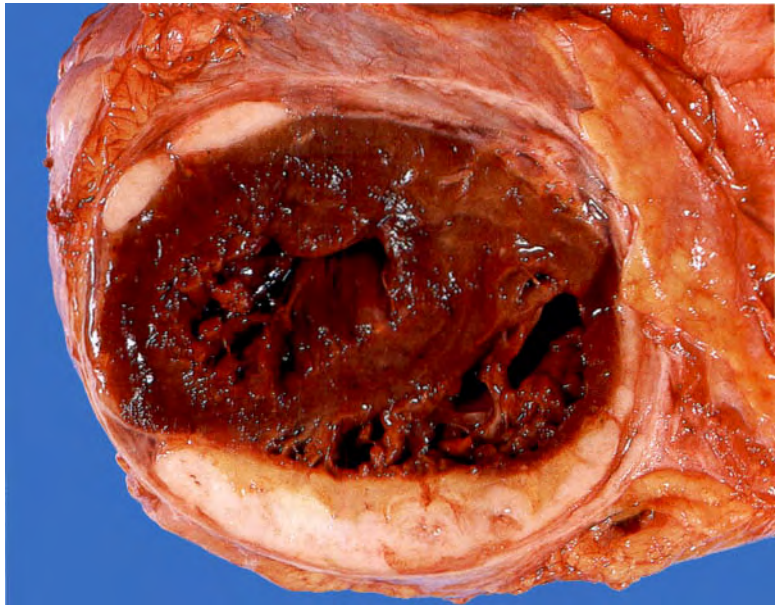


Fig. 3.63



Fig. 3.64

Fig. 3.64 Pleural mesothelioma. M/67. This vertical slice of the right lung shows the manner in which a pleural mesothelioma causes thickening of the pleura and encases the whole lung and mediastinum.

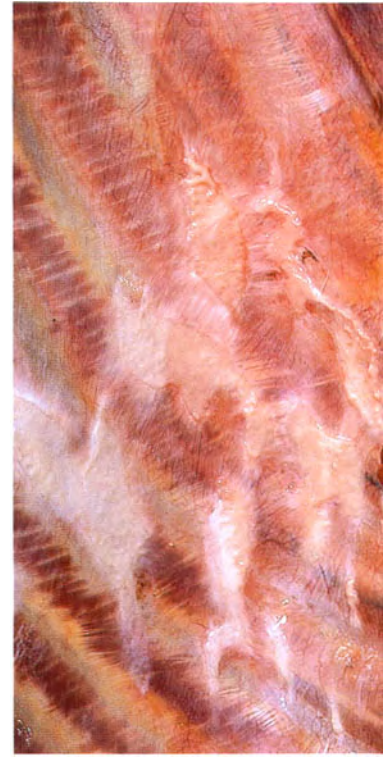


Fig. 3.65

Fig. 3.65 Pleural plaques. The left parietal pleura of the patient in Figure 3.64 showing fibrous plaques running in the line of the ribs. Pleural plaques indicate previous exposure to asbestos, but they may occur without causing clinical symptoms, and without necessarily being associated with any other manifestations of asbestosis.



Fig. 3.66



Fig. 3.67

Fig. 3.66 Bronchoalveolar carcinoma (alveolar cell carcinoma) of the lung. F/72. This is a variety of adenocarcinoma of the lung which accounts for about 5% of lung cancers. It is characterized by the fact that the well differentiated cuboidal tumour cells spread along the intact alveolar walls without causing destruction of the lung architecture. The round tumour nodules may involve a segment of a lobe, a whole lobe, or almost the whole lung, as in this case.

Fig. 3.67 Secondary carcinoma of the lung. F/59. There are a number of rounded nodules of tumour through the lung. The primary was a breast carcinoma.

**ALIMENTARY
SYSTEM**



Fig. 4.1



Fig. 4.2



Fig. 4.3

Fig. 4.1 Haemangioma of the buccal mucosa. F/20.

Fig. 4.2 Congenital epulis. F/Neonate. Microscopically this was a granular cell tumour.

Fig. 4.3 Mucus retention cyst of a minor salivary gland on the under surface of the tongue. M/40. This cyst developed within a few hours, persisted for 4 days, then ruptured.



Fig. 4.4



Fig. 4.5



Fig. 4.6

Fig. 4.4 Macroglossia. F/2. This is the normal resting position of her mouth.

Fig. 4.5 Intraoperative photograph of the same case as in Figure 4.4. The enlargement of the tongue has been caused by a lymphangioma. The variably sized lymph channels have produced multiple nodules on the surface of the tongue.

Fig. 4.6 Candida infection of the tongue. M/70. The patient died from malignant lymphoma, so this was an opportunistic infection.



Fig. 4.7



Fig. 4.8



Fig. 4.9

Fig. 4.7 Squamous cell carcinoma of the base of the tongue. F/60.

Fig. 4.8 Squamous cell carcinoma of the lower lip. M/60.

Fig. 4.9 Squamous cell carcinoma of the floor of the mouth. F/77. This cancer was removed surgically and the patient lived for another 10 years before dying of an unrelated condition.



Fig. 4.10



Fig. 4.11

0 cm 1

Fig. 4.10 Squamous cell carcinoma of the buccal mucosa. Indian M/40 from Bombay. Cancer of this type is very common in all cultures where betel nut is chewed.

Fig. 4.11 Calculus impacted in the duct of a submandibular gland. M/40. Surgically removed to relieve the symptoms of pain and swelling during salivation.

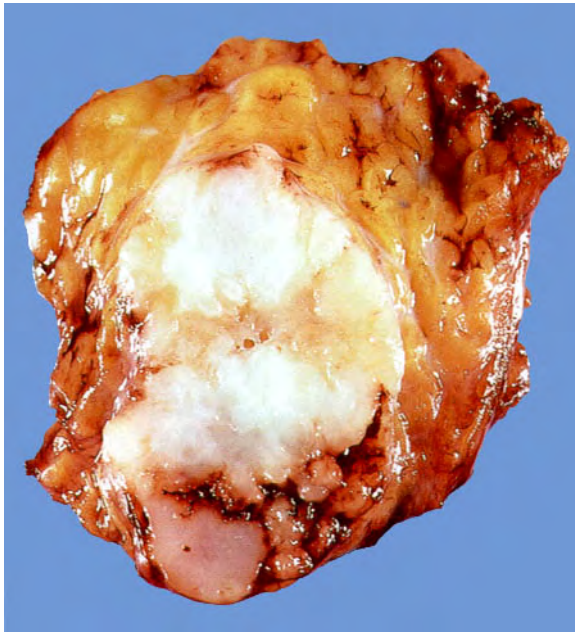


Fig. 4.12

0 cm 1

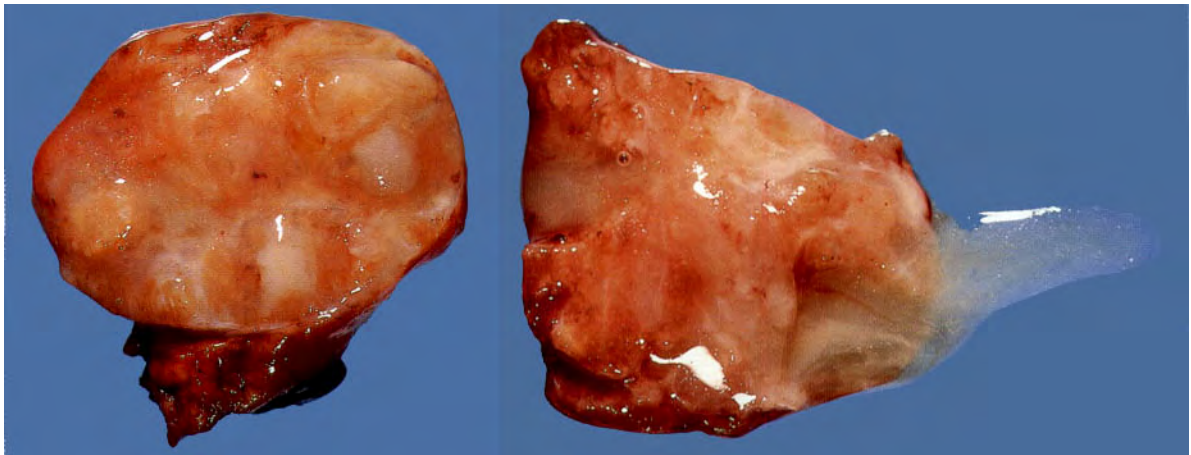


Fig. 4.13

0 cm 1

Fig. 4.12 Pleomorphic adenoma of parotid gland. F/52. The multilobulated appearance of this tumour is shown. It must be removed together with some surrounding parotid gland, or else some of the irregular projections around its margins will be left behind and the tumour will recur.

Fig. 4.13 Warthin's tumour (adenolymphoma) of the parotid gland. M/63. These tumours are multicystic. The cysts are filled with mucus, as indicated. They are benign tumours and are the second most frequent tumour of the parotid gland, following pleomorphic adenoma.

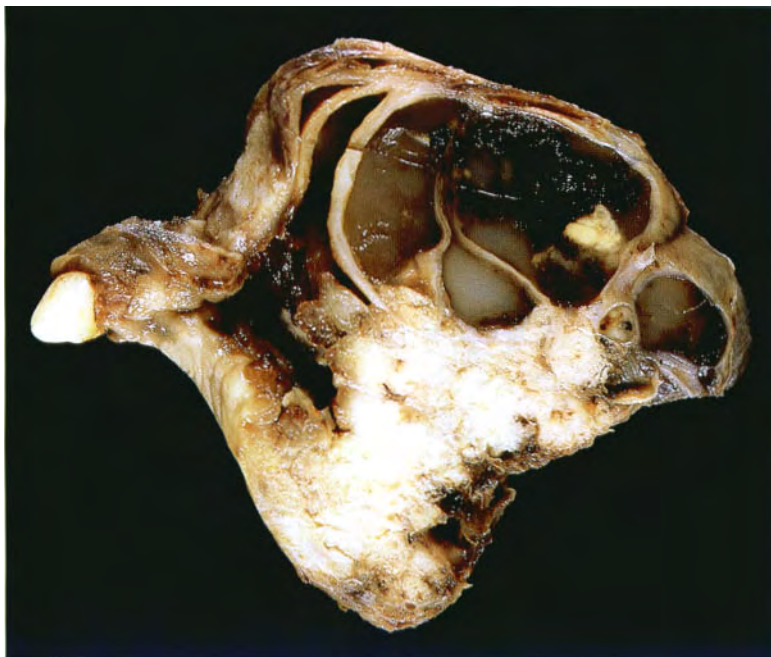


Fig. 4.14

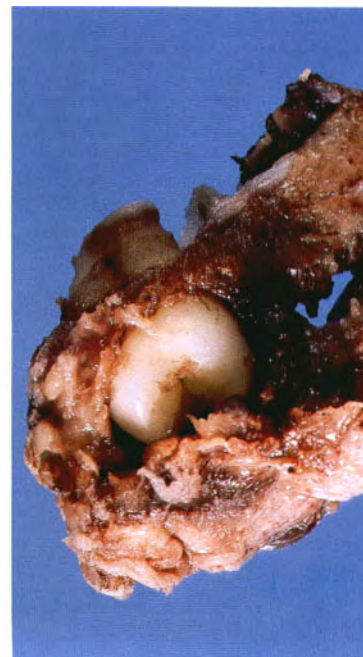


Fig. 4.15



Fig. 4.16

Fig. 4.14 Ameloblastoma of maxilla. F/30. A benign, multiloculated neoplasm within the maxilla arising from the enamel organ.

Fig. 4.15 Dentigerous cyst, shelled out from the mandible. M/14. The cyst contains an unerupted tooth.

Fig. 4.16 X-ray. Dentigerous cyst in the ramus of the right mandible. The unerupted tooth is clearly seen.



Fig. 4.17

0 cm 1



Fig. 4.18

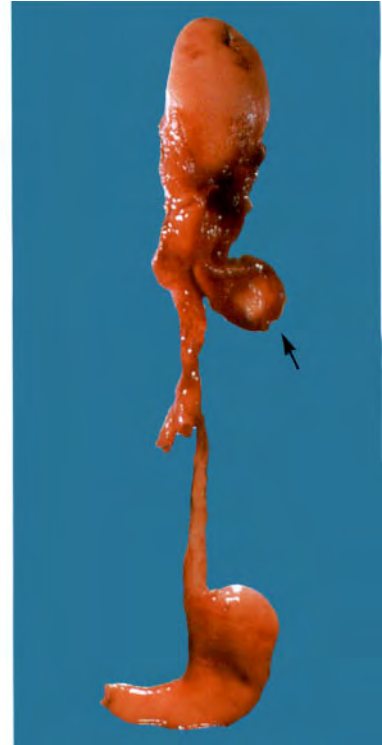


Fig. 4.19



Fig. 4.20

Fig. 4.17 Tracheo-oesophageal fistula. Newborn child. The upper end of the oesophagus terminates as a blind pouch.

Fig. 4.18 The lower half of the abnormality shown in Figure 4.17. The distal end of the oesophagus opens into the trachea just above the carina.

Fig. 4.19 This shows the entire abnormality, with a blindly ending upper oesophageal pouch (arrowed) and the lower part of the oesophagus opening into the trachea proximal to the carina. There are a number of different types of tracheo-oesophageal fistula. This one is the most common.

Fig. 4.20 Acute-on-chronic oesophagitis resulting from reflux associated with a hiatus hernia. F/70.

Fig. 4.21 Candida oesophagitis. M/50. The patient died from malignant lymphoma. The thick, greenish membrane is composed of *Candida* hyphae and purulent exudate.

Fig. 4.22 Pharyngeal diverticulum. M/73. This was removed surgically to relieve symptoms of dysphagia.

Fig. 4.23 Oesophageal varices. M/70. The patient died from the effects of alcoholic cirrhosis.

Fig. 4.24 Same specimen as Figure 4.23 transilluminated to accentuate the varices.



Fig. 4.21

0 cm 5



Fig. 4.22

0 cm 1



Fig. 4.23

0 cm 5



Fig. 4.24

0 cm 5



Fig. 4.25



Fig. 4.26



Fig. 4.27

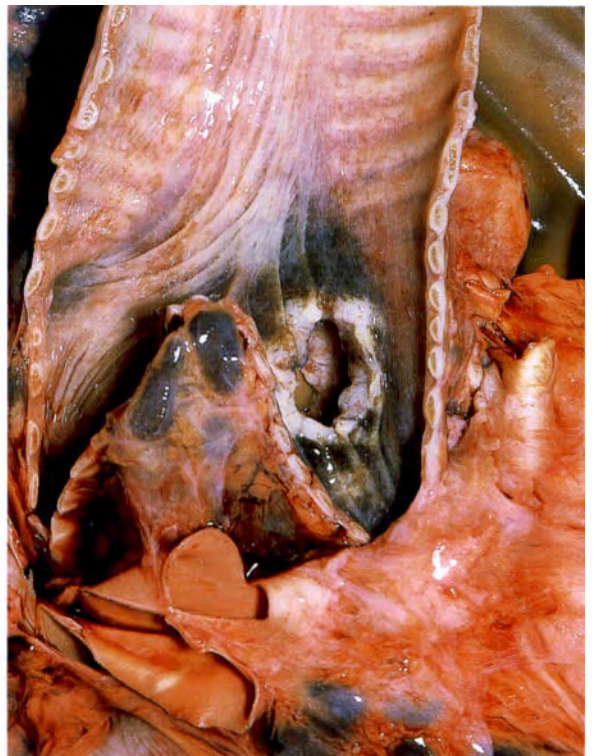


Fig. 4.28



Fig. 4.25

Fig. 4.25 Leiomyoma of the oesophagus. M/51. The mucosa over the tumour is intact.

Fig. 4.26 Squamous cell carcinoma of the lower third of the oesophagus. M/61. Note the heaped up, ulcerated lesion with an irregular edge. The oesophagus has been opened to display the tumour, which involves almost the whole circumference of the oesophagus. As the tumour grows it narrows the lumen, resulting in dysphagia, the presenting symptom of carcinoma of the oesophagus.

Fig. 4.27 Squamous cell carcinoma of the upper third of the oesophagus. M/63. Note the extensive ulceration in this tumour.

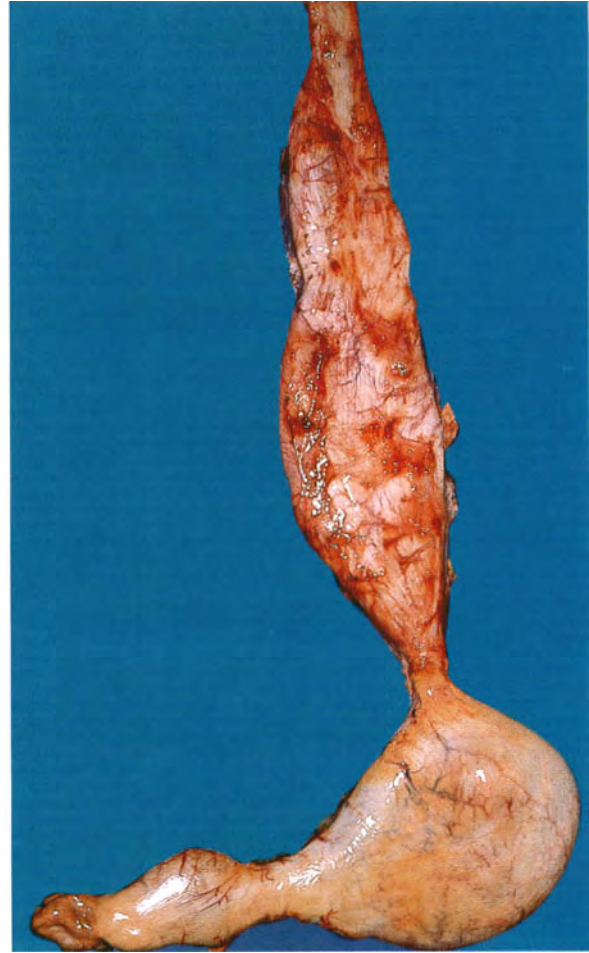


Fig. 4.28

Fig. 4.28 Squamous cell carcinoma of the middle third of the oesophagus (viewed from the front) eroding into the left main bronchus. M/58.

Fig. 4.29 Oesophageal stricture. F/51. Surgical specimen. The oesophageal wall is fibrotic and the lumen is greatly reduced. This resulted from swallowing caustic soda with suicidal intent.

Fig. 4.30 Megaoesophagus due to achalasia of the lower end. M/84. Every day for the 30 years before his death the patient had swallowed a mercury-filled rubber bougie to dilate the lower end of his oesophagus and relieve his symptoms of dysphagia. He had suffered from a number of episodes of aspiration pneumonia before the one that finally caused his death.

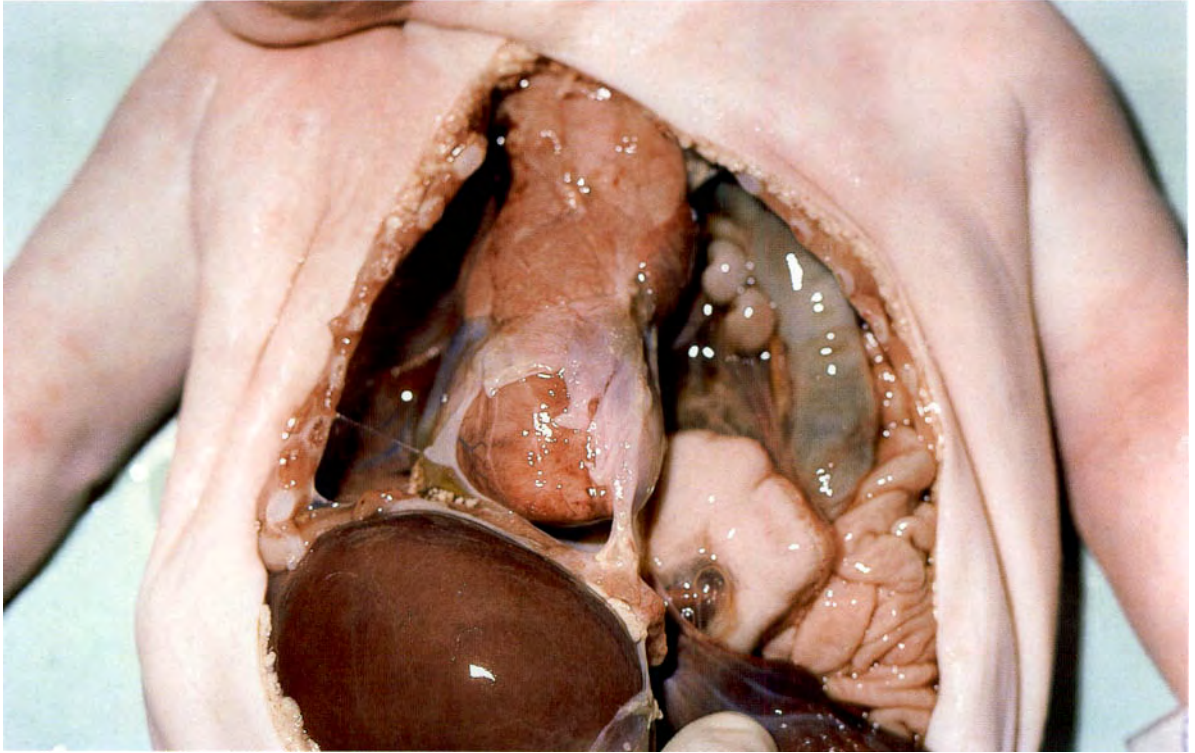


Fig. 4.31



Fig. 4.32

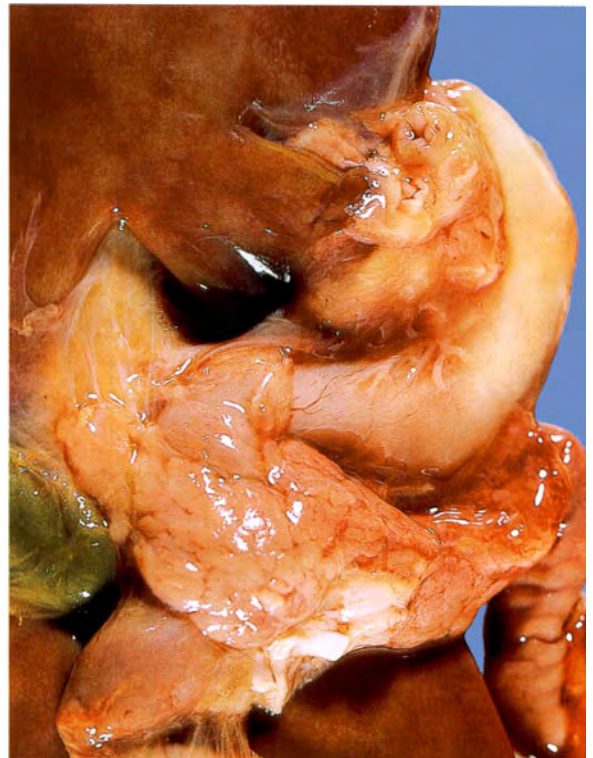


Fig. 4.33

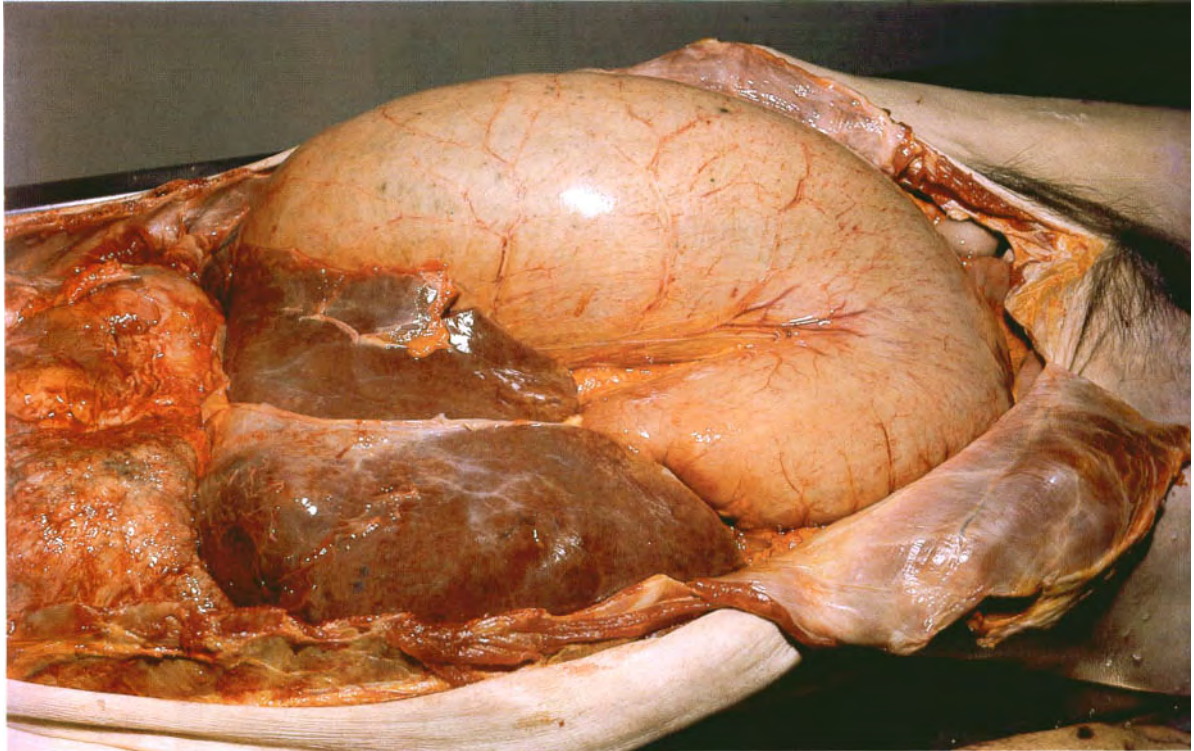


Fig. 4.34

Fig. 4.31 Left-sided congenital diaphragmatic hernia. M/neonate. Abdominal contents are present in the thorax. There is hypoplasia of the left lung and the mediastinum is pushed to the right. Death occurred shortly after delivery.

Fig. 4.32 Duodenal atresia. Neonatal death. The pylorus has been opened and ends blindly. The second part of the duodenum has been opened and terminates blindly at both ends.

Fig. 4.33 Annular pancreas. M/4 weeks. The head of the pancreas has wrapped around the first and second parts of the duodenum, causing pyloric obstruction.

Fig. 4.34 Acute dilatation of the stomach. F/60. This is a rare complication of trauma. The exact mechanism is not known. Suddenly the stomach dilates and is filled with fluid. It requires urgent diagnosis, gastric aspiration through a nasogastric tube, and fluid replacement to avoid the complication indicated in this photograph.

Fig. 4.35 Gastric diverticulum. F/71. Incidental postmortem finding.



Fig. 4.35

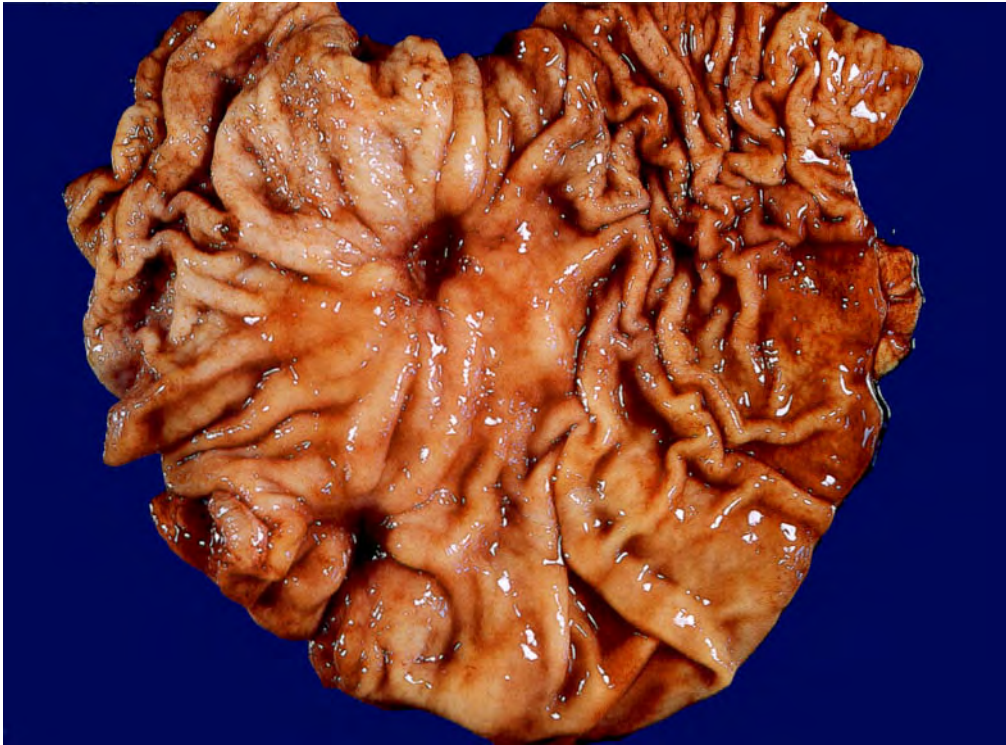


Fig. 4.36

0 cm 5

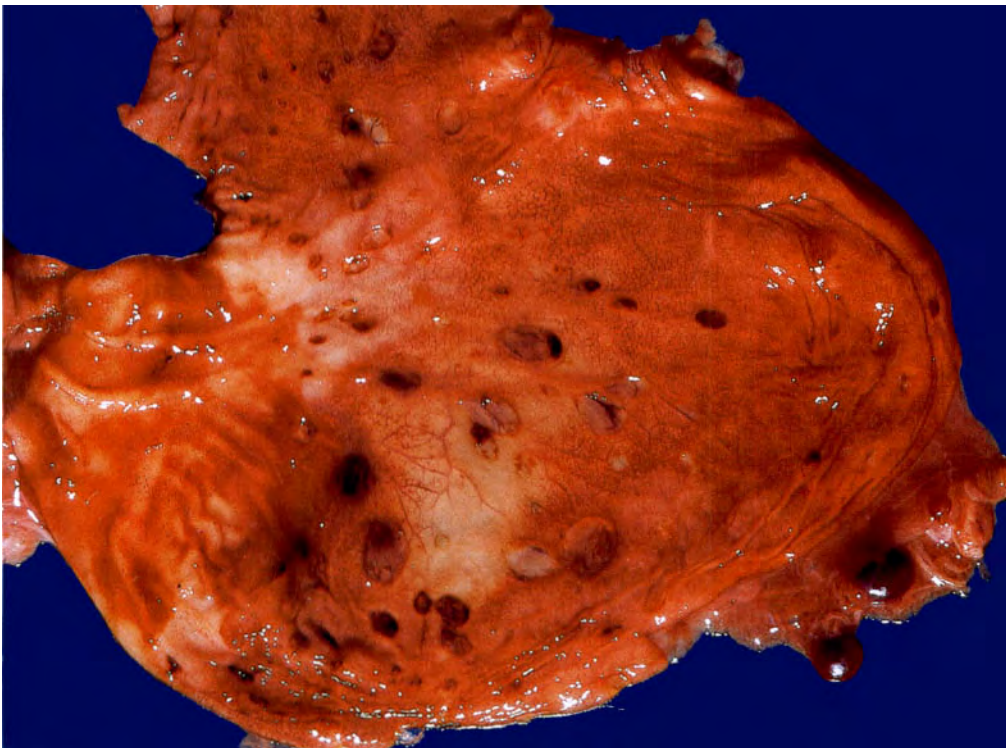


Fig. 4.37

0 cm 5



Fig. 4.38

Fig. 4.36 Chronic peptic ulcer. M/44. A partial gastrectomy was performed because of haematemesis. There was a bleeding artery in the base of the ulcer.

Fig. 4.37 Acute gastric erosions. M/78. These occurred just prior to death.

Fig. 4.38 Candida gastritis. F/11. This child died of aplastic anaemia. The dark green fungal membrane is adherent to the surfaces of the rugal folds. In the opened stomach this results in a linear pattern.

Fig. 4.39 Mallory-Weiss tear at the oesophagogastric junction. F/56. The patient died from a massive haematemesis resulting from this tear. A tear in the mucosa at this point characteristically follows an episode of severe vomiting, frequently associated with a bout of heavy drinking.

Fig. 4.39



Fig. 4.40



Fig. 4.41

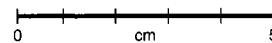


Fig. 4.40 Multiple benign adenomatous gastric polyps. M/75. Incidental postmortem finding.

Fig. 4.41 Giant rugal hypertrophy. M/65. Partial gastrectomy performed because a space-occupying lesion was seen on a barium meal examination and erroneously diagnosed as cancer. This patient was treated before the advent of flexible gastroscopes.

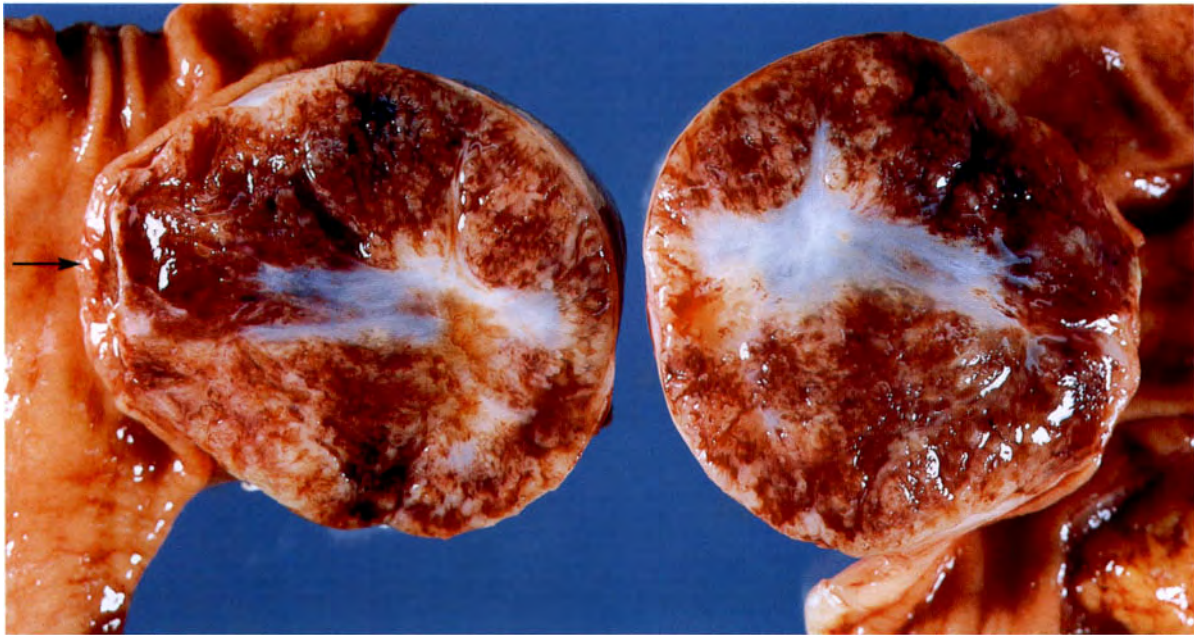


Fig. 4.42



Fig. 4.43

Fig. 4.42 Large leiomyoma of the stomach. F/40. This patient presented with haematemesis from mucosal ulceration on the surface of the tumour (arrow). This lesion characteristically presents with haematemesis. Endoscopic examination reveals a tumour protruding into the lumen of the stomach, and there is a small mucosal ulceration in the middle of the protrusion.

Fig. 4.43 Bezoar removed from the stomach. M/12. It is composed predominantly of hair and straw. This mentally defective child's usually placid behaviour was replaced by hypermania, which caused serious management problems for his carers. A lump was discovered in his upper abdomen. Laparotomy revealed this bezoar, which was removed. Postoperatively he returned to his usual placid self.



Fig. 4.44

0 cm 5

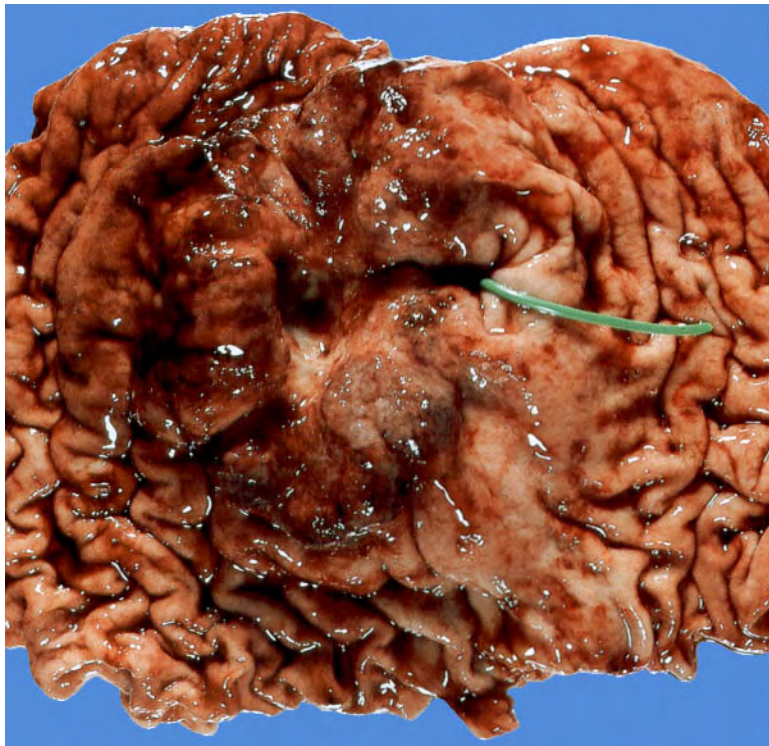


Fig. 4.45

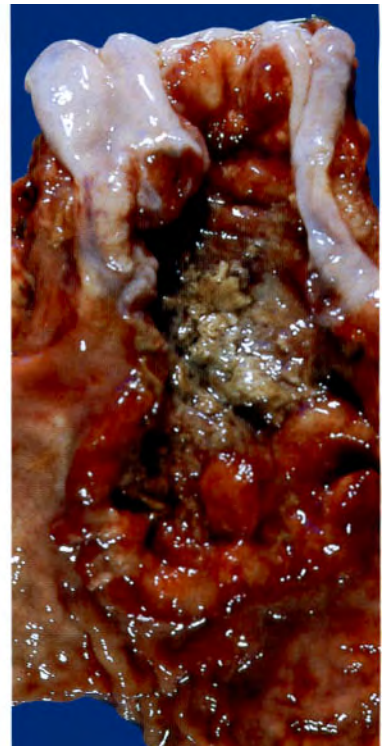


Fig. 4.46



Fig. 4.47

Fig. 4.44 Polypoid adenocarcinoma of the stomach. F/86. The patient was treated by partial gastrectomy.

Fig. 4.45 Ulcerated adenocarcinoma of stomach. M/32. The patient was treated by partial gastrectomy. The probe is in the pylorus, which was partially obstructed.

Fig. 4.46 Ulcerating adenocarcinoma at the oesophagogastric junction. M/50. The tumour was locally resected.

Fig. 4.47 Linitis plastica. F/68. In this type of adenocarcinoma of the stomach the tumour cells infiltrate beneath the mucosa and produce marked fibrosis and thickening of the stomach wall.

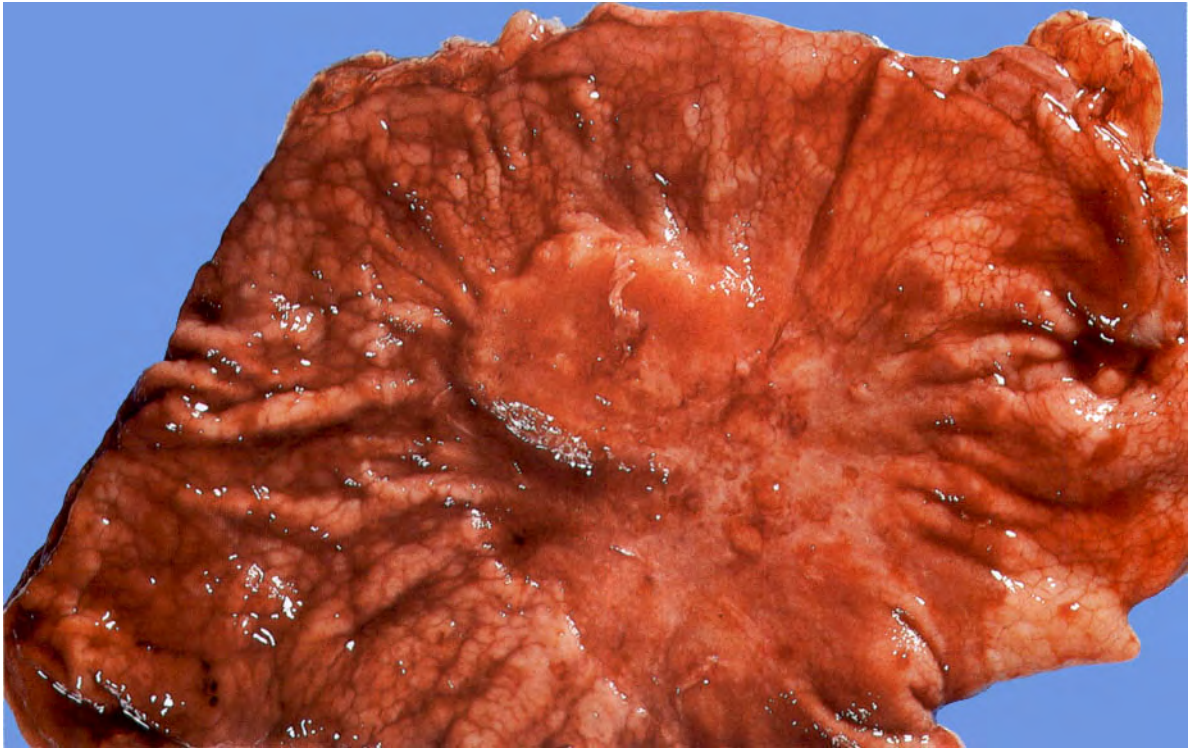


Fig. 4.48

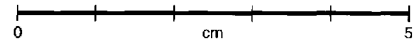


Fig. 4.49



Fig. 4.50

× 16



Fig. 4.51

× 16

Fig. 4.48 Early gastric cancer (superficial adenocarcinoma of the stomach). F/38. The patient was treated by partial gastrectomy. Note the firm, plateau-like area on the stomach mucosa, with loss of the rugal folds. The abnormal area in such cases may be better seen by holding the specimen up to the light. This patient had rather vague, non-specific upper abdominal symptoms, and diagnosis was made by gastroscopy and biopsy.

Fig. 4.49 Malignant lymphoma of the stomach. M/60. Note the multiple areas of creamy tumour on the stomach mucosa. The mucosa is ulcerated over some of the deposits.

Fig. 4.50 Normal small intestinal mucosa. F/66. This tissue was obtained by means of a small bowel biopsy capsule and was examined under a dissecting microscope. The intestinal villi appear as fingers, leaves and ridges. This is a very much bigger piece of tissue than that obtained by present-day fiberoptic flexible endoscopes.

Fig. 4.51 Flat mucosa (total villus atrophy) in coeliac disease. F/31. The patient had had lifelong mild diarrhoea. The jejunal biopsy was performed because her child was diagnosed as having malabsorption syndrome caused by coeliac disease. The atrophic mucosal pattern is well seen in this large, capsule biopsy. Using present-day fiberoptic flexible endoscopes, the flat mucosa of coeliac disease can be visualized directly (see Figure 4.51a).

Fig. 4.51a Coeliac disease. The flat mucosal pattern of the duodenum seen through a gastroscope.



Fig. 4.51a

Fig. 4.52 Strangulated right inguinal hernia. M/2 months.

Fig. 4.53 The strangulated hernia from Figure 4.52 was reduced through an incision in the right iliac fossa and the contents were withdrawn from the scrotum. A loop of necrotic bowel can be seen, and this was resected.

Fig. 4.54 Richter's hernia. F/82. In this type of hernia a portion of the bowel wall slips into the hernial orifice, frequently femoral, giving rise to intermittent and incomplete intestinal obstruction. This woman died from the effects of complete obstruction when the hernia became impacted in the femoral hernial orifice. The diagnosis was not made during life.



Fig. 4.52



Fig. 4.53

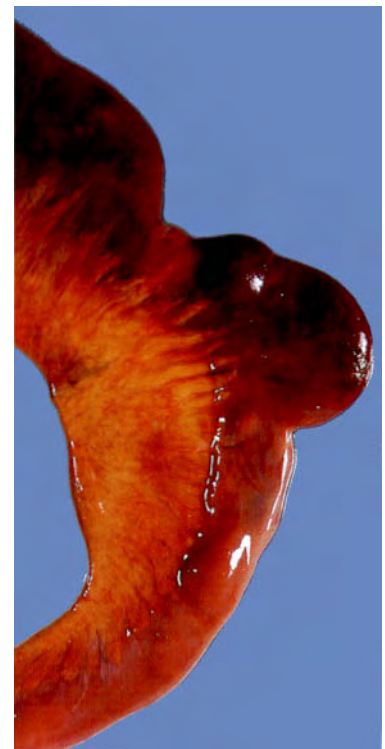


Fig. 4.54

0 cm 5



Fig. 4.55

0 cm 1

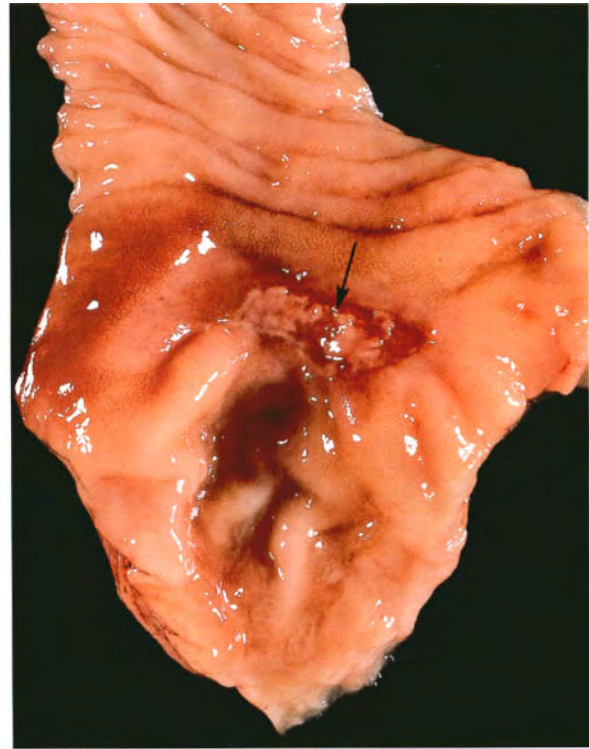


Fig. 4.56



Fig. 4.57

0 cm 5

Fig. 4.55 Meckel's diverticulum. M/3 weeks. The Meckel's diverticulum and the adjacent loop of small intestine had become incarcerated in an inguinal hernia and the necrotic bowel segment was resected. Note the serosal peritonitis affecting the small intestine on the left.

Fig. 4.56 Meckel's diverticulum with a bleeding peptic ulcer. M/25. The ulcer is present at the junction between the diverticulum and the adjoining ileal mucosa at the upper end of the specimen. His presenting symptoms were typical of this condition: sudden onset of abdominal pain, closely followed by the passage of bright red blood per rectum.

Fig. 4.57 Meckel's diverticulum. Acute inflammation. M/58. Symptoms of acute appendicitis. The patient had already had an appendectomy. Laparotomy revealed an acute Meckel's diverticulitis. The diverticulum was removed, together with a segment of terminal ileum. The mucosal surface of the diverticulum is red and inflamed. The serosal surface is covered by fibrinous exudate.



Fig. 4.58

Fig. 4.59



Fig. 4.58 Jejunal diverticula. M/76. An incidental postmortem finding. Note that the diverticula are on the mesenteric border of the bowel, whereas Meckel's diverticulum is on the antimesenteric border.

Fig. 4.59 Exomphalos. M/1 day. There is a defect in the abdominal wall at the umbilicus. The herniated bowel is covered by a thin membrane. Untreated, death occurs from infection when the membrane ruptures.

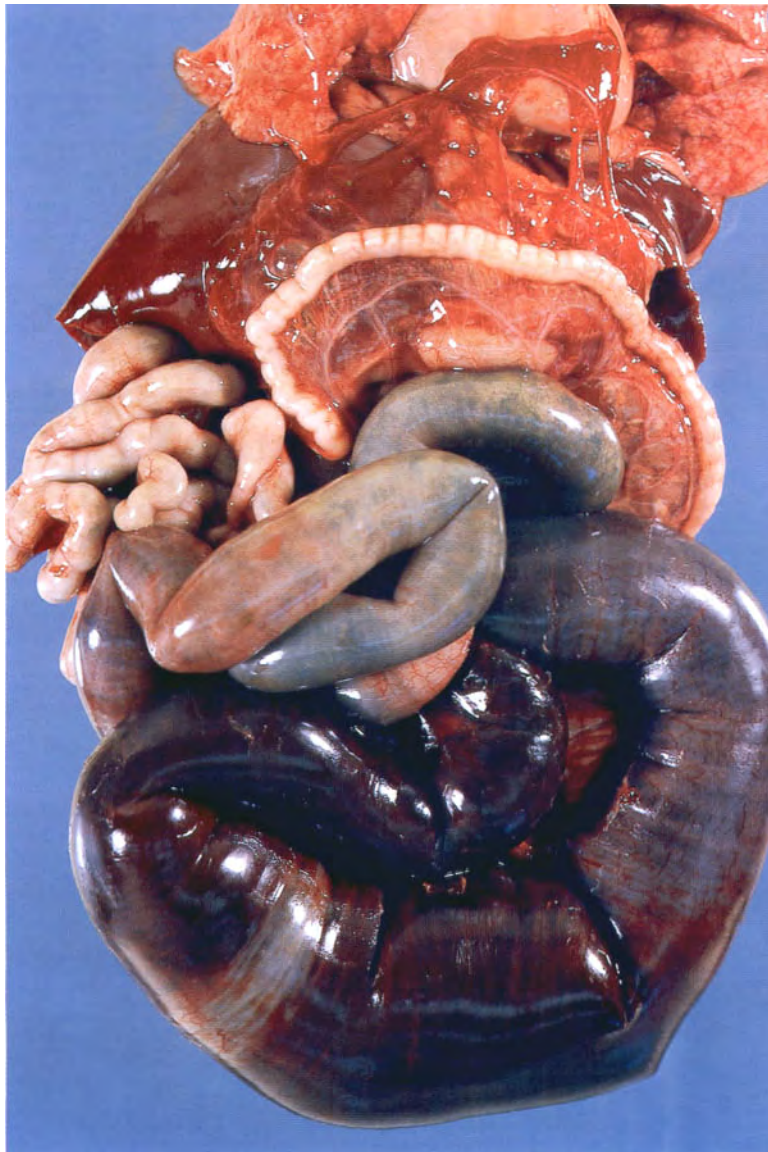


Fig. 4.60

Fig. 4.60 Volvulus of the small intestine. M/2 days. Most of the small intestine is gangrenous, resulting from twisting on its mesentery at the duodenojejunal junction.



Fig. 4.61

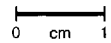


Fig. 4.62

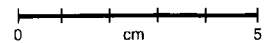


Fig. 4.61 Multiple areas of atresia in the jejunum. M/2 days. This child presented with intestinal obstruction, which was cured by resection of the atretic segment. The atresia consists of multiple small blindly ending segments of intestine.

Fig. 4.62 Meconium ileus. M/6 hours. The neonate presented with intestinal obstruction shortly after delivery. The small intestine is dilated and filled with green, sticky material. This condition represents the presentation of mucoviscidosis in the neonatal period. The segment of atresia is not related to the mucoviscidosis.



Fig. 4.63

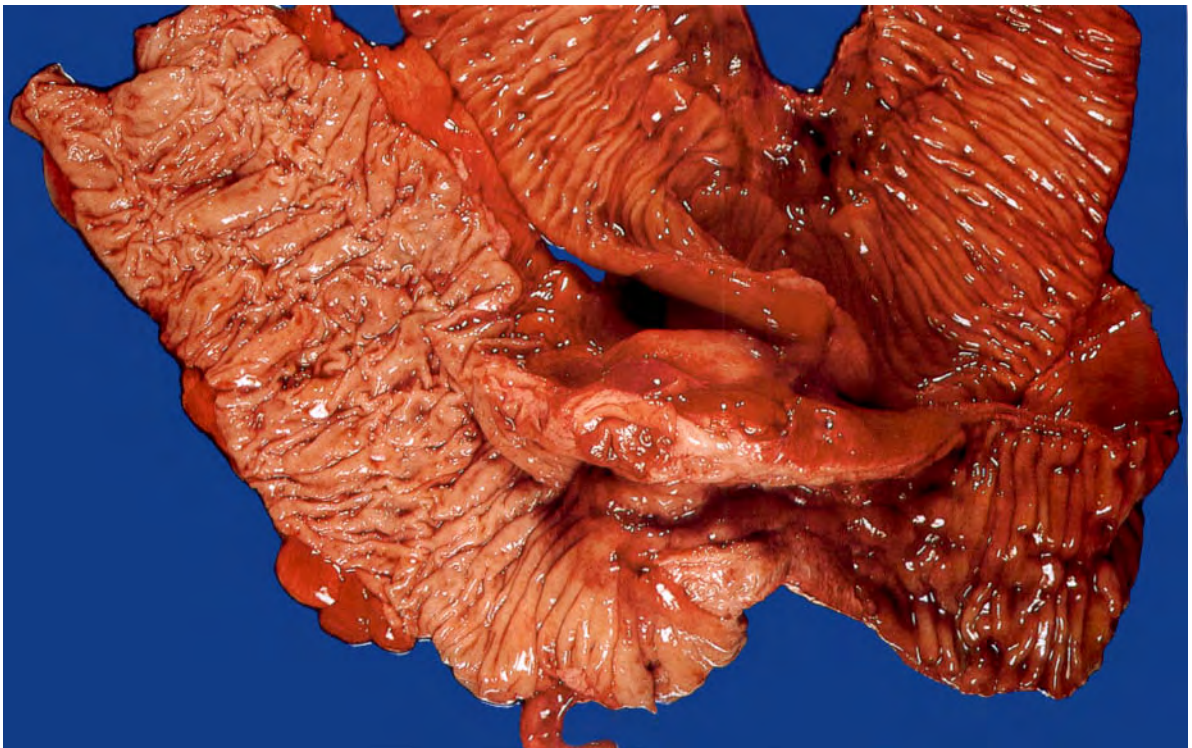


Fig. 4.64



Fig. 4.63

Fig. 4.63 Ischaemic necrosis of the small intestine. F/65. This was caused by thrombosis of the superior mesenteric artery (arrow). Postmortem finding.

Fig. 4.64 Crohn's disease of the terminal ileum. M/21. The patient presented with recurrent attacks of lower abdominal pain and vomiting for 6 weeks. A mass was palpable in the right iliac fossa. The surgical specimen shows terminal ileum with a thickened wall and thickening of its mucosal surface—the so-called 'cobble stone' appearance. An adjacent loop of ileum has become adherent to it and an ileo-ileal fistula is in the process of developing.



Fig. 4.65

Fig. 4.65 Typhoid. M/23. Postmortem specimen of small intestine. The Peyer's patches are prominent. There is ulceration and haemorrhage into most of them. The pathologist's finger identified the site of a perforation in the middle of the largest area of ulceration and haemorrhage.

Fig. 4.66 Tuberculosis. F/28. Postmortem specimen of small intestine. There are multiple oval ulcers running transversely across the bowel. The patient died from untreated disseminated tuberculosis.

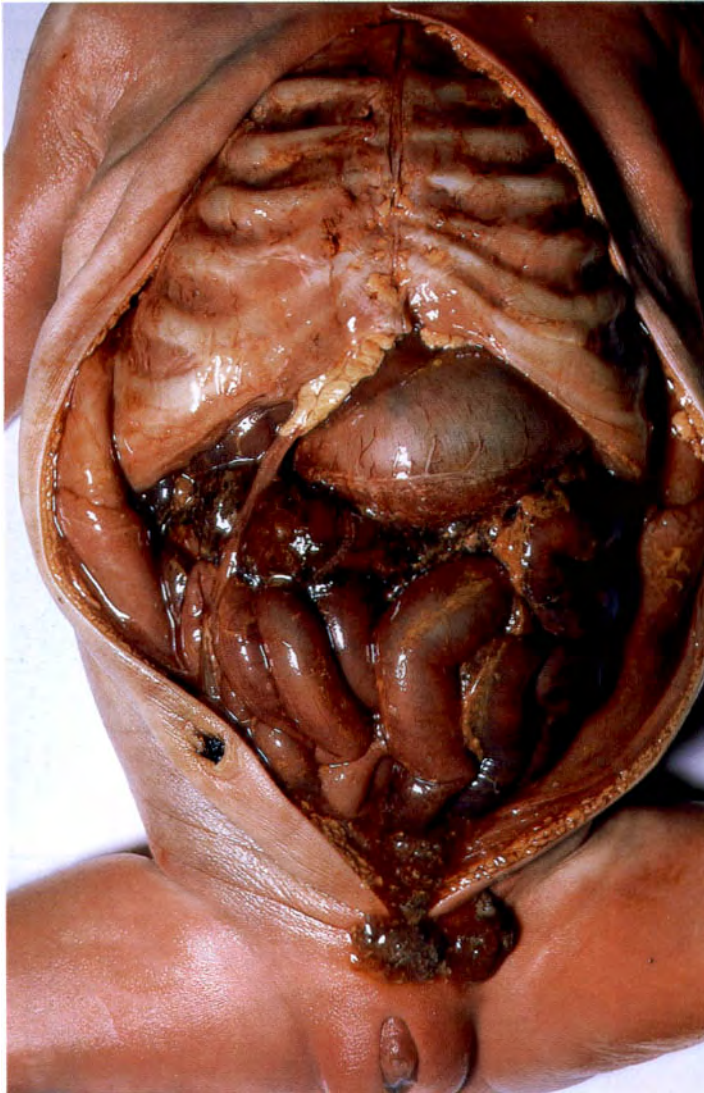


Fig. 4.67

Fig. 4.67 Acute peritonitis resulting from a small perforation in the caecum. Newborn child with **neonatal necrotizing enterocolitis**. Note the dilated bowel with a dull red serosal surface, on which there is a fibrinous exudate.

Fig. 4.68 Radiation enteritis. M/83. The patient had a carcinoma of the prostate which had been treated by radiotherapy. Some time after this he developed symptoms of intestinal obstruction, and this loop of small intestine which had become incarcerated in the pelvis was resected. The mucosa is ulcerated and lined by a greenish-yellow purulent membrane.



Fig. 4.68

Fig. 4.69 Intussusception causing acute intestinal obstruction. M/33. The apex of the intussusceptum consists of an adenocarcinoma.

Fig. 4.70 Acute obstruction of the ileum. F/80. Examination of the resected bowel showed that the obstruction was caused by a partially dissolved potassium tablet. The bowel on the left is dilated proximal to the obstruction.

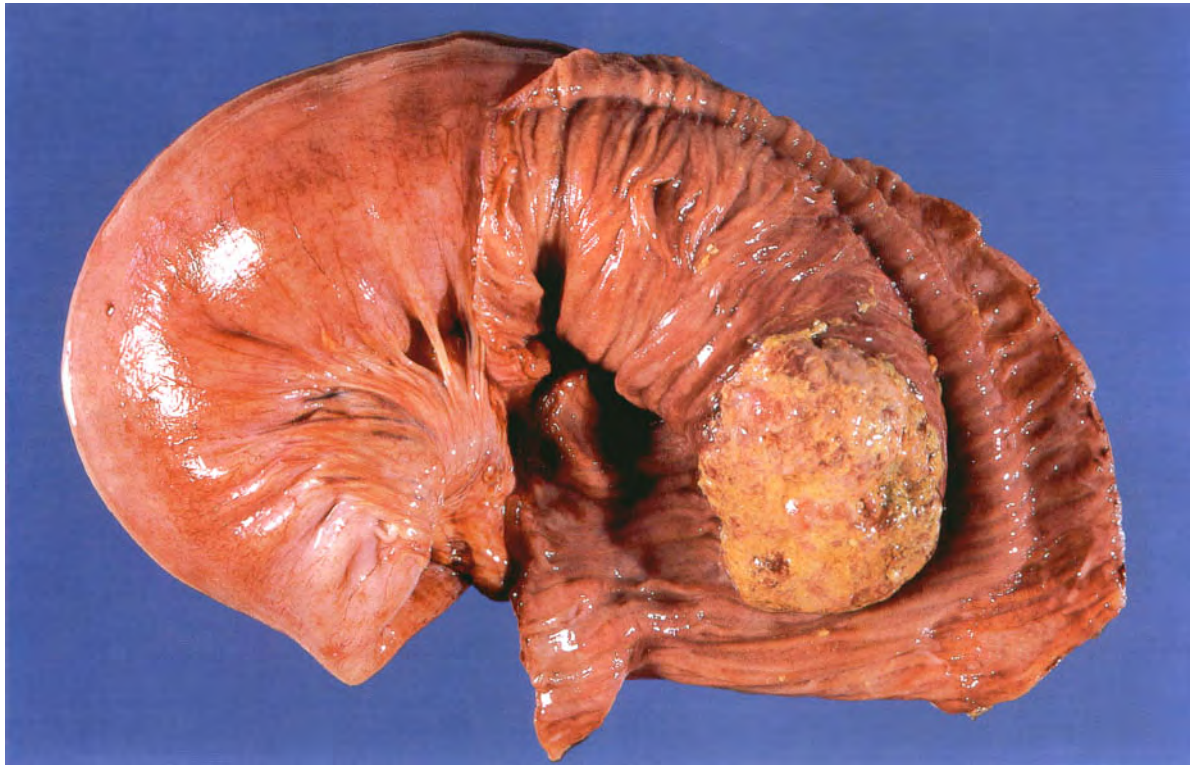


Fig. 4.69

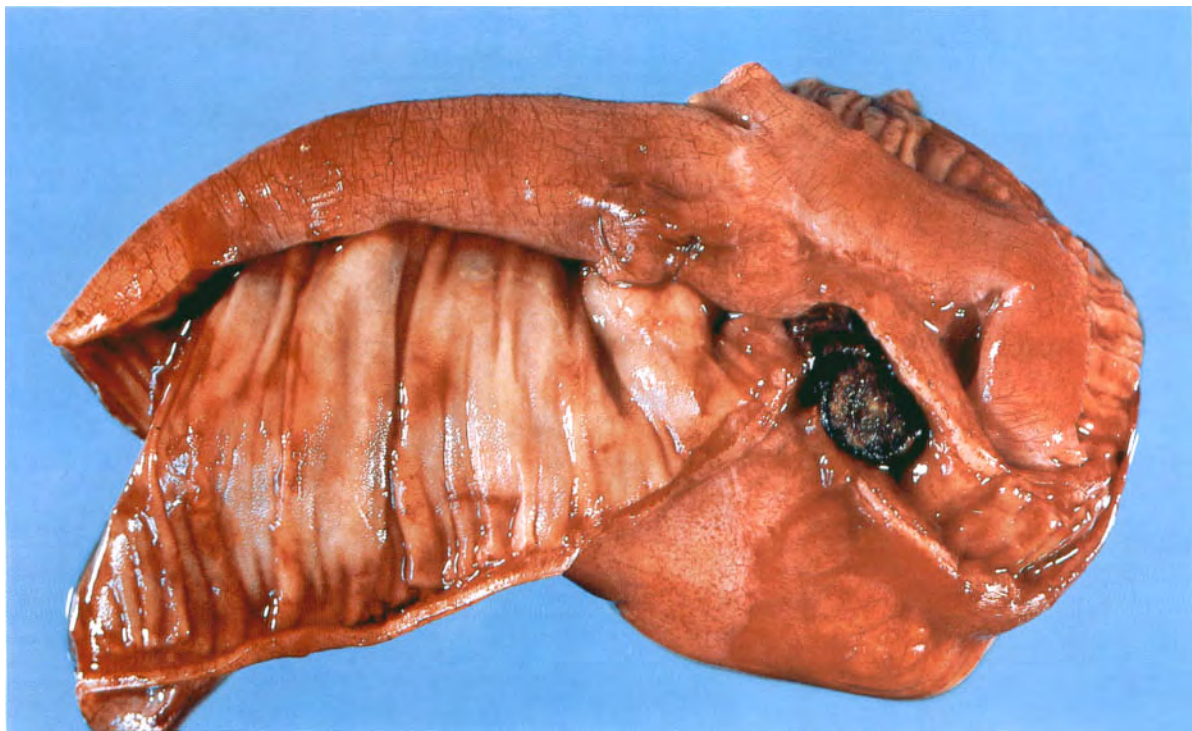


Fig. 4.70

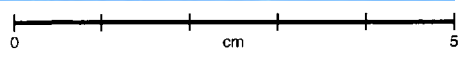




Fig. 4.71

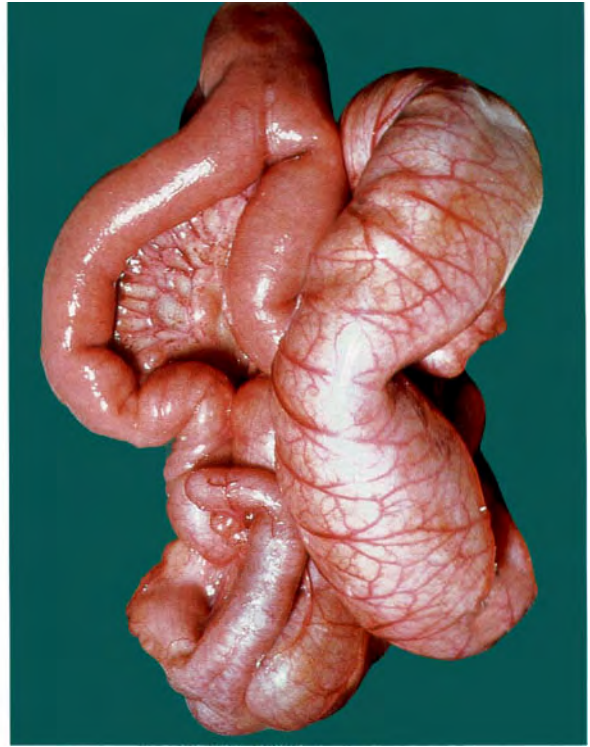
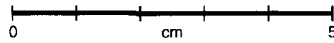


Fig. 4.72



Fig. 4.73

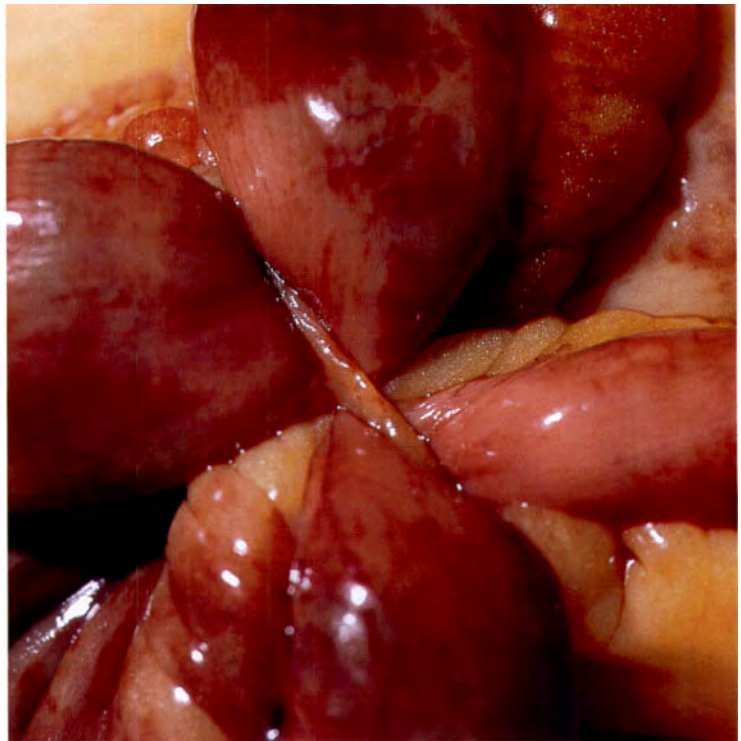
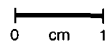


Fig. 4.74



Fig. 4.75



Fig. 4.76

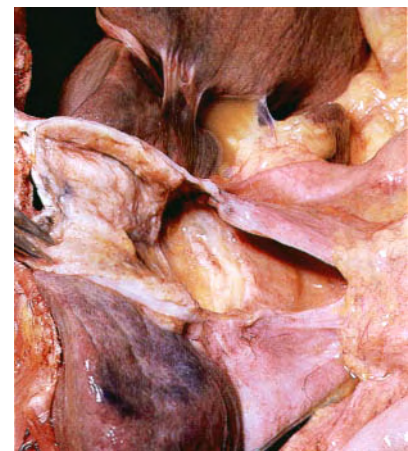
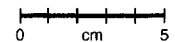


Fig. 4.77

Fig. 4.71 Enterogenous cyst of the ileum. M/48. The small cyst in the ileal wall had caused intestinal obstruction. It consists of a partial duplication of the bowel. Duplications can occur anywhere along the gastrointestinal tract. They are usually short segment duplications, and when they cause symptoms they are those of obstruction.

Fig. 4.72 Duplication of the proximal portion of the ascending colon. F/2.

Fig. 4.73 Endometriosis of the terminal ileum. F/50. This blood-filled cyst had caused intestinal obstruction.

Fig. 4.74 Intestinal obstruction with infarction of a loop of small bowel caused by a fibrous band. M/60. The patient had had an appendectomy 25 years previously.

Fig. 4.75 Gallstone ileus. F/77. This woman had complained of intermittent abdominal pain for some months. She finally developed complete obstruction, the cause of which was undiagnosed prior to death. There is an obstruction in the small intestine with dilatation proximal to it. The thickened gallbladder is adherent to the second part of the duodenum (arrow).

Fig. 4.76 On opening the bowel shown in Figure 4.75, a single large gallstone was found to be the cause of the obstruction.

Fig. 4.77 Same case as Figure 4.75. A large fistula was present between the gallbladder and the second part of the duodenum. Repeated attacks of cholecystitis resulted in adhesion of the gallbladder to the duodenum. Necrosis of the intervening tissue allowed the gallstone to pass into the duodenum. Gallstone ileus and Richter's hernia (Figure 4.54) are causes of difficult-to-diagnose intermittent abdominal pain in elderly patients.



Fig. 4.78

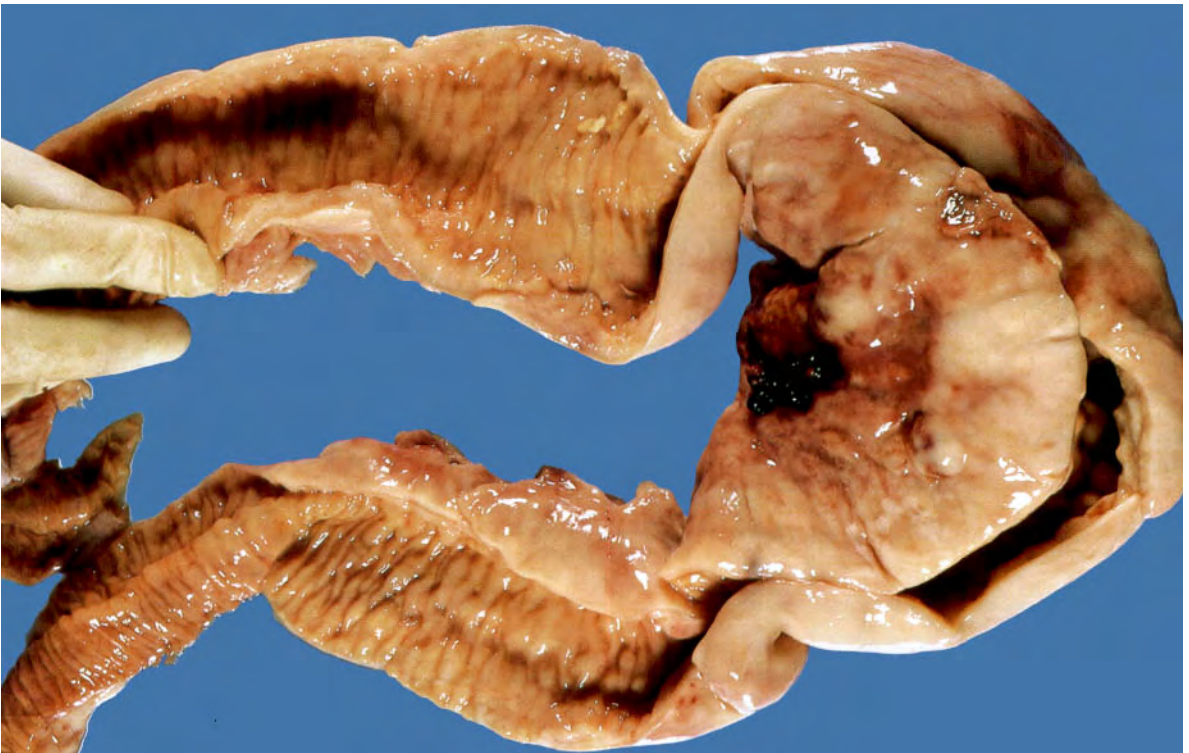


Fig. 4.79



Fig. 4.80



Fig. 4.81

Fig. 4.78 Focal nodular lymphoid hyperplasia of the ileum. F/9. On the right, small nodules of lymphoid hyperplasia can be seen. On the left, this hyperplasia has become so gross as to produce a tumour which resulted in intestinal obstruction necessitating resection.

Fig. 4.79 Malignant lymphoma of the small intestine. M/3½. The bowel wall over a long segment has been thickened by a creamy mass of soft tumour. The mesenteric lymph nodes are also enlarged.

Fig. 4.80 Carcinoid tumour in the terminal ileum. F/80. The yellow tumour is protruding into the lumen of the ileum. This resulted in intestinal obstruction. The bowel wall is thickened by fibrosis and puckered so as to be drawn into the lumen. This appearance is very characteristic of carcinoid tumours. Such tumours frequently metastasize to the liver and cause the carcinoid syndrome, but this patient showed no evidence of that.

Fig. 4.81 Multiple carcinoids in the small intestine. F/61. Incidental postmortem finding. Carcinoids of the small intestine are frequently multiple.



Fig. 4.82



Fig. 4.83

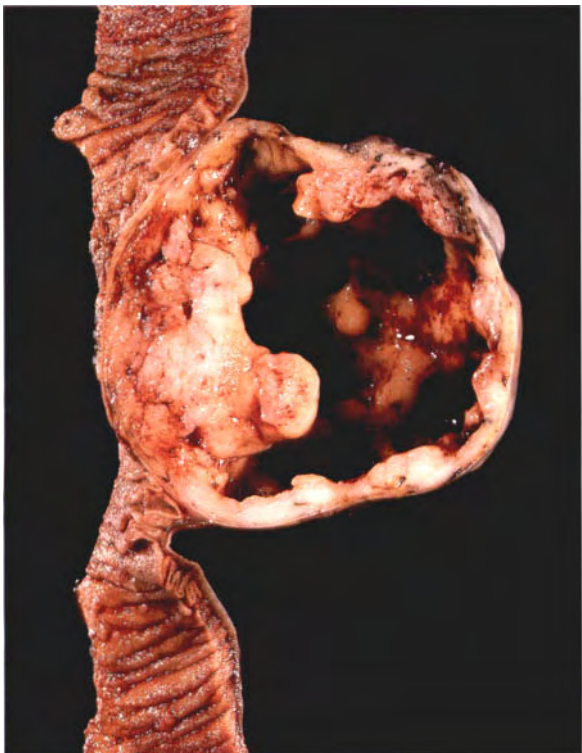


Fig. 4.84

Fig. 4.82 Adenocarcinoma of the ileum. F/63. The patient had had recurrent attacks of abdominal pain and finally came to laparotomy because of acute intestinal obstruction. The obstruction was caused by the lodging of a large fruit seed at the site of partial obstruction caused by the carcinoma. Intestinal obstruction occurs later in small bowel carcinomas than in large bowel carcinomas, because the bowel contents are more liquid in the small intestine.

Fig. 4.83 Secondary melanoma in the small intestine. M/51. This had resulted in intestinal obstruction. This manifestation of disseminated melanoma is seen fairly frequently in communities in which malignant melanoma is a common tumour.

Fig. 4.84 Leiomyosarcoma of the small intestine. M/55. The patient presented with intestinal obstruction. The tumour is large, cystic, and partially necrotic.

Fig. 4.85 Acute peritonitis associated with appendicitis. F/18 months. Peritonitis complicates appendicitis more frequently in children than in adults, because in adults the greater omentum is more likely to seal off an acutely inflamed appendix. The thin, greenish pus can be seen in the lower skin flap.

Fig. 4.86 Normal appendix.

Fig. 4.87 Acute appendicitis. M/18. The appendix is dilated and its serosal surface is reddened and covered by a fibrinopurulent exudate.

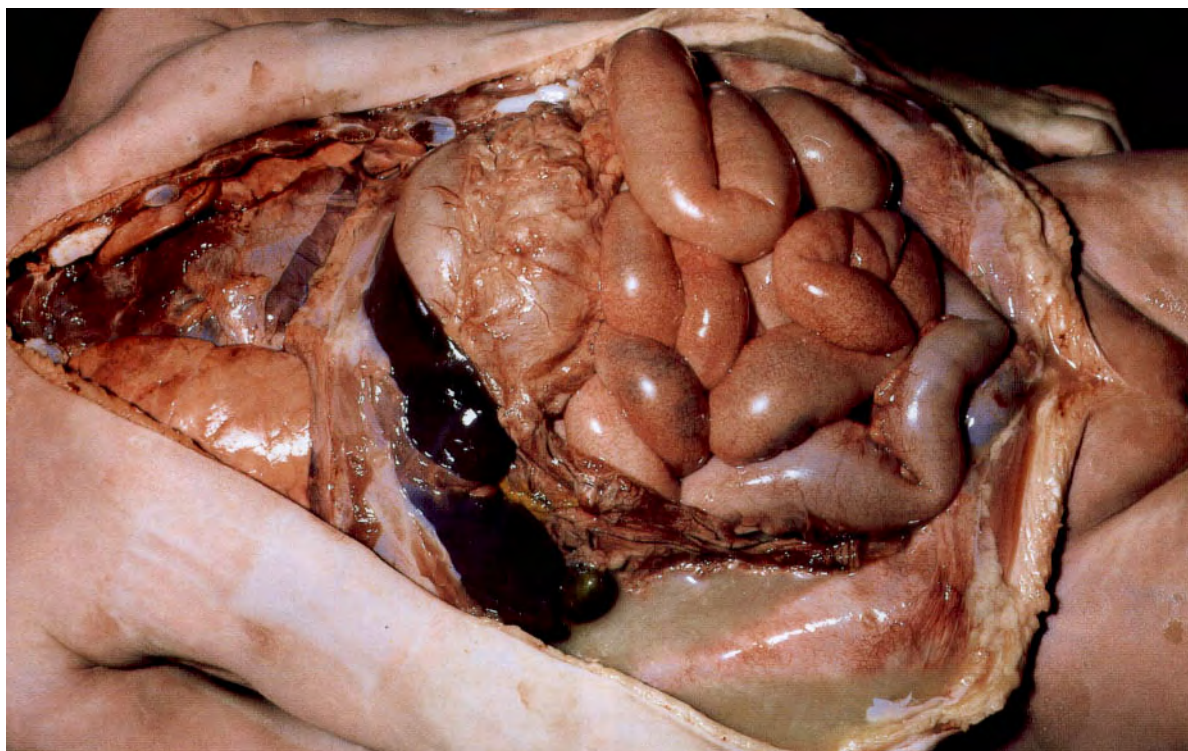


Fig. 4.85



Fig. 4.86

0 cm 1



Fig. 4.87

0 cm 1



Fig. 4.88

0 cm 1

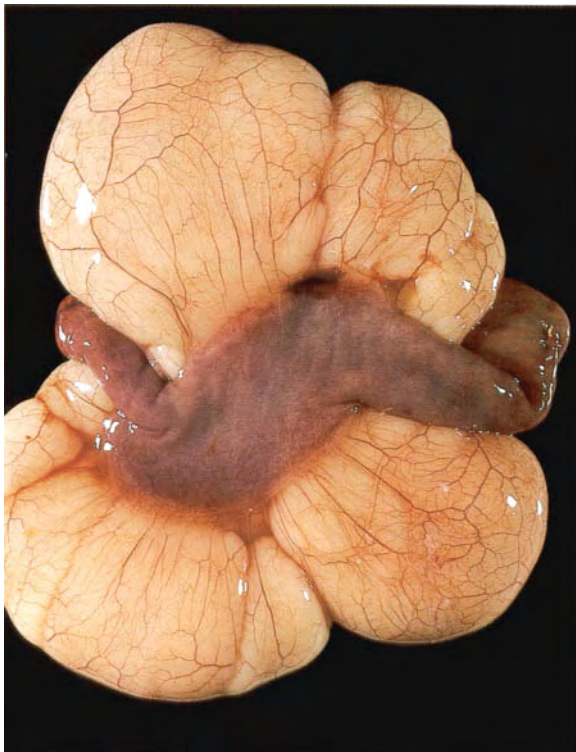


Fig. 4.90

0 cm 5



Fig. 4.89

0 cm 5

Fig. 4.88 Carcinoid tumour in the appendix. M/24. This was an incidental finding during an appendectomy for acute appendicitis. The tumour is usually yellow or cream coloured. In this case it is in the middle of the appendix, but it is more often situated at the tip.

Fig. 4.89 Mucocoele of the appendix. F/40. The appendix is dilated and filled with clear mucus.

Fig. 4.90 Chylous cyst of the mesentery of the small intestine. M/3. The child presented with an abdominal mass.

Fig. 4.91 Acquired megacolon. M/23. The patient was mentally retarded and living in an institution. The megacolon was not related to the cause of death.

Fig. 4.92 Hirschsprung's disease. M/1 week. The baby had been constipated since birth and exhibited signs of intestinal obstruction. Barium enema showed a narrowed lower rectal segment with dilated rectum above it. This operative photograph shows the typical appearance of Hirschsprung's disease. There are no ganglion cells in the narrowed segment. The suture (arrow) is at the site of biopsy of the intermediate zone, in which there are no ganglion cells but nerve fibres between the two muscle layers of the bowel wall. There are normal ganglion cells in the dilated segment – the 'cone'.

Fig. 4.93 Imperforate anus. M/newborn.

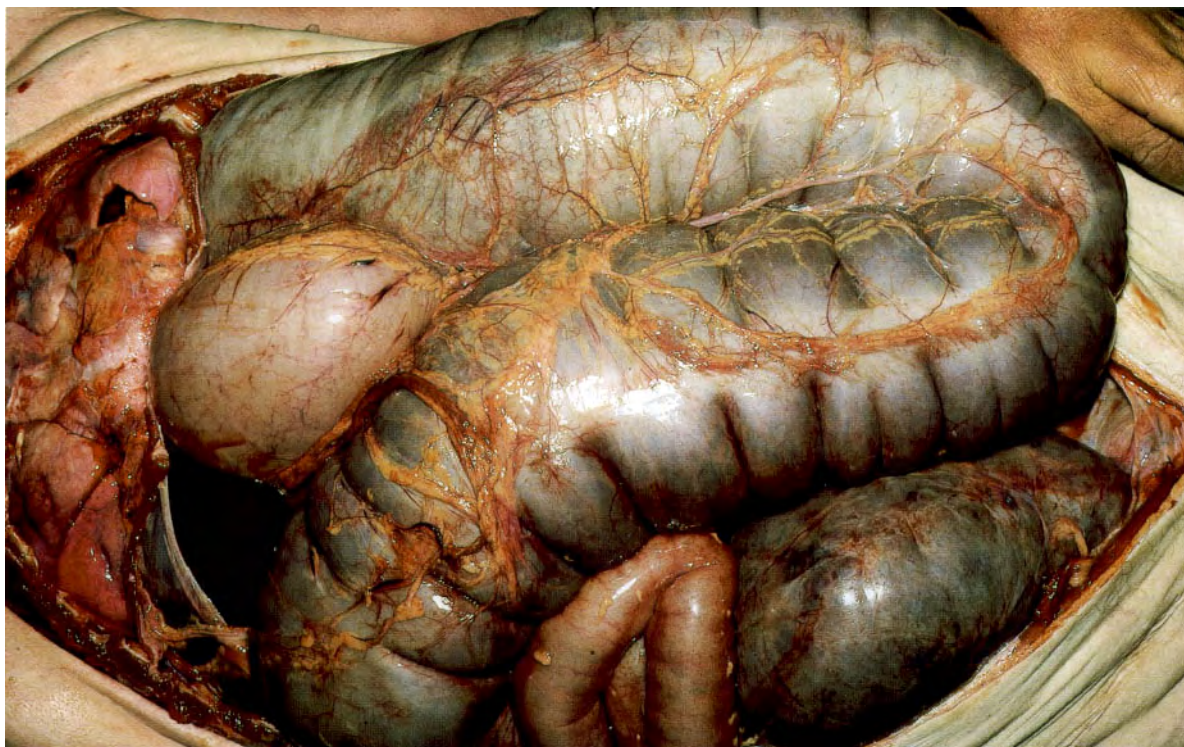


Fig. 4.91



Fig. 4.92



Fig. 4.93



Fig. 4.94

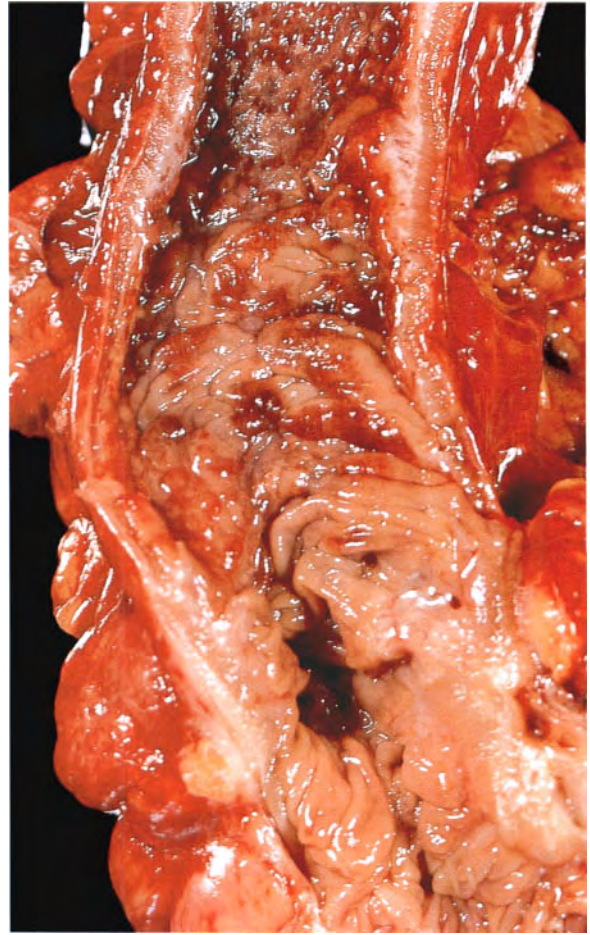


Fig. 4.95



Fig. 4.96

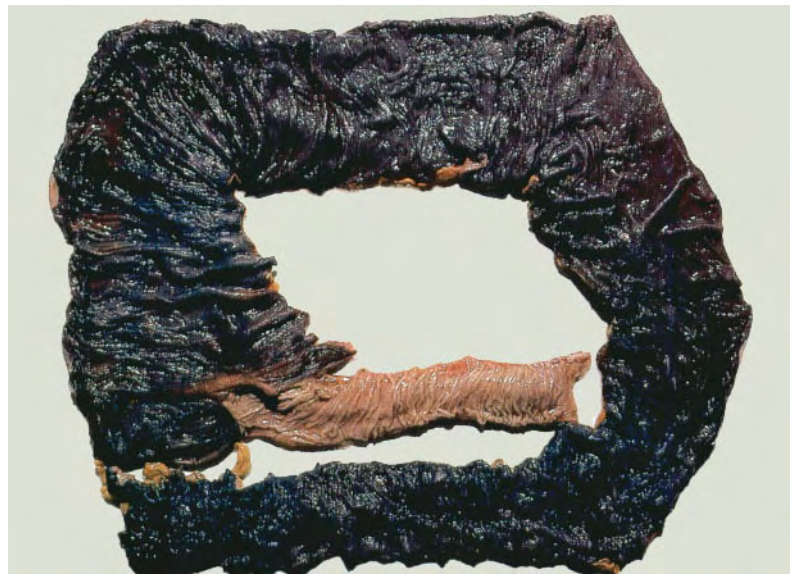


Fig. 4.97

0 cm 10

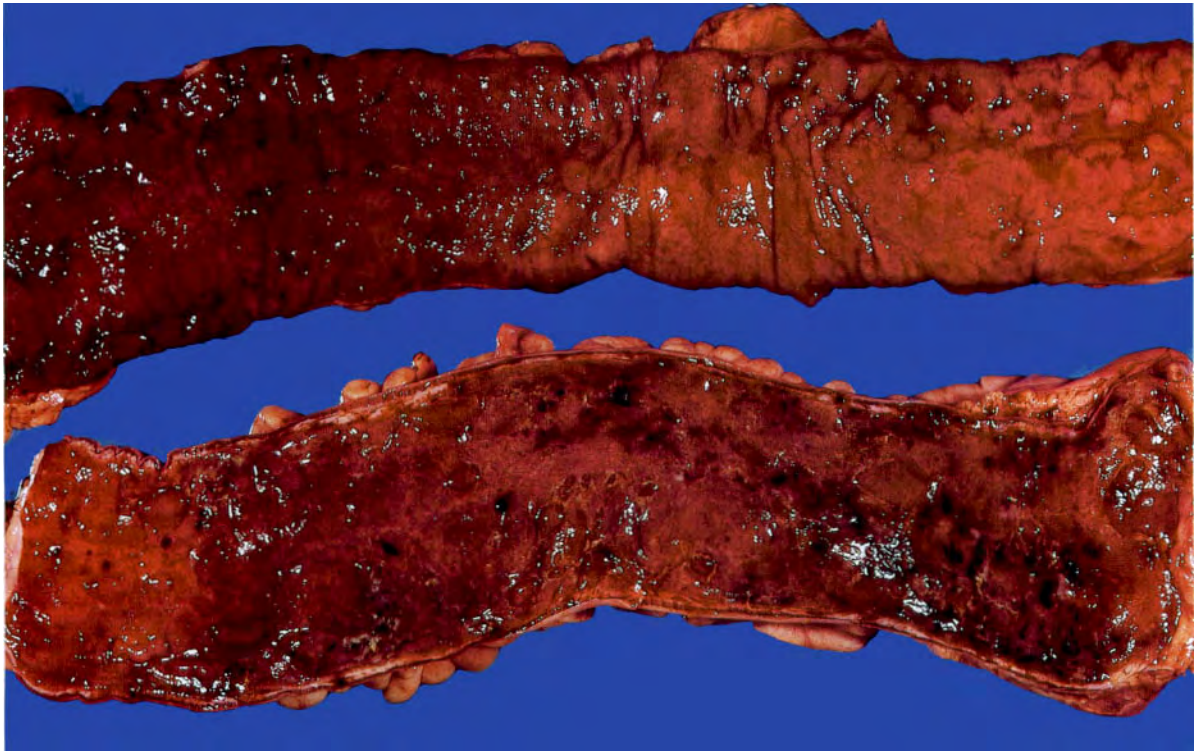


Fig. 4.98

Fig. 4.94 Diverticulosis of the sigmoid colon. F/59. An incidental postmortem finding.

Fig. 4.95 Chronic diverticulitis. F/75. A resected segment of thickened, fibrotic sigmoid colon that had caused obstruction. There is acute colitis proximal to the obstruction.

Fig. 4.96 Diverticulosis of the colon. The thin-walled diverticulum extends through the fibrotic wall of the colon into the pericolic fat. Characteristically, the colon in areas of diverticulosis shows submucosal fibrosis and muscle hypertrophy, as shown here.

Fig. 4.97 Melanosis coli. F/73. Note the black coloration of the mucosa throughout the whole length of the colon, whereas the terminal ileum is a normal colour.

Fig. 4.98 Acute ulcerative colitis. F/16. The mucosa throughout the length of the colon is reddened, oedematous, ulcerated and bleeding. Colectomy was performed because the patient was not responding to medical treatment.

Fig. 4.99 Chronic ulcerative colitis. F/58. The bowel is shortened and its wall is fibrotic. The mucosa is reddened and atrophic. The disease had been present for over 10 years and colectomy was performed, partly to relieve symptoms of diarrhoea and partly to prevent the development of cancer.

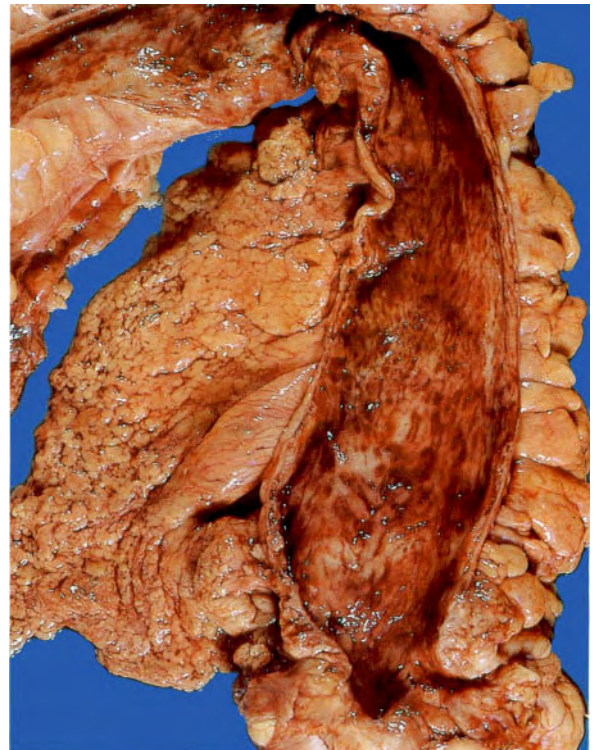


Fig. 4.99

0 cm 5



Fig. 4.100

0 cm 5



Fig. 4.101

Fig. 4.100 Chronic ulcerative colitis with hyperplastic polyps. F/40. Colectomy was performed because of long-standing disease. Virtually the whole of the mucosal surface has been converted into polyps, which have resulted from re-epithelialization after the initial ulceration.

Fig. 4.101 Chronic ulcerative colitis with mucosal dysplasia in the sigmoid colon. F/49. The abnormal areas were seen during routine colonoscopy to assess the progress of the disease. Biopsy showed severe dysplasia, and colectomy was performed to prevent the development of carcinoma.

Fig. 4.102 Chronic ulcerative colitis with a carcinoma arising in the caecum. F/30. A total colectomy was performed. The patient had had long-standing ulcerative colitis and the carcinoma was found on colonoscopy.



Fig. 4.102

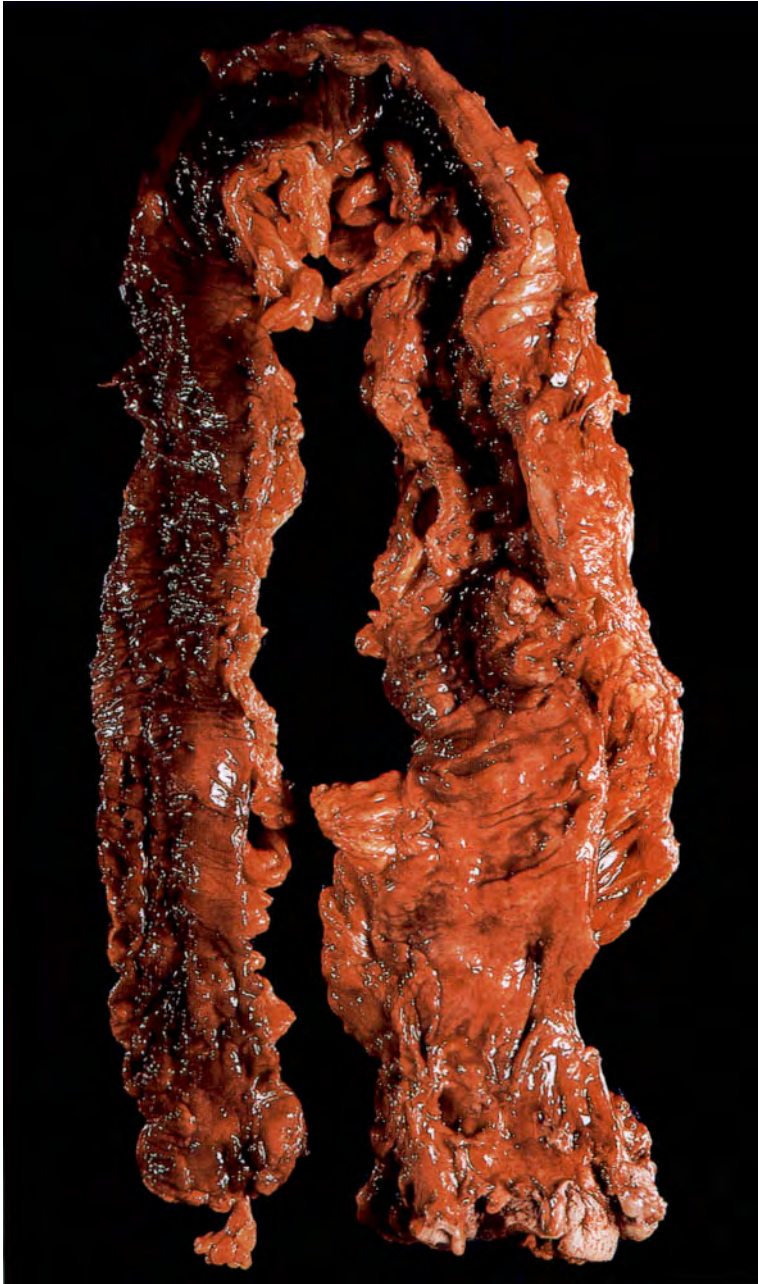


Fig. 4.103

Fig. 4.103 Crohn's disease of the colon. F/60. Total colectomy performed for disease which could not be controlled by medical treatment. Nearly the whole length of the colon is involved, but there is a segment in the sigmoid colon that is less involved than the rest. In advanced cases such as this it is not easy to identify the segmental involvement characteristic of Crohn's disease of the colon.



Fig. 4.104

Fig. 4.104 Closer view of the splenic flexure of the specimen in Figure 4.103 showing thickening of the wall and a 'cobblestone' appearance of the mucosal surface.



Fig. 4.105



Fig. 4.106

0 cm 5



Fig. 4.107

0 cm 5



Fig. 4.108



Fig. 4.109

Fig. 4.105 Pseudomembranous colitis. F/68. Colectomy was performed because the patient developed toxic megacolon. She was taking ampicillin and this allowed overgrowth of the *Clostridium difficile* which produced the multiple, discrete white plaques of purulent exudate on the mucosal surface.

Fig. 4.106 Ischaemic colitis. M/64. Surgical resection of the splenic flexure following abdominal pain and diarrhoea. The mucosal surface is reddened and covered by a fibrinopurulent exudate. The colon adjacent to this area appears normal.

Fig. 4.107 Amoebic colitis. M/49. Multiple, undermined mucosal ulcers can be seen in the caecum and ascending colon. This man had colitis and liver abscess. While undergoing treatment he suddenly developed an acute pericardial effusion and died.

Fig. 4.108 Acute colitis. F/9 This had a rapid onset and quickly led to death from dehydration. No causative organism was found. The colonic mucosa is thickened and bright red.

Fig. 4.109 Acute enterocolitis. F/19 months. A *Shigella* organism was isolated from the faeces prior to death. The mucosal surface is reddened and slightly thickened. The macroscopic changes are less florid than those seen in Figure 4.108. Acute enterocolitis is now a very rare cause of death in children in countries where there is 'clean' water and ready access to medical services.

Fig. 4.110 Villous papilloma of the rectum. F/48. These polyps are sessile, soft on palpation, and cover quite a large area. They carry a high risk of developing carcinoma.

Fig. 4.111 Benign tubular adenomatous polyps of the colon. M/46. These were asymptomatic.



Fig. 4.110

0 cm 5



Fig. 4.111

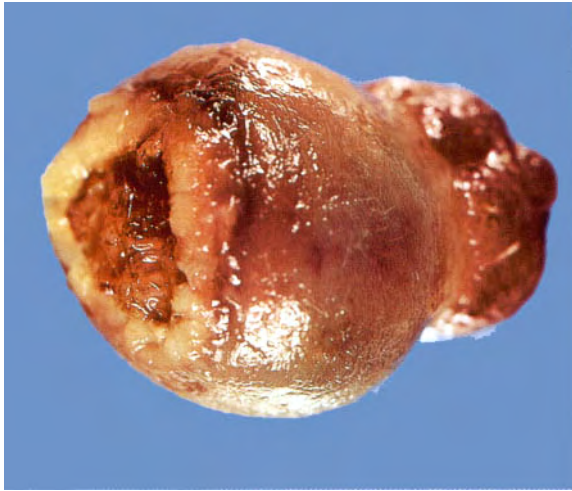


Fig. 4.112

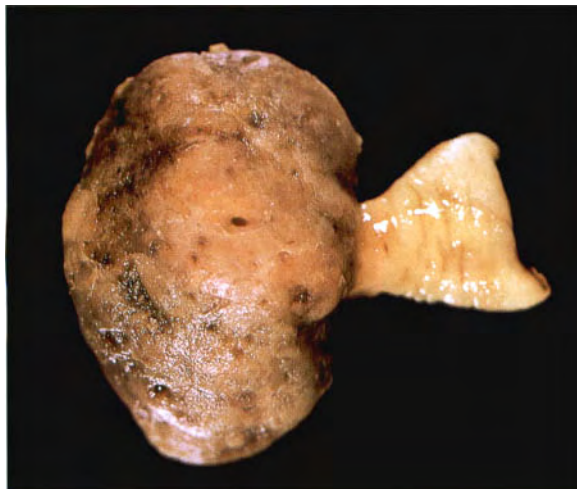


Fig. 4.113

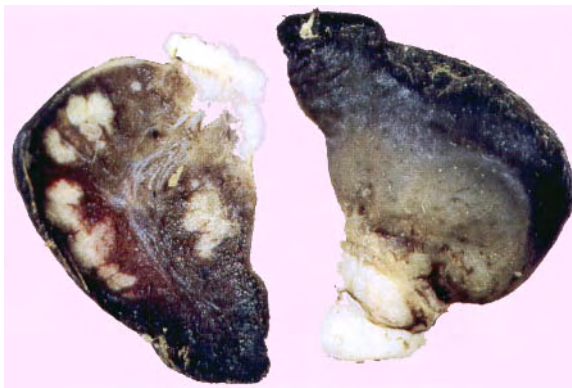


Fig. 4.114



Fig. 4.115

Fig. 4.112 Tubular adenoma removed via a colonoscope. M/73. This polyp was causing rectal bleeding from the ulcer on its surface.

Fig. 4.113 Juvenile polyp. F/7½. This was removed via a colonoscope. These polyps are characterized by the presence of greatly dilated mucus glands, which can be seen on its surface.

Fig. 4.114 Hamartomatous polyp from the rectum. M/6 weeks. This had caused rectal bleeding. It is composed of vascular fibrofatty tissue.

Fig. 4.115 Multiple polyposis coli. F/25. This patient's father had been treated for carcinoma of the colon, and colectomy was performed because of the high risk of her developing a carcinoma. Polyps cover virtually the whole of the mucosal surface of the colon.



Fig. 4.116

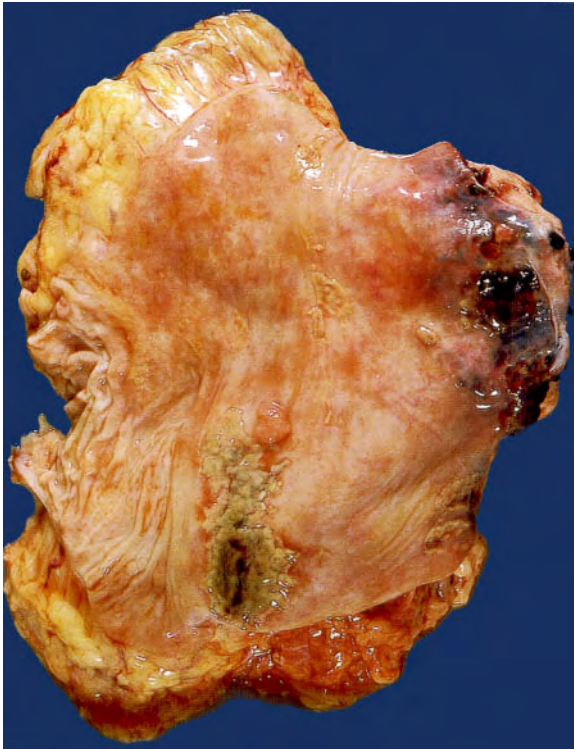


Fig. 4.117

Fig. 4.116 Pneumatosis intestinalis. M/70. The gas-filled cysts caused marked thickening of the colonic wall. This condition can be found in both small and large intestine, but it is most often seen in the colon, where it usually involves a short segment only. This man had the whole length of his colon involved and it was an incidental postmortem finding.

Fig. 4.117 Solitary ulcer of the rectum. M/48. Local resection was performed because of recurrent pain and bleeding. These ulcers are usually found on the anterior wall of the rectum.



Fig. 4.118

0 cm 5

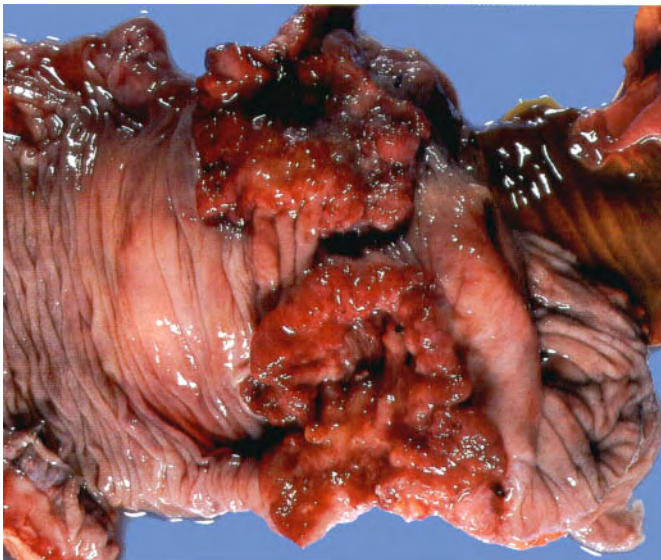


Fig. 4.120



Fig. 4.119



Fig. 4.121

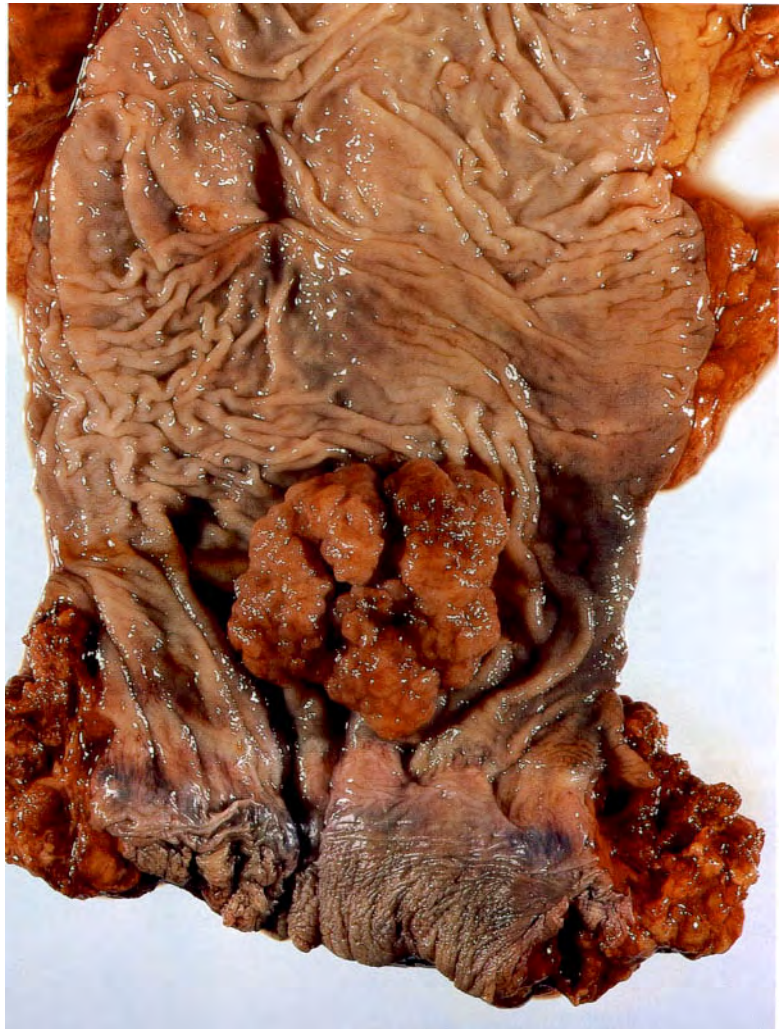


Fig. 4.118 Adenocarcinoma of the caecum. M/53. This tumour is large and its surface is ulcerated and bleeding. These tumours often present in an advanced stage, and frequently because of symptoms of iron deficiency anaemia resulting from chronic blood loss.

Fig. 4.119 Polypoid adenocarcinoma of the colon. M/26. When a carcinoma appears at this young age it is necessary to exclude the presence of some premalignant condition, for example polyposis coli. There was no such history in this man.

Fig. 4.120 Adenocarcinoma of the transverse colon. F/87. This tumour is partly polypoid, but it had encircled the bowel wall and caused obstruction.

Fig. 4.121 Adenocarcinoma of the descending colon. M/48. This is an infiltrating sclerosing lesion which has invaded the full thickness of the bowel wall. The central portion of the tumour is ulcerated. The proximal margin has a polypoid projection into the lumen.

Fig. 4.122 Adenocarcinoma of the rectum. M/70. This is a polypoid type of tumour. These tumours frequently present at an early stage in their development with bloodstained diarrhoea. They are readily palpable by digital examination of the rectum.

Fig. 4.123 Squamous cell carcinoma of the anus. M/62.

Fig. 4.122



Fig. 4.123



Fig. 4.124

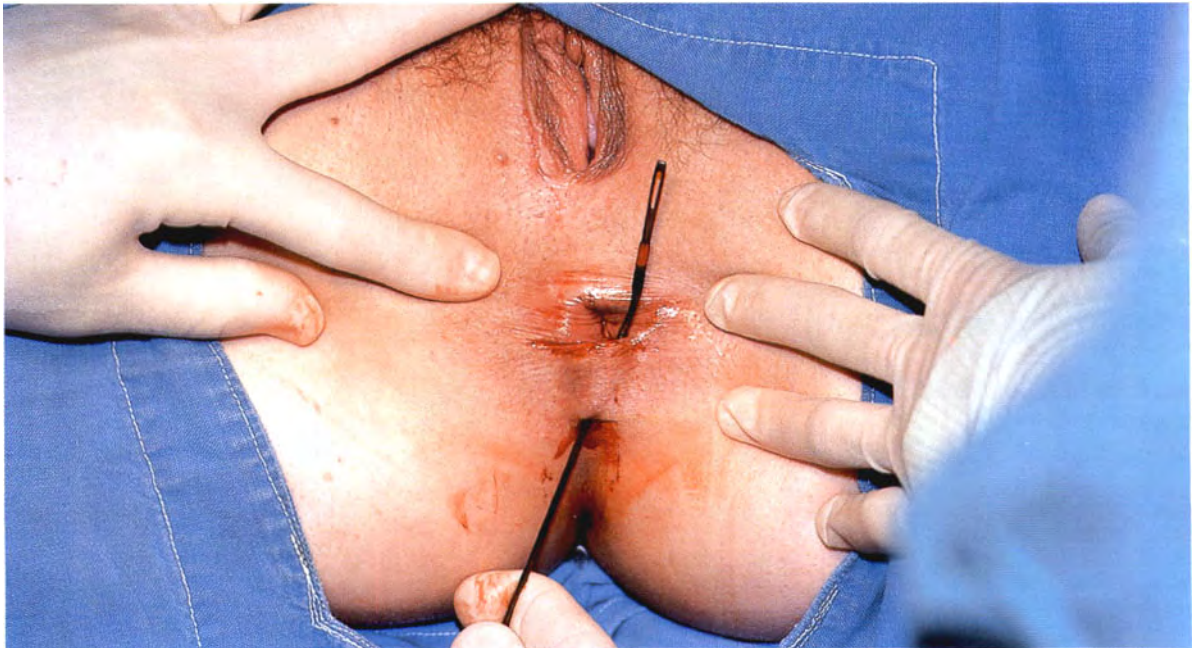


Fig. 4.125

Fig. 4.124 Perianal abscesses and fistulae. F/72. This complicated the patient's long-standing Crohn's disease of the colon.

Fig. 4.125 Simple fistula in ano. F/40.

**PANCREAS, BILIARY
SYSTEM AND LIVER**

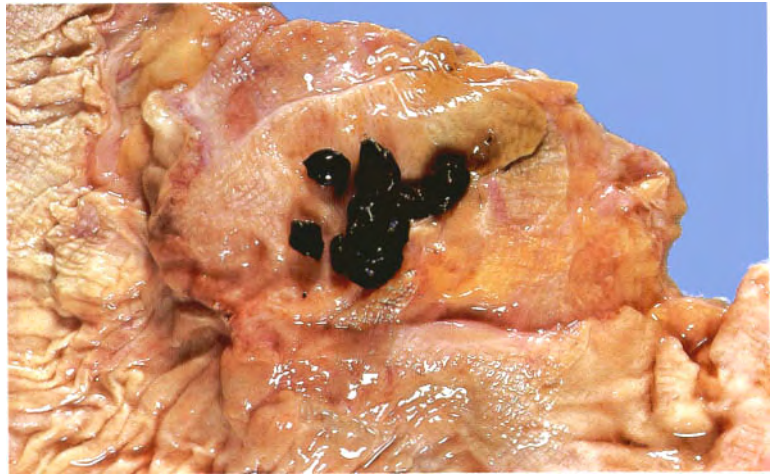


Fig. 5.1

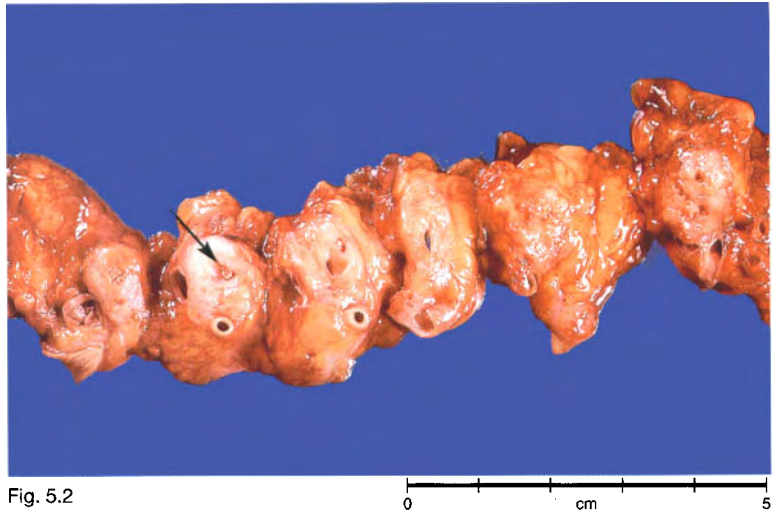


Fig. 5.2

Fig. 5.1 Calculi in the ampulla of Vater. F/87. There are multiple calculi impacted in the ampulla. The duodenal surface on the left is ulcerated as a result of a failed endoscopic attempt to remove them prior to death from liver failure.

Fig. 5.2 Pancreatic atrophy caused by obstruction of the pancreatic duct by a calculus. M/44. The pancreas has been sliced along its length. The pancreatic duct in the middle of the gland is dilated, and there is atrophy of the acinar tissue. This was an incidental finding in a patient who died from a carcinoma of the pharynx.

Fig. 5.3 Nodule of ectopic pancreas on the surface of the jejunum. F/69. An incidental postmortem finding. Ectopic pancreatic tissue is found especially in the pylorus, duodenum and jejunum.

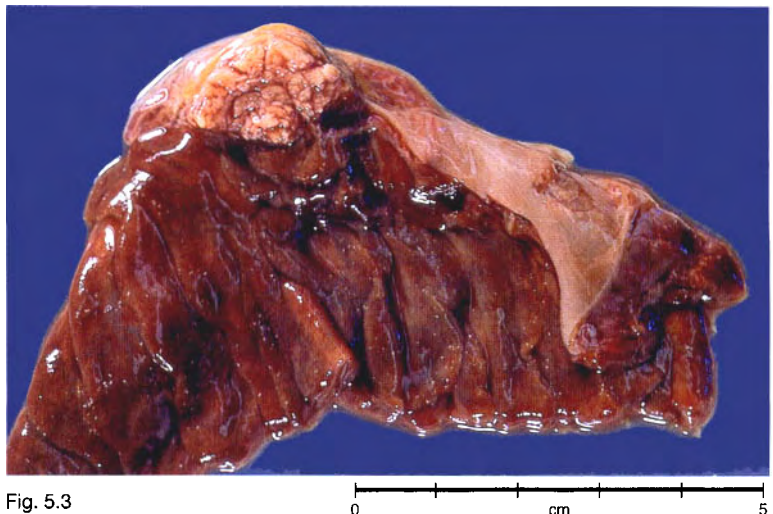


Fig. 5.3



Fig. 5.4

0 cm 5

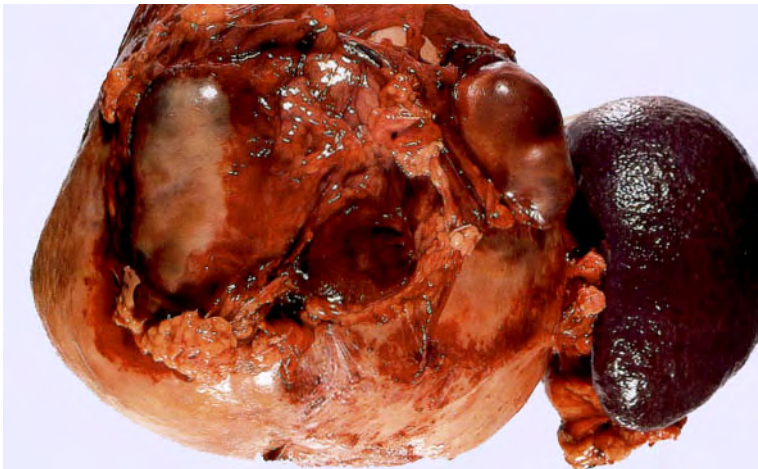


Fig. 5.5

0 cm 5



Fig. 5.6

0 cm 5

Fig. 5.4 Acute haemorrhagic pancreatitis. M/44. This was the cause of death. Note the haemorrhage, necrosis, and yellow spots of enzymatic fat necrosis.

Fig. 5.5 Pseudocyst in the body and tail of the pancreas. F/67. This is a well recognized complication of acute pancreatitis.

Fig. 5.6 Chronic pancreatitis. F/43. The pancreas is atrophic and fibrotic. The main pancreatic duct is dilated and there are calculi in the ducts in the head of the pancreas. The patient was an alcoholic.

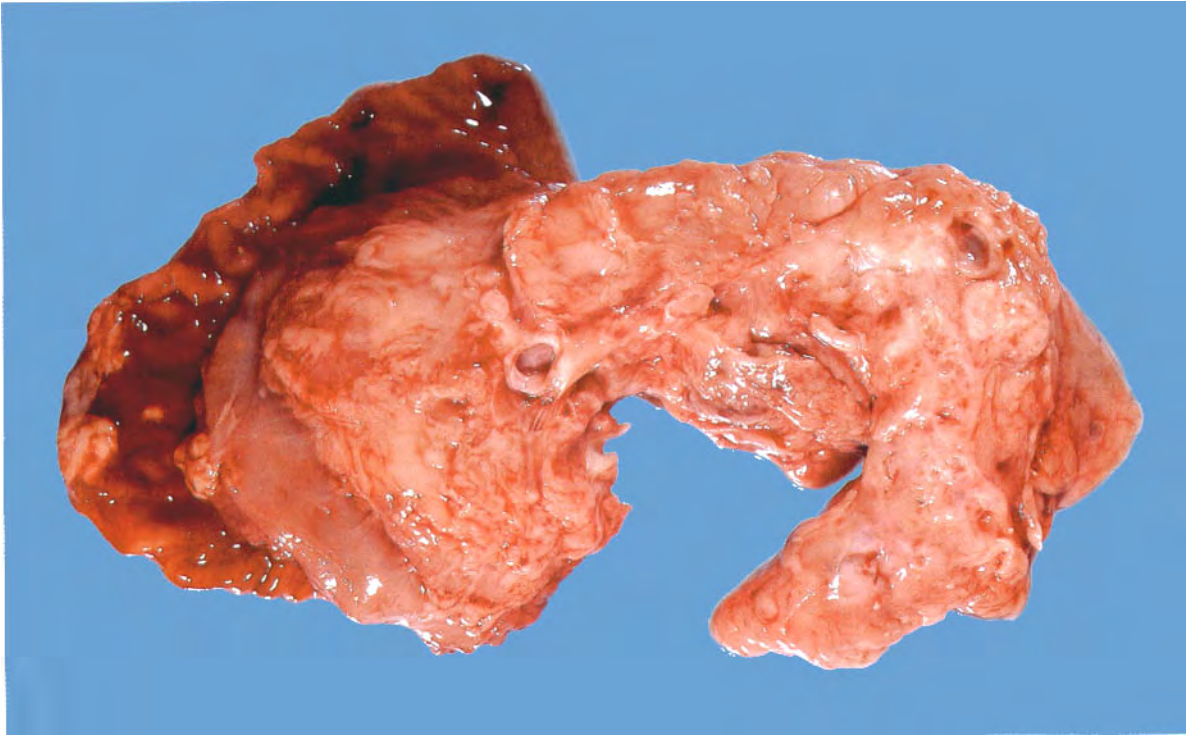


Fig. 5.7

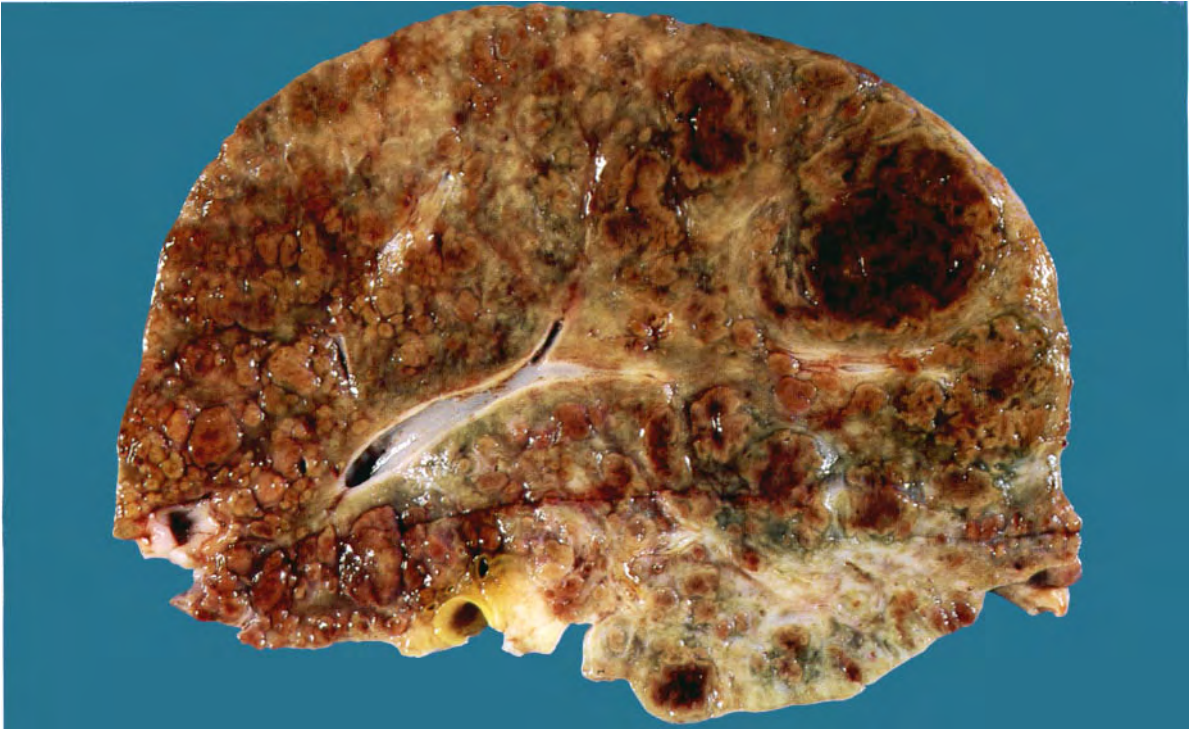


Fig. 5.8

0 cm 5

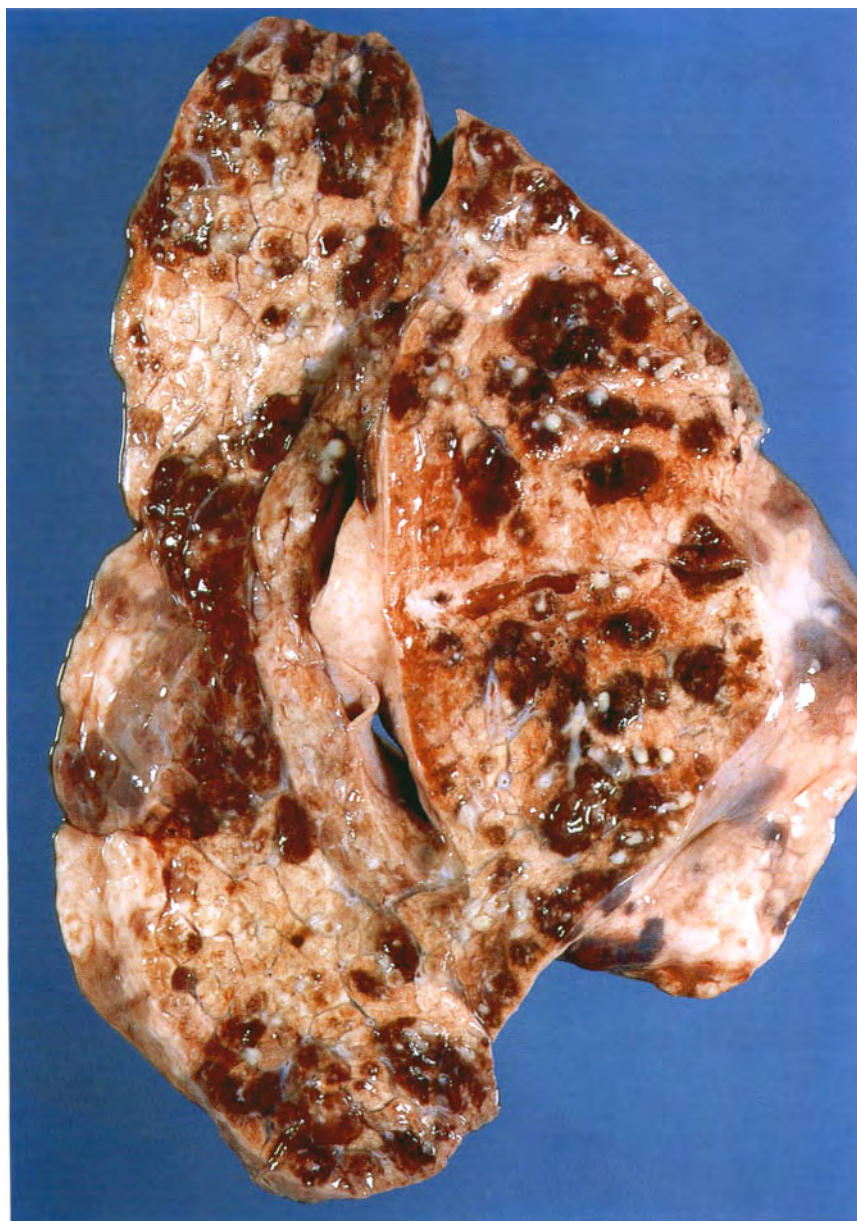


Fig. 5.9

Fig. 5.7 Mucoviscidiosis (fibrocystic disease of the pancreas). M/11. The pancreas is attached to the second part of the duodenum. The main pancreatic duct in the head of the pancreas is dilated. The body and tail are fibrotic, and numerous cysts can be seen.

Fig. 5.8 Hepatic cirrhosis in mucoviscidiosis. M/6. Cirrhosis complicates mucoviscidiosis in a proportion of cases, usually presenting about this age as haematemesis.

Fig. 5.9 Lung from a patient with mucoviscidiosis. F/2. The lung shows widespread bronchopneumonia with pus issuing from dilated bronchi and bronchioles. Recurrent respiratory tract infection is one of the main complications of this disease.

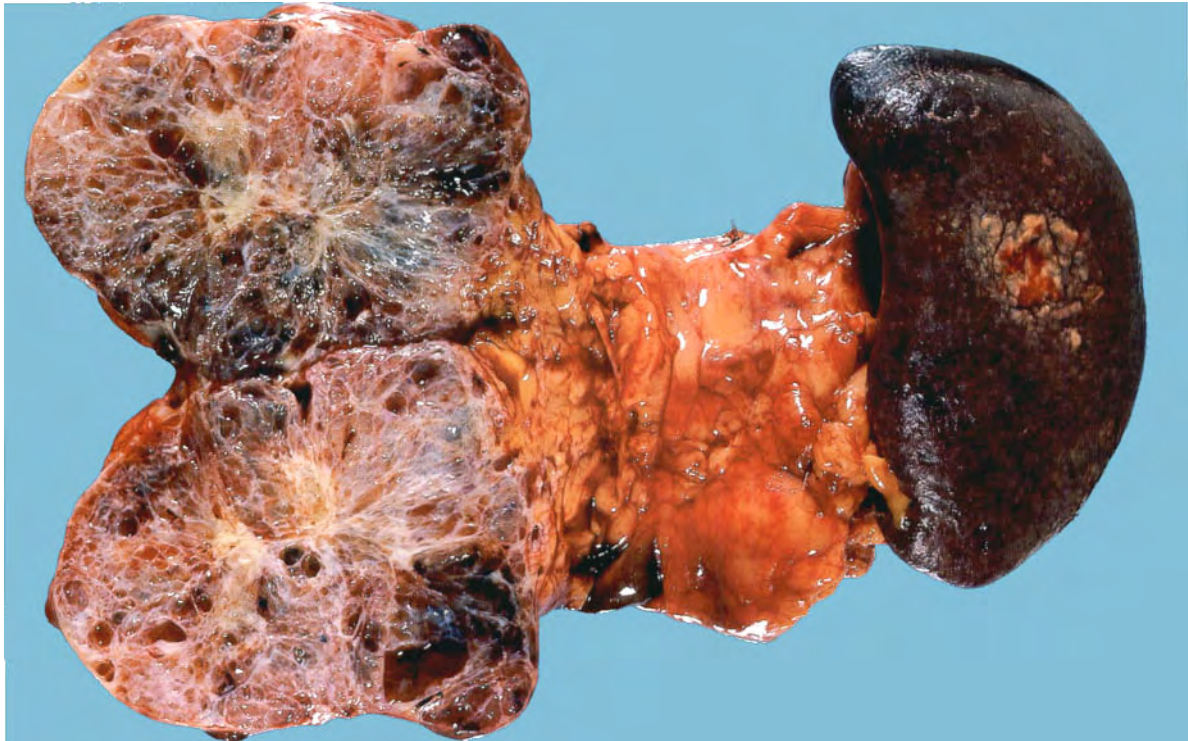


Fig. 5.10

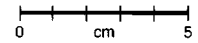


Fig. 5.11

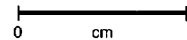


Fig. 5.10 Benign cystadenoma of the head of the pancreas. F/74. The patient presented with an epigastric mass.

Fig. 5.11 Insulin-secreting islet cell adenoma of the pancreas. F/45. For many years the patient had had difficulty in

waking in the morning, using an alarm clock for this purpose. After a cup of tea with milk and sugar she would feel better and ready for the day. This ultimately became such a problem that she sought medical advice. The diagnosis was made and the removal of the adenoma relieved her symptoms.

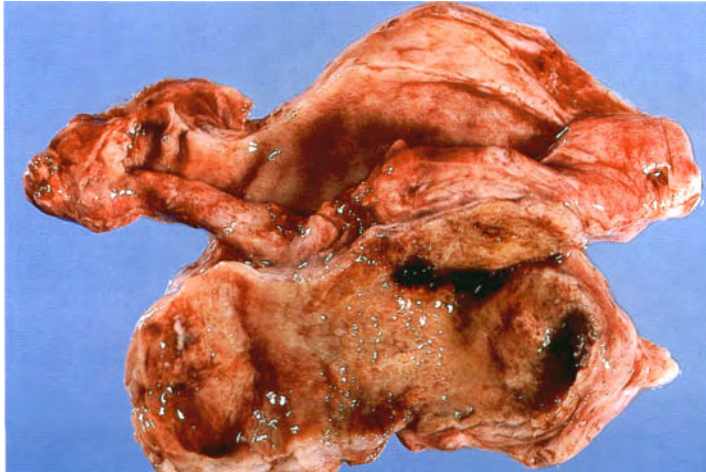


Fig. 5.12



Fig. 5.13



Fig. 5.15



Fig. 5.14

0 cm 1

Fig. 5.12 Double gallbladder. F/45.

This congenital abnormality was discovered when cholecystectomy was being performed for chronic calculous cholecystitis.

Fig. 5.13 Calculi removed from the gallbladder in Figure 5.12. One gallbladder contained a single large calculus and the other contained multiple calculi.**Fig. 5.14 Acute-on-chronic cholecystitis.** F/38. The gallbladder is distended. Both serosal and mucosal surfaces are reddened and inflamed. The wall of the gallbladder is thickened and there are a few mixed calculi within it.**Fig. 5.15 Chronic cholecystitis.** F/48. The gallbladder shows the features of chronic cholecystitis and is packed with small, multifaceted mixed gallstones.



Fig. 5.16



Fig. 5.17



Fig. 5.18

Fig. 5.16 Cholesterolosis. F/36. The gallbladder shows chronic cholecystitis. There are multiple yellow spots on its mucosal surface. This is due to the accumulation of lipid in the lamina propria.

Fig. 5.17 Mucocoele of the gallbladder. M/38. The unopened gallbladder has been transilluminated to show that its wall is thin and it contains semitransparent fluid.

Fig. 5.18 Adenomyoma of the gallbladder. F/50. There is a cream-coloured thickening of the fundus at the lower end of the specimen. As is usual, the gallbladder was removed for symptoms of chronic cholecystitis and the presence of the benign tumour was an incidental finding.

Fig. 5.19 Gallstones in the common bile duct. M/73. This patient died from liver failure. The presence of the gallstones was not diagnosed during life.

Fig. 5.20 Calculus left in the common bile duct after cholecystectomy. M/73. During the operation the common bile duct was explored, as can be seen by the ulceration in its lower part just proximal to the ampulla of Vater. A small gallstone, missed at the operation, is impacted above the opening of the cystic duct near the bifurcation of the main hepatic ducts. The patient died a few days postoperatively from an acute myocardial infarction.

Fig. 5.21 Carcinoma of the gallbladder. F/74. A large calculus is present in the gallbladder. Tumour has extended into the adjacent liver.

Fig. 5.22 Adenocarcinoma arising from the bile ducts in the porta hepatis. F/78. The patient died from the effects of obstructive jaundice.



Fig. 5.19



Fig. 5.20

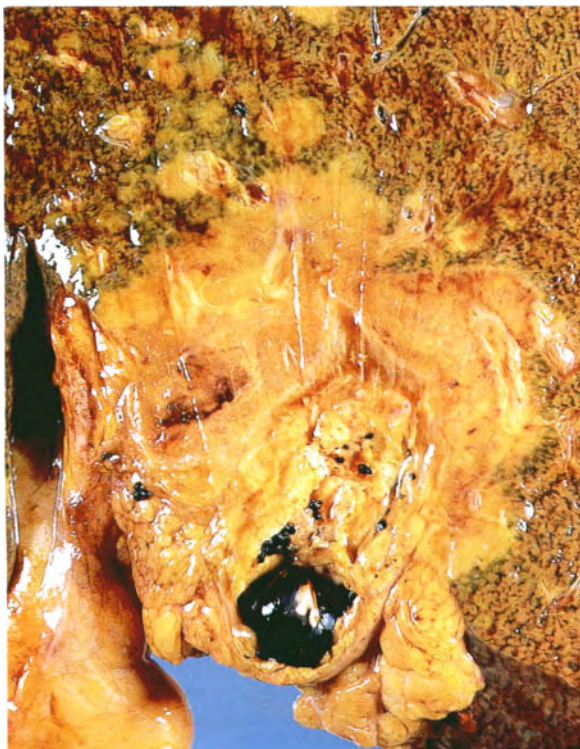


Fig. 5.21



Fig. 5.22



Fig. 5.23

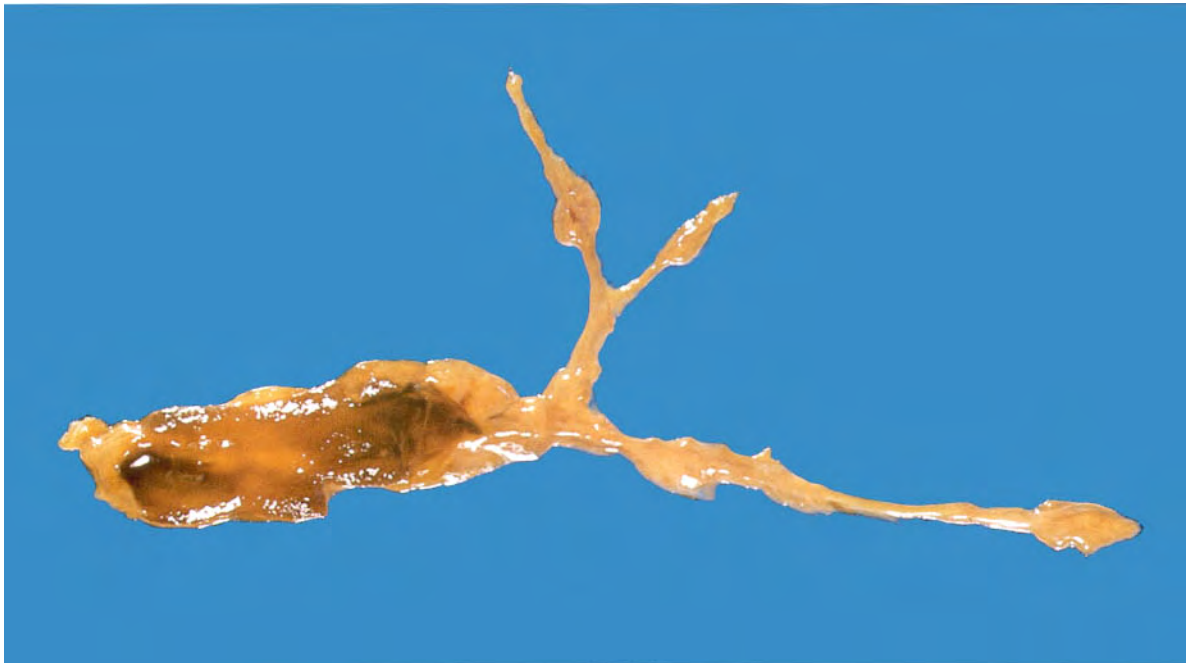


Fig. 5.24

Fig. 5.23 Choledochal cyst. F/5. The patient had been jaundiced since birth. At laparotomy this large cyst was found in the middle of the common bile duct and excised. The structure to the left is the attached gallbladder.

Fig. 5.24 Congenital biliary atresia. M/6. This child died from hepatic failure and the thin, stenosed extrahepatic biliary system was dissected. The right and left hepatic ducts and the common bile duct with the gallbladder attached on the left, are displayed. Sections showed the presence of only a microscopic lumen.

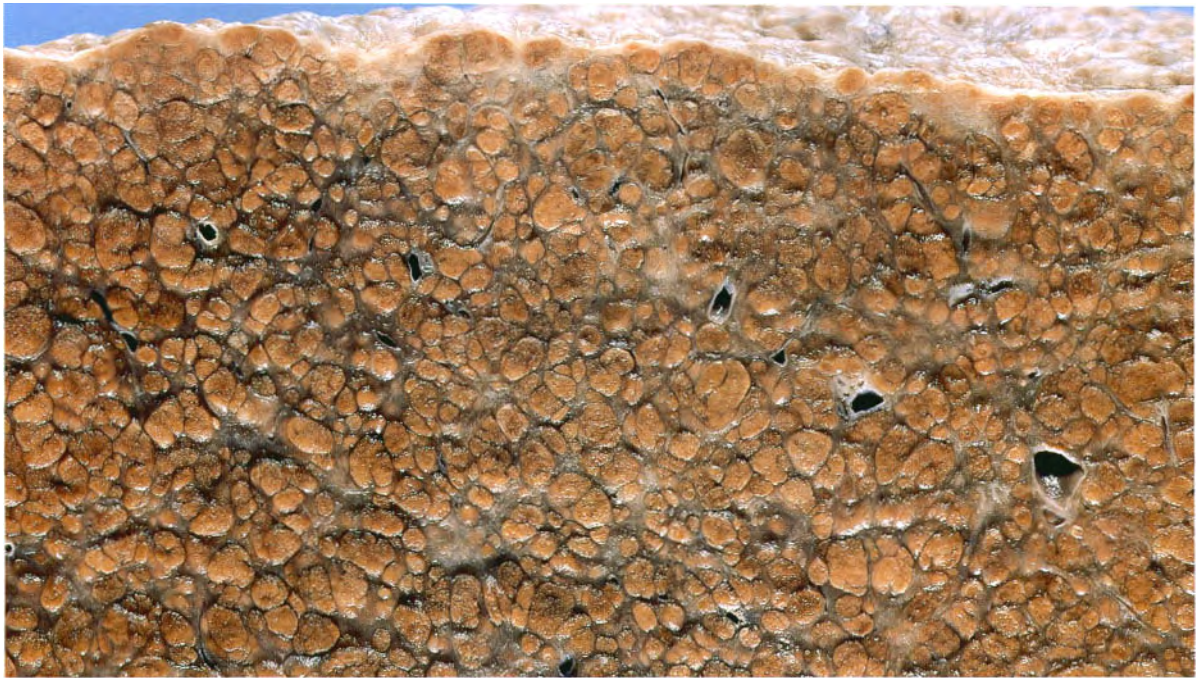


Fig. 5.25

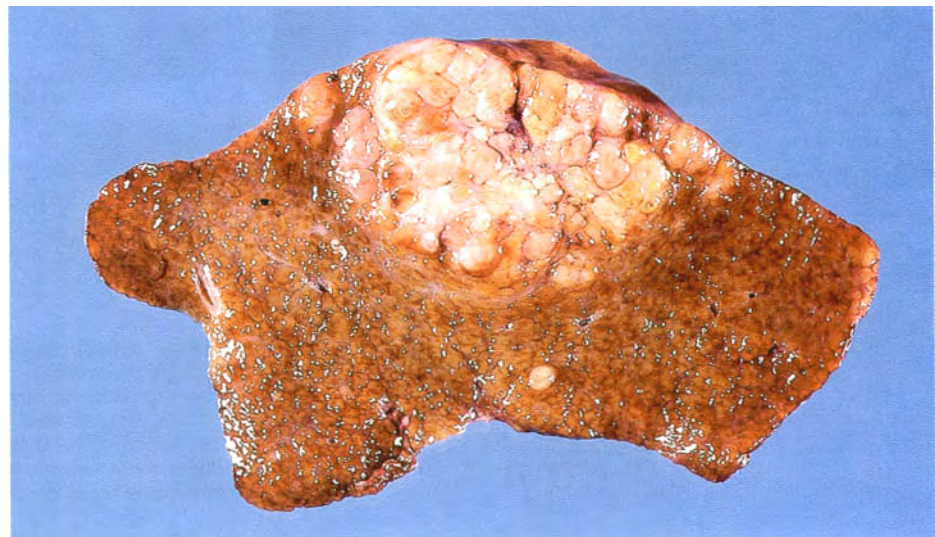


Fig. 5.26

Fig. 5.25 Haemochromatosis. M/56. This patient died from liver failure. The cirrhotic nodules are clearly seen. The liver is dark brown because of the heavy iron deposition within the hepatocytes.

Fig. 5.26 Haemochromatosis with hepatocellular carcinoma. M/56. This is a common complication of haemochromatosis. In this case there is one main focus of tumour, with a smaller lesion near the inferior margin of the specimen. HCC may occur as a single lesion or as multiple foci throughout the liver.



Fig. 5.27



Fig. 5.28



Fig. 5.29

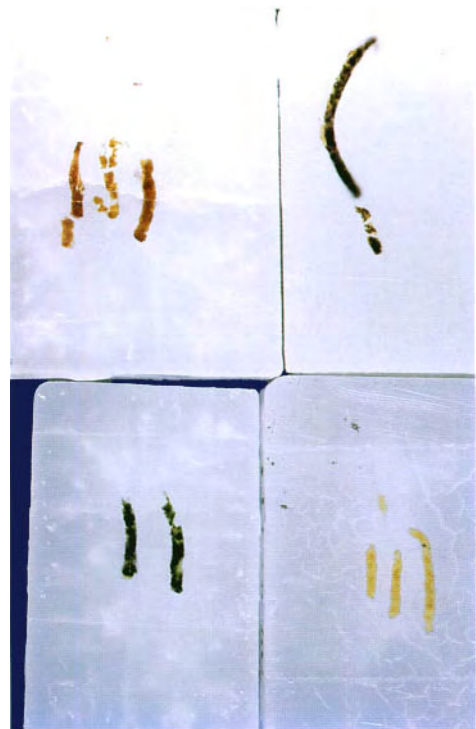


Fig. 5.30

Fig. 5.27 Arthritis in haemochromatosis. M/61. The brown pigmentation of the skin which is a feature of haemochromatosis can be seen, and the ankle joint is swollen. The arthritis is associated with the deposition of iron in the synovium of the joint. Arthritis of the ankles, knees and hips may be the presenting symptoms of haemochromatosis.

Fig. 5.28 Pancreas in haemochromatosis. M/50. The pancreas is a red colour owing to the deposition of iron. Diabetes is a common complication of haemochromatosis.

Fig. 5.29 Dubin-Johnson syndrome. M/20. This needle biopsy shows the black colour of the liver in this type of congenital hyperbilirubinaemia.

Fig. 5.30 Paraffin blocks containing liver biopsies which show the colours of biopsies in various conditions. Clockwise from the bottom right: normal, obstructive jaundice, haemochromatosis, and Dubin-Johnson syndrome.



Fig. 5.31



Fig. 5.32

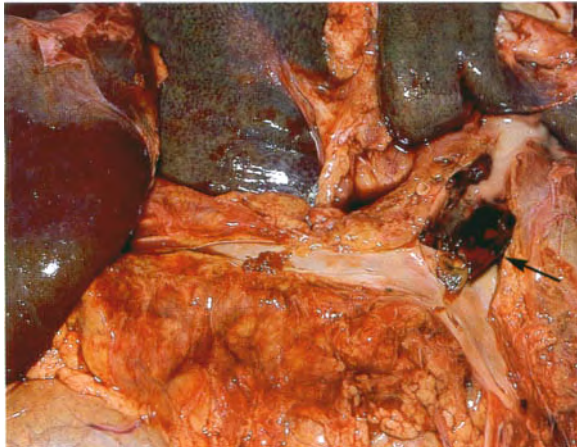


Fig. 5.33

Fig. 5.31 Hepatocellular carcinoma in macronodular cirrhosis. M/60. The dark brown nodules are the tumour. Both cirrhosis and HCC are caused by hepatitis B virus infection. Hence, these two conditions are common in countries where infection with this virus is prevalent.

Fig. 5.32 Cirrhosis and HCC. This man from Papua New Guinea, where hepatitis B virus infection, cirrhosis and HCC are common diseases, presented with ascites and a greatly enlarged, hard liver. Needle biopsy confirmed the diagnosis.

Fig. 5.33 Thrombosis of the portal vein. F/24. This is one of the complications of hepatocellular carcinoma. The specimen is viewed from the back (posteriorly). The portal vein forms as a



Fig. 5.34

result of the confluence of the splenic vein (running from the left along the inferior border of the pancreas) and the superior mesenteric vein (running vertically).

Fig. 5.34 Secondary deposits of hepatocellular carcinoma in a lymph node in the porta hepatis. The common bile duct can be recognized to the left of the enlarged, tumour-filled lymph node.

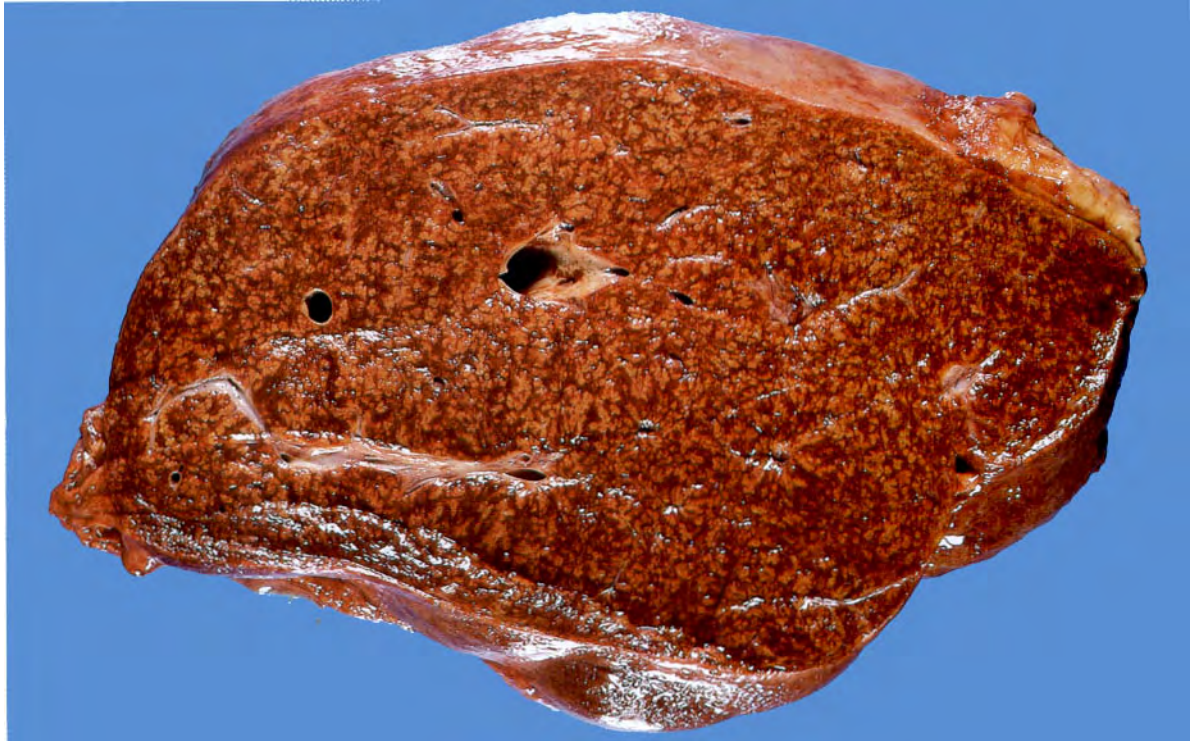


Fig. 5.35

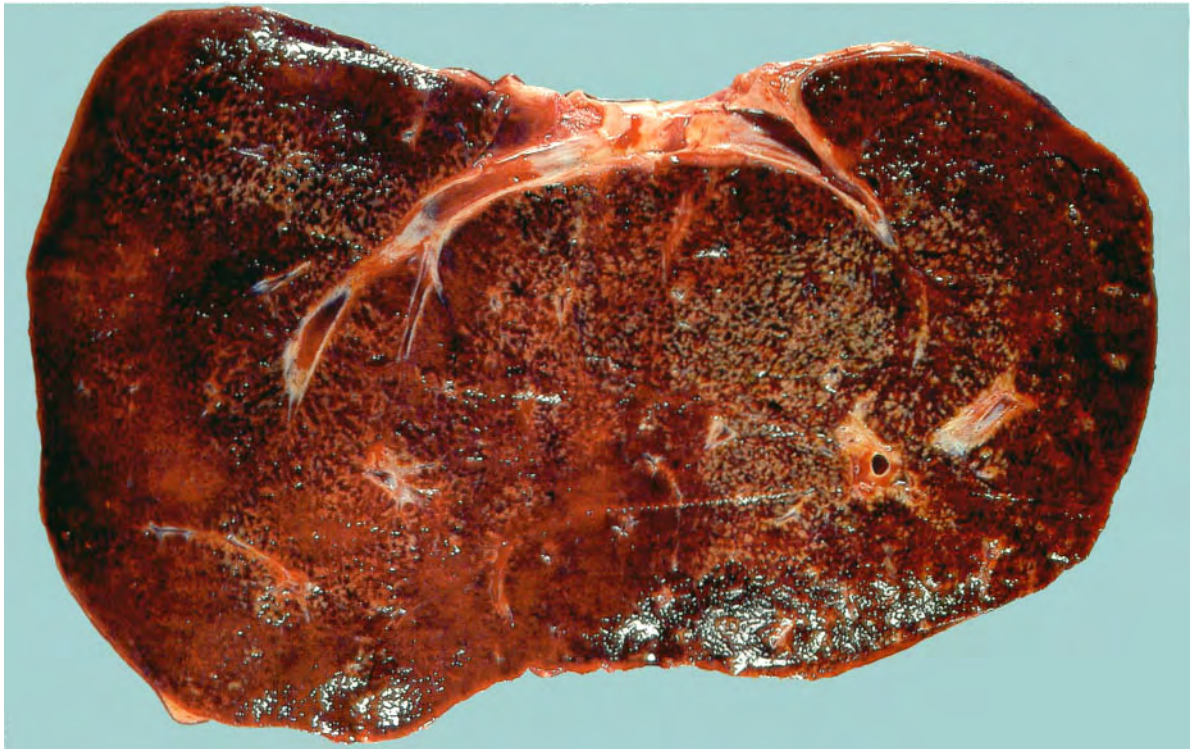


Fig. 5.36



Fig. 5.37



Fig. 5.38

Fig. 5.35 Liver showing the effects of long-standing cardiac failure resulting from a cardiomyopathy. M/35. The congested centrilobar areas are red. The creamy nodular areas are accentuated portal tracts and foci of regenerating hepatocytes.

Fig. 5.36 Budd–Chiari syndrome. F/21. The liver has been sliced coronally, with the caudate lobe in the middle. Thrombus can be seen in the hepatic veins. This caused obstruction, which resulted in venous congestion of the liver, most marked in the caudate lobe.

Fig. 5.37 Recent infarction in the liver. M/48. At postmortem there was a thrombus in the right hepatic artery.

Fig. 5.38 Subcapsular and intrahepatic haematoma. F/79. Bleeding had occurred from an intrahepatic vascular malformation. Such haematomas occur more frequently as a result of blunt trauma to the abdomen.



Fig. 5.39

0 cm 5



Fig. 5.40

0 cm 5

Fig. 5.39 Congenital polycystic liver. M/54. This was associated with polycystic kidneys and the patient died from renal failure.

Fig. 5.40 Massive necrosis of the liver. F/67. The patient died 3 months after an attack of acute hepatitis. In the upper half of the specimen the capsule is intact and multiple yellow areas can be seen through it. The lower half shows a cut surface. On the left there is an area of complete necrosis of hepatocytes, with condensation of the connective tissue (arrow). The

remainder of the cut surface shows small, yellow nodules of regenerating hepatocytes.

Fig. 5.41 Suppurative cholangitis. F/45. The patient died from liver failure due to extrahepatic obstruction caused by carcinoma of the head of the pancreas. The dilated bile ducts are filled with green, bile-stained pus.

Fig. 5.42 Liver abscesses. F/87. This patient died from Gram-negative septicaemia and the abscesses are a complication of this. The site of the original infection was not found.

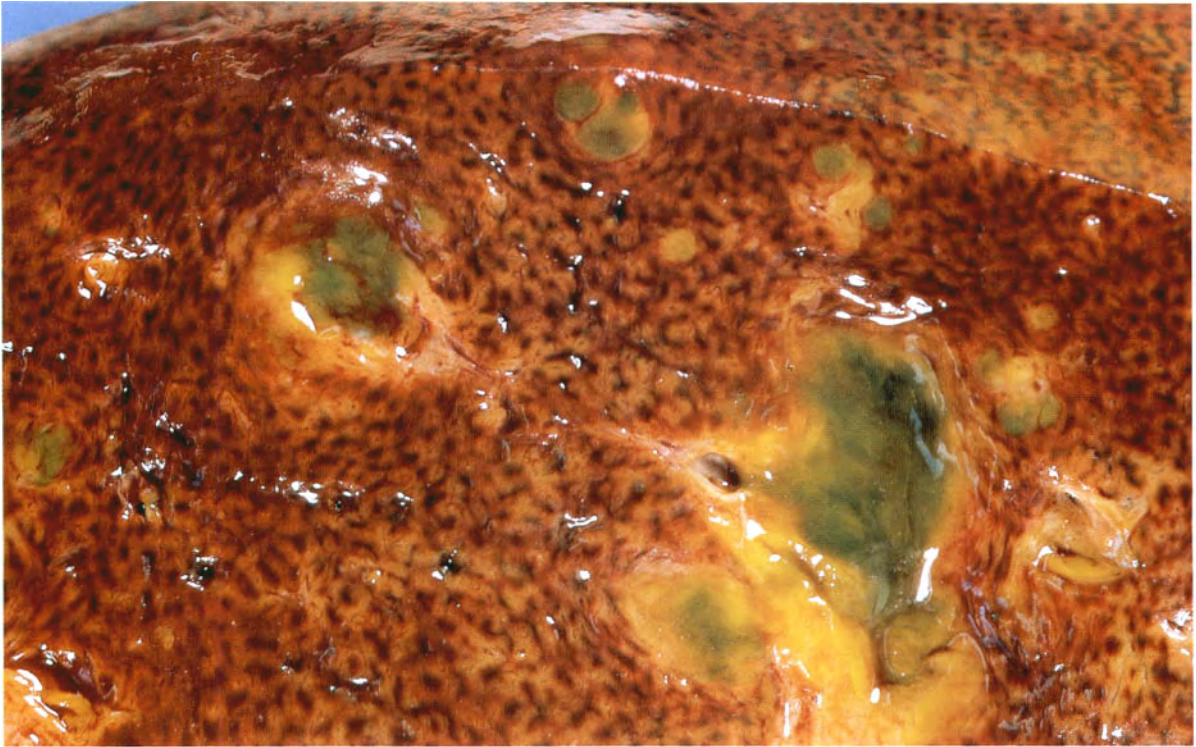


Fig. 5.41

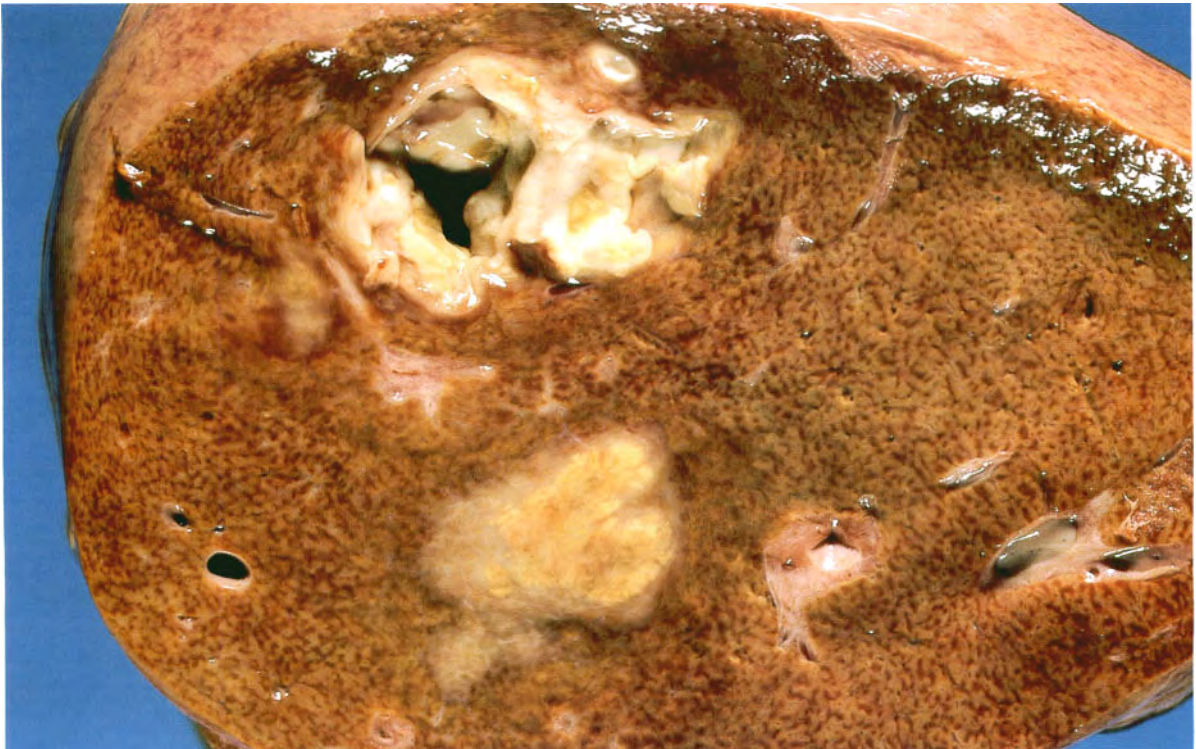


Fig. 5.42

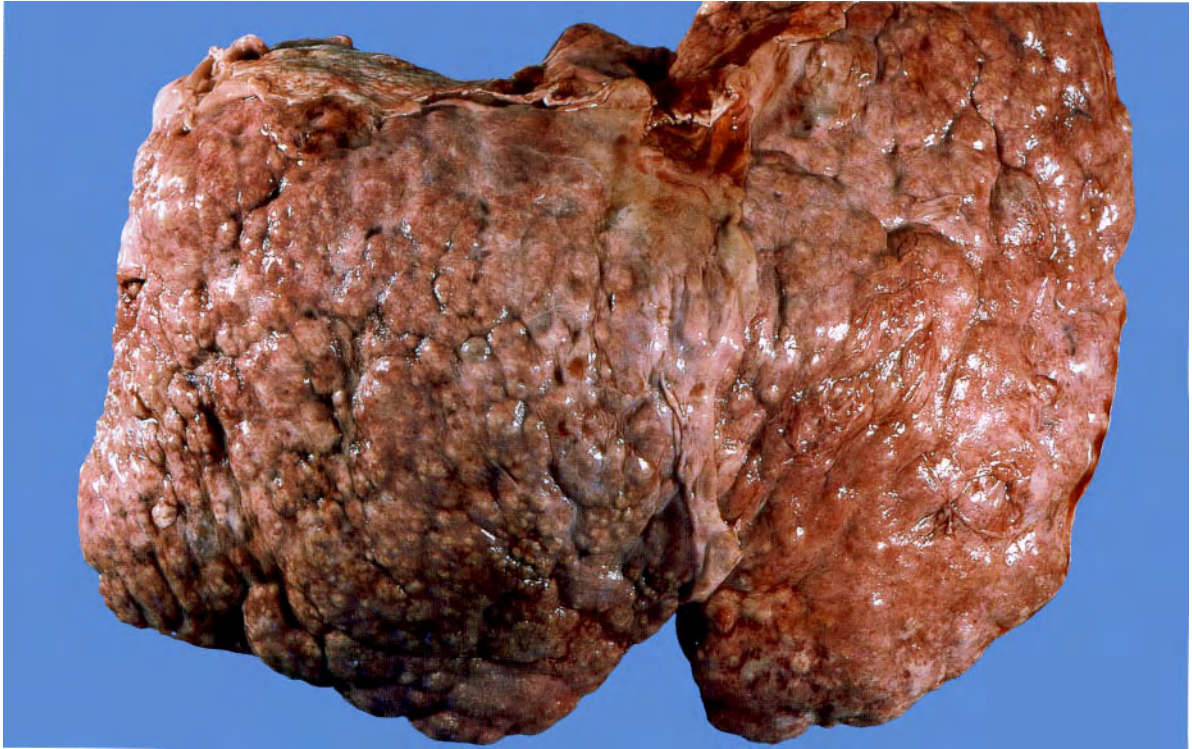


Fig. 5.43

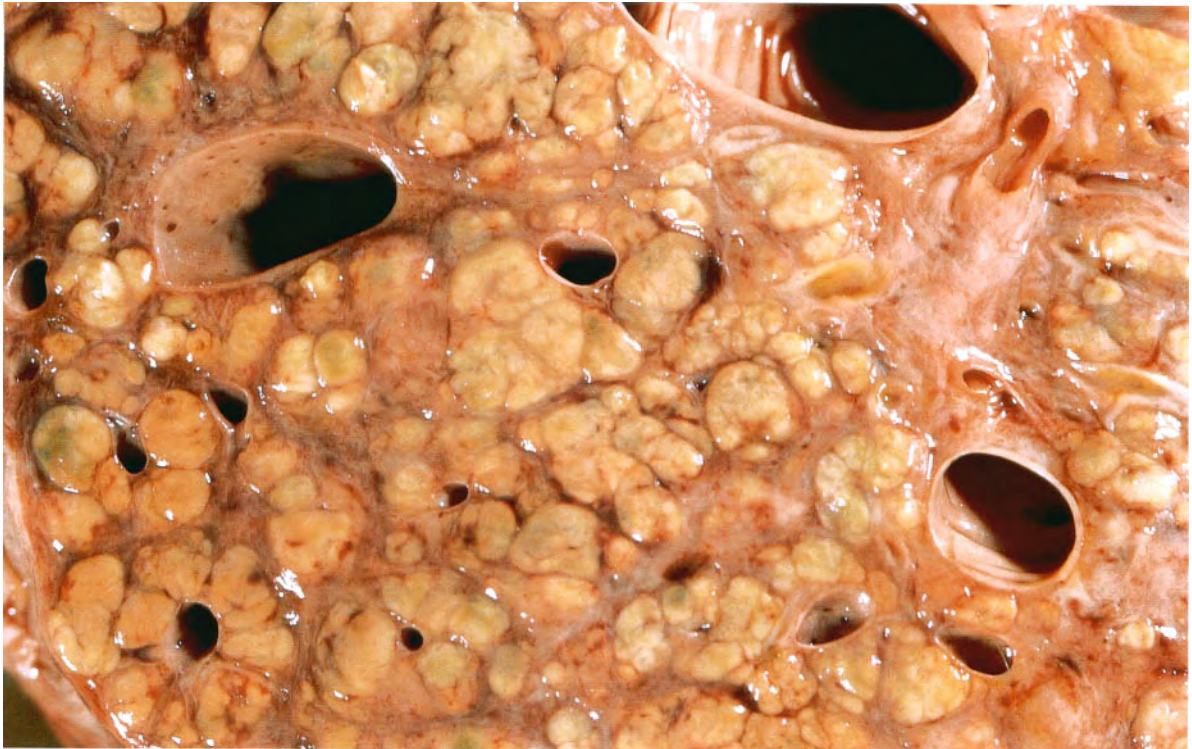


Fig. 5.44



Fig. 5.45

Fig. 5.43 Macronodular cirrhosis. M/39. The liver is greatly enlarged and weighed 1720 g. Its surface is coarsely nodular. This type of cirrhosis is common in populations with a high incidence of hepatitis B infection.

Fig. 5.44 Cut surface of the specimen in Figure 5.43.

Fig. 5.45 Micronodular cirrhosis and congestive cardiac failure. Livers from two chronic alcoholics of similar age. One died from 'alcoholic cirrhosis' and the other from 'alcoholic cardiomyopathy'. The cirrhotic liver is pale and fatty and its architecture is replaced by multiple small nodules. Compare the appearances of this type of cirrhosis with those in Figures 5.43 and 5.44.

Fig. 5.46 Subdiaphragmatic abscess. M/50. The right leaf of the diaphragm has been partially removed to demonstrate the pus on the upper surface of the right lobe of the liver. This was a complication that followed surgery to the patient's biliary tract.

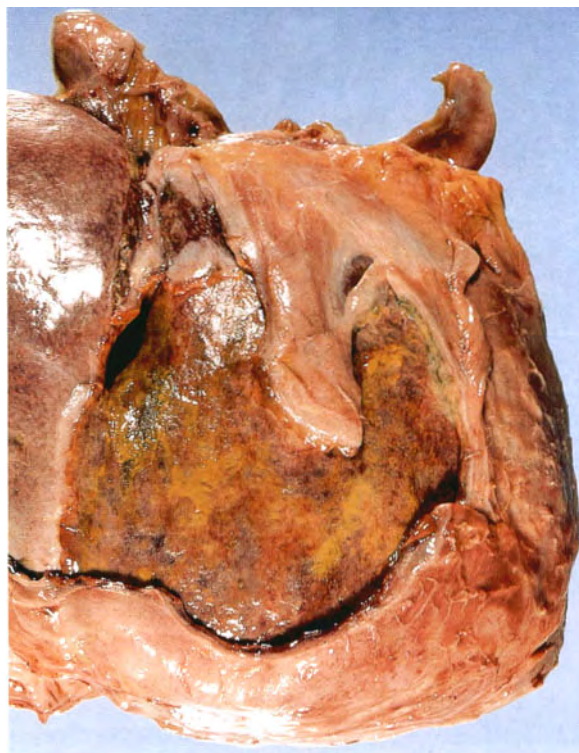


Fig. 5.46

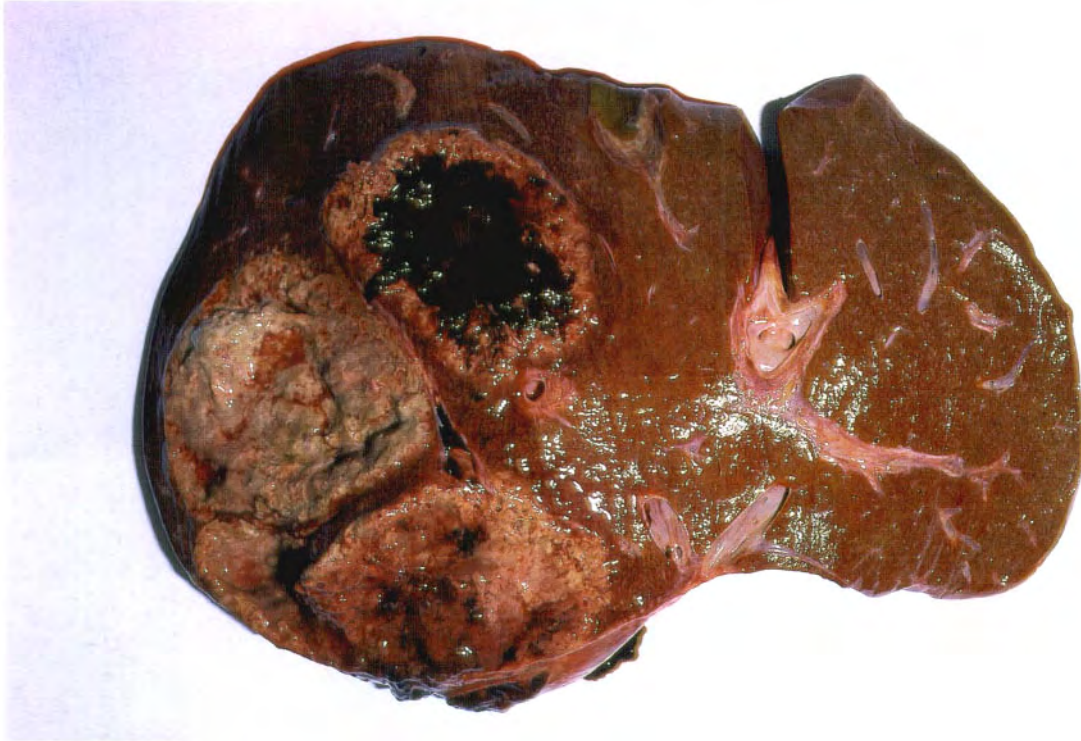


Fig. 5.47



Fig. 5.48

Fig. 5.47 Amoebic abscess of the liver. M/49. There are three distinct loculi in this abscess, which occupied most of the right lobe of the liver. The abscess was drained and a large amount of brown pus (anchovy sauce pus) was removed (see Figure 5.48). During treatment the patient suddenly developed pericardial effusion and died.

Fig. 5.48 Brown pus removed from the amoebic abscess of the liver shown in Figure 5.47.

Fig. 5.49 Hydatid cyst of the liver. M/53. The patient had lived in a sheep-raising area of Australia, but this was an incidental postmortem finding. The outer, thick fibrotic wall of the cyst is clearly seen and the cyst is filled with multiple daughter cysts of varying sizes.

Fig. 5.50 *Clonorchis sinensis* infestation of the liver. Korean seaman aged 35 years. The whole of the intrahepatic biliary system is filled with flukes. There is some thickening of the walls of the intrahepatic bile ducts, but the infestation appeared to be essentially asymptomatic.

Fig. 5.51 *Clonorchis sinensis* fluke (×10) removed from the specimen in Figure 5.50.

Fig. 5.52 *Hepar lobatum*. M/70. There was no other evidence of syphilis.



Fig. 5.49

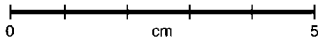


Fig. 5.50

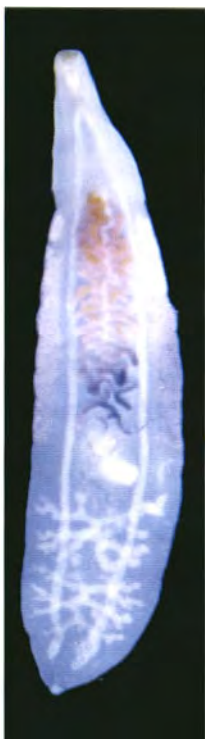


Fig. 5.51



Fig. 5.52

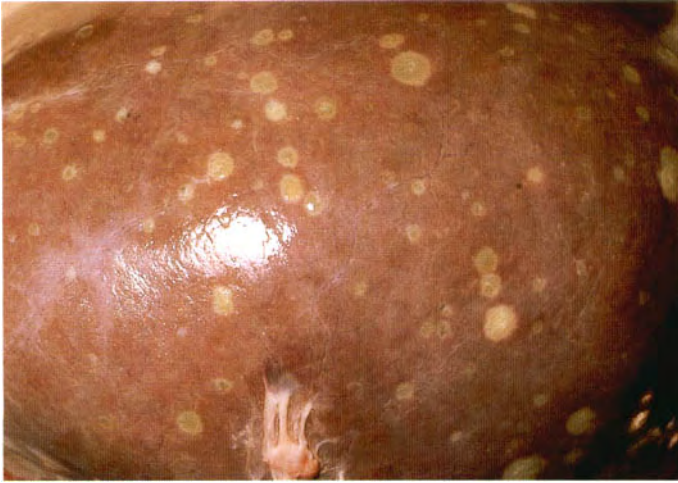


Fig. 5.53

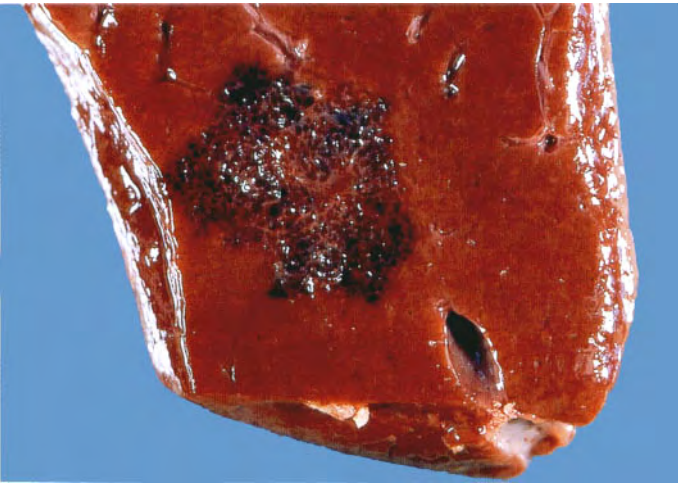


Fig. 5.54

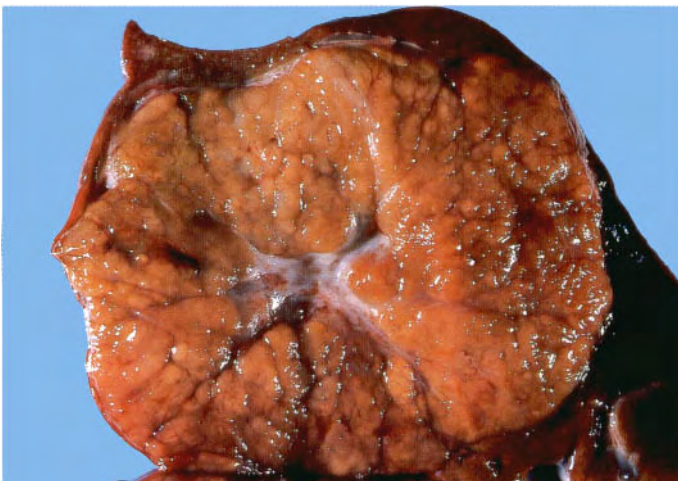


Fig. 5.55

Fig. 5.53 Multiple bile duct hamartomas. F/54. Microscopically these creamy nodules consist of proliferations of bile ducts. The condition is of no clinical significance. When a liver with this appearance is seen during surgery for bowel cancer, the surgeon often wonders whether they are secondary deposits of tumour. One or two of them are often biopsied to check that they are not secondaries.

Fig. 5.54 Haemangioma in the liver. M/40. This was an incidental postmortem finding. Occasionally these haemangiomas may bleed, as in Figure 5.38, but mostly they are asymptomatic.

Fig. 5.55 Focal nodular hyperplasia. F/25. This tumour presented as an upper abdominal mass, and was treated by local resection. This well circumscribed mass in the liver is a benign lesion. It is regarded as being a hamartoma and is distinguished from a true adenoma by the presence of the central stellate scar, which contains bile ductules. This is a large example of FNH. The abnormal areas are usually multiple and smaller than this one.

Fig. 5.56 Hepatocellular carcinoma. M/17. This is an example of a large, single lesion. It was treated by local resection. The liver is not cirrhotic and there is no obvious cause for the HCC. Grossly, the differential diagnosis of this lesion is benign hepatoma (an adenoma). The final diagnosis depends on the microscopic appearances. Benign hepatomas occur in non cirrhotic livers, and occur especially in women of reproductive age who are taking contraceptive medication. The most common presentation is with haemorrhage into the tumour.

Fig. 5.57 Hepatoblastoma. F/12 weeks. This tumour presented as a large upper abdominal mass. It was treated by partial hepatectomy. Its cut surface shows a creamy neoplasm with multiple cystic areas. These tumours sometimes secrete endocrine substances and their first presentation may be with endocrine abnormalities.



Fig. 5.56

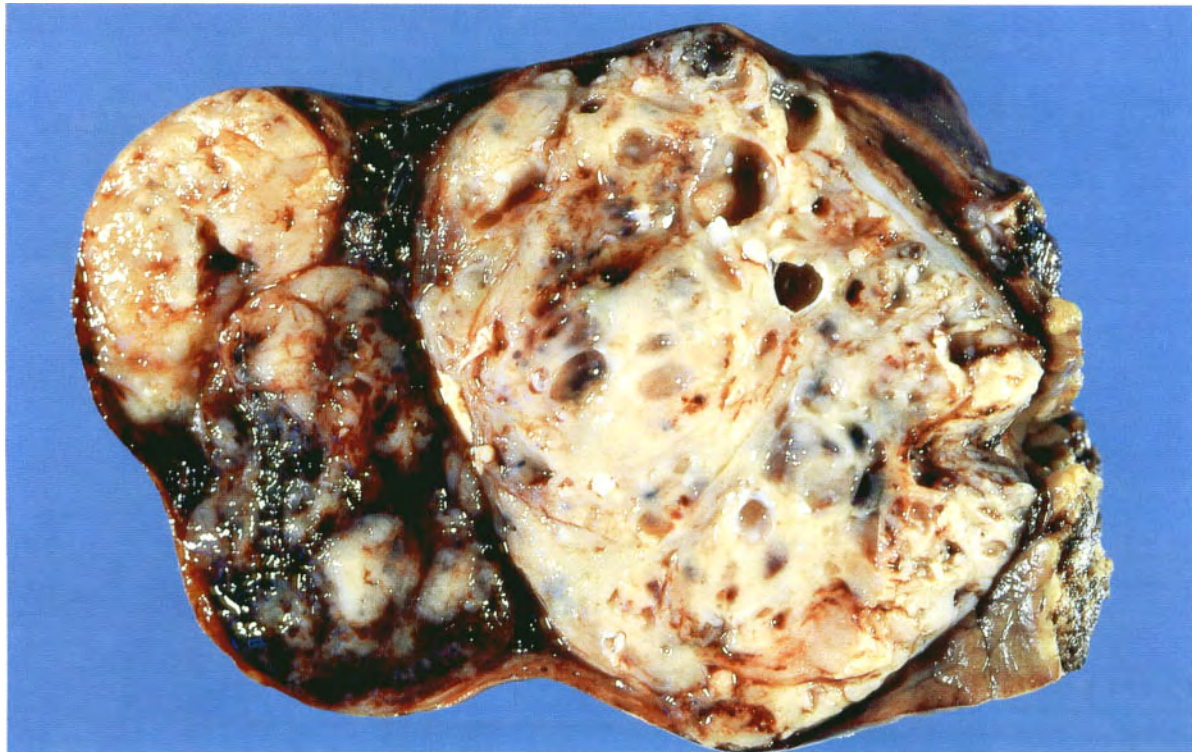
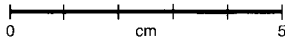
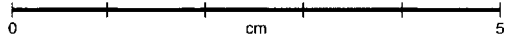


Fig. 5.57



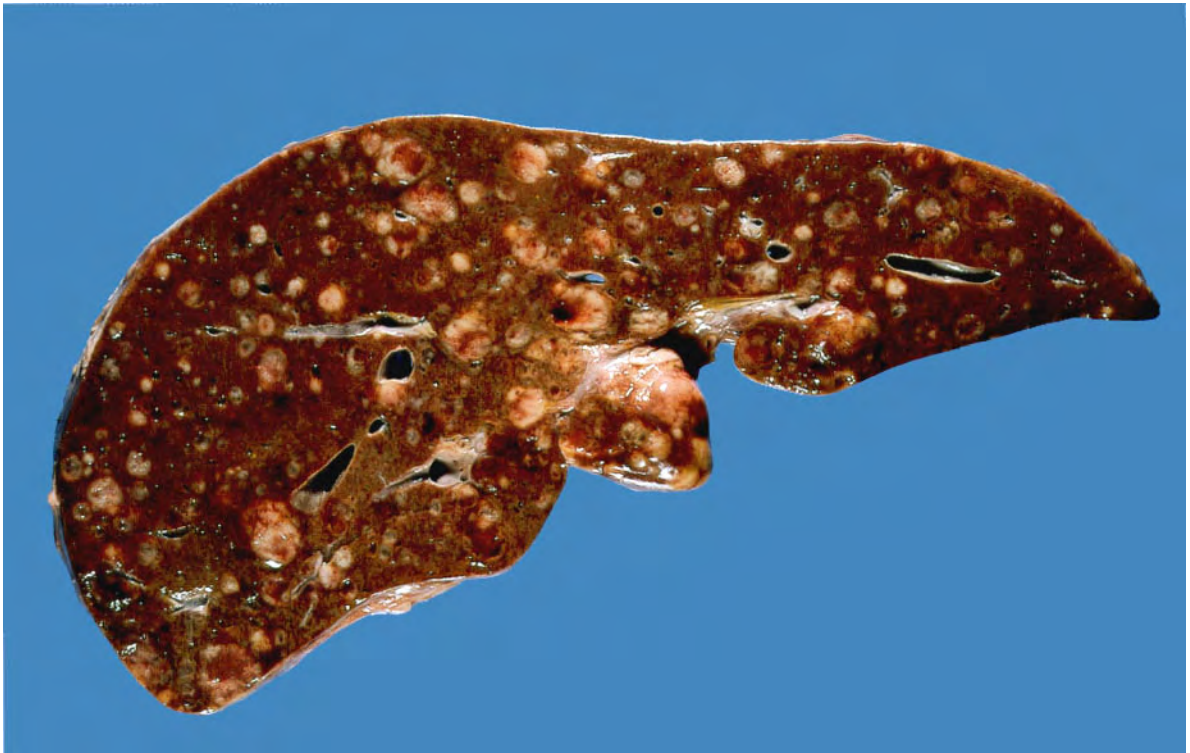


Fig. 5.58

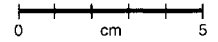


Fig. 5.58 Secondary tumour in the liver. M/68. There are multiple secondaries in both right and left lobes, and in the caudate lobe. The primary was a bronchogenic carcinoma of the lung.

RENAL SYSTEM

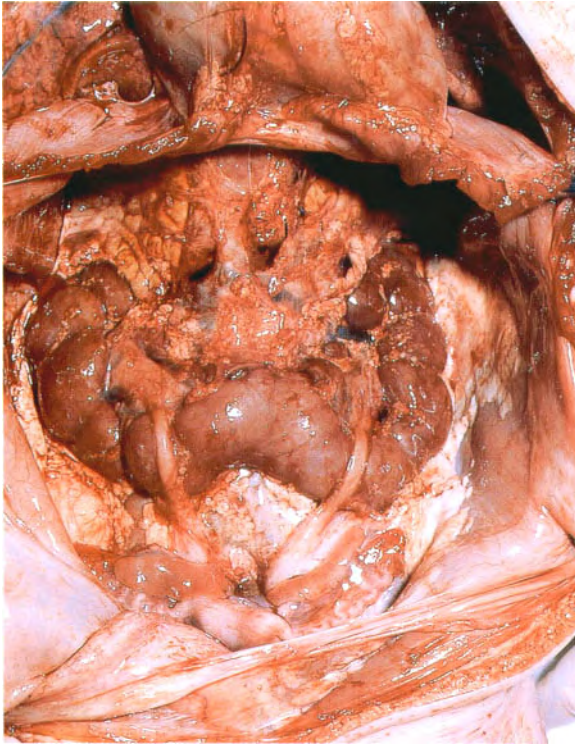


Fig. 6.1



Fig. 6.2



Fig. 6.3

0 cm 5



Fig. 6.4

0 cm 5



Fig. 6.5



Fig. 6.6

Fig. 6.1 Horseshoe kidney. F/9 days. The lower poles of both kidneys are joined across the midline and the ureters pass anterior to the renal substance. This child died as a result of multiple congenital abnormalities.

Fig. 6.2 Double ureters. Neonate. Both ureters are bifid and join to form a single ureter before opening into the bladder.

Fig. 6.3 Megaloureter. M/11. This was caused by stenosis at the ureterovesical junction. The patient had recurrent urinary tract infections, and finally the kidney and ureter were surgically removed.

Fig. 6.4 Triple ureter. Neonate. Double ureters are fairly common, but triple ureter is very rare.

Fig. 6.5 Polycystic disease of the kidneys. M/54. The kidney substance is almost completely replaced by cysts of varying size. The kidneys may be not much bigger than normal, but usually they are quite large.

Fig. 6.6 Cut surface of specimen in Figure 6.5, showing the cysts with very little normal renal tissue remaining. Polycystic kidneys characteristically cause symptoms of hypertension or renal failure after the age of 40 years. In women they may be diagnosed at an earlier age during antenatal investigations, either as palpable masses or as impaired renal function.

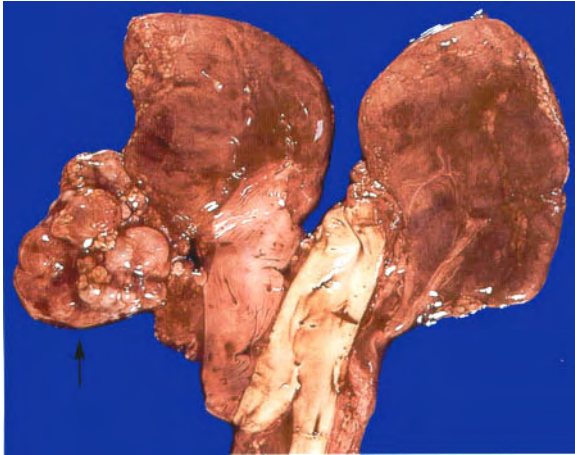


Fig. 6.7

0 cm 5



Fig. 6.8



Fig. 6.9

0 cm 5



Fig. 6.10

0 cm 5



Fig. 6.11

Fig. 6.7 Cystic dysplastic kidney. Stillborn. There is a very small multicystic kidney on the right (arrow) and no kidney on the left. The adrenal glands are relatively large in neonates, but they are accentuated in this case because of the very small size of the kidney.

Fig. 6.8 Cystic dysplastic kidney. F/24 hours. The right kidney is normal but the left is grossly cystic. Microscopic examination showed malformed renal substance together with areas of cartilage. Cystic dysplastic kidney may be unilateral or bilateral.

Fig. 6.9 Multiple simple cysts in the kidney. M/70. This was an incidental postmortem finding.

Fig. 6.10 Sponge kidney in a neonate who died a few minutes after birth. This type of cystic kidney is usually large and bilateral and may interfere with delivery of the fetus.

Fig. 6.11 Ureteritis cystica. M/80. Incidental autopsy finding. This condition may be associated with chronic urinary tract infection.

Fig. 6.12 Multicystic kidneys resulting from long-term haemodialysis for chronic renal disease. M/68.

Fig. 6.13 Hydatid cyst of the kidney. M/10. The unruptured, white laminated membrane of the cyst can be seen in the upper pole. It had compressed the calyceal system, causing hydronephrosis. The kidney was removed because the clinical and radiological features resembled those of a primary renal tumour. There was no history of exposure to sheep farming.

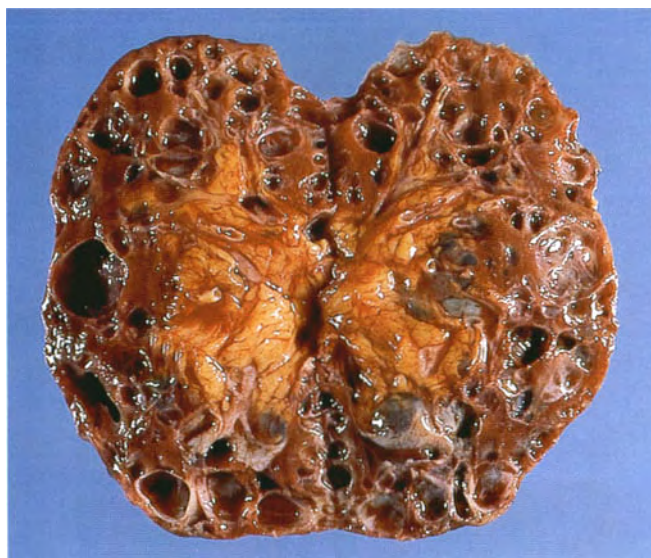


Fig. 6.12

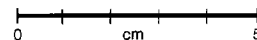
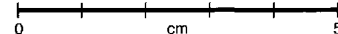


Fig. 6.13



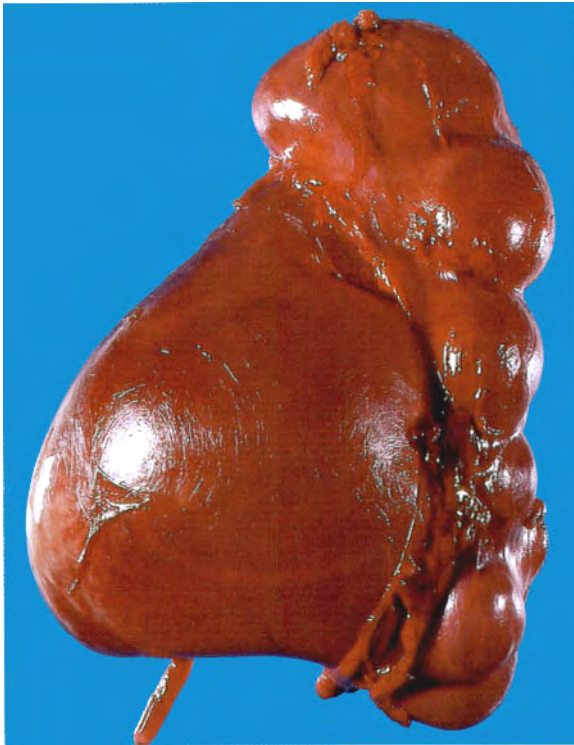


Fig. 6.14

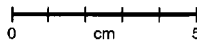


Fig. 6.15



Fig. 6.16

Fig. 6.14 Hydronephrosis due to congenital pelviureteric obstruction. F/46. There is marked dilatation of the renal pelvis and atrophy of renal substance. The upper end of the ureter is atrophic and its lumen was microscopic. The patient had experienced no symptoms until just prior to the nephrectomy, when she presented with abdominal pain.

Fig. 6.15 Hydronephrosis. F/73. There is marked dilatation of all of the calyces, with atrophy of the renal papillae. These are the results of ureteric obstruction, which in this case was caused by a transitional cell carcinoma of the bladder.

Fig. 6.16 'Uric acid infarcts'. Neonate. The yellow streaks in the renal papillae are due to the deposition of uric acid crystals. This does not appear to have any clinical significance.

Fig. 6.17 Multiple renal cortical infarcts. M/15 months. The creamy areas of infarction are surrounded by areas of haemorrhage. The renal damage resulted from a sudden drop in blood pressure following haemorrhage.

Fig. 6.18 Renal tubular necrosis. M/8 weeks. The tubular necrosis is shown by the presence of haemorrhagic streaking in the medulla and renal papillae. It was a complication of peritonitis.

Fig. 6.19 Infarction of the kidney due to thrombosis of the renal vein. M/10 months. The whole kidney was infarcted. The child was severely dehydrated due to gastroenteritis. Thrombosis of renal, pulmonary or cerebral veins may occur as a complication of dehydration in children.

Fig. 6.20 Infarction of the kidney caused by thrombosis of a large branch of the renal artery. M/55. The infarcted area has become discoloured and depressed below the adjacent kidney surface. The thrombus was a complication of atherosclerosis of the renal artery.

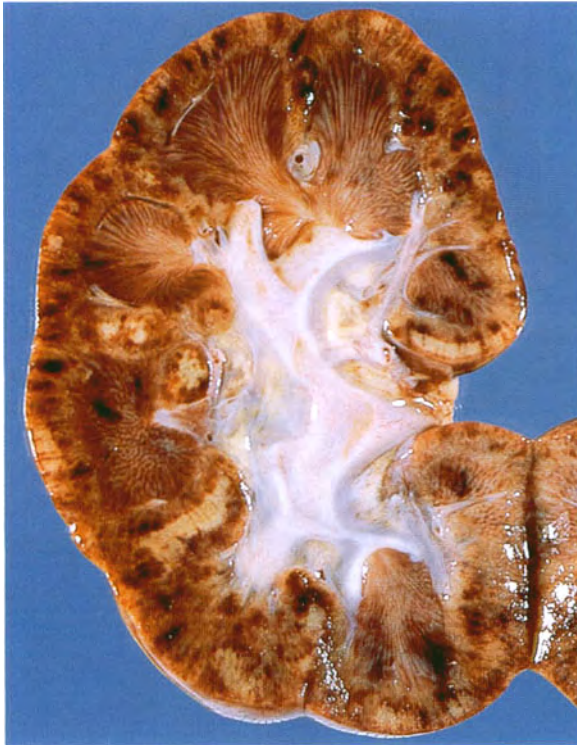


Fig. 6.17

0 cm 1



Fig. 6.18



Fig. 6.19

0 cm 5



Fig. 6.20

0 cm 5

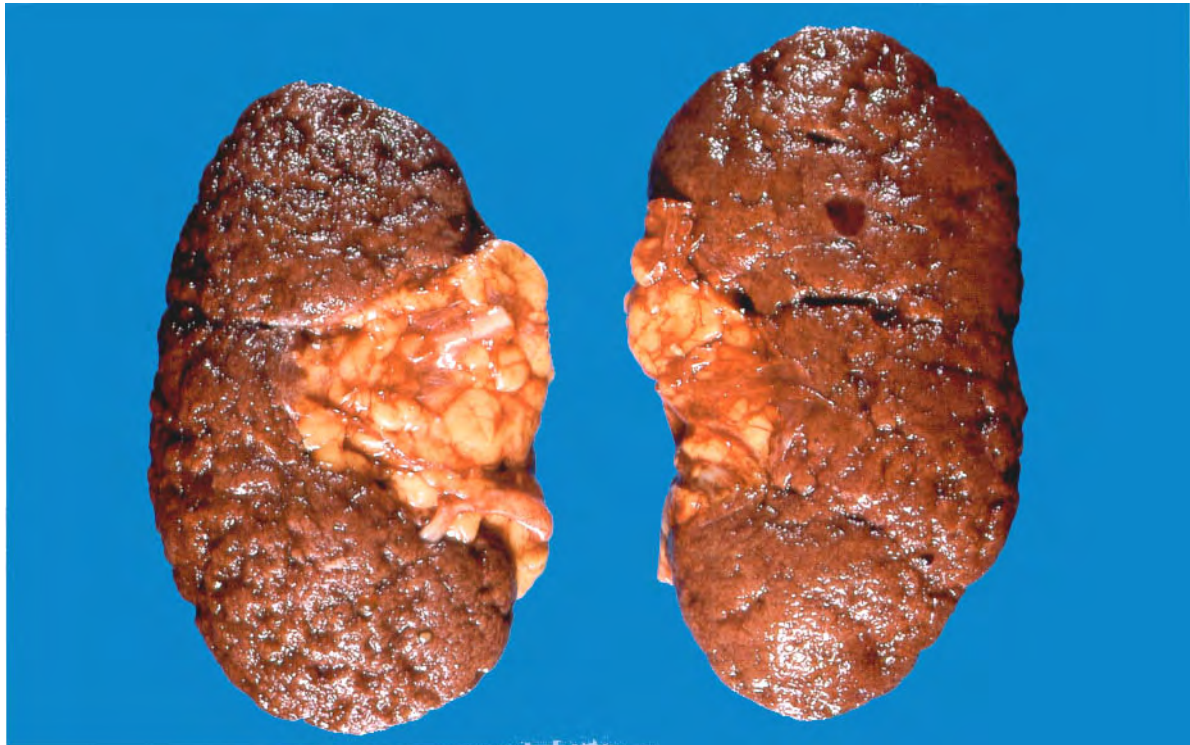


Fig. 6.21

0 cm 5

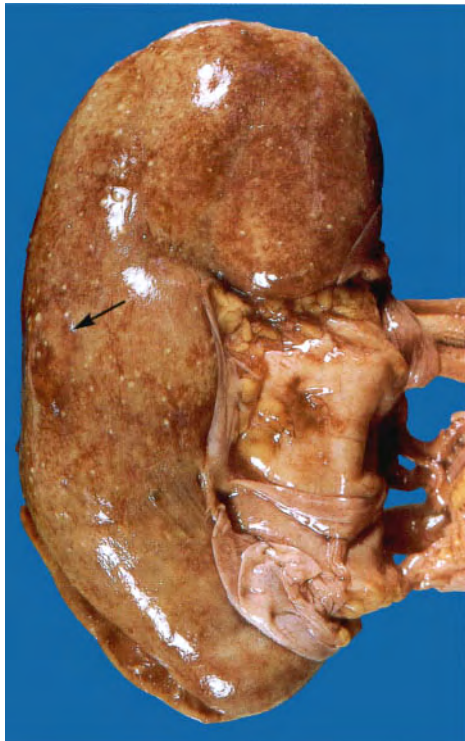


Fig. 6.22

0 cm 5

Fig. 6.21 Benign nephrosclerosis. M/77. Both kidneys are slightly reduced in size. The capsular surface is nodular. This resulted from atherosclerosis of the renal arteries.

Fig. 6.22 Acute pyelonephritis. F/71. The outer surface of the kidney shows multiple creamy spots. These are abscesses, and when the capsule is stripped from the cortical surface pus is released from the most superficial of them.

Fig. 6.23 Acute pyelonephritis. M/58. The cut surface of the kidney shows reddening of the mucosa of the calyceal system. There are multiple yellow abscesses throughout the renal cortex, which itself appears to be hyperaemic.

Fig. 6.24 Diabetic kidneys with pyelonephritis and papillary necrosis. M/47. Infection is an important complication of diabetes and renal infection may sometimes cause death, as in this case.



Fig. 6.23

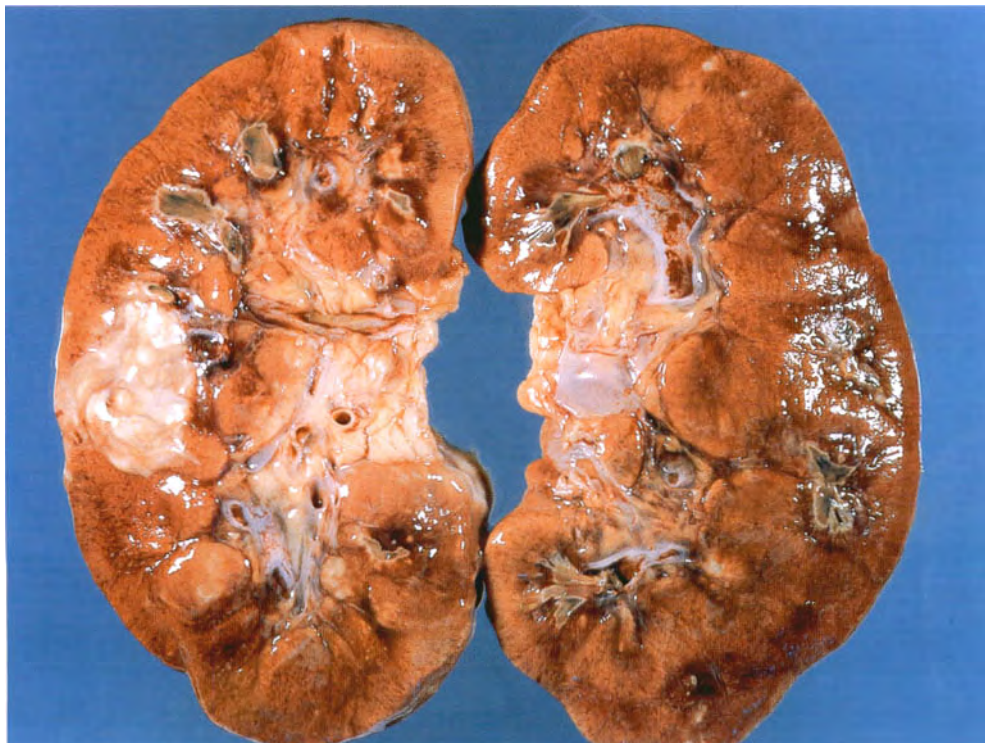


Fig. 6.24

0 cm 5



Fig. 6.25



Fig. 6.26

0 cm 5



Fig. 6.27



Fig. 6.28

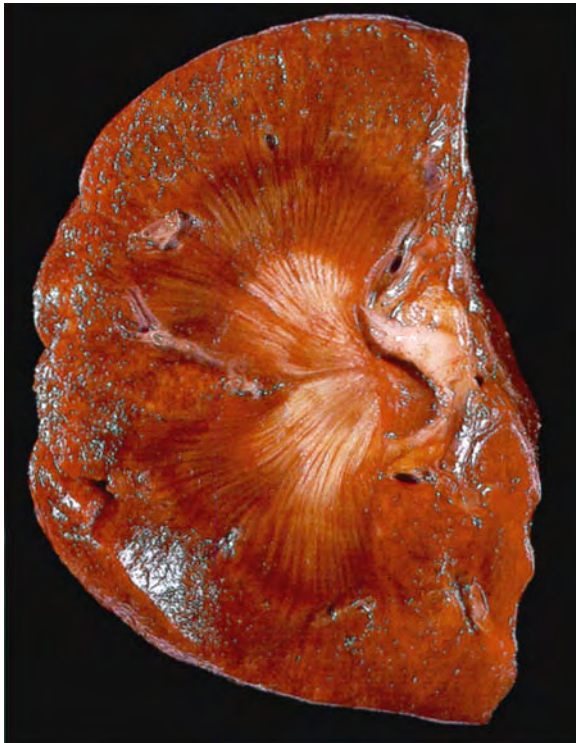


Fig. 6.29

Fig. 6.25 Xanthogranulomatous pyelonephritis. F/60. The kidney is opened to show the features of acute pyelonephritis already displayed in Figure 6.23, together with large areas of haemorrhage and lipid accumulation. These features occur in a small percentage of cases of pyelonephritis, but do not appear to have any special significance.

Fig. 6.26 Pyonephrosis. M/26 weeks. This child had congenital abnormalities of the lower urinary tract which predisposed to infection. As well as acute pyelonephritis there is a large amount of pus in the calyceal system.

Fig. 6.27 Nephrolithiasis and hydronephrosis. F/42. Fragments of a staghorn calculus are impacted in the calyces at the upper pole of the kidney.

Fig. 6.28 Renal tuberculosis. M/28. In the lower third of the kidney there is a caseous inflammatory mass extending through the whole thickness of the renal cortex. Numerous acid-fast bacilli were demonstrated in the microscopic sections. This patient presented with the classic symptom of painless haematuria. Investigations confirmed the diagnosis of tuberculosis, and nephrectomy was performed.

Fig. 6.29 Early analgesic nephropathy. F/54. There is a heavy deposition of lipid in the renal papillae. The remainder of the kidney is still relatively normal.

Fig. 6.30 More advanced analgesic nephropathy. M/60. There is acute necrosis of the renal papillae, especially in the lower pole, and shrinkage and scarring of the renal substance is beginning.



Fig. 6.30



Fig. 6.31

Fig. 6.31 Advanced analgesic nephropathy. F/41. The kidneys are small and irregularly scarred. The renal papillae have virtually all disappeared and the cortex is very thin.

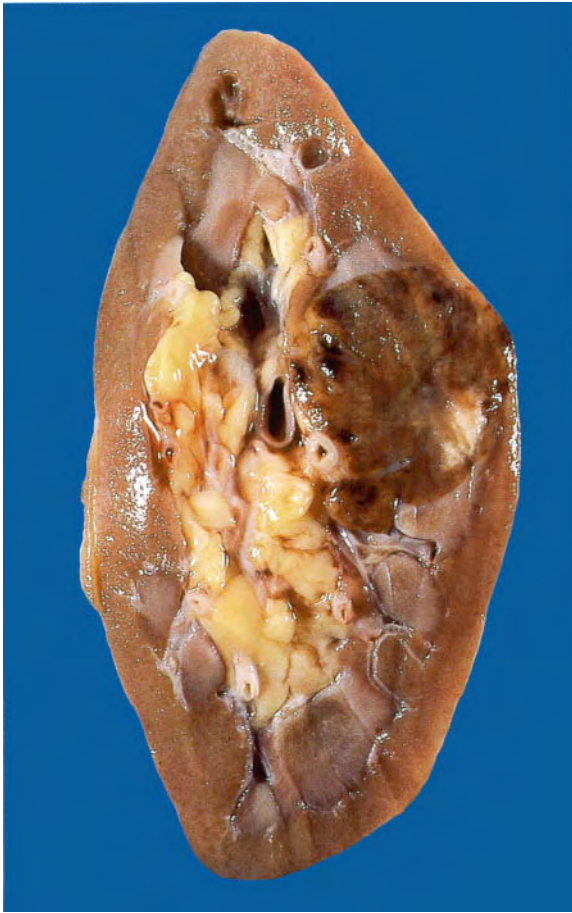


Fig. 6.32

0 cm 5



Fig. 6.33

Fig. 6.32 Oncocytoma (renal tubular adenoma). M/65. Vertical slice through the middle of the right kidney. In the anterior portion of the right upper pole there is a well circumscribed spherical tumour 30 mm in diameter. It has a dark reddish-brown, homogeneous cut surface. These tumours are benign, but this kidney was removed because of a radiological diagnosis of renal carcinoma.

Fig. 6.33 Intramedullary fibroma. F/58. This is a small, pale, benign tumour which causes no clinical symptoms and is frequently found in examination of postmortem kidneys.



Fig. 6.34

0 cm 5

Fig. 6.34 Kidneys in acute lymphoblastic leukaemia. F/3. The kidneys are pale because of the anaemia. The normal architecture has been replaced by an infiltration of creamy, haemorrhagic tissue. The kidneys have been enlarged by this infiltrate.

Fig. 6.35 Wilms' tumour. F/5. The tumour occupies the whole upper pole of the kidney. Its cut surface shows some firm, homogeneous areas and other areas of necrosis.

Fig. 6.36 Renal cell carcinoma. There is a well circumscribed, spherical tumour 30 mm in diameter bulging through the cortical surface of the kidney. Its cut surface is bright yellow. It shows solid areas, cystic areas, and areas of haemorrhage.

Fig. 6.37 Transitional cell carcinoma of the renal pelvis. These tumours frequently have a papilliferous appearance.

Fig. 6.38 Transitional cell carcinoma of the ureter. M/52. This tumour is more solid and less papillary than the one illustrated in Figure 6.37. It caused obstruction, and the ureter proximal to the tumour has become somewhat dilated.



Fig. 6.35

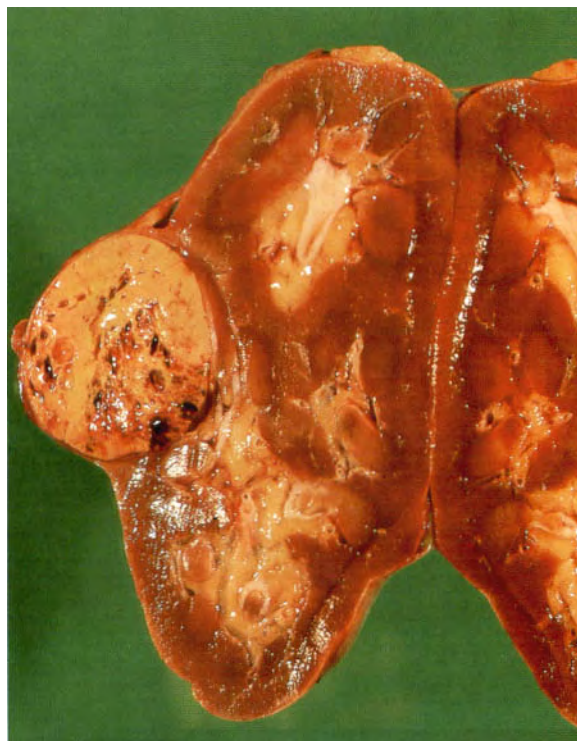
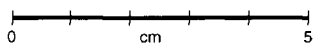


Fig. 6.36

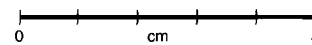


Fig. 6.37

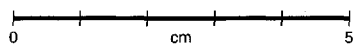


Fig. 6.38

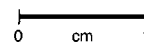




Fig. 6.39

Fig. 6.39 Carcinoma of the bladder. M/88. The entire mucosal surface is replaced by a transitional cell carcinoma. It has caused obstruction with bilateral hydroureter and hydronephrosis.

Fig. 6.40 Renal calculus which has been cut and its surface polished to show its laminations.

Fig. 6.41 Ureteric calculus.

Fig. 6.42 Bossellated vesical calculus.



Fig. 6.40 0 cm 1



Fig. 6.41 0 cm 1



Fig. 6.42 0 cm 1

MALE GENITAL SYSTEM

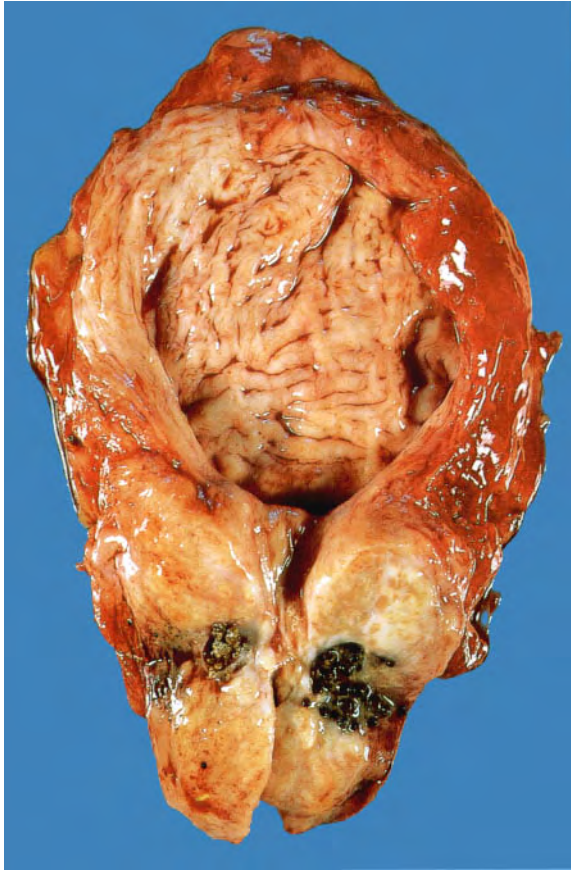


Fig. 7.1



Fig. 7.2

Fig. 7.1 Benign prostatic hypertrophy. M/84. The prostate is considerably enlarged. Its cut surface shows a creamy, lobulated appearance. There are a number of calculi in the prostatic ducts. The middle lobe has extended into the base of the bladder and the long-standing prostatic obstruction has caused thickening and trabeculation of the bladder wall.

Fig. 7.2 Bladder outlet obstruction caused by posterior urethral valves. M/6. This boy had suffered from repeated attacks of urinary tract infection since birth, and died during one of these episodes. The valves can be seen arising from the verumontanum. The bladder is hypertrophied and the mucosal surface is grossly trabeculated.

Fig. 7.3 Acute cystitis. F/36. The mucosal surface is red and inflamed. The patient had an indwelling catheter for many weeks before death from other pathology.



Fig. 7.3

0 cm 5

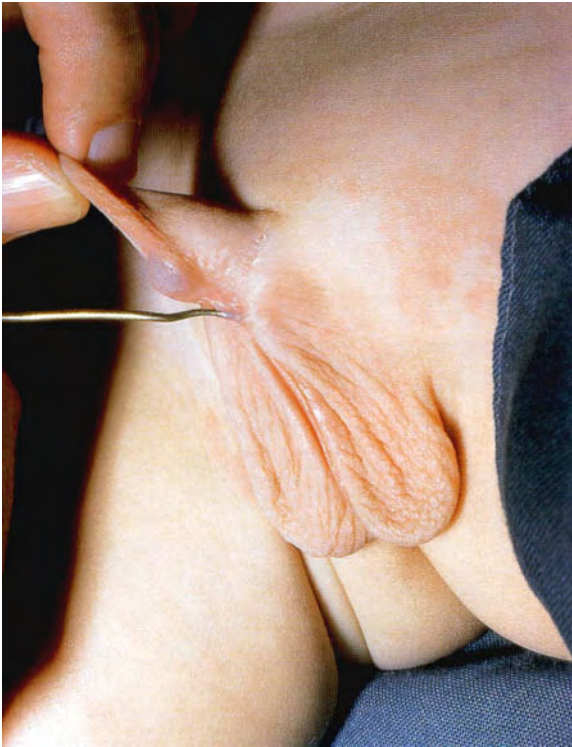


Fig. 7.4



Fig. 7.5



Fig. 7.6

Fig. 7.4 Hypospadias. M/1. The urethra opens at the base of the penis. The penis itself is short and bent.

Fig. 7.5 Epispadias. M/2.

Fig. 7.6 Phimosis. M/8. This is caused by partial stenosis of the prepuce. Urine collects under the prepuce during micturition.



Fig. 7.7

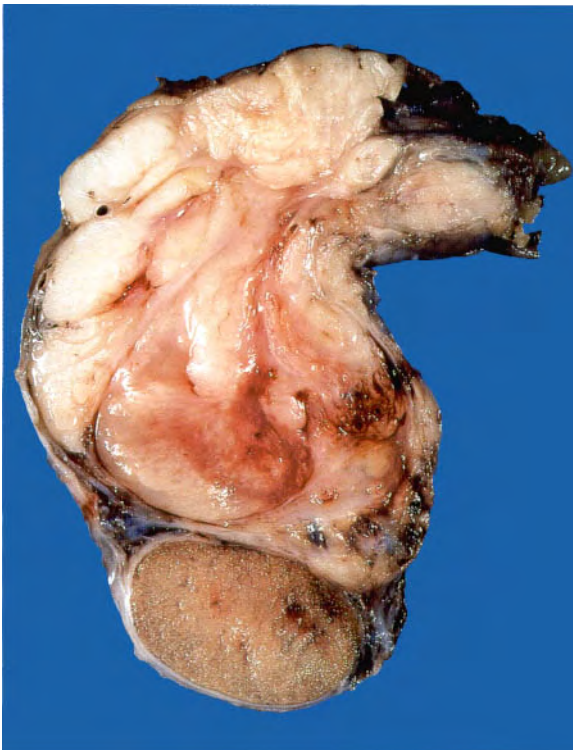


Fig. 7.8

Fig. 7.7 Squamous cell carcinoma of the penis. M/69. There is an ulcerating squamous cell carcinoma eroding the prepuce and the dorsal surface of the glans.

Fig. 7.8 Liposarcoma of the spermatic cord. M/52. This tumour had been growing slowly for at least a year. A fleshy, cream-coloured homogeneous tumour surrounds the spermatic cord. The testis is intact and normal. Microscopically, this was a low-grade liposarcoma. Local recurrence occurs unless the tumour is completely excised.

Fig. 7.9 Torsion of the testis. M/14 days. The testis is swollen, black and necrotic. The twist in the cord is demonstrated. When this occurs in babies, it presents as a lump in the scrotum. In adults it presents with sudden onset of severe pain.

Fig. 7.10 Hydrocoele. M/3 months. The tunica vaginalis is filled with clear fluid. In children, the tunica still retains its connection with the abdominal cavity.

Fig. 7.11 Chronic hydrocoele. M/56. In adults, the tunica vaginalis has lost its connection with the abdominal cavity and fluid collects locally. As time passes, the tunica becomes fibrotic and sometimes calcifies.

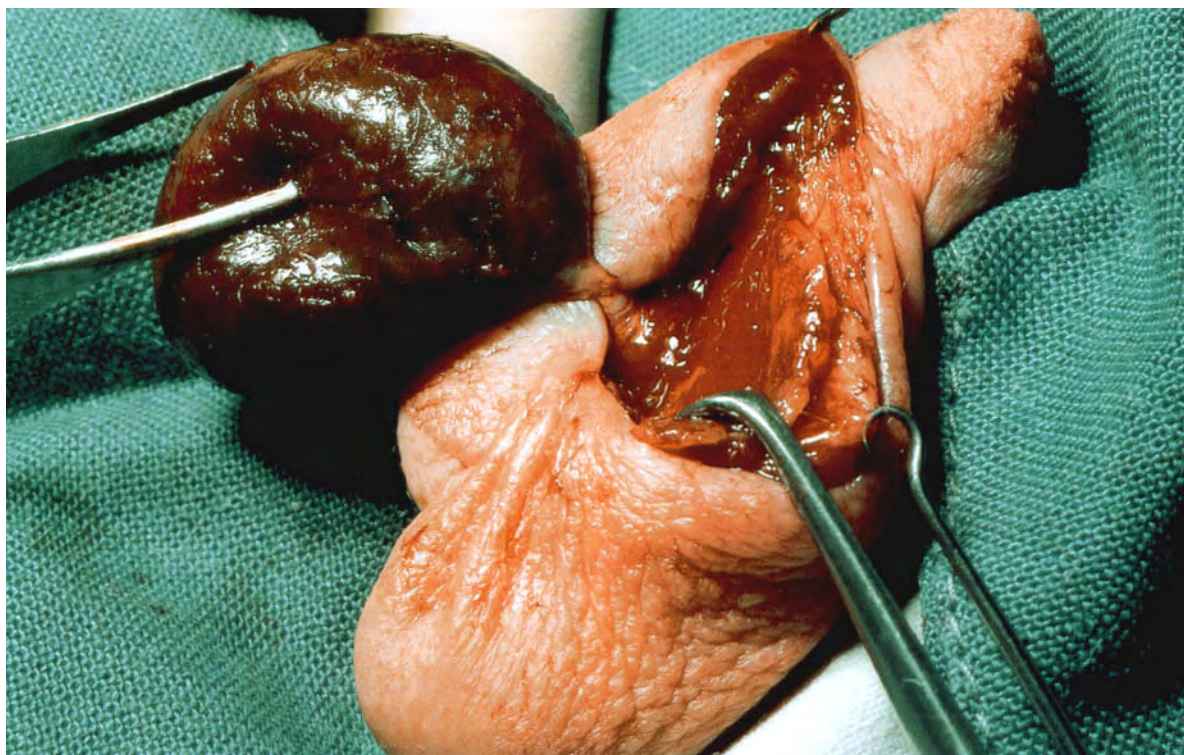


Fig. 7.9



Fig. 7.10

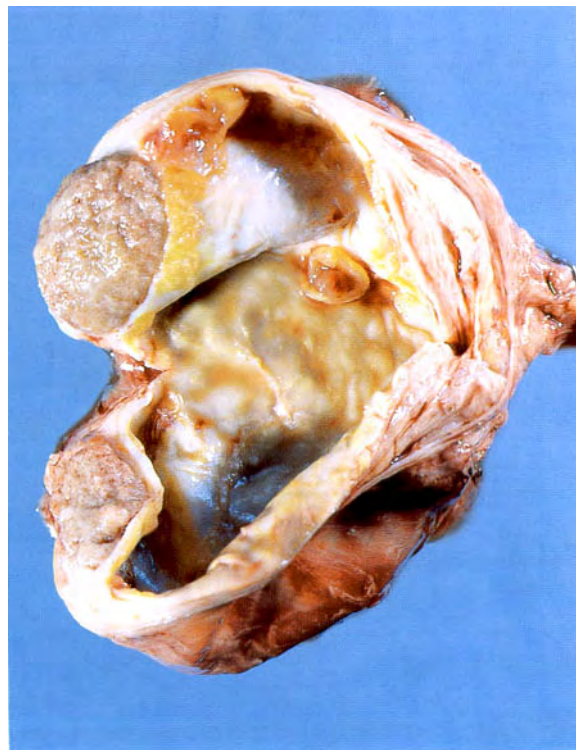


Fig. 7.11

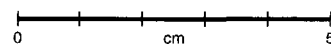




Fig. 7.12

0 cm 5



Fig. 7.13

0 cm 5



Fig. 7.14

0 cm 1

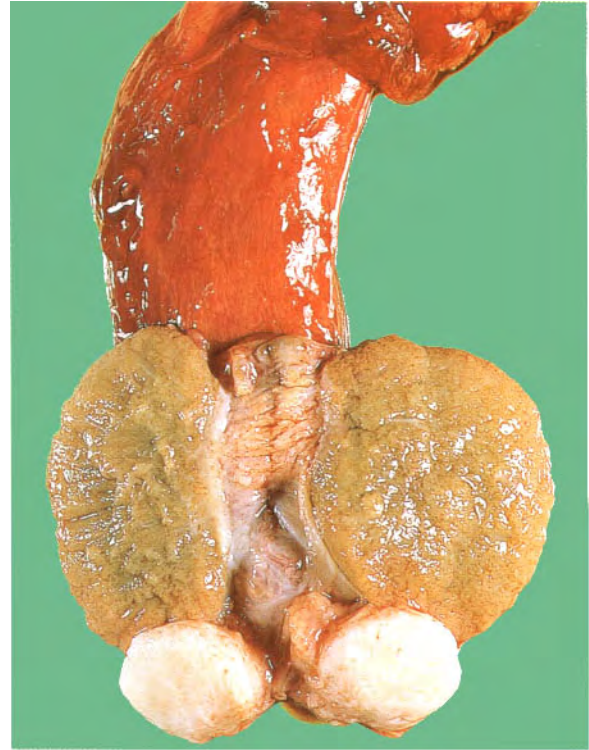


Fig. 7.15

0 cm 5



Fig. 7.16

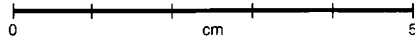


Fig. 7.17

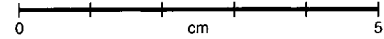


Fig. 7.12 Cyst of the epididymis. M/34. The cyst is thin walled, multiloculated and filled with clear fluid. It developed behind the testis.

Fig. 7.13 Abscess in the epididymis. M/78. Thick purulent material is replacing the epididymis. The patient presented with a mass in the scrotum.

Fig. 7.14 Tuberculosis of the testis and epididymis. M/23. The testis contains multiple rounded granulomatous lesions. The epididymis is almost completely replaced by similar tissue. The patient had disseminated tuberculosis.

Fig. 7.15 Adenomatoid tumour of the epididymis. M/54. There is a creamy, well circumscribed tumour in the epididymis.

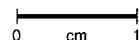
Fig. 7.16 Seminoma of the testis. M/40. The testis is enlarged and completely replaced by fleshy, lobulated, homogeneous creamy tissue.

Fig. 7.17 Combined teratoma and seminoma of the testis. M/20. The cut surface of this tumour shows some areas which are homogeneous (the seminoma) (arrow), and other areas that are necrotic and haemorrhagic (the teratoma).

Fig. 7.18 Regressing seminoma of the testis. M/26. This man died from disseminated malignancy. The main bulk of the tumour involved the para-aortic and mediastinal lymph nodes, and there were pulmonary secondaries. After careful slicing of both testes this small, creamy focus of tumour was found (arrow). Microscopically it consisted of small numbers of seminoma cells surrounded by an inflammatory cell reaction.



Fig. 7.18



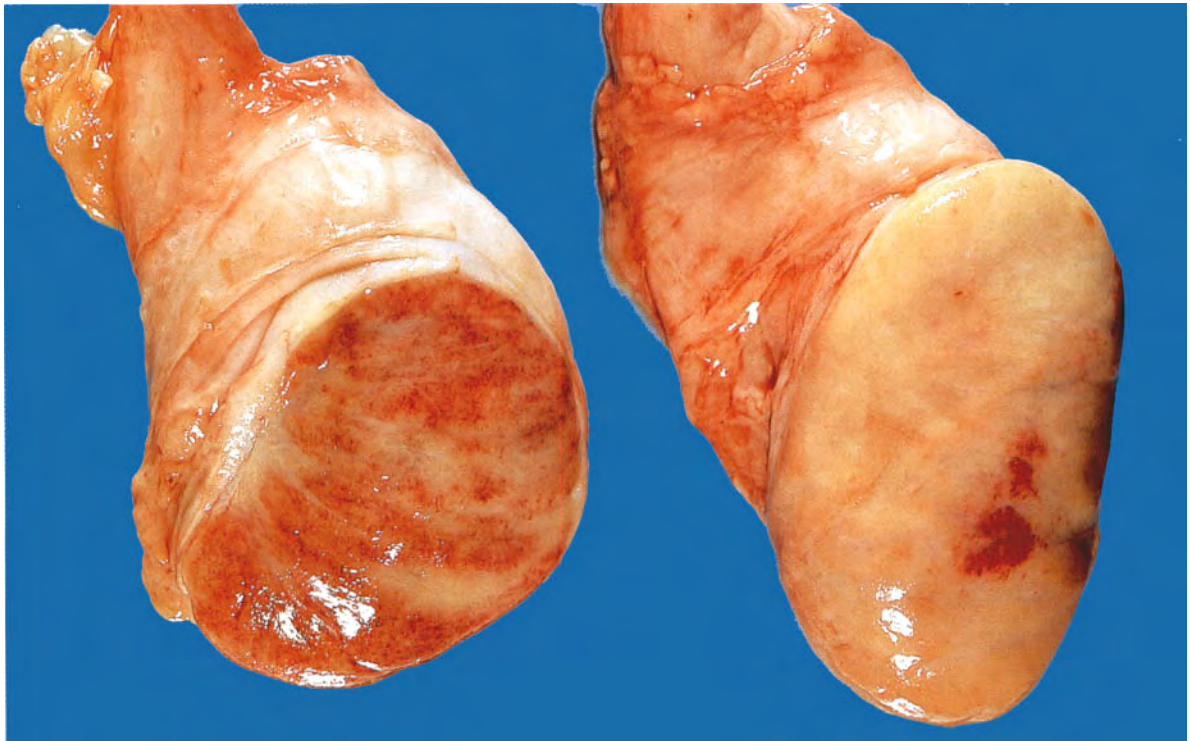


Fig. 7.19

0 cm 5

Fig. 7.19 Acute lymphoblastic leukaemia infiltrating both testes. M/12. The normal testicular tissue has been completely replaced by creamy, slightly haemorrhagic tumour tissue. When patients have responded to chemotherapeutic treatment of acute lymphoblastic leukaemia, the first manifestation of recurrence is frequently in the testes.

Fig. 7.20 Infantile embryonal carcinoma. M/9 months. The tumour has a homogeneous, creamy cut surface and has completely replaced the normal testicular tissue. This is a special type of malignant tumour of the testis that occurs in children. Its old name was orchioblastoma.



Fig. 7.20

0 cm 1

BREAST AND FEMALE GENITAL SYSTEM

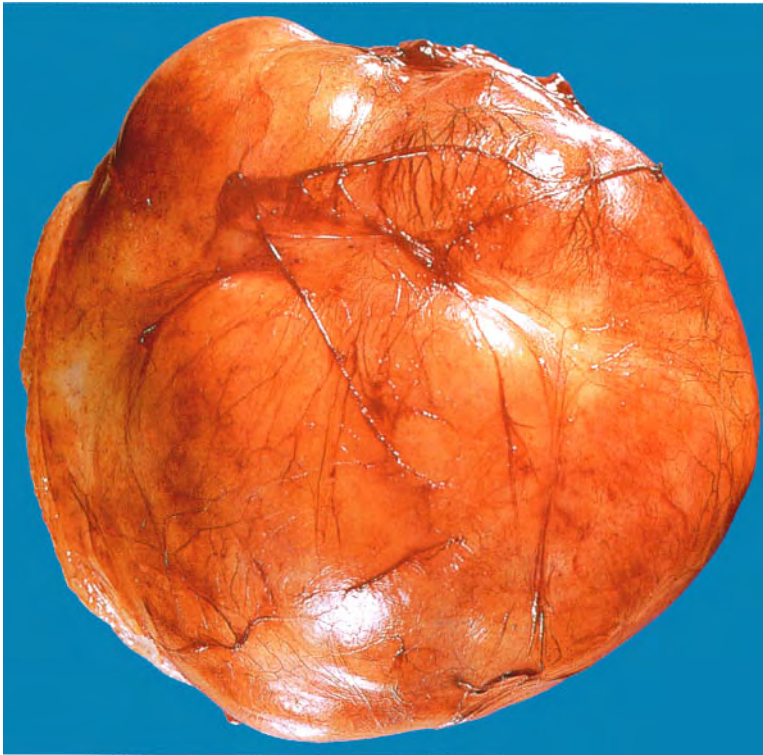


Fig. 8.1

0 cm 5



Fig. 8.2

0 cm 5

Fig. 8.1 Fibroadenoma. F/18. This well circumscribed and mobile nodule was removed surgically.

Fig. 8.2 Cut surface of Figure 8.1 showing a lobulated appearance. The tissue bulges outwards.

Fig. 8.3 Mammary duct ectasia. F/55. Lump removed from just below the nipple. When cut across it showed many dilated ducts filled with cheesy material, some of which can be seen on the right of the specimen.

Fig. 8.4 Intraduct papilloma. F/83. Presented with bleeding from the nipple associated with a breast lump. A large breast duct has been opened and contains a fleshy tumour arising from its wall.

Fig. 8.5 Fibrocystic disease of the breast. F/35. The breast lump shows multiple small, blue-coloured fluid-filled cysts. The adjacent breast tissue is somewhat fibrous. Since the introduction of mammographic and ultrasound imaging of the breast this condition can be diagnosed without having to perform surgical excision.



Fig. 8.3



Fig. 8.4

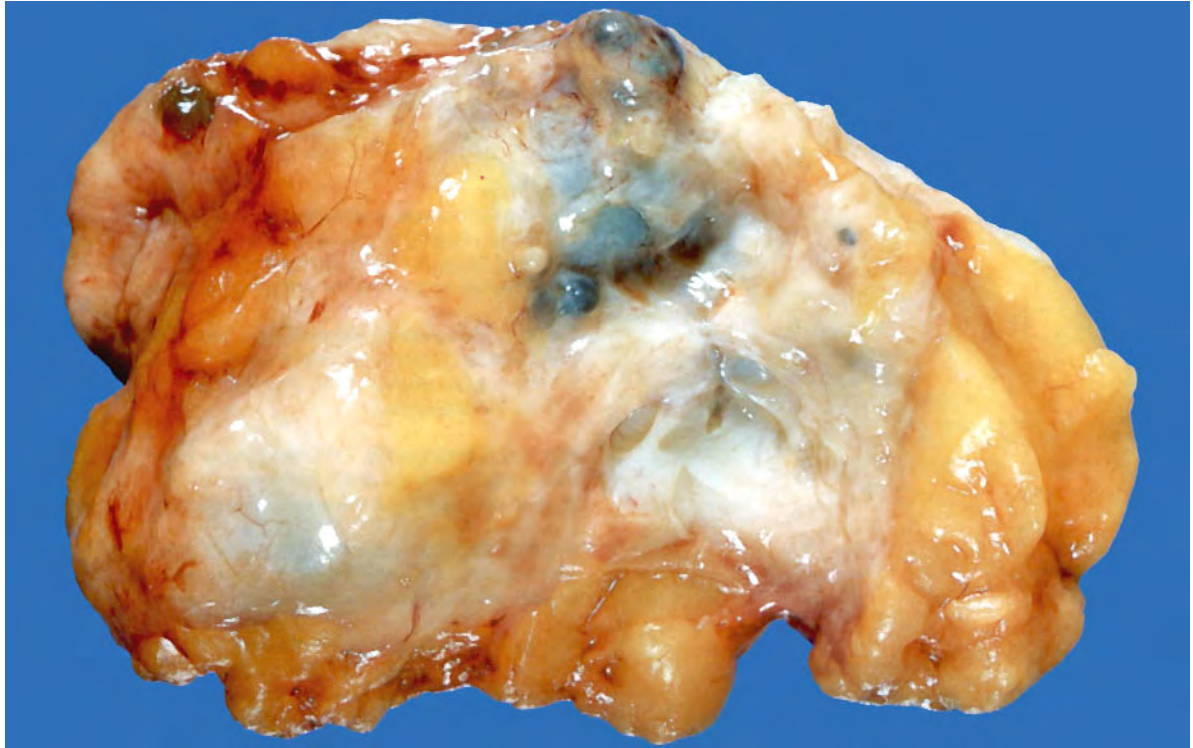


Fig. 8.5

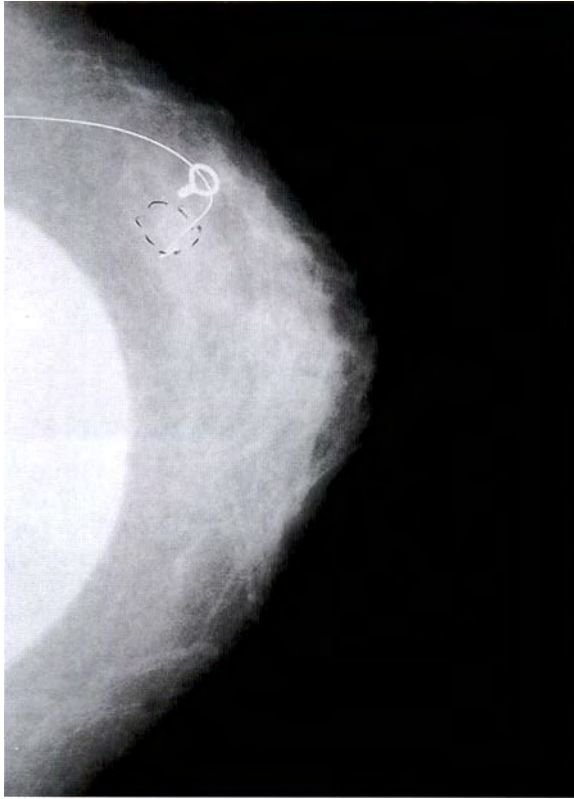


Fig. 8.6



Fig. 8.8



Fig. 8.7

Fig. 8.6 Mammogram showing a breast prosthesis in place. In the breast adjacent to the well defined margin of the prosthesis there are opacities which represent a lipogranulomatous reaction to the leaked contents of the implanted prosthesis.

Fig. 8.7 **Lipogranuloma** caused by rupture of a paraffin-filled polythene sac implanted some 30 years previously as a device for breast augmentation. F/47. This is a very old-fashioned type of breast implantation.

Fig. 8.8 **Fat necrosis.** F/42. Note the variegated colour and areas of haemorrhage on the cut surface of this lump. It was gritty to cut because of the presence of spotty calcification.

Fig. 8.9 **Carcinoma of the left breast.** F/60. A small lump was palpable, and when the hands were raised above the head tethering to the skin was accentuated.

Fig. 8.10 **Carcinoma of the breast.** F/70. A breast lump removed for frozen section. When cut across, it was hard and gritty and the cut surface bulged inwards.

Fig. 8.11 **Carcinoma of the breast.** F/35. A larger lump than in Figure 8.10, but again showing inward bulging.

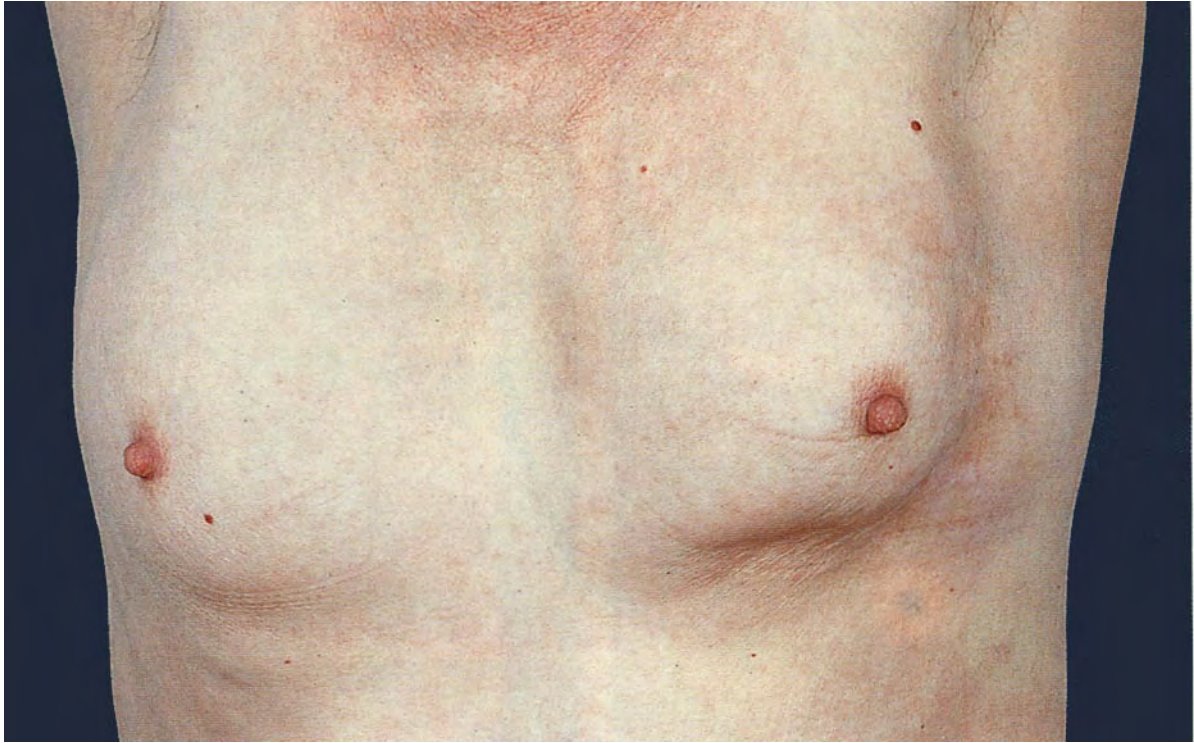


Fig. 8.9



Fig. 8.10

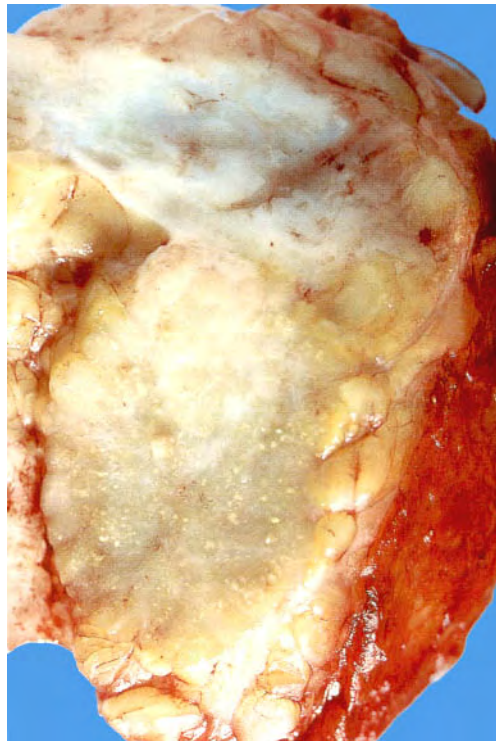


Fig. 8.11



Fig. 8.12

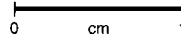


Fig. 8.13

Fig. 8.12 Medullary carcinoma of the breast. F/50. Well circumscribed, soft breast lump. The diagnosis of carcinoma was confirmed on microscopic examination.

Fig. 8.13 Colloid carcinoma of the breast. F/70. This sagittal slice of the breast shows that it is completely replaced by mucoid tumour.

Figs 8.14–8.16 Angiosarcoma of the right upper arm. F/57. This lady had a radical mastectomy performed for treatment of a carcinoma in the right breast in 1968. She developed gross lymphoedema of the arm, which was a usual consequence of this radical surgery. Occasionally, angiosarcomas arose in the skin and subcutaneous tissue of these grossly oedematous arms some years after the surgery. Figure 8.14 is the clinical appearance of this lesion, which presented for treatment in 1979. Figure 8.15 shows the skin surface of the excised lesion. Figure 8.16 shows the appearance of the cut surface of the specimen. There is a large amount of haemorrhagic tumour in the subcutaneous tissue.



Fig. 8.14

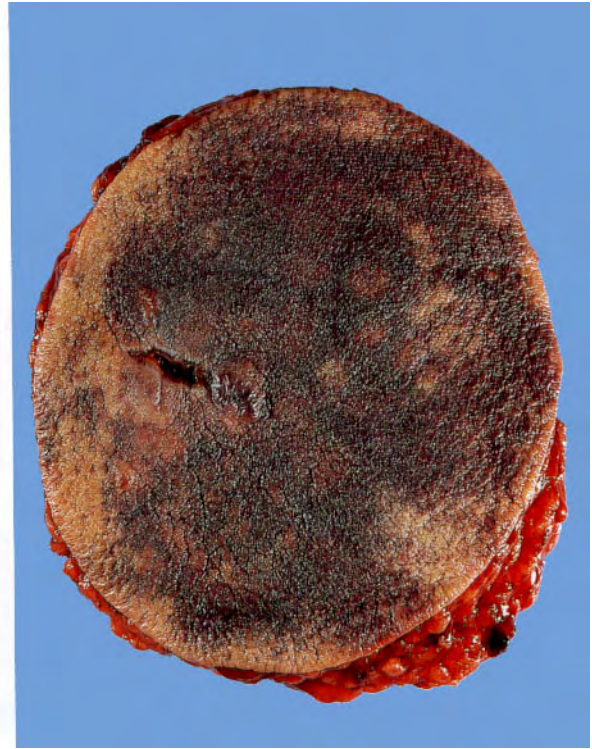


Fig. 8.15

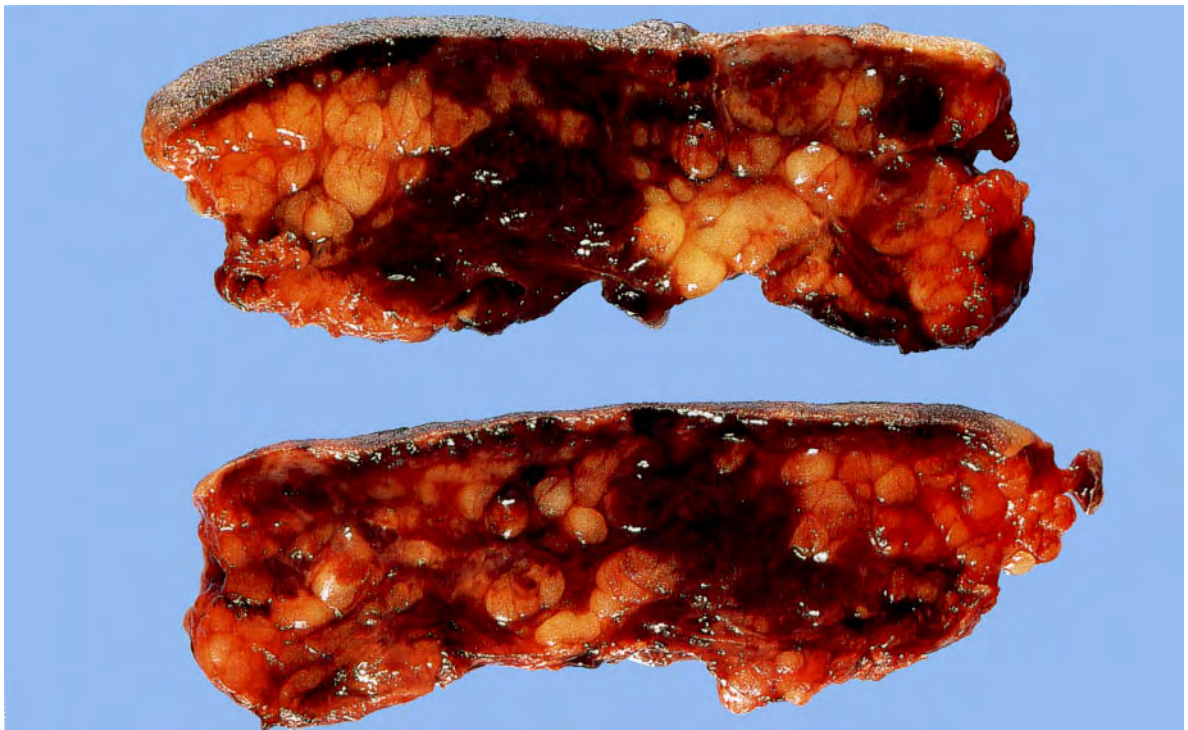


Fig. 8.16



Fig. 8.17

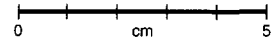


Fig. 8.17 Angiosarcoma of the breast. F/42. This patient had a 1-cm diameter infiltrating duct carcinoma treated by complete local resection (lumpectomy) and radiotherapy. The tumour was detected by routine mammographic screening. Ten years later she developed a few tiny red spots on the skin near the lumpectomy scar. Excision biopsy showed that this was an angiosarcoma involving the skin and the breast tissue. The tumour extended to some margins of excision. A simple mastectomy was performed. The patient had no evidence of tumour recurrence 2 years after the mastectomy.

Angiosarcoma is a rare form of primary breast cancer. In this case, however, it was most likely caused by the radiotherapy. Angiosarcoma is a well known complication of radiotherapy, arising in treated areas about 10 years after the radiation therapy was administered.

Comment: These two cases illustrate the changed treatment of breast cancer in the last half of the 20th century, with radical surgery being replaced by conservative surgery followed by radiotherapy. With both methods of treatment unwanted iatrogenic disease occasionally occurs. The cause of the iatrogenically induced tumour is different in each of these modes of treatment.



Fig. 8.18

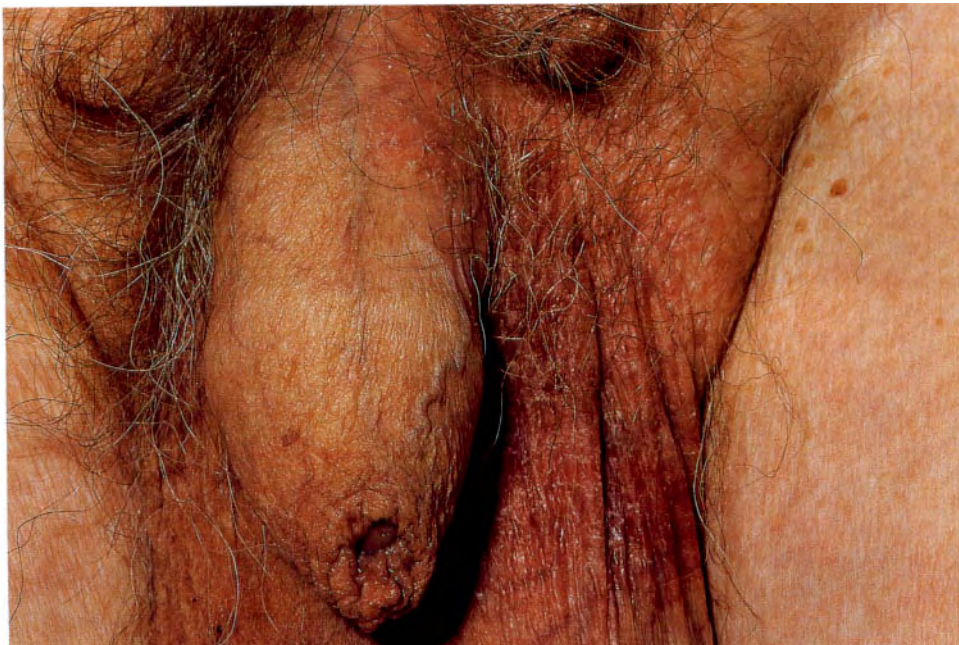


Fig. 8.19

Fig. 8.18 Paget's disease of the nipple. F/39. The crusted, eroded surface is characteristic of this condition. There is always an associated carcinoma present in the breast. This condition is more frequently found in women older than this patient.

Fig. 8.19 Extramammary Paget's disease of the scrotum. M/58. Note the red, scaling skin. The commonest site for extramammary Paget's disease is the anogenital region in both sexes. Only a small proportion of cases have carcinoma in the underlying apocrine glands.

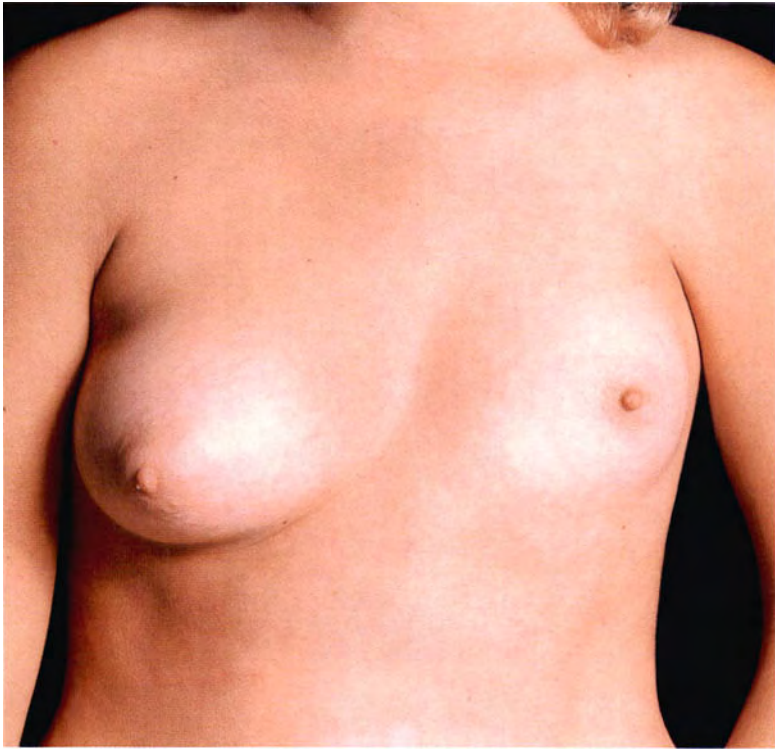


Fig. 8.20

Fig. 8.20 Congenital hypoplasia of the left breast. F/18. Absence of the underlying pectoralis muscles is often associated with this condition, as is seen in this case.

Fig. 8.21 Juvenile hypertrophy of the left breast. F/13. The redness is due to cellulitis from ulceration caused by wearing a bra that was too tight. The benign tumorous tissue was removed and the breast was reconstructed.

Fig. 8.22 Accessory nipple, left pectoral region. M/23. Accessory nipples occur in both sexes and may be found anywhere on the 'milk line' from the axilla to the groin.



Fig. 8.21



Fig. 8.22



Fig. 8.23



Fig. 8.24

Fig. 8.23 Carcinoma of the right breast. M/55. There is already ulceration of the skin in spite of the fact that the tumour is quite small. Cancer of the male breast is rare and is often advanced at the time of first presentation.

Fig. 8.24 Gynaecomastia. M/20. This condition occurs most commonly at about puberty, presumably resulting from mild hormonal imbalance. It may occur also during adult life. Only very occasional cases of gynecomastia are caused by an endocrine tumour (see Figure. 9.18).



Fig. 8.25

Fig. 8.25 Acute vulvitis. F/40. The exact cause can only be determined by the results of bacteriological culture.

Fig. 8.26 Condylomata lata. F/20. Spirochaetes were seen on dark-ground microscopic examination of smears from the lesions. Serological tests for syphilis were positive.



Fig. 8.26

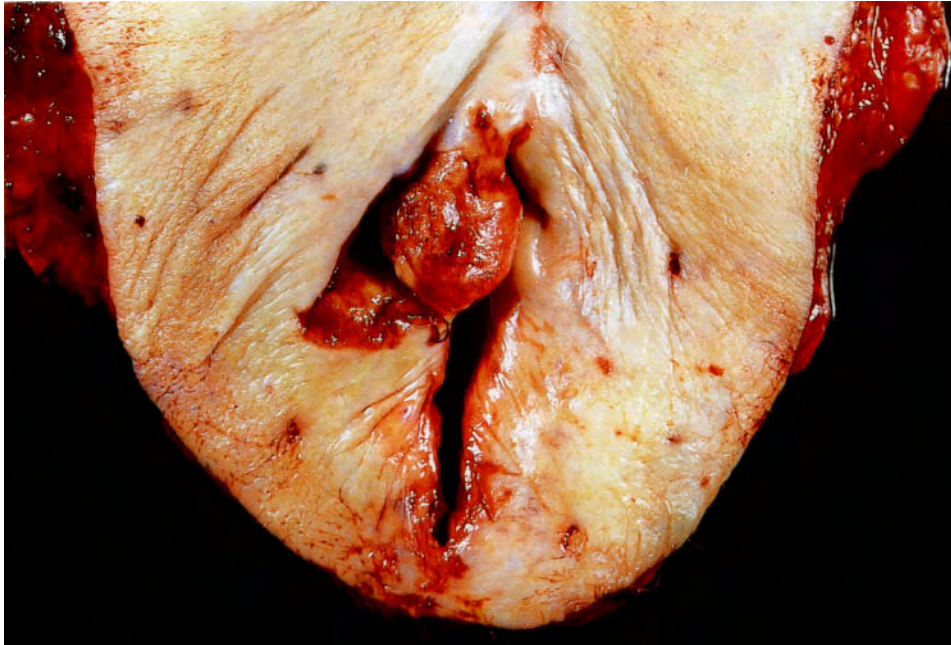


Fig. 8.27



Fig. 8.28

Fig. 8.27 Squamous cell carcinoma arising from the right labium minus. F/79. Treated by radical vulvectomy. Squamous cell carcinoma of the vulva usually occurs as a complication of long-standing lichen sclerosis et atrophicus in older women, or as a complication of HPV (human papilloma virus) infection in younger women.

Fig. 8.28 Malignant melanoma arising in the vagina. F/78. This is one of the uncommon sites for a primary melanoma.



Fig. 8.29

0 cm 5



Fig. 8.30

Fig. 8.29 Advanced squamous cell carcinoma of the cervix. F/41. The panhysterectomy specimen shows that the cervix has been completely eroded by a malignant neoplasm.



Fig. 8.31

Fig. 8.30 Carcinoma in situ plus early invasive squamous cell carcinoma of the cervix. F/41. The cervix is eroded. The diagnosis was made on Papanicolaou smear and biopsy.

Fig. 8.31 Squamous cell carcinoma arising in a long-standing procidentia. F/72.



Fig. 8.32



Fig. 8.33

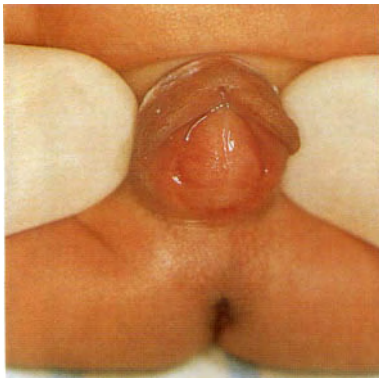


Fig. 8.34

Fig. 8.32 Embryonal rhabdomyosarcoma. F/2. The mother noticed soft nodules protruding from the vagina.

Fig. 8.33 Pelvic exenteration was performed on the patient in Figure 8.32. Soft tumour masses can be seen covering the vagina and cervix – the so-called botryoid sarcoma.

Fig. 8.34 Imperforate hymen. F/neonate.



Fig. 8.35

Fig. 8.35 Double uterus.



Fig. 8.36

0 cm 5

Fig. 8.36 Pyometra. F/67. There is cervical stenosis and the uterine cavity is filled with pus.

Fig. 8.37 Benign endometrial polyp. F/37. The soft polyp is attached to the endometrium. The patient presented with menorrhagia.

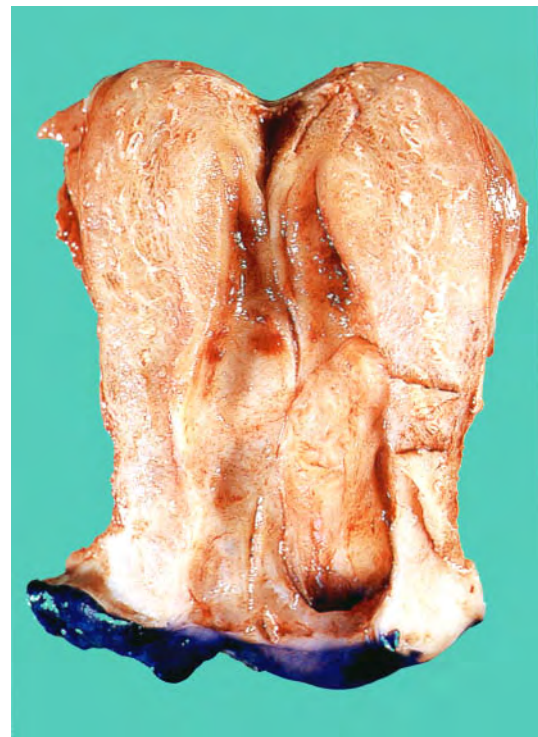


Fig. 8.37

0 cm 5

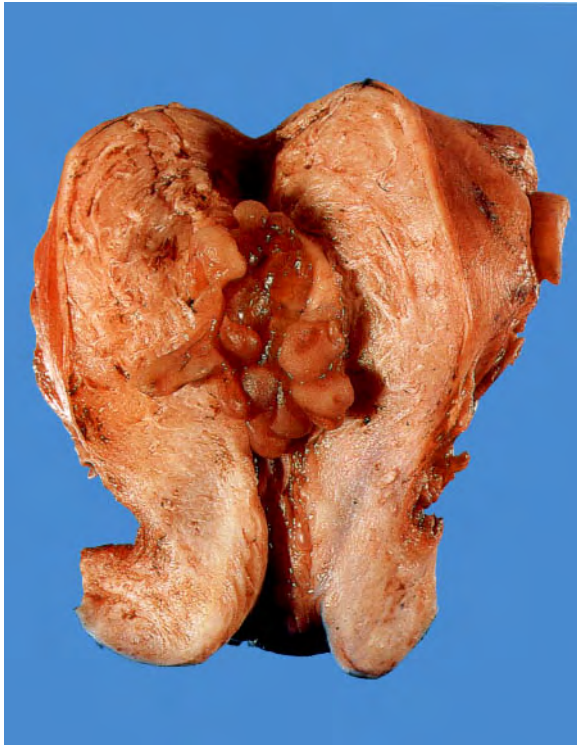


Fig. 8.38



Fig. 8.40



Fig. 8.39

0 cm 5

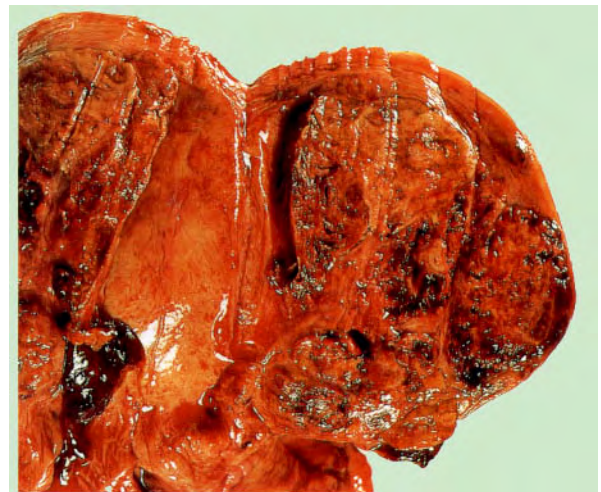


Fig. 8.41

Fig. 8.38 Endometrial hyperplasia. F/45. The patient presented with postmenopausal bleeding. The whole endometrium is involved, rather than there being a discrete polyp.

Fig. 8.39 Adenocarcinoma of the endometrium. F/76. There is a large, rather ragged mass of tissue filling the endometrial cavity.

Fig. 8.40 Choriocarcinoma. F/25. Hysterectomy specimen. There is secondary tumour in the right ovary, and the black nodules in the vagina are also secondary tumour.

Fig. 8.41 Cut surface of specimen in Figure 8.40 showing the haemorrhagic tumour invading the myometrium.

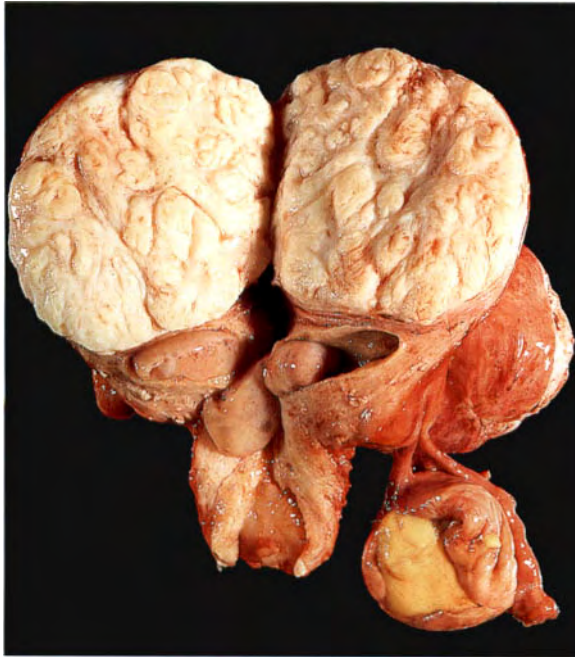


Fig. 8.42

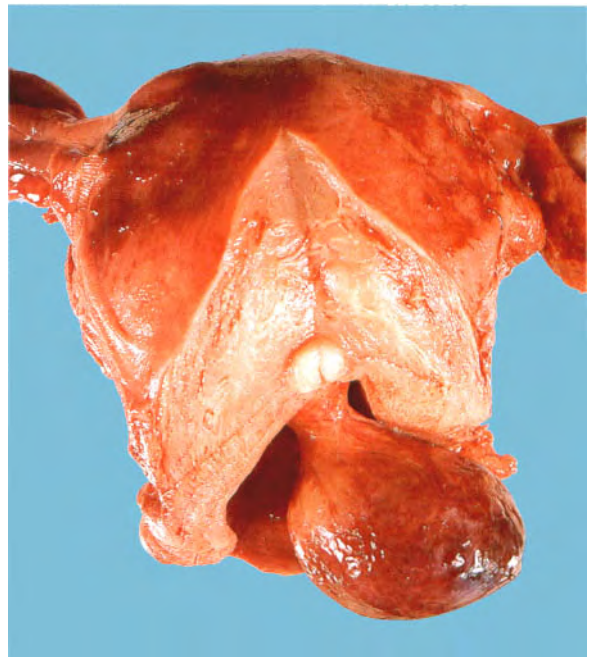


Fig. 8.43

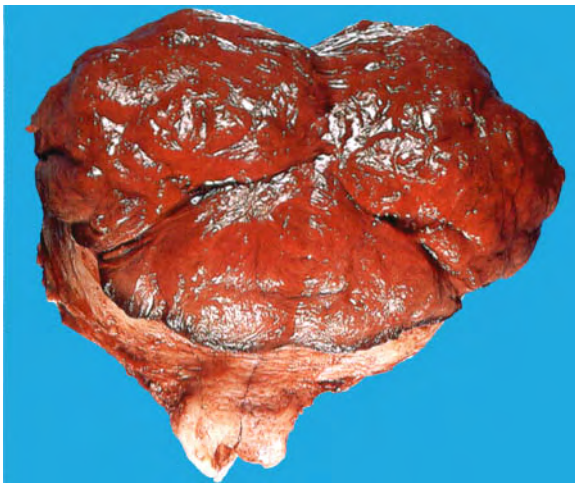


Fig. 8.44

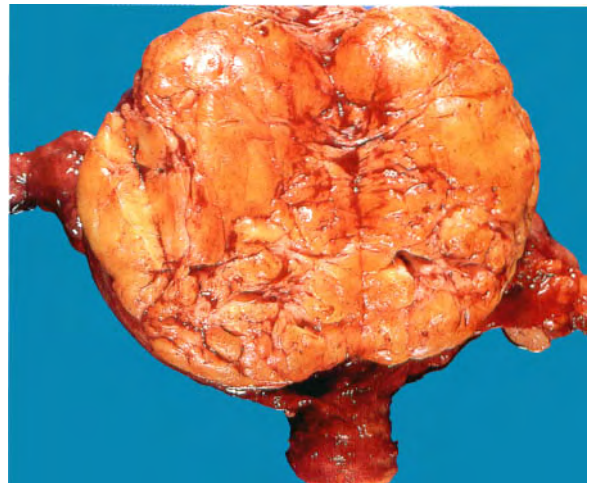


Fig. 8.45

Fig. 8.42 Intramural leiomyoma. F/40. The typical whorled, lobulated pattern of these tumours is apparent.

Fig. 8.43 Pedunculated leiomyoma protruding through the cervix. F/48.

Fig. 8.44 Red degeneration in a leiomyoma. F/42. The red, meaty appearance is characteristic.

Fig. 8.45 Lipoleiomyoma. F/45. The yellow appearance of the tumour is due to lipid infiltration.



Fig. 8.46

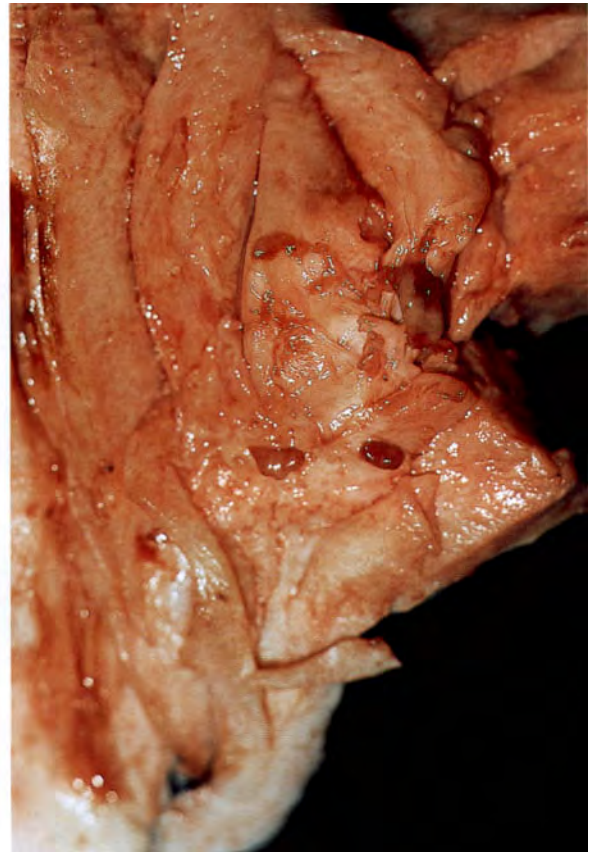
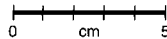


Fig. 8.47

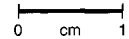


Fig. 8.46 Leiomyoma of the uterus. F/44. The cut surface shows cystic areas and areas of necrosis. This suggested the presence of malignant change, but this was not confirmed on microscopic examination.

Fig. 8.47 Endolymphatic stromal myosis. F/51. Note the red, worm-like areas of tumour in the myometrium.

Fig. 8.48 Adenomyoma of the uterus. F/48. The fundus of the uterus shows marked thickening of the myometrium by cream-coloured tissue which contains many small blood-filled spaces.



Fig. 8.48



Fig. 8.49

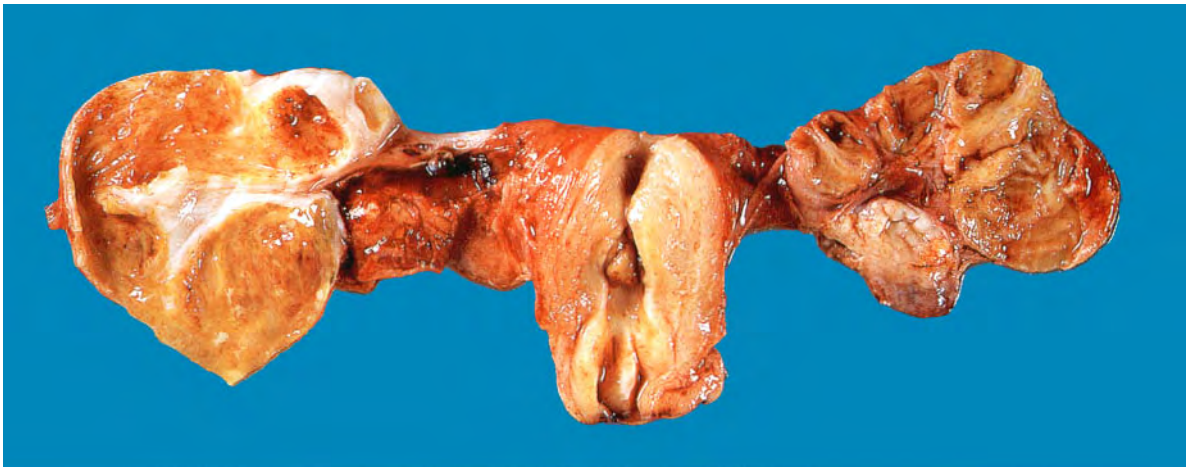
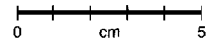


Fig. 8.50

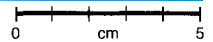


Fig. 8.49 Bilateral pyosalpinx. F/49. The fallopian tubes are dilated and their serosal surfaces are reddened.

Fig. 8.50 Same specimen as in Figure 8.49. The tubes have been opened to show the pus. A small endometrial polyp is also present.

Fig. 8.51 Hydrosalpinx. F/33. This is an end result of chronic salpingitis. The fallopian tube is greatly enlarged and filled with clear fluid.



Fig. 8.51

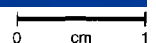




Fig. 8.52

0 cm 5



Fig. 8.53

0 cm 1

Fig. 8.52 Simple follicular cysts in the ovary. F/40. The unopened cysts have a blue colour. There is an unrelated endometrial polyp in the fundus of the uterus.

Fig. 8.53 Bilateral polycystic ovaries. F/23. Most of the cysts are follicular, but the one on the left in the upper ovary is a corpus luteum.

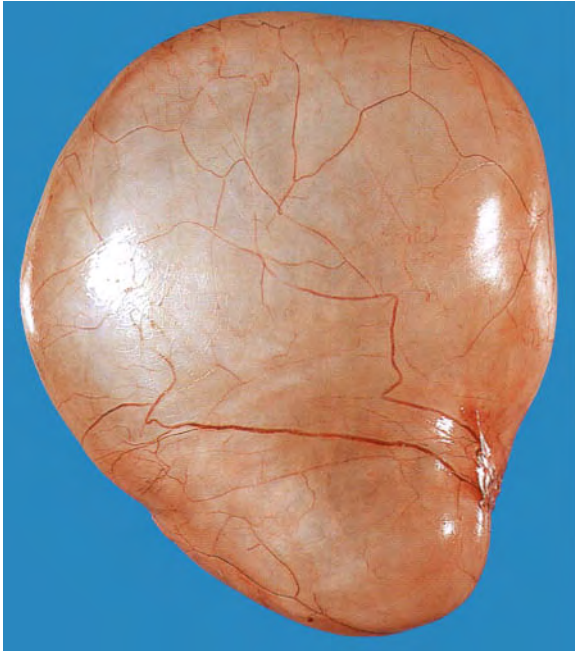


Fig. 8.54

0 cm 5

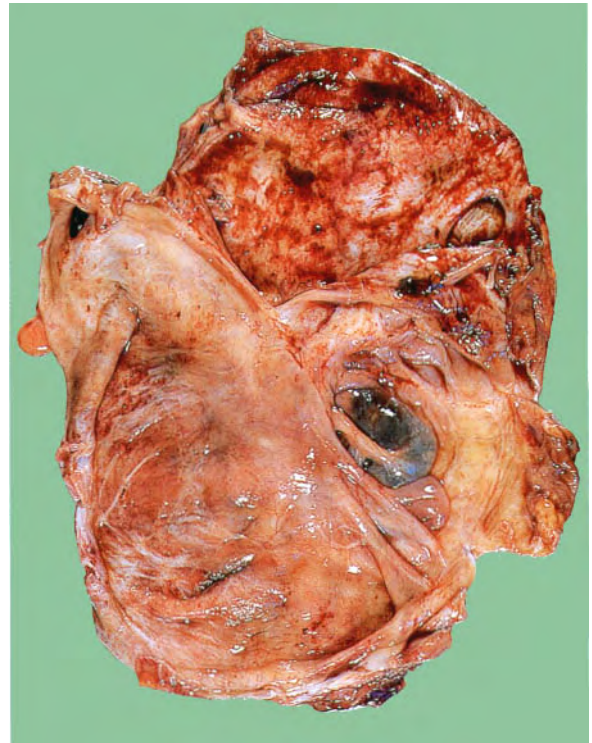


Fig. 8.55

0 cm 5

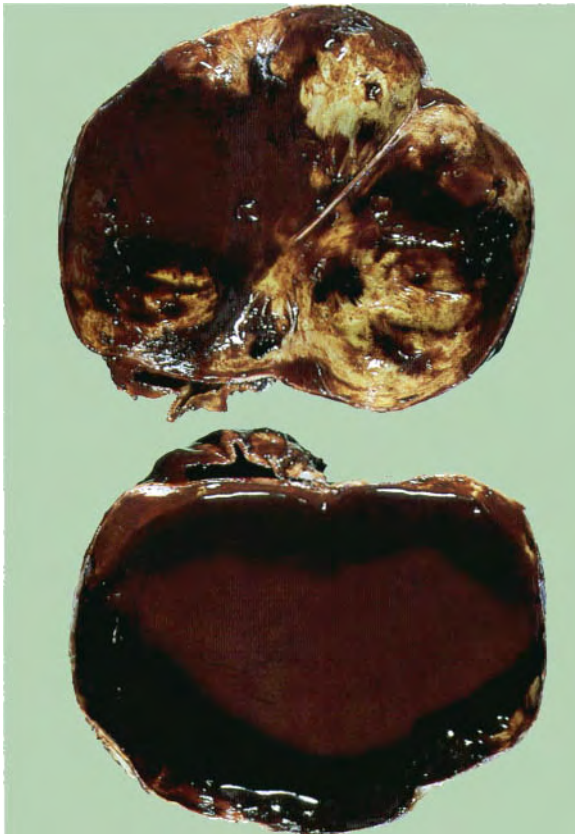


Fig. 8.56

0 cm 5

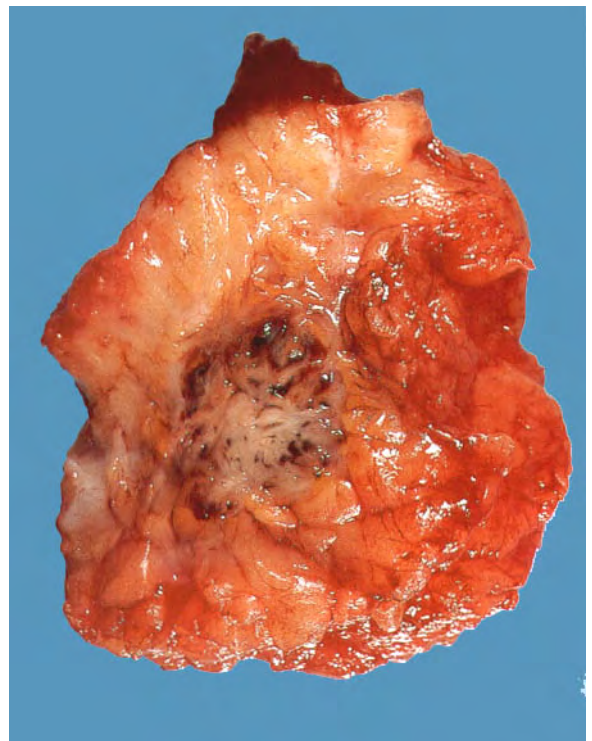


Fig. 8.57

0 cm 1

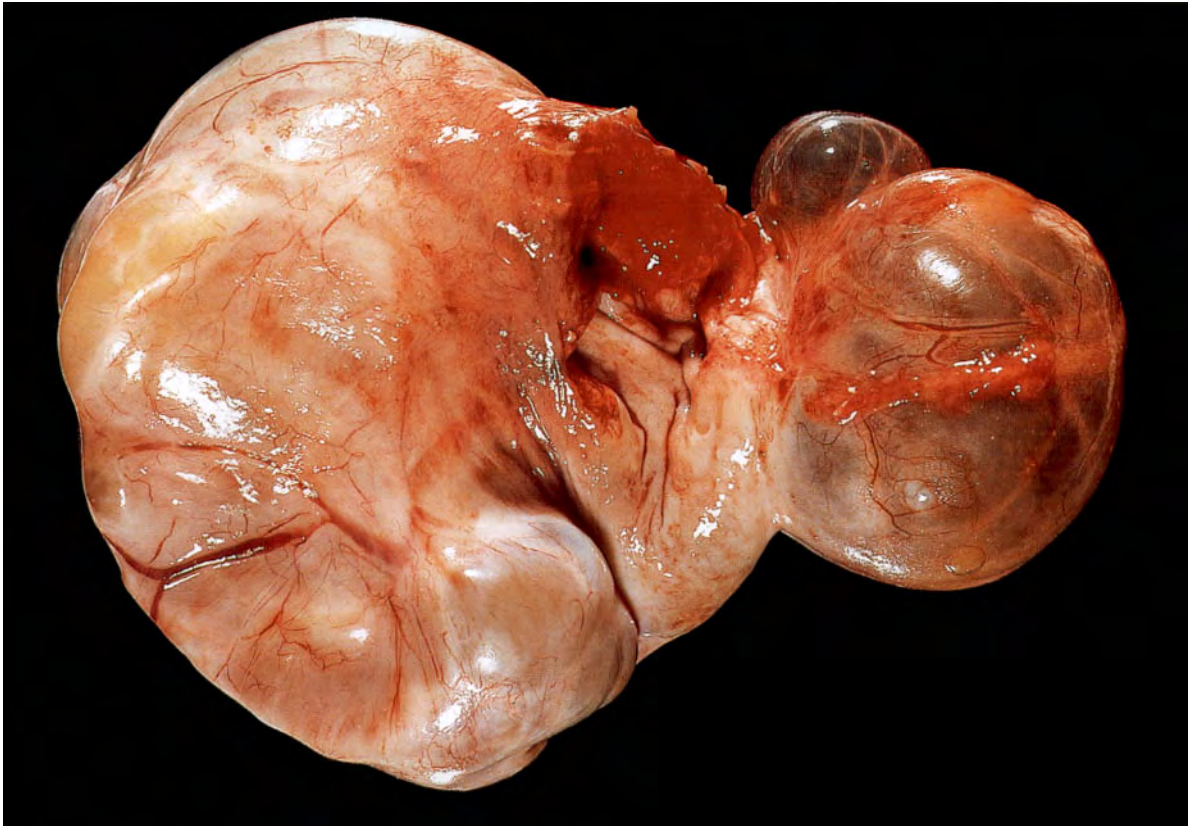


Fig. 8.58

Fig. 8.54 Benign serous cystadenoma of the ovary. F/19. This is a unilocular, thin-walled cyst containing clear fluid.

Fig. 8.55 Endometriosis of the ovary. F/40. The ovarian cyst is multiloculated. The blood has been removed from most of the loculi.

Fig. 8.56 Endometriosis of the ovary. F/31. Blood has not been removed so as to demonstrate the so-called 'chocolate cyst'.

Fig. 8.57 Extrapelvic endometriosis. F/43. A subcutaneous lump appeared at the site of an abdominal scar, the result of Caesarian section 5 years previously. This was excised, and on cross-section the blood-filled cysts can be seen in the centre of the specimen.

Fig. 8.58 Benign mucinous cystadenoma of the ovary. F/76. The solid tumour on the left is a benign Brenner tumour. This combination is quite frequent.

Fig. 8.59 The cut surface of the specimen in Figure 8.58 shows a multiloculated cyst containing mucin, most of which has been removed.

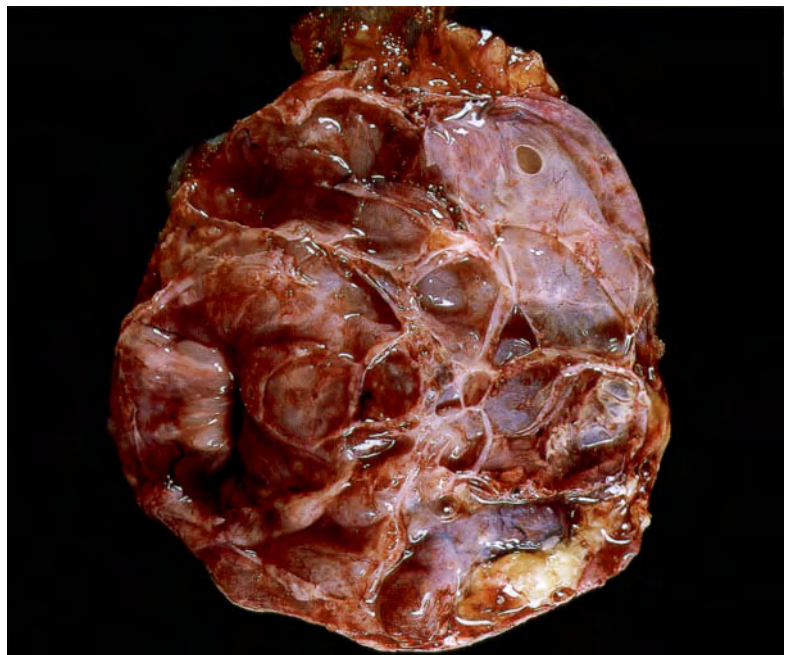


Fig. 8.59

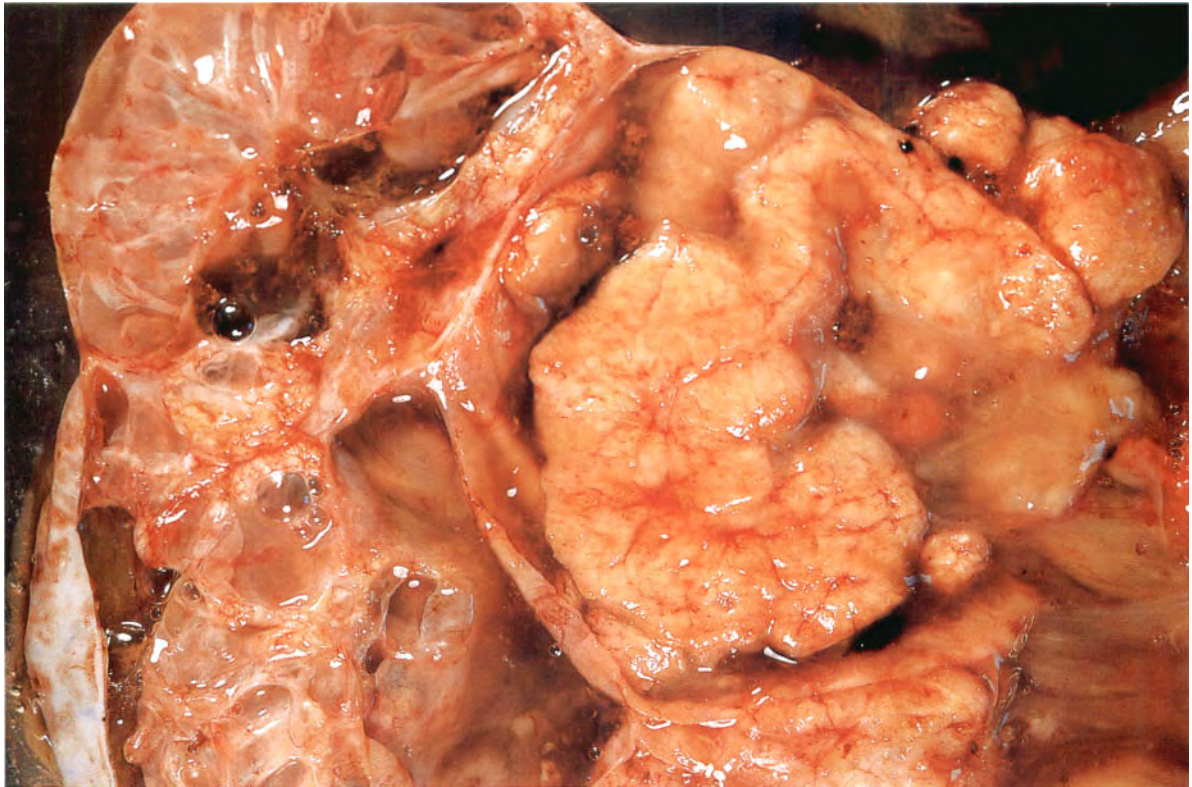


Fig. 8.60

Fig. 8.60 Mucinous cystadenocarcinoma of the ovary. F/47. Solid areas of tumour are present as well as multiple loculi of benign mucinous cystadenoma.

Fig. 8.61 Papillary cystadenocarcinoma of the ovary. F/32. Note the papillary projections in the lumen of the cyst, and also on its surface. In a benign papillary cystadenoma the papillae are present only on the inner surface of the cyst.

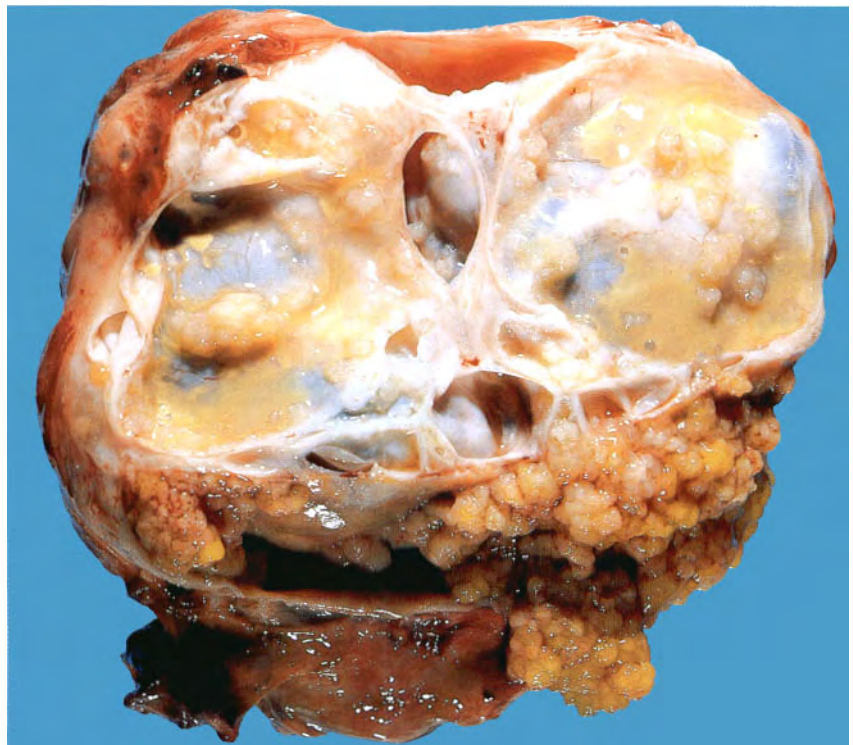


Fig. 8.61

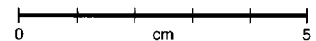




Fig. 8.62

0 cm 5



Fig. 8.63

0 cm 1

Fig. 8.62 Krukenberg tumour. F/44. Both ovaries are fairly symmetrically enlarged and replaced by secondary adenocarcinoma.

Fig. 8.63 Dermoid cyst (benign teratoma) of the ovary. F/26. It contains sebaceous material, hair and a tooth.

Fig. 8.64 Torsion of an ovarian dermoid cyst and the attached fallopian tube. F/23.



Fig. 8.64

0 cm 5



Fig. 8.65

0 cm 1

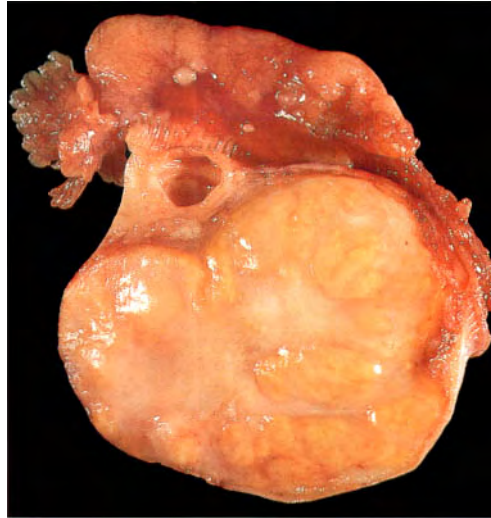


Fig. 8.66

0 cm 1



Fig. 8.67

0 cm 1



Fig. 8.68

0 cm 5

Fig. 8.65 Fibroma of the ovary. F/30. The cut surface of the tumour shows a homogeneous white appearance.

Fig. 8.66 Thecoma of the ovary. F/66. This is distinguished from fibroma by the presence of lipid, which gives it a yellow colour.

Fig. 8.67 Granulosa cell tumour of the ovary. F/84. These tumours, too, are usually yellow. Positive diagnosis depends on the microscopic appearances. They sometimes secrete oestrogen.

Fig. 8.68 Dysgerminoma of the ovary. F/30. The tumour has a cream-coloured, fleshy appearance on its cut surface, with some areas of haemorrhage. This tumour has the same microscopic appearances as a seminoma of the testis.



Fig. 8.69

0 cm 1



Fig. 8.70

0 cm 1

Fig. 8.69 Ruptured tubal ectopic pregnancy. F/24. Blood and placental tissue are exuding from the greatly distended fallopian tube.

Fig. 8.70 Ovarian pregnancy. F/32. The placental tissue is embedded in the ovary.

Fig. 8.71 Lithopaedion. F/55. This was removed from the pelvic wall of an African patient. It was an incidental finding during pelvic surgery. This condition results from fossilization of an untreated intra-abdominal pregnancy.



Fig. 8.71

0 cm 1



Fig. 8.72

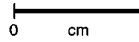


Fig. 8.73

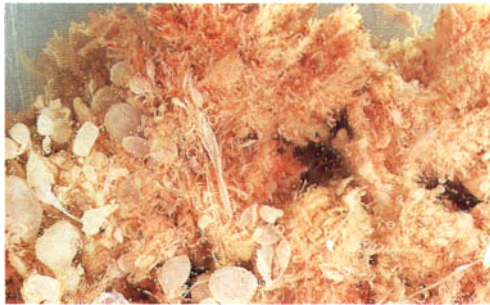
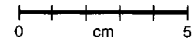


Fig. 8.74

Fig. 8.72 Hydatidiform mole. F/26. Cured specimen. Note variably sized vesicles, no normal placenta and no fetus.

Fig. 8.73 Partial mole. F/30. Note the presence of normal placenta plus some variably sized vesicles. The fetus is abnormal, and chromosomal studies showed it to be triploid – 69, XXX.

Fig. 8.74 Close-up view of Figure 8.73 shows areas of normal placenta plus vesicles of varying size.

Fig. 8.75 Chorangioma (benign haemangioma) of the placenta. This tumour usually occurs at the site of insertion of the cord and is the commonest tumour of the placenta.

Fig. 8.76 Placenta with retroplacental haemorrhage.

Fig. 8.77 Placenta with broad, depressed areas of infarction.

Fig. 8.78 Erythroblastosis fetalis due to rhesus incompatibility. Large oedematous placenta.

Fig. 8.79 Erythroblastosis fetalis due to rhesus incompatibility. Oedematous stillborn fetus (the so-called hydrops fetalis).

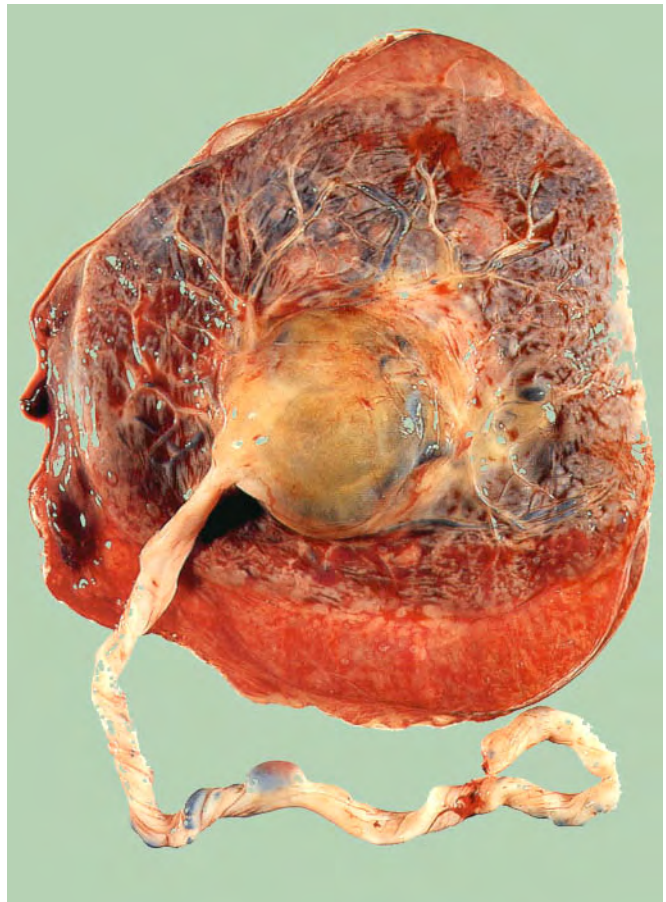
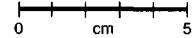


Fig. 8.75



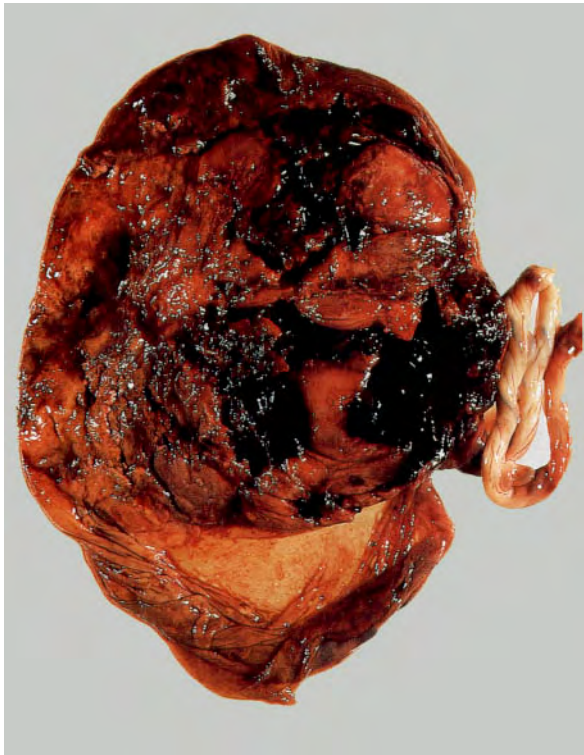


Fig. 8.76



Fig. 8.77

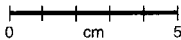


Fig. 8.78



Fig. 8.79



Fig. 8.80

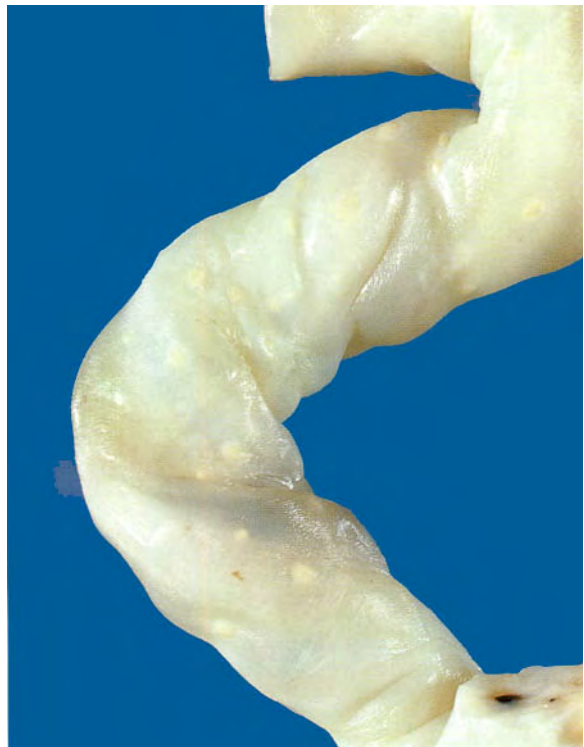


Fig. 8.81

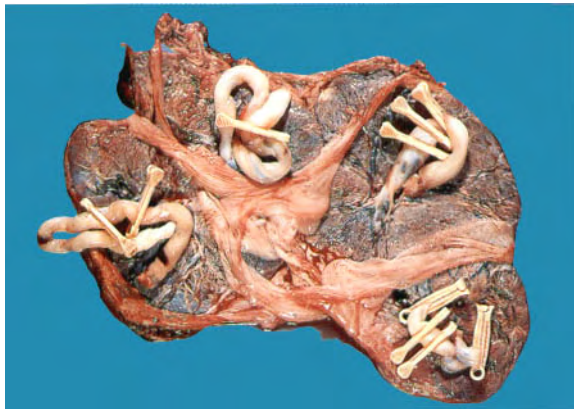


Fig. 8.82

Fig. 8.80 Knotting of the umbilical cord around the neck of the fetus. This resulted in intrauterine death.

Fig. 8.81 Intrauterine candidiasis. White spots of *Candida* colonies are present on the surface of the umbilical cord.

Fig. 8.82 Placenta from the birth of quadruplets.

Fig. 8.83 Placenta accreta. F/30. Hysterectomy was performed to stop the postpartum haemorrhage when the placenta could not be removed manually after delivery of the baby.



Fig. 8.83

ENDOCRINE SYSTEM



Fig. 9.1



Fig. 9.3



Fig. 9.2

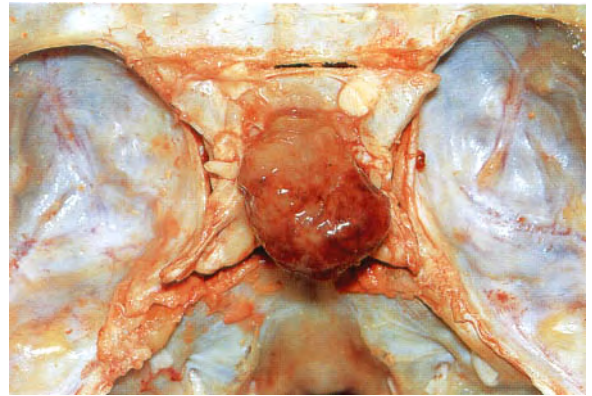


Fig. 9.4

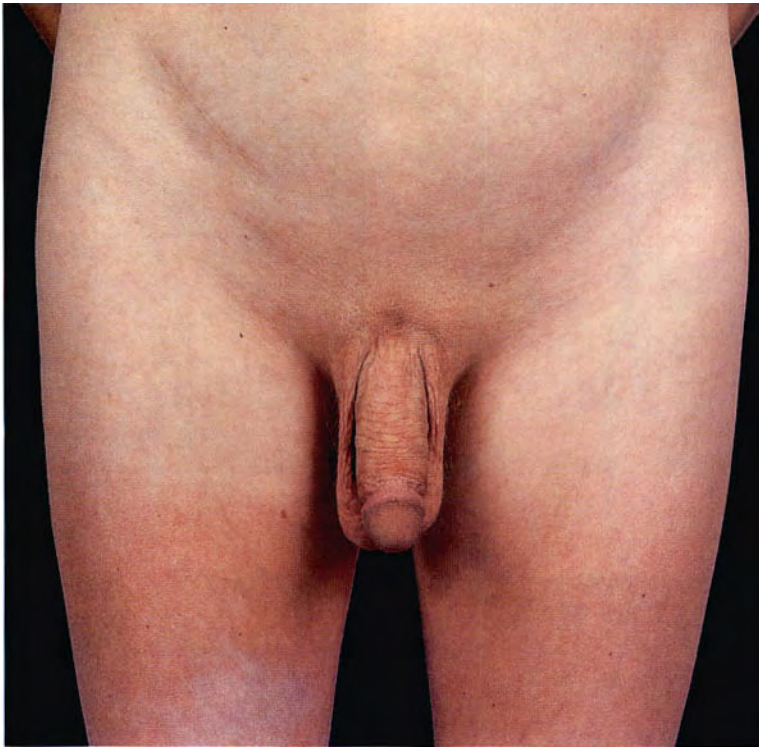


Fig. 9.5

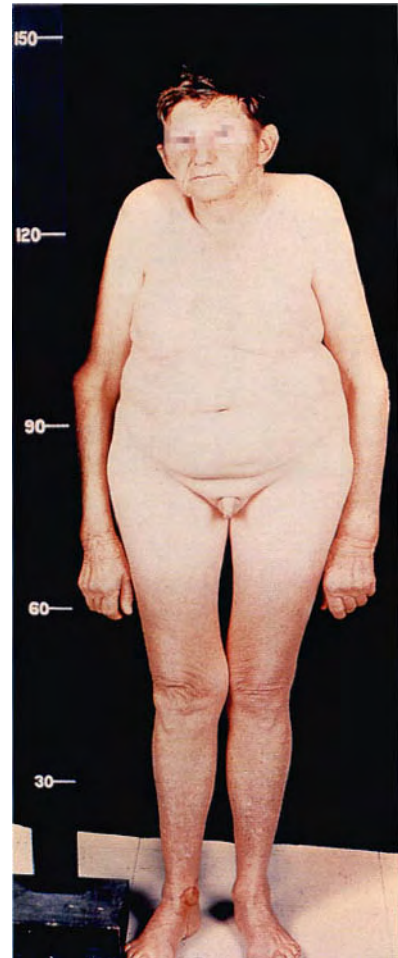


Fig. 9.6

Fig. 9.1 Hyperpituitarism. Gigantism. F/19. Family photographs showed that this young woman had consistently outgrown her twin brother and was always the biggest child in the school class. She had a pituitary adenoma secreting growth hormone. The tumour developed before puberty and before bone growth was complete. She is shown with two staff members, one short and one tall.

Fig. 9.2 Acromegaly. F/36. This is the condition that occurs when the growth hormone-secreting tumour develops during adult life. The photograph shows the characteristic malocclusion of the teeth resulting from the overgrowth of the mandible. The patient had noticed that over the past few years her facial appearance had been changing.

Fig. 9.3 Acromegaly. The enlarged, spade-shaped hand of the patient in Figure 9.2 is shown on the left, with a normal hand for comparison.

Fig. 9.4 Pituitary adenoma in the pituitary fossa. The majority of pituitary adenomas are chromophobe tumours tinctorially. Some cause symptoms because of their compression of adjacent structures, whereas others do so because of their secretion of hormones. Immunoperoxidase stains make it possible to identify the cells that secrete the various pituitary hormones (see Figure 11.98).

Fig. 9.5 Hypopituitarism. Hypogonadism. M/20. There are many causes for failure of the gonads, one of which is primary pituitary failure.

Fig. 9.6 Hypopituitarism. M/60. Clinical photograph of a man with eunuchoid features resulting from primary hypopituitarism. He had no beard and had not developed any secondary sex characteristics. He had a somewhat female type of body habitus and a high-pitched voice.

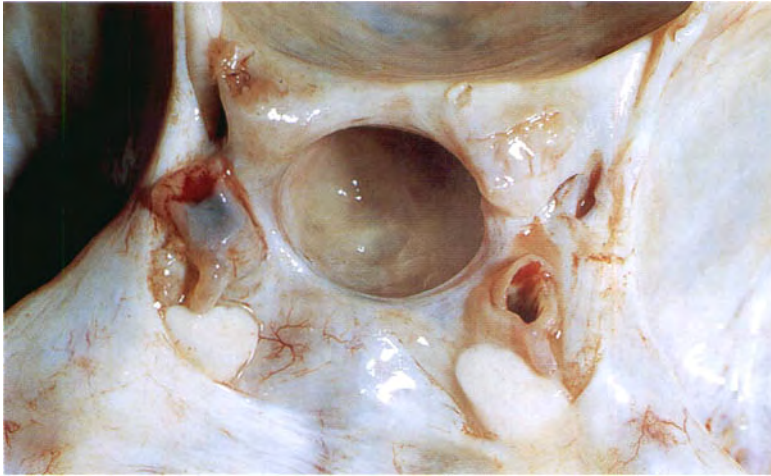


Fig. 9.7

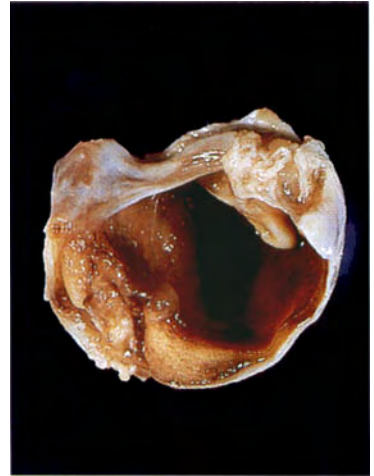


Fig. 9.8

0 cm 1



Fig. 9.9

Fig. 9.7 Hypopituitarism. M/64. Empty pituitary fossa found at postmortem in another patient who had primary hypopituitarism.

Fig. 9.8 Cystic pituitary gland. F/55. The patient had had hypopituitarism since the birth of her last child, which was associated with heavy postpartum bleeding. Presumably this caused infarction of the pituitary – Sheehan's syndrome. Features of this condition are failure to lactate, cessation of menstruation, and hypothyroidism. Some patients die soon after delivery as a result of the postpartum pituitary infarction.

Fig. 9.9 This syndrome was described by Harold Sheehan, pathologist at the Women's Hospital, Glasgow, Scotland, in the 1930s. Industrial workers were housed in very crowded conditions in these tenement buildings close to the River Clyde, with one family per room and four families sharing cooking, washing and toilet facilities. Women had their babies here with a minimal amount of medical assistance. The maternal and infant mortality rates were high. Sheehan made his observations from this concentrated accumulation of cases. The buildings have been cleaned, and are now much sought after real estate in the centre of Glasgow.

Fig. 9.10 Cushing's syndrome. F/45. Over a period of approximately 2 years this woman had noticed increasing obesity associated with a round face, red cheeks and hirsutism.

Fig. 9.11 The same patient as in Figure 9.10, showing truncal obesity and abdominal striae.



Fig. 9.10



Fig. 9.11



Fig. 9.12

0 cm 1

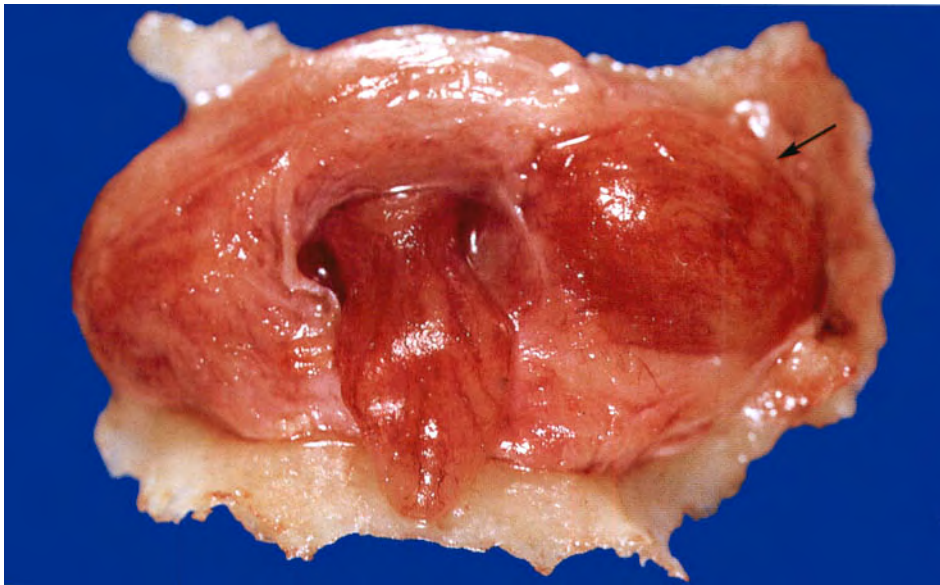


Fig. 9.13

0 cm 1

Fig. 9.12 Cushing's syndrome. Adrenal cortical adenoma. F/29. This tumour was removed surgically, resulting in a cure of the condition.

Fig. 9.13 Basophil adenoma of the pituitary. F/66. This patient died with Cushing's syndrome and the basophil adenoma (arrow) was found at postmortem.



Fig. 9.14

0 cm 1

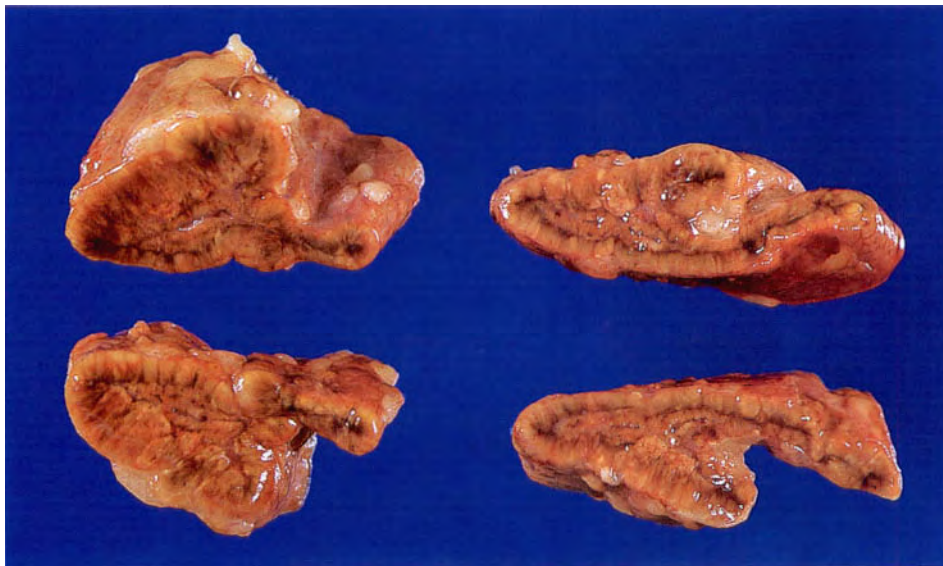


Fig. 9.15

0 cm 1

Fig. 9.14 Bilateral focal nodular hyperplasia of the adrenal. F/31. This patient had Cushing's syndrome and the left adrenal gland was removed. When this failed to control the Cushing's, a right adrenalectomy was performed. The periadrenal fat was removed with the gland to ensure that the nodules of adrenal tissue that extended into it were completely removed. This resulted in a cure.

Fig. 9.15 Bilateral adrenal hyperplasia. F/66. The adrenals from the patient in Figure 9.13. Both adrenals are markedly enlarged and are a brown colour because the hyperplasia occurs mainly in the zona reticularis. Adrenal hyperplasia such as this may be primary, in which case it is a cause of Cushing's syndrome, or it may be secondary to endogenous secretion or the exogenous administration of ACTH.



Fig. 9.16

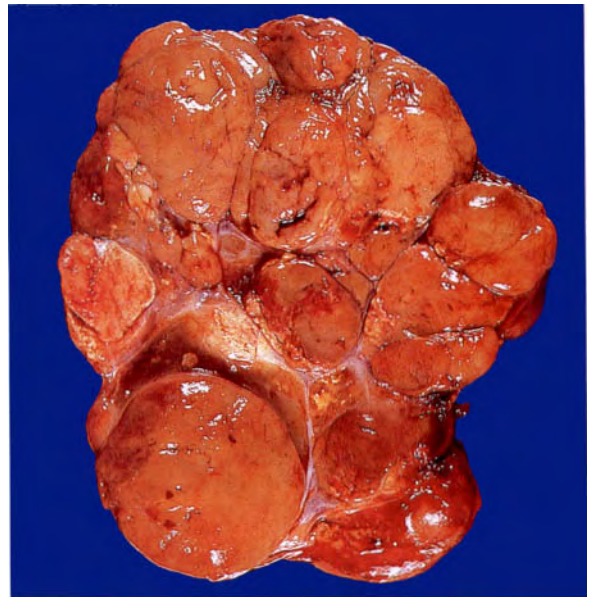


Fig. 9.17



Fig. 9.18

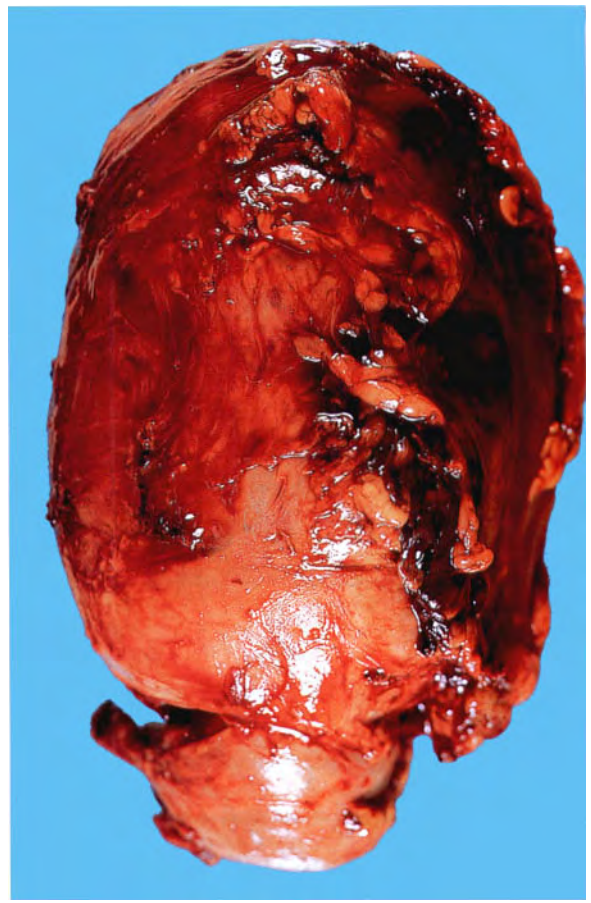


Fig. 9.19



Fig. 9.20



Fig. 9.21

Fig. 9.16 Precocious puberty. M/11 months.

Fig. 9.17 Adrenal cortical adenoma.

This was removed surgically from the patient in Figure 9.16. The cut surface is multilobulated and a homogeneous brown colour. This adenoma was secreting androgens.

Fig. 9.18 Gynaecomastia. M/5.

Fig. 9.19 Adrenal cortical tumour. This large adrenal tumour was removed surgically from the patient in Figure 9.18. It was secreting oestrogens. The tumour was somewhat adherent to adjacent structures and was torn during removal. It is impossible to predict which adrenal tumours will be malignant, because cellular pleomorphism does not correlate with their behaviour. In spite of the local adhesions and raggedness of this specimen, the gynaecomastia subsided and the patient was alive and well 30 years later.

Fig. 9.20 Conn's syndrome. M/58. Surgical specimen of the left adrenal gland, showing a bright yellow cortical adenoma. The patient presented with hypertension and hypokalaemia. Both of these were reversed by the adrenalectomy.

Fig. 9.21 Adrenogenital syndrome. F/2 $\frac{1}{2}$. These patients have pseudohermaphrodite genitalia because of hypertrophy of the clitoris. The condition is caused by enzyme deficiency in the adrenal gland, resulting in overproduction of androgens.



Fig. 9.22

Fig. 9.22 Addison's disease. M/40. This man presented with weakness, heavy pigmentation of the skin and blotchy pigmentation of the tongue.

Fig. 9.23 On the right is the hand of the patient in Figure 9.22, showing increased pigmentation, particularly in the palmar creases, and on the left is a normal hand for comparison.

Fig. 9.24 Adrenal atrophy in Addison's disease. The atrophic adrenal is compared with a normal one.

Fig. 9.25 Addison's disease. This is a wax model of one of Thomas Addison's original cases, crafted by Joseph Towne and housed in the Gordon Museum in Guy's Hospital, London. It shows the deeply pigmented skin.



Fig. 9.23



Fig. 9.24

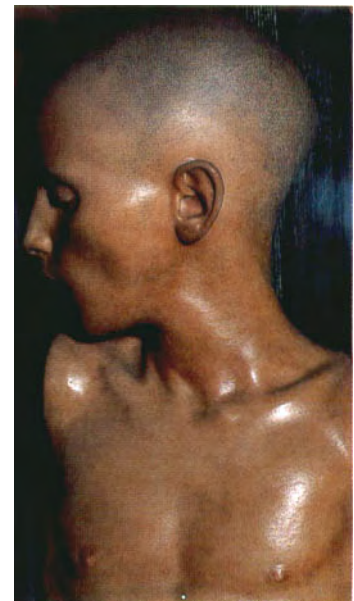


Fig. 9.25

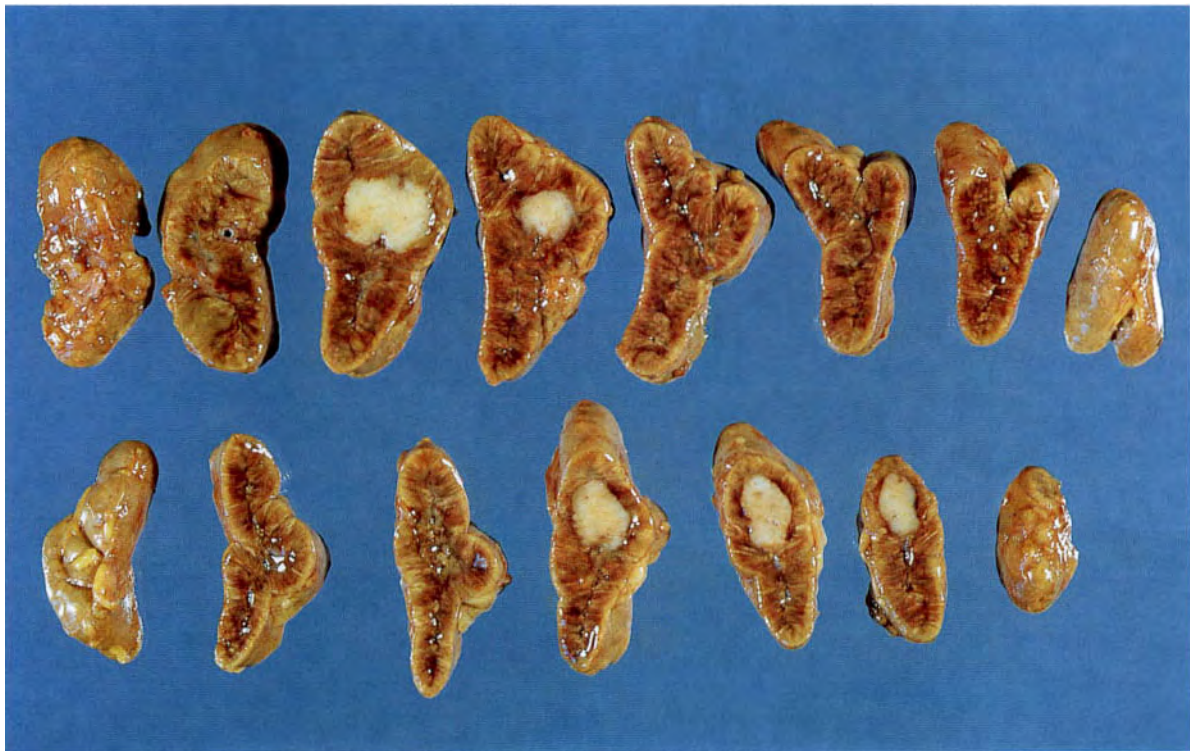


Fig. 9.26

0 cm 5



Fig. 9.27



Fig. 9.28

0 cm 1

Fig. 9.26 Bilateral adrenal hyperplasia caused by an oat cell carcinoma of the lung. M/56. Both adrenals have been sliced to show that they are enlarged and brown – features of adrenal hyperplasia. There are secondary deposits from the lung cancer in the medulla of both adrenals. Towards the end of his life, the patient had clinical features of Cushing's syndrome. This is an example of hormone secretion by a non-endocrine tumour.

Fig. 9.27 Secondary lung cancer in the medulla of the adrenal. M/51. Sometimes secondary tumour completely replaces both adrenals, and the patient suffers from Addison's disease in the last few weeks of life. Often in such cases the skin becomes deeply pigmented.

Fig. 9.28 Myelolipoma in the medulla of the adrenal. F/84. An incidental postmortem finding.

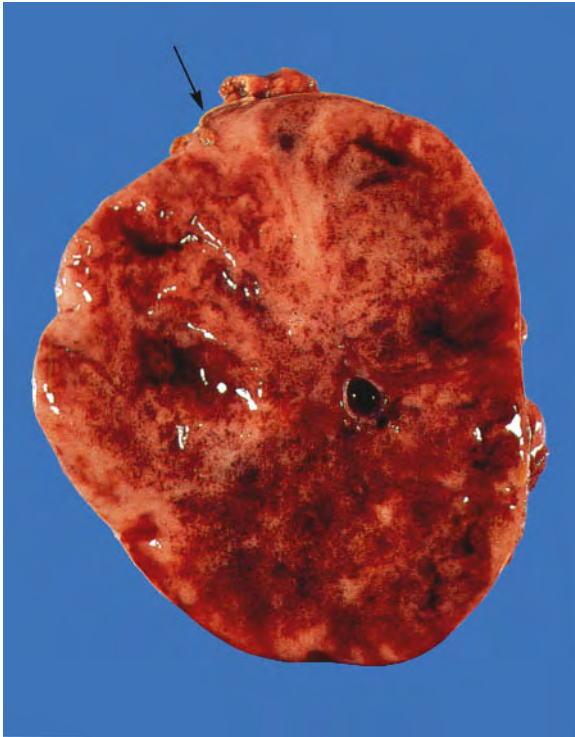


Fig. 9.29

0 cm 1

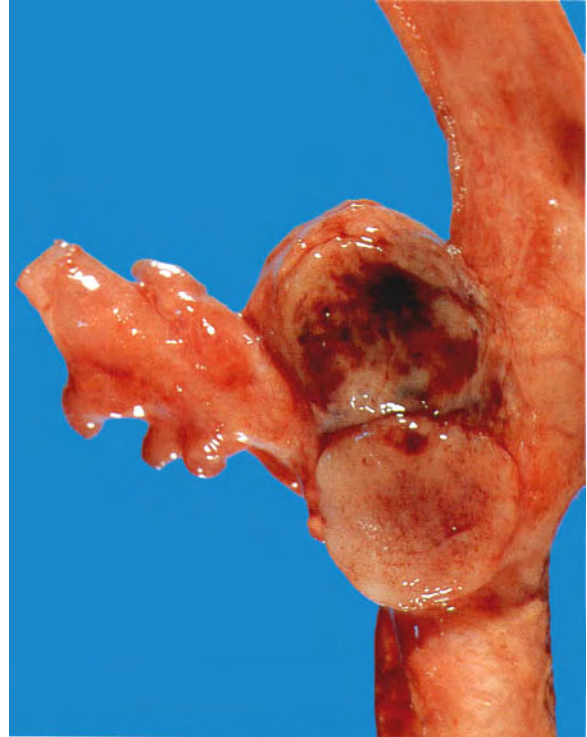


Fig. 9.30

0 cm 1



Fig. 9.31

0 cm 5

Fig. 9.29 Pheochromocytoma almost completely replacing the left adrenal gland. F/35. The patient presented with intermittent hypertension, which was cured by removal of the tumour. The cut surface of the tumour shows a red, haemorrhagic appearance. There is a tiny remnant of adrenal cortex at the top of the specimen (arrow).

Fig. 9.30 Carotid body tumour. F/80. This tumour situated in the bifurcation of the common carotid artery is an example of a chemodectoma. This particular one was an incidental postmortem finding. These tumours are usually intimately attached to the wall of the artery, which causes technical difficulty during surgical removal. They may be associated with the presence of pheochromocytoma of one or both adrenals. This association may be familial.

Fig. 9.31 Neuroblastoma. M/4½. The haemorrhagic tumour has replaced the right adrenal gland. The child presented with a mass in the right upper quadrant of the abdomen. It was surgically removed. This treatment formed part of the combined surgical, radiotherapy and chemotherapeutic treatment. This is one of the more common tumours in childhood.

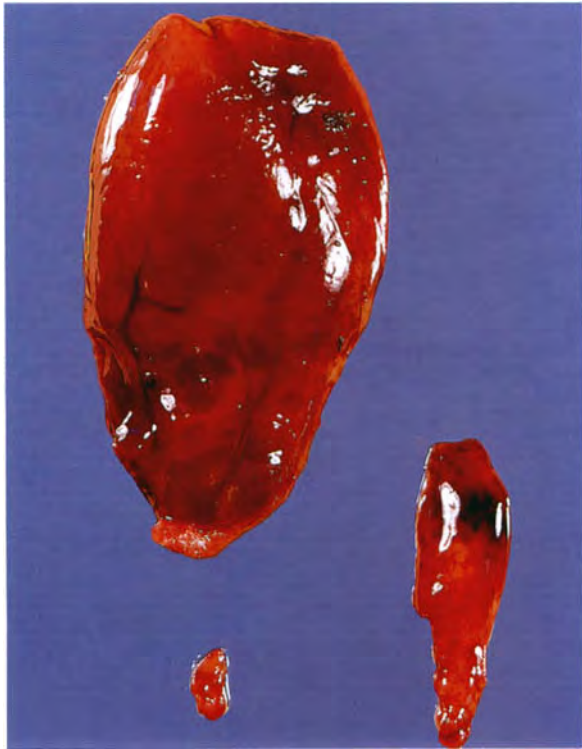


Fig. 9.32

0 cm 1



Fig. 9.33

Fig. 9.32 Hyperparathyroidism. M/51. Three glands were removed at parathyroidectomy and laid out in accordance with their anatomical position. The right upper gland is very large and weighed 3.8 g. The right lower is a biopsy, and the left lower is a little larger than normal. The patient presented with asymptomatic hypercalcaemia. The calcium returned to normal postoperatively and remained normal. Terminology in this condition is somewhat difficult. 'What constitutes an adenoma and what constitutes hyperplasia?' This one could be regarded as being one large and one small adenoma.

Fig. 9.33 Hyperparathyroid bone disease. F/72. The segment of vertebral column shows bands of dense bone on each side of the intervertebral discs. This is seen particularly in secondary hyperparathyroidism.

Fig. 9.34 X-ray taken during life of the spine of the patient in Figure 9.33. The bands of osteosclerosis in the vertebral bodies are clearly demonstrated.



Fig. 9.34



Fig. 9.35

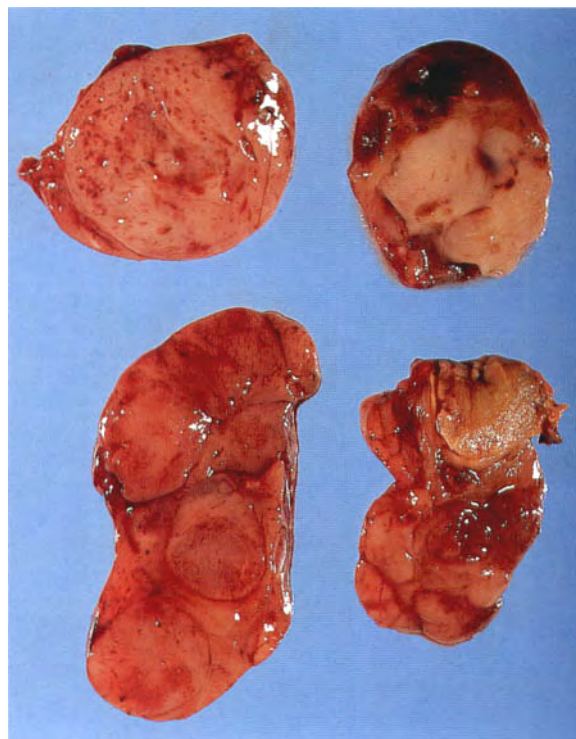
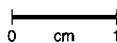


Fig. 9.36

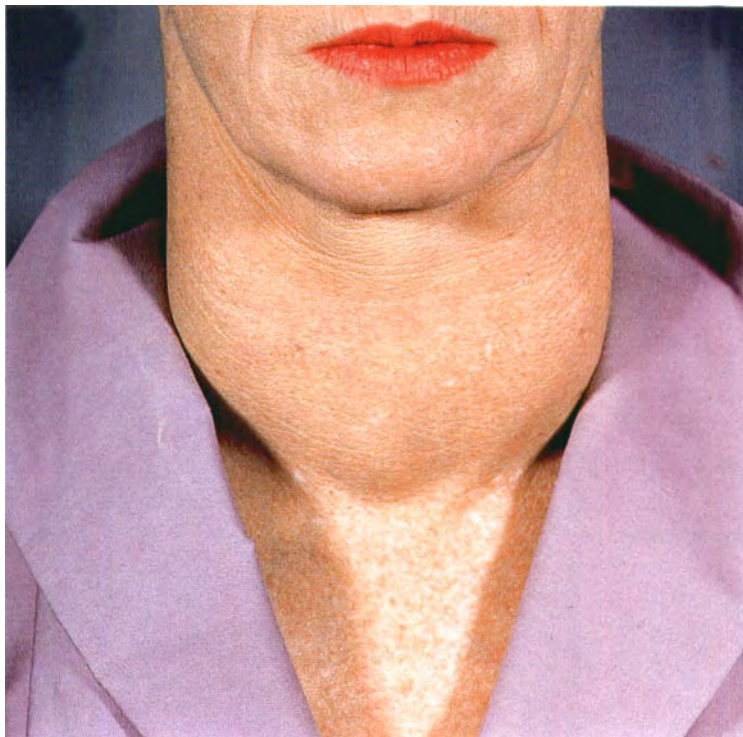
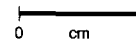


Fig. 9.37

Fig. 9.35 Secondary hyperparathyroidism. M/40. All four parathyroid glands are very markedly enlarged. The patient had chronic renal disease and the hyperplastic parathyroids were becoming autonomous and were removed. The surgeon left a small piece of one parathyroid gland in situ in order to preserve some parathyroid function.

Fig. 9.36 The cut surfaces of the parathyroids in Figure 9.35. This shows the multilobulated appearance of the hyperplastic parathyroid glands.

Fig. 9.37 Goitre. F/45. An enlarged thyroid gland. Non-functioning goitres are usually caused by dietary iodine deficiency. They are especially common in the high mountainous areas of the world.

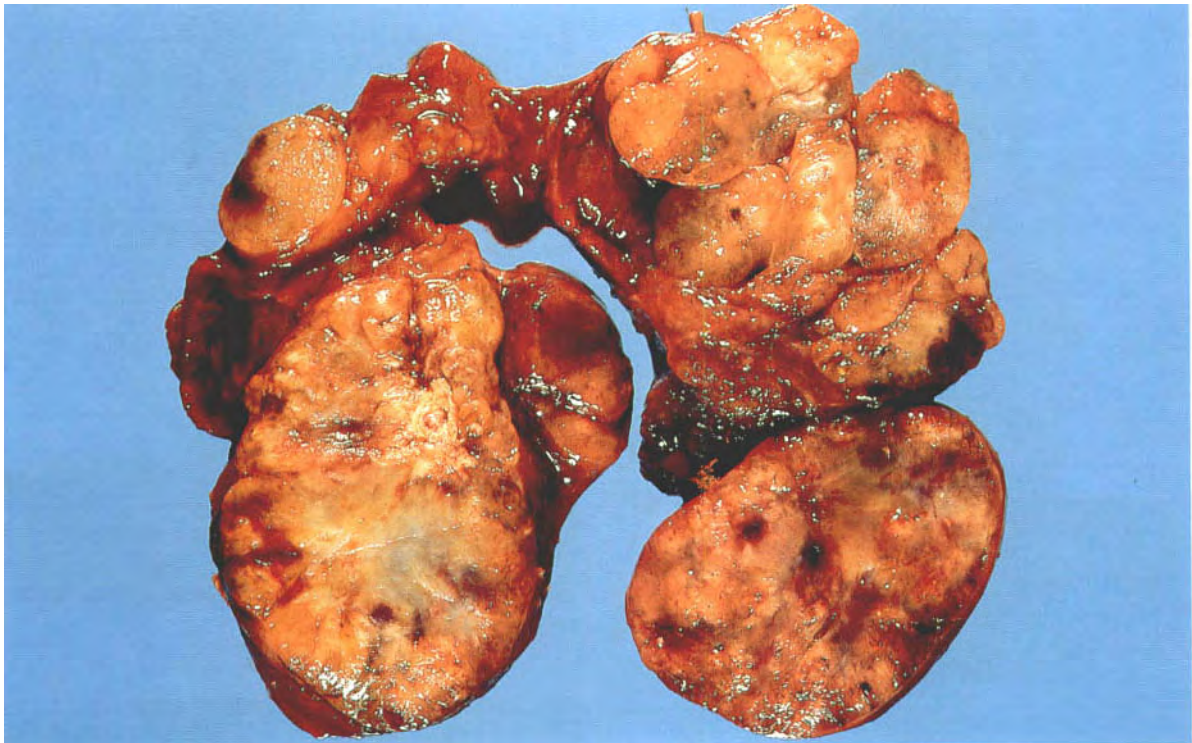


Fig. 9.38

0 cm 5

Fig. 9.38 Multinodular colloid goitre. The cut surface of the gland is multilobulated and the lobules vary in size. Glistening colloid can be seen on the surface of some lobules. Elsewhere there is fibrosis, and some of the yellowish areas in the lower poles are areas of calcification. This is the commonest pathology seen in non-functioning goitres.

Fig. 9.39 Thyroid cyst. F/46. This presented as a unilateral enlargement of the thyroid. It was hard on palpation because of the presence of calcification in its wall.

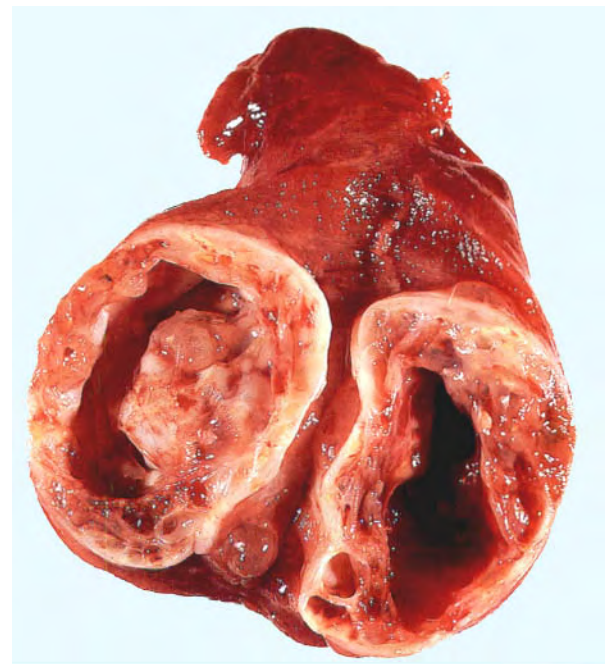


Fig. 9.39

0 cm 1

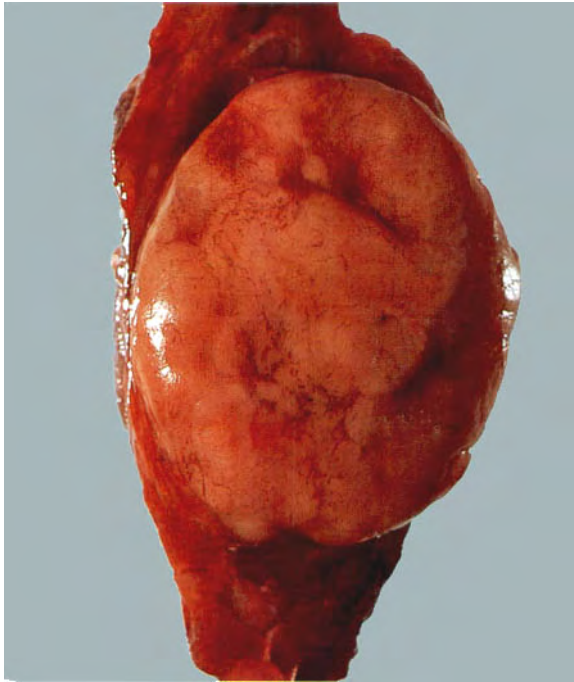


Fig. 9.40



Fig. 9.41

Fig. 9.40 Follicular adenoma of thyroid. F/35. This presented as a solitary enlargement of one lateral lobe of the thyroid. The cut surface shows a single, well circumscribed nodule of brownish-coloured tissue.

Fig. 9.41 Thyrotoxicosis. F/26. Note the presence of the smooth symmetrical goitre and a minor degree of exophthalmos of the left eye. These are two of the many physical signs of thyrotoxicosis. It is now rare to see surgical specimens of untreated thyrotoxicosis, because medical treatment is very effective.

Fig. 9.42 Cretin. F/4 months. The baby had a hoarse cry, was floppy, could not sit up, and the hair was coarse and reddish. This type of cretinism is caused by a congenital absence of the thyroid gland. It results in profound mental retardation.



Fig. 9.42

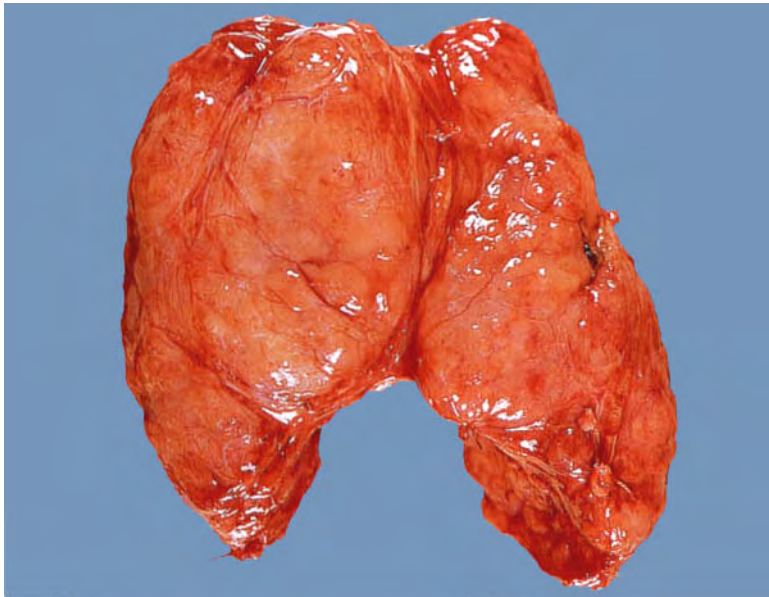


Fig. 9.43



Fig. 9.44

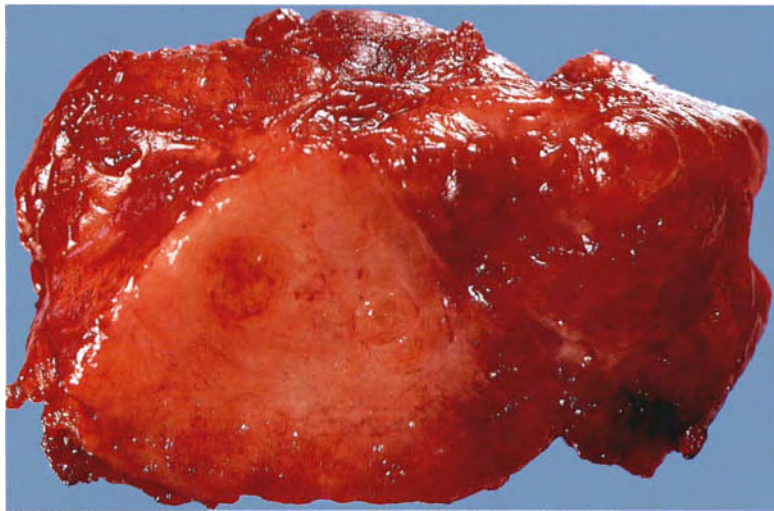


Fig. 9.45

Fig. 9.43 Hashimoto's thyroiditis. F/45. Subtotal thyroidectomy of a moderately enlarged thyroid gland. Patients with this condition are usually middle-aged women who have a slightly enlarged thyroid gland (rather like that illustrated in Figure 9.37) and mild hypothyroidism.

Fig. 9.44 Cut surface of the gland from Figure 9.43. It shows the nodular, fleshy appearance characteristic of this condition. No colloid can be seen.

Fig. 9.45 Granulomatous thyroiditis. F/60. This woman presented with a unilateral thyroid enlargement. There is a firm, homogeneous area in the middle of the specimen. Microscopic sections showed granulomatous thyroiditis. These patients sometimes present with thyrotoxicosis due to the release of thyroxin as the thyroid follicles are destroyed by the inflammation.



Fig. 9.46

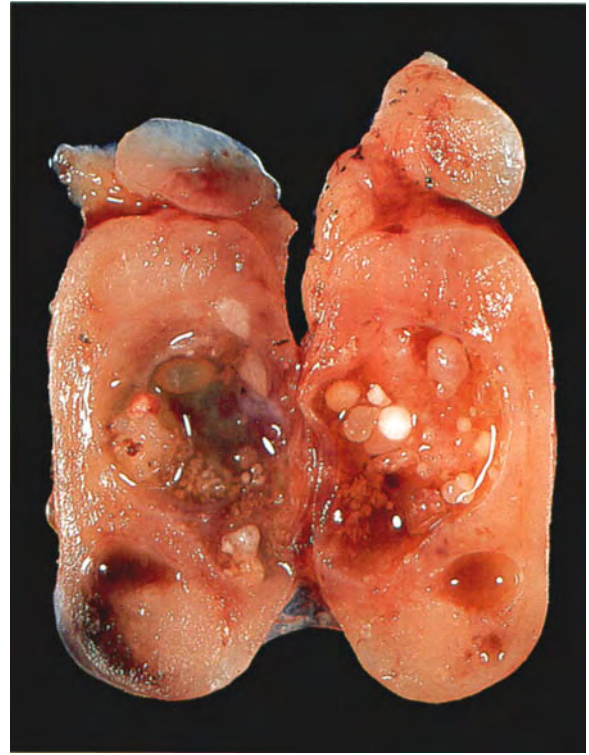


Fig. 9.47

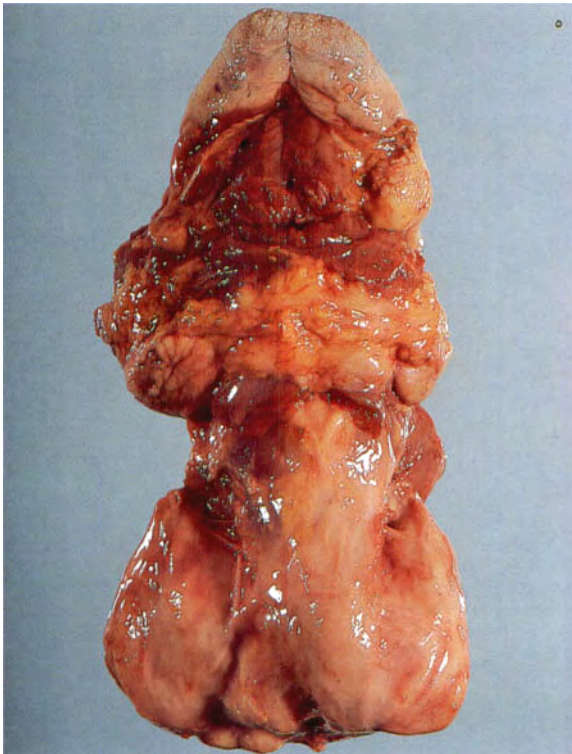


Fig. 9.48

Fig. 9.46 Riedel's thyroiditis. F/60. The abnormal thyroid was an unexpected postmortem finding. The gland was hard and woody, and was firmly attached to the strap muscles of the neck. This is a very rare condition.

Fig. 9.47 Follicular carcinoma of the thyroid. F/46. The patient presented with unilateral enlargement of the thyroid and a single thyroid nodule was removed. It appears to be well circumscribed, with a fairly homogeneous cut surface. The diagnosis of follicular carcinoma depends on the microscopic demonstration of vessel invasion, or the presence of metastases.

Fig. 9.48 Secondary papillary carcinoma of the thyroid in a cervical lymph node. F/25. This patient presented with cervical lymphadenopathy. One of the nodes was removed, and when it was cut across a focus of colloid-containing thyroid tissue was visible.



Fig. 9.49



Fig. 9.50

Fig. 9.49 Multifocal papillary carcinoma of the thyroid. F/21. Tumour is present throughout the enlarged gland.

Fig. 9.50 Solitary papillary carcinoma of the thyroid. F/43. This presented as a localized lump in the left lateral lobe of the thyroid.

Figures 9.48 to 9.50 demonstrate the three main ways in which papillary carcinoma of the thyroid presents. When the presentation is because of cervical lymphadenopathy, the thyroid may not be palpable. It is necessary to remove the whole gland, because the primary tumour may be multifocal and only identifiable by microscopic examination.

Fig. 9.51 Medullary carcinoma of the thyroid. F/40. Tumour involved both lobes of the gland, causing considerable enlargement, as shown in this operative photograph.

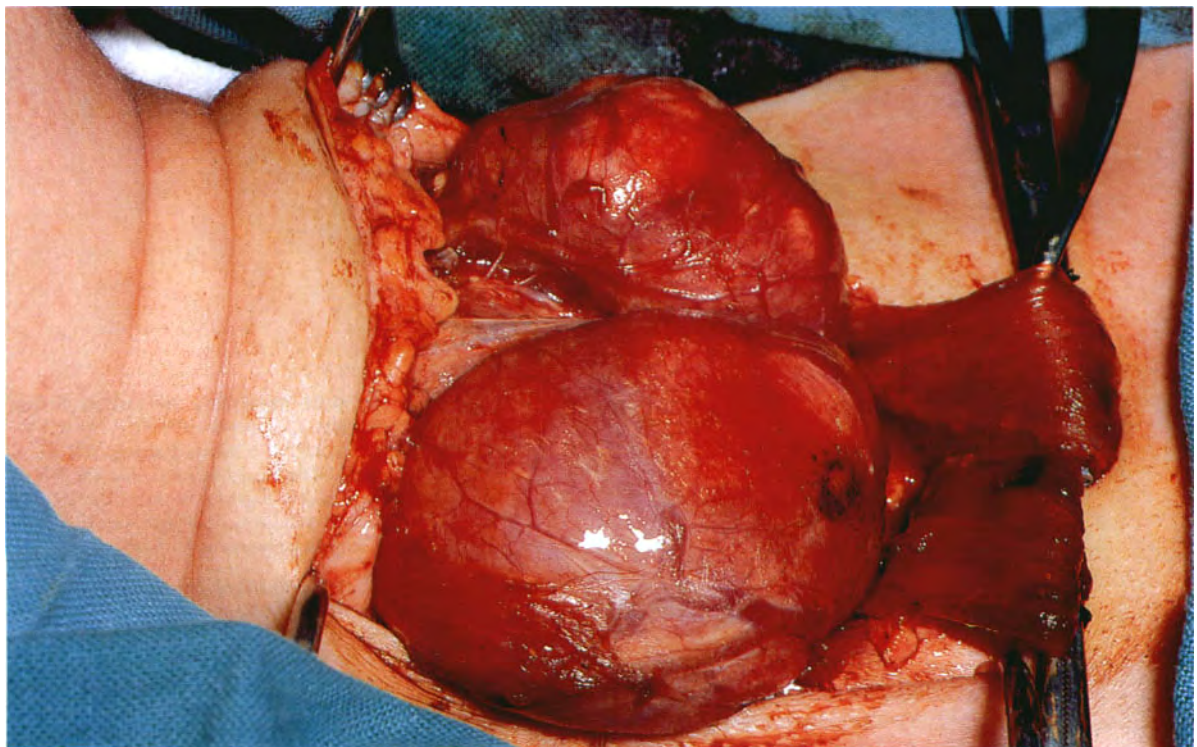


Fig. 9.51

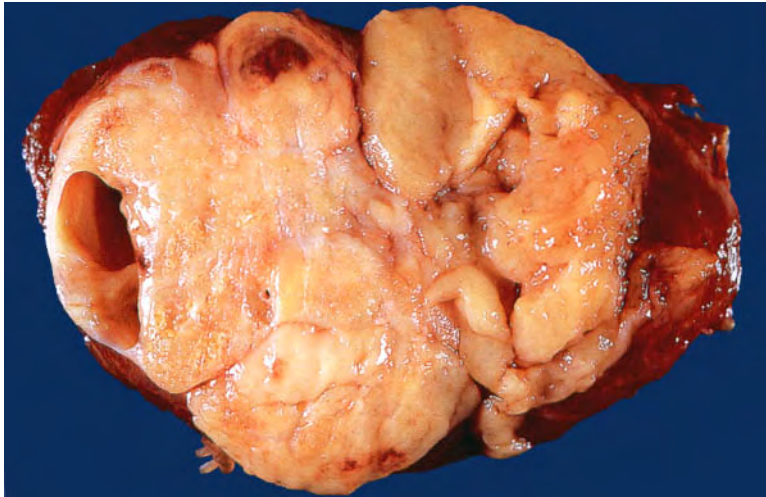


Fig. 9.52

0 cm 1



Fig. 9.53

Fig. 9.52 Medullary carcinoma of the thyroid. Cut surface of the tumour from Figure 9.51. It is fleshy and yellowish in colour. One would need to examine the microscopic sections to see the anaplastic tumour with amyloid stroma before making a confident diagnosis in this case.

Fig. 9.53 Multiple neurofibromas on the tip of the tongue of the patient in Figure 9.51. During life she had mild dysphagia and diarrhoea. Postmortem examination, 15 years after her first diagnosis, revealed the presence of ganglioneuromatosis of the oesophagus and small intestine.

Fig. 9.54 Pheochromocytoma. One of the bilateral pheochromocytomas removed from the patient in Figure 9.51. There appear to be two larger, fairly discrete areas of tumour (one of them being partially cystic) and two smaller, discrete areas of tumour within this adrenal gland. The patient exhibited the features of **multiple endocrine adenopathy syndrome type 2B**. Two of her siblings were tested and they did not have it, but her mother probably died from secondary medullary carcinoma of the thyroid.

Fig. 9.55 Secondary medullary carcinoma of the thyroid in the liver. F/55. This woman had had a medullary carcinoma of the thyroid removed 21 years before she presented with Cushing's syndrome, 3 months before her death. This demonstrates two of the other features of medullary carcinoma: (1) that it grows slowly and metastases may not appear until many years after removal of the primary; (2) that it is one of the tumours that produces ACTH, and the clinical presentation may occur because of the effects of this.

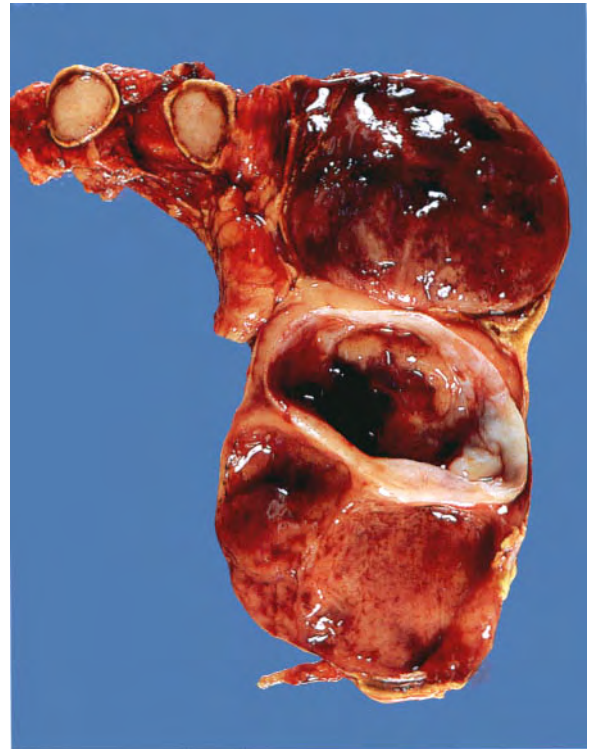


Fig. 9.54

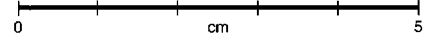


Fig. 9.55

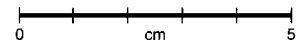




Fig. 9.56

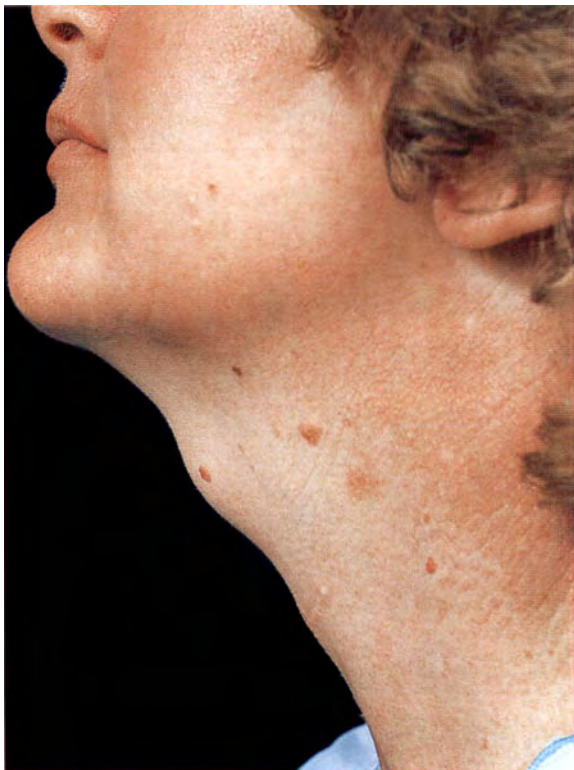


Fig. 9.57

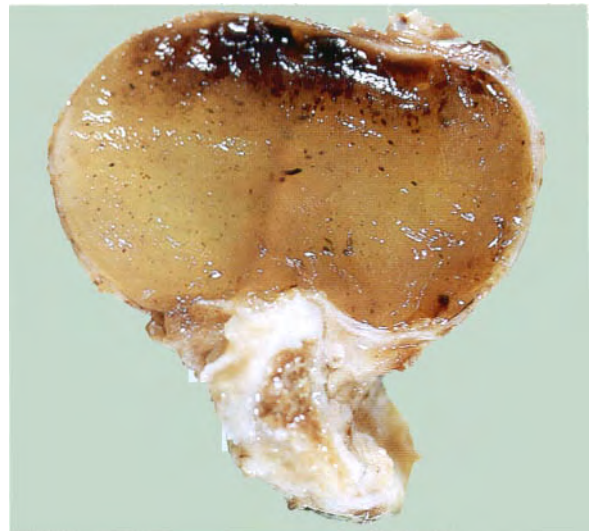


Fig. 9.58

0 cm 1

Fig. 9.56 Amyloid goitre. F/12 from Papua New Guinea. The thyroid has been almost completely replaced by firm, homogeneous pale tissue which microscopically was amyloid. Amyloid goitre is relatively common in Papua New Guinea, where it occurs as part of a primary amyloidosis syndrome, the other main feature of which is normotensive renal failure.

Fig. 9.57 Thyroglossal cyst. F/40. Situated in the midline, just above the thyroid cartilage.

Fig. 9.58 Thyroglossal cyst. Surgical specimen showing the cyst filled with glistening colloid.

**BONES, JOINTS
AND CONNECTIVE
TISSUE**

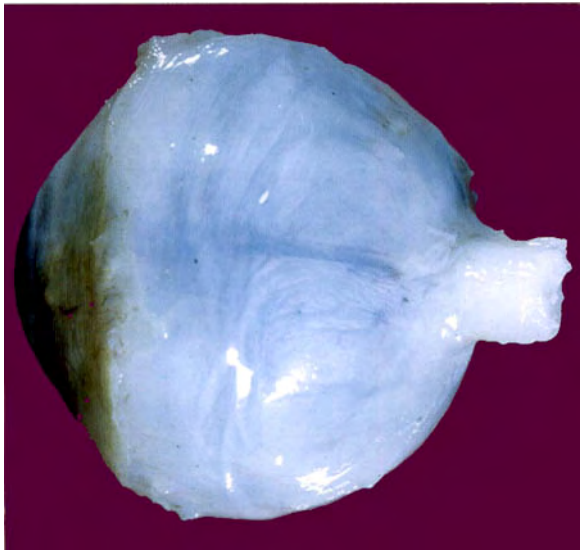


Fig. 10.1

0 cm 1



Fig. 10.3

0 cm 1



Fig. 10.2

Fig. 10.1 Osteogenesis imperfecta. Patients with this condition have abnormally fragile bones and suffer multiple repeated fractures. They usually have blue-coloured sclerotics, as is shown in this eye from a child who died from this condition.

Fig. 10.2 Achondroplasia. M/6. The patient demonstrates the short arms and legs of this inherited abnormality of endochondral ossification.

Fig. 10.3 Multiple enchondromata (Ollier's disease). M/28. The head of the humerus is greatly expanded by the intramedullary chondromas.

Fig. 10.4 Acute osteomyelitis. F/21. There is a large collection of pus in the medullary cavity of the shaft of the femur. This patient died from acute leukaemia, and the infection resulted from her immune deficiency state.

Fig. 10.5 Chronic osteomyelitis. This specimen shows death of the bone of the shaft of the tibia. This has separated completely as a sequestrum. New bone – an involucrum – has formed around the dead bone. Lacunae open through the involucrum and result in *discharging sinuses on the skin surface*. This specimen was prepared in the 1770s by John Hunter and is displayed in the Museum of the Royal College of Surgeons in London. It demonstrates the long-term complications of acute osteomyelitis before the days of antibiotics. The pressure of the pus causes death of the bone. Pus then forms an abscess, which ruptures through the skin, producing chronic discharging sinuses. Then, progressively, new bone forms on the scaffolding of the dead bone. Progressively, some or all of the dead bone (sequestrum) discharges through the sinuses. The Museum catalogue does not record an age or sex for this specimen.



Fig. 10.4



Fig. 10.5



Fig. 10.6



Fig. 10.7

Fig. 10.6 Tuberculosis of the spine. F/4. This child from Papua New Guinea is grossly emaciated from the disseminated infection. The deformity in the lumbar region is characteristic of involvement of the lumbar vertebrae by tuberculous infection. The diseased vertebrae 'collapsed'.

Fig. 10.7 Tuberculosis of the spine. F/4. X-ray of the child shown in Figure 10.6. The collapsed lumbar vertebrae are easily seen.



Fig. 10.8



Fig. 10.9

Fig. 10.8 Tuberculosis in the spine of a young boy (Pott's fracture of the vertebrae). This is a specimen from one of Percival Pott's original cases from about 1770. It is housed in the Pathology Museum of St Bartholomew's Hospital, London.

Fig. 10.9 Tuberculous psoas abscess. Two lumbar vertebrae involved by tuberculosis with extension of the caseation into the psoas muscle. When such infection spreads along the psoas, the abscess may 'point' in the groin.

Fig. 10.10 Secondary carcinoma in the lumbar vertebrae. M/68. Cream-coloured homogeneous deposits can be seen in each vertebral body, the biggest being in the lower one. The primary tumour was a bronchogenic carcinoma of the lung.



Fig. 10.10



Fig. 10.11

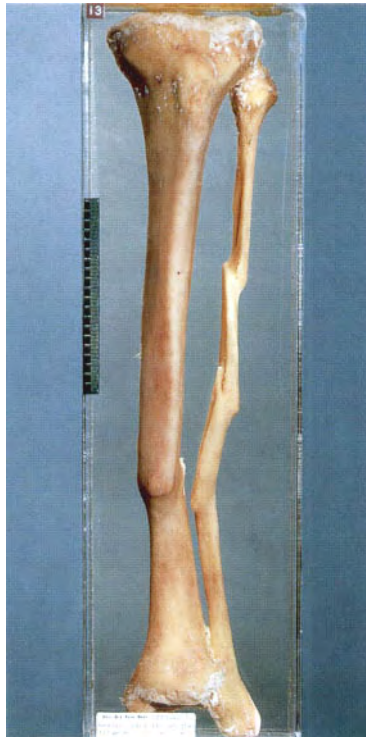


Fig. 10.12



Fig. 10.13



Fig. 10.14

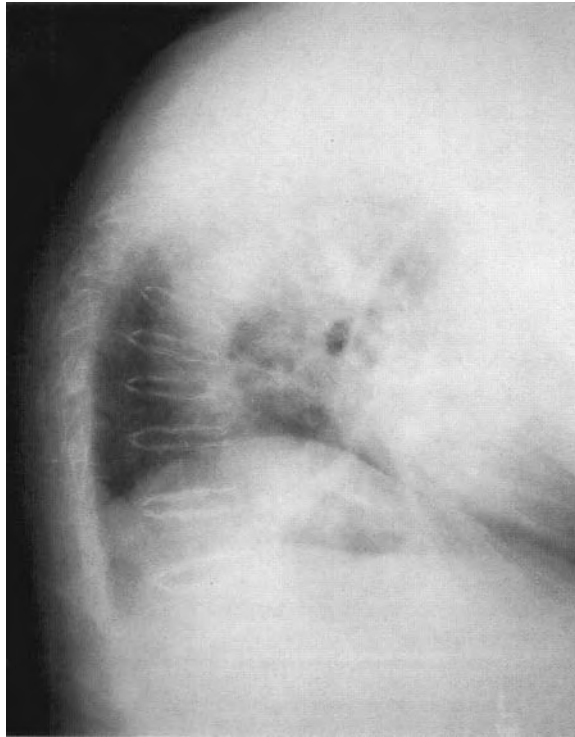


Fig. 10.15



Fig. 10.16

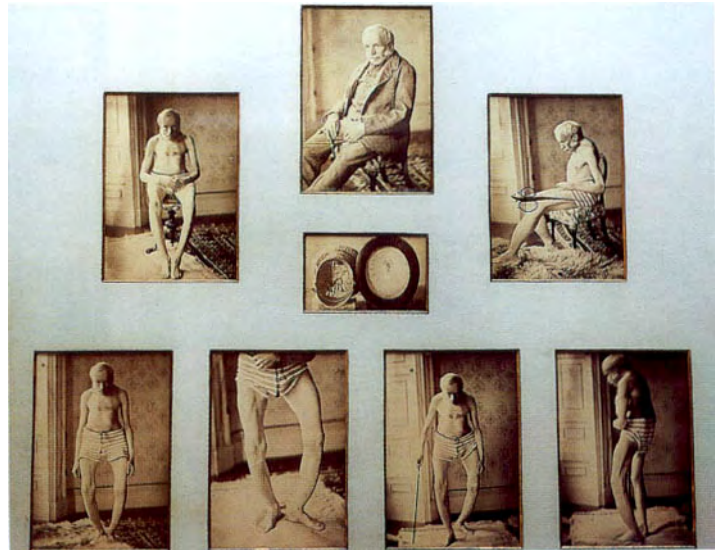


Fig. 10.17

Fig. 10.11 Healed fracture. Femur recovered by archaeologists from a burial about 200 years ago. There has been a fracture, which has healed with a great deal of callus formation.

Fig. 10.12 Multiple fractures of the tibia and fibula which have healed with very little callus – a tribute to modern splinting methods for the treatment of fractures.

Fig. 10.13 Osteoporosis. F/65. The trabecular bone in the vertebral bodies is very thin and the two lower vertebrae show the effects of crush fracture – a complication of this condition.

Fig. 10.14 Osteoporosis. M/40. This vertical slice through the thoracic spine shows severe osteoporosis of the vertebrae, with the characteristic 'bowing' or 'curvature' of the spine caused by collapse of the anterior portions of the vertebral bodies. Osteoporosis of this severity is more common in postmenopausal women. It is frequently associated with nerve pain caused by compression of the nerves as they pass through the intervertebral foramina. The cause of the osteoporosis was not found in this case.

Fig. 10.15 Osteoporosis. X-ray of the patient shown in Figure 10.14 taken some months before his death.

Paget's disease

James Paget (1814–1899) studied medicine at St Bartholomew's Hospital, London, and went on to become a surgeon at that hospital. His name is given to some of the diseases which he was the first to describe. Paget's disease of bone and Paget's disease of the nipple are the two most famous of these.

Fig. 10.16 Portrait of James Paget displayed in the Pathology Museum of St Bartholomew's Hospital, London.

Fig. 10.17 Photographs of the first case of Paget's disease of bone (osteitis deformans), described by Paget in 1876. These photographs were taken of a 68-year-old man, 6 months before he died. He demonstrates the features of Paget's disease. The hats indicate the increase in size of his head between 1844 and 1876. The deformation of the bones of the lower limbs is well illustrated.



Fig. 10.18



Fig. 10.19

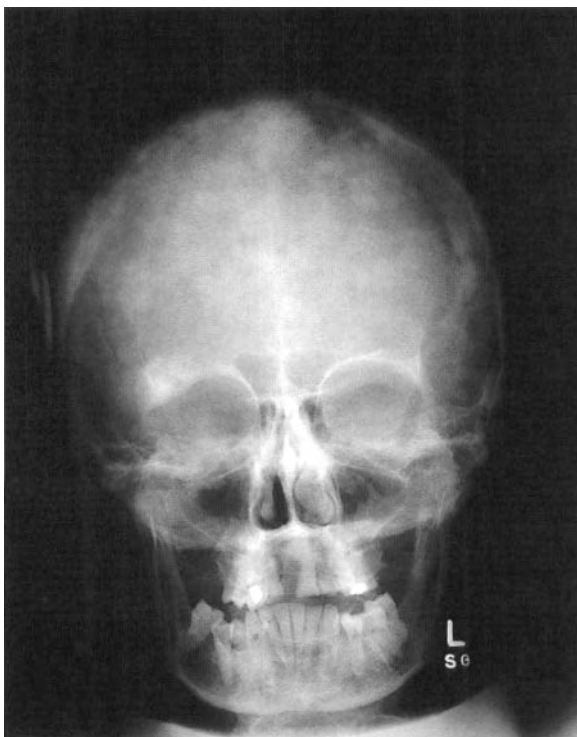


Fig. 10.20

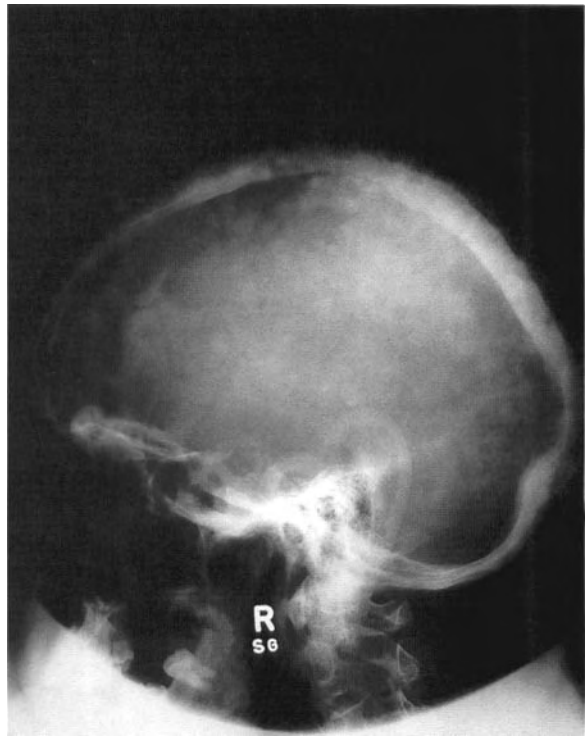


Fig. 10.21



Fig. 10.22

Fig. 10.18 Sample bones from the original case of Paget's disease. They show the marked thickening of the cortical bone of the tibia, the skull and the patella.

Fig. 10.19 **Paget's disease.** M/66. Clinical photograph showing the characteristic enlarged head. Patients often complain of headaches.

Fig. 10.20 Anteroposterior X-ray of the skull of the man shown in Figure 10.19.

Fig. 10.21 Lateral view of the same skull, showing marked thickening of the diploe.

Fig. 10.22 **Paget's disease.** X-ray changes in the pelvis.



Fig. 10.23

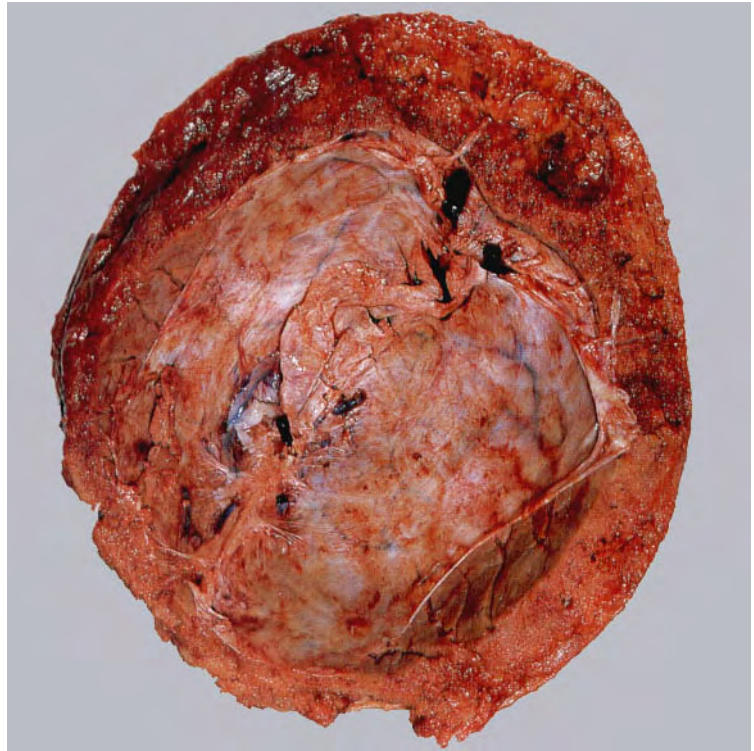


Fig. 10.24

Fig. 10.23 Paget's disease. Longitudinal slice of a tibia from another case, showing the marked thickening of the cortical bone. This specimen looks very much like the tibia from Paget's original case. The bone is thick, but softer than normal bone. As a result there is anterior bowing of the tibia, and the bones are more liable to fracture than are normal bones.

Fig. 10.24 Paget's disease of the skull. F/81. Note the gross thickening of the diploe of the skull. The bone is extremely vascular. This vascularity sometimes results in cardiac failure in patients with Paget's disease.



Fig. 10.25

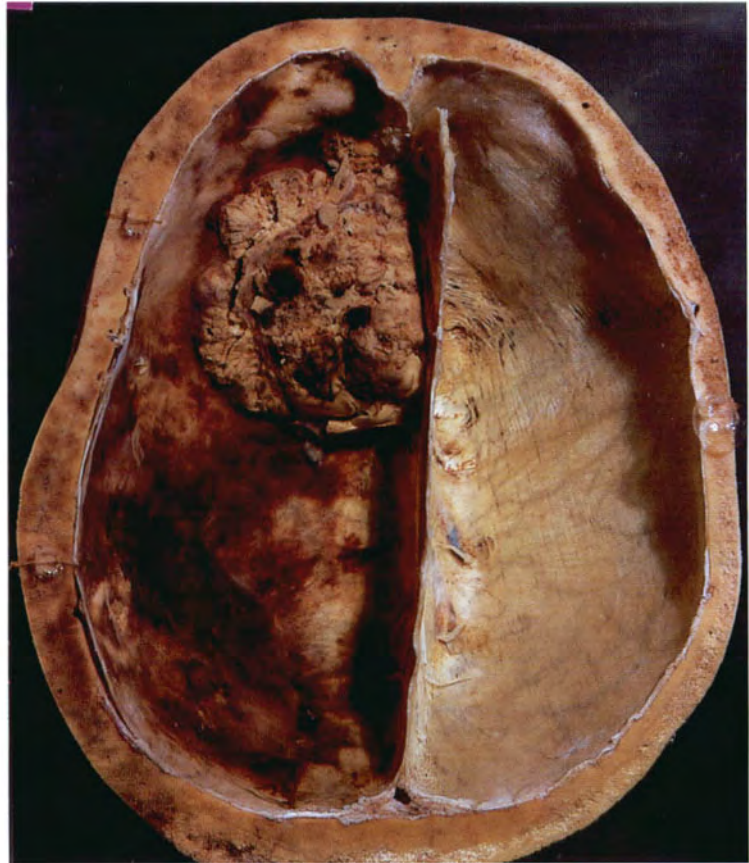


Fig. 10.26

Fig. 10.25 Paget's disease. The sliced femur shows thickening of the cortical bone. An osteogenic sarcoma has arisen at the distal end of the bone. Osteogenic sarcoma is a well recognized complication of Paget's disease. There are two age peaks for osteogenic sarcoma, one in adolescents and young adults, and the second in older people with Paget's disease.

Fig. 10.26 Paget's disease of the skull complicated by the development of an osteogenic sarcoma.

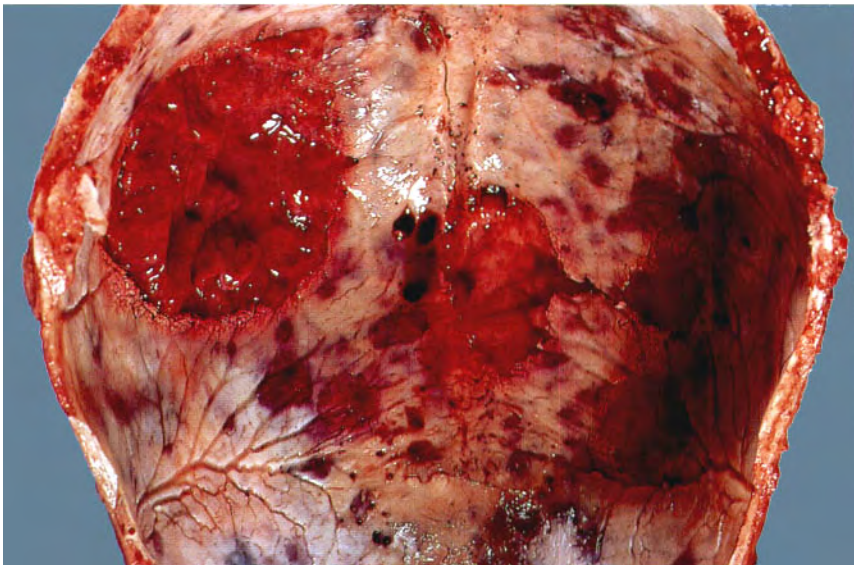


Fig. 10.27



Fig. 10.28

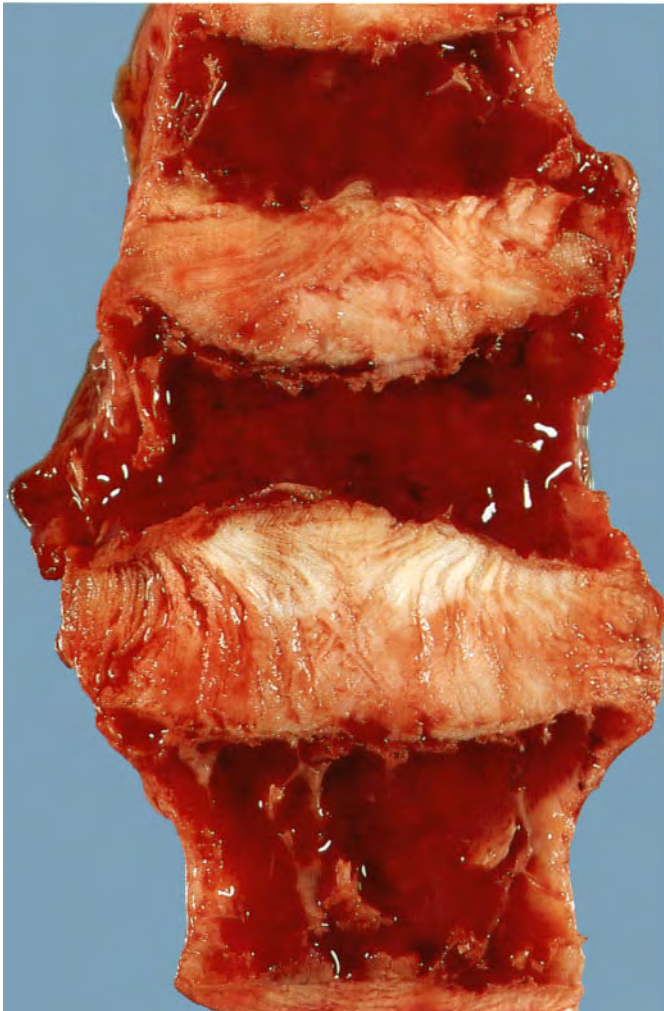


Fig. 10.29



Fig. 10.30

Fig. 10.27 Skull in multiple myeloma. M/39. Multiple, rounded red deposits of myeloma are present in the calvarium.

Fig. 10.28 Multiple myeloma. A lateral X-ray of the skull showing the punched-out defects of deposits of multiple myeloma.

Fig. 10.29 Vertebral column in multiple myeloma. The same patient as in Figure 10.27. The myeloma deposits in the vertebrae cause loss of bone and consequent crush fractures, as demonstrated here.

Fig. 10.30 Multiple myeloma. Humerus and femur showing localized areas of deposition of myeloma in the long bones.

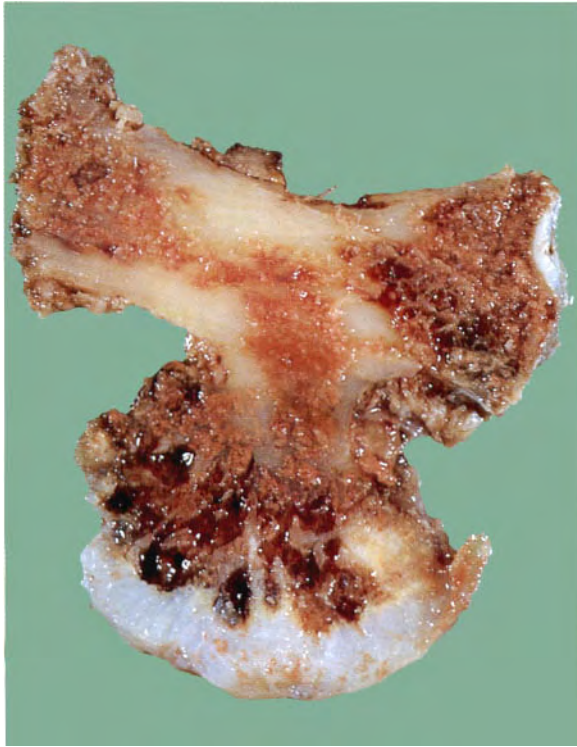


Fig. 10.31

0 cm 1



Fig. 10.32

0 cm 1



Fig. 10.33

0 cm 1



Fig. 10.34

0 cm 1



Fig. 10.35



Fig. 10.36

Fig. 10.31 Osteochondroma on a rib. F/22. This is a common benign tumour which usually occurs in the region of the epiphyses of long bones. It is characterized by having a distinct cartilage cap. Such tumours are easily excised.

Fig. 10.32 Osteoid osteoma in the proximal phalanx of a finger. M/30. There is a benign, well circumscribed tumour within the medullary cavity. The treatment of choice is local curettage. Amputation such as this is overtreatment. The commonest site for an osteoid osteoma is the upper end of the tibia.

Fig. 10.33 Benign chondroma. M/27. This small cartilage tumour was resected from the tibia.

Fig. 10.34 Fibrous dysplasia in the medullary cavity of the midshaft of the tibia. F/14.

Fig. 10.35 Multiple benign haemangiomas in the vertebrae. F/68. This was an incidental postmortem finding. Haemangiomas of bone may be single or multiple. In the vertebrae they may be large enough to destroy cancellous bone, which may result in crush fractures.

Fig. 10.36 Aneurysmal bone cyst in the lower end of the right ulna. M/40. The large angiomatous spaces are expanding the cortex of the bone, hence the name 'aneurysmal'.

Fig. 10.37 Osteogenic sarcoma. F/11. The creamy tumour has involved the lower end of the femur and has broken through the cortical bone and caused elevation of the periosteum.



Fig. 10.37

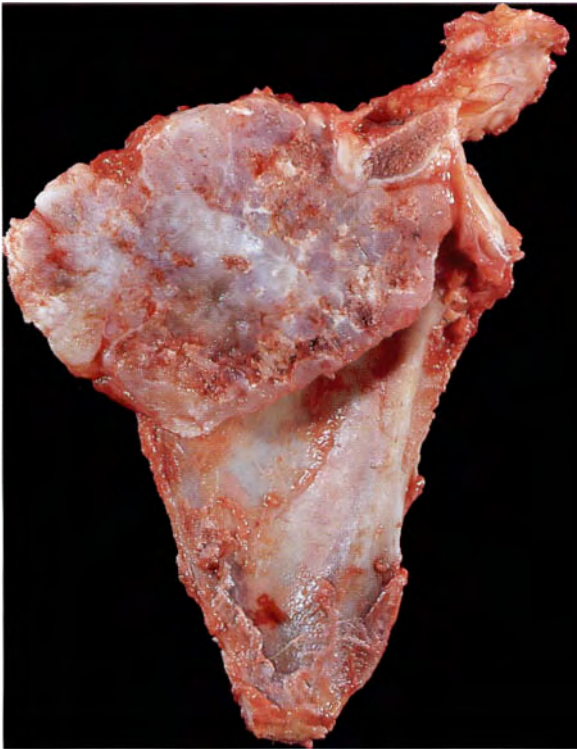


Fig. 10.38



Fig. 10.39



Fig. 10.40



Fig. 10.41

0 cm 5

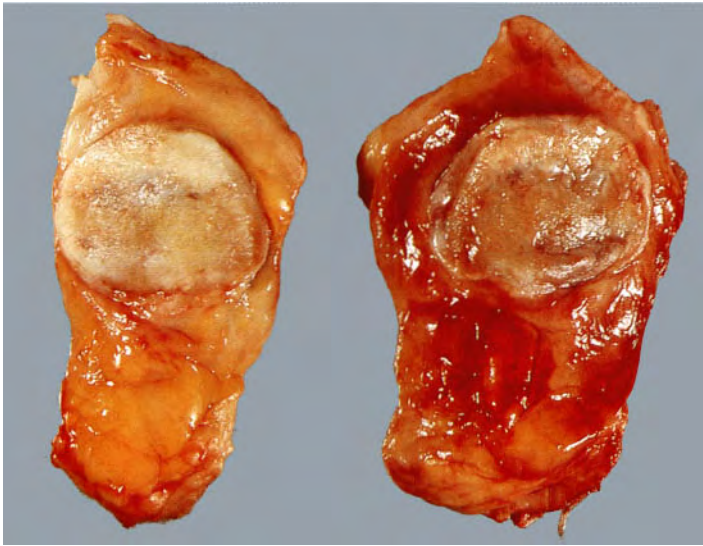


Fig. 10.42

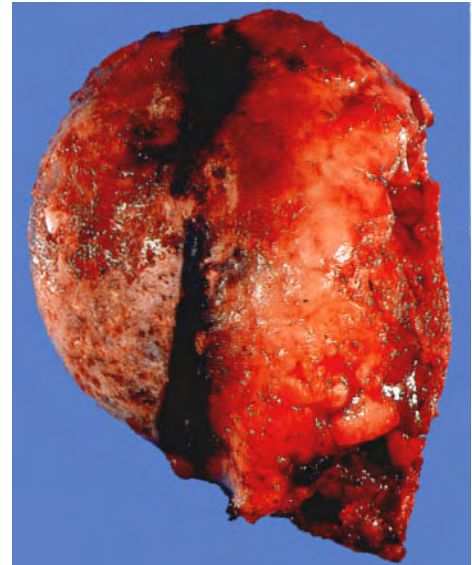
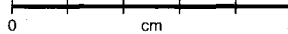


Fig. 10.43

Fig. 10.38 Chondrosarcoma arising in the scapula. F/35. This tumour had grown rapidly. Its cut surface shows a lobulated pattern with the white, glistening appearance of cartilage.

Fig. 10.39 Giant cell tumour in the lower end of the femur. M/38. There is a haemorrhagic tumour expanding the lateral condyle and destroying the normal bone.

Fig. 10.40 Ewing's tumour. M/13. A large tumour in the upper third of the tibia has eroded the cortical bone and extended beneath the periosteum. There is a pathological fracture through the tumour.

Fig. 10.41 Chordoma removed from the pelvis anterior to the sacrum. M/58. The tumour is haemorrhagic and has a rather mucoid cut surface. Microscopic examination was required to make a definitive diagnosis.

Fig. 10.42 Chronic osteoarthritis. F/67. Both patellae have been removed. They show irregular eburnation of their articular surfaces.

Fig. 10.43 Osteoarthritis and ochronosis. M/58. The head of the femur was amputated during an operation for insertion of an artificial hip joint. The patient had had painful, osteoarthritic hips for some years. The specimen shows overgrowth of bone with the formation of osteophytes along the line of the resection, and irregularity of the articular cartilage. These are features of osteoarthritis and the only special feature is the wide band of black pigment running across the articular cartilage. Ochronosis is characterized by melanin pigmentation of articular cartilage. Patients with this abnormality are particularly prone to develop osteoarthritis.

Fig. 10.44 Ochronosis. The right eye of the patient from Figure 10.43 shows deposition of melanin in the sclera. He also had patches of pigmentation in the cartilage of his ears.

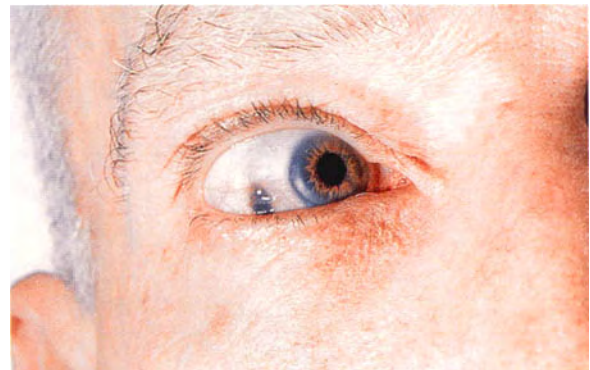


Fig. 10.44

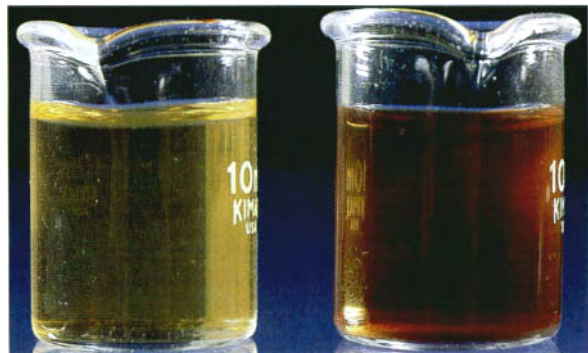


Fig. 10.45

Fig. 10.45 Urine from the same patient as in Figure 10.44. The sample on the left is freshly voided and that on the right has been standing for 2 hours, during which time it has turned dark brown. Figures 10.43 to 10.45 illustrate the main features of the hereditary metabolic disease alkaptonuria.



Fig. 10.46

0 cm 5

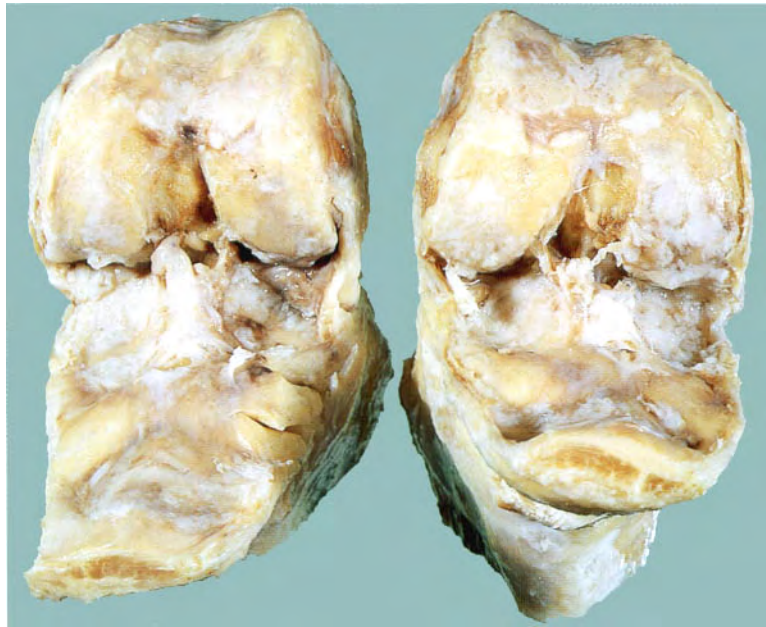


Fig. 10.47

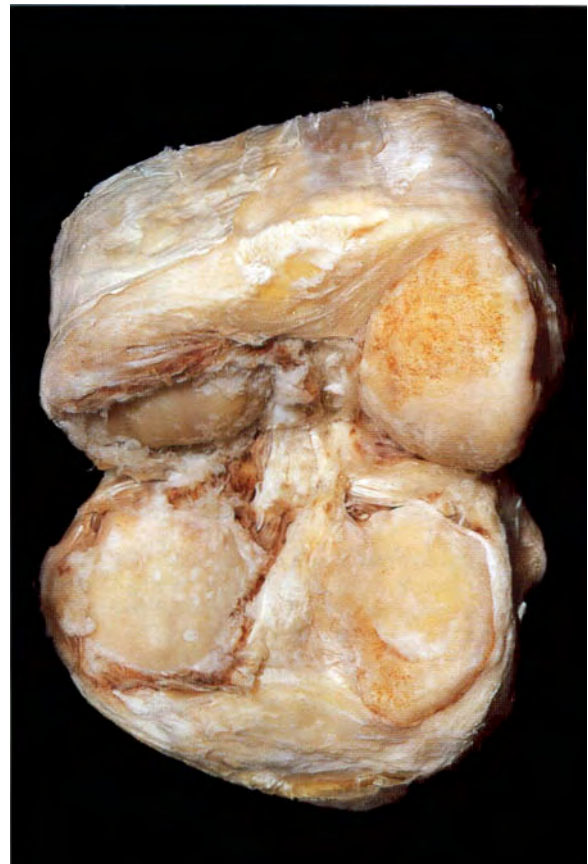


Fig. 10.48

Fig. 10.46 Knee joint in gout. M/76. The knee joint has been opened to show the heavy deposition of urate crystals in the articular cartilage.

Fig. 10.47 Knee joints in rheumatoid arthritis. F/63. The joints have been opened to show the gross destruction of the articular cartilages by the overgrowth of pannus. A fibrous ankylosis had occurred and the ragged appearance of the articular surfaces is partly due to the tearing of this during the opening of the joints.

Fig. 10.48 Chronic arthritis resulting from multiple haemarthroses. M/50 with haemophilia. The articular surfaces of the knee joint are markedly pitted and destroyed. The yellow pigmentation is due to the deposition of iron. The knee joints of patients with haemophilia are especially vulnerable to bleeding, which results from mild trauma.



Fig. 10.49



Fig. 10.50

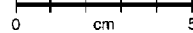


Fig. 10.51



Fig. 10.52

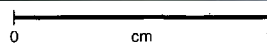


Fig. 10.49 Ankylosing spondylitis. M/46. This man demonstrates the posture adopted to compensate for the fact that his spinal column is rigid.

Fig. 10.50 Spinal column of ankylosing spondylitis. M/50. The calcification of the interspinous ligaments is demonstrated.

Fig. 10.51 Kyphoscoliosis. F/47. There are many causes for this deformity of the spine. They include congenital and acquired diseases of bone, muscle and nerves.

Fig. 10.52 Giant cell tumour of tendon sheath (benign synovioma) excised from the finger. F/58. The tumour is lobulated and the brown colour is due to the deposition of haemosiderin. When a similar lesion occurs in the synovial membrane within a joint it is called pigmented villonodular synovitis.



Fig. 10.53



Fig. 10.54

0 cm 1



Fig. 10.55

0 cm 1

Fig. 10.53 Cyst of the lateral meniscus of the knee. F/50.

Fig. 10.54 The lateral meniscus has been removed and the cut surface shows a multiloculated cyst containing sticky synovial fluid.

Fig. 10.55 Synovial cyst or ganglion removed from near a joint. F/52. The thin-walled multiloculated cyst has been cut open. Some of the synovial fluid it contained is still present.

Fig. 10.56 Benign subcutaneous lipoma. F/27. The cut surface shows a lobulated appearance, which is accentuated by thin bands of fibrous tissue.

Fig. 10.57 Intramuscular myxoma. F/79. This tumour was removed from the right buttock. It is well circumscribed within the muscle and its cut surface shows a glistening appearance.

Fig. 10.58 Liposarcoma. M/34. The cut surface is multilobulated and contains some solid areas and some areas of haemorrhage. All malignant soft-tissue tumours appear macroscopically to be well encapsulated. This leads surgeons to 'shell them out' as one would remove a pea from a pod. This invariably leaves residual tumour, which will regrow if further resection is not performed.

Fig. 10.59 Rhabdomyosarcoma. F/44. This tumour was removed from the forearm with a good margin of muscle around it. The tumour is brown, with a central area of haemorrhage. Wide local resection, wherever possible, is currently accepted as the treatment of choice for malignant soft tissue tumours. Classification of malignant soft tissue tumours has been greatly refined by the use of immunoperoxidase stains.



Fig. 10.56

0 cm 1

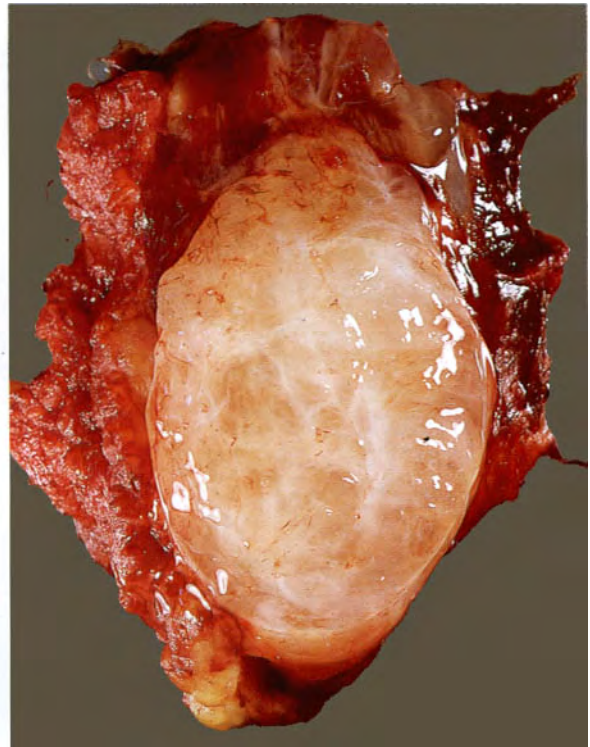


Fig. 10.57

0 cm 5

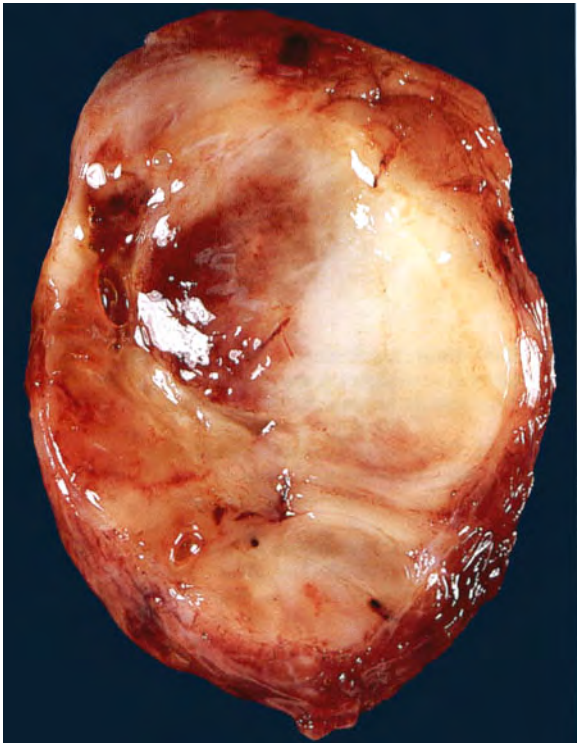


Fig. 10.58

0 cm 1

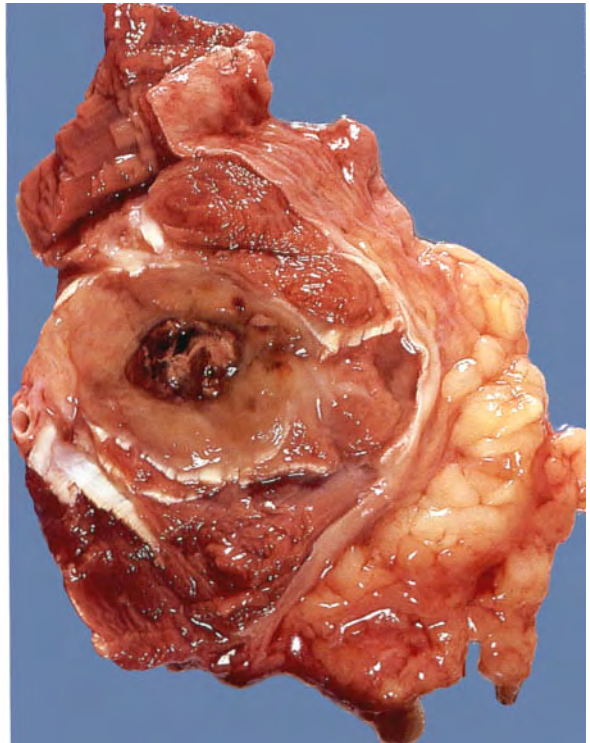


Fig. 10.59

0 cm 5

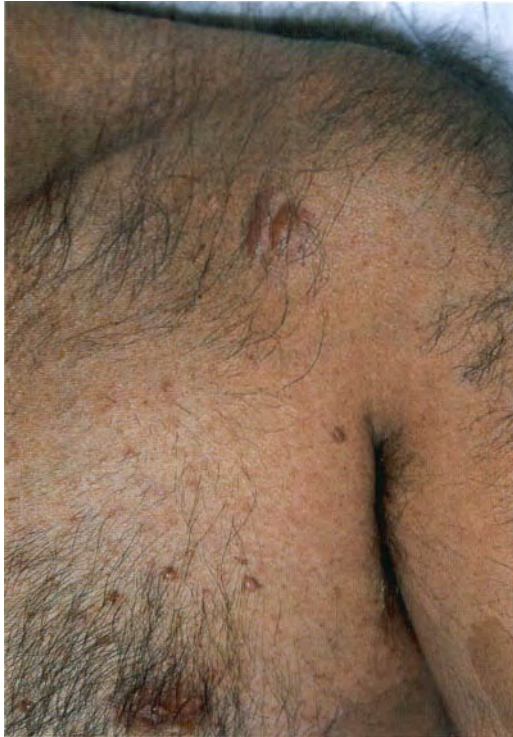


Fig. 10.60



Fig. 10.62

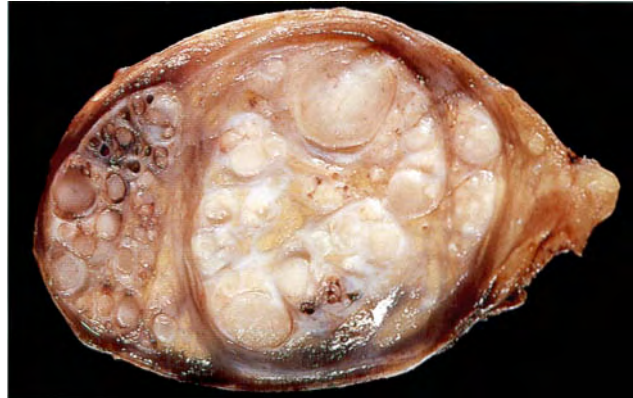


Fig. 10.61

0 cm 1

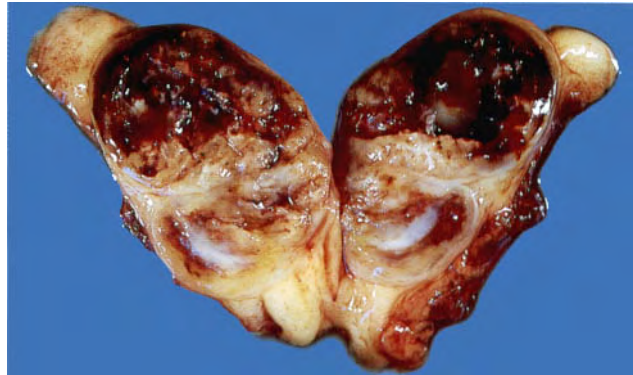


Fig. 10.63

0 cm 1

Fig. 10.60 Neurofibromatosis. M/20. The multiple brown subcutaneous neurofibromas are readily visible. There is a *café-au-lait* spot on the inner aspect of the left arm.

Fig. 10.61 Transverse section of a plexiform neurofibroma of the sciatic nerve. M/34. This benign proliferation of nerve is often associated with neurofibromatosis.

Fig. 10.62 Neurofibrosarcoma of the sciatic nerve. M/8. This is another complication of neurofibromatosis. A large, irregular, partly necrotic tumour has developed on the sciatic nerve. Microscopically it showed numerous mitoses. Treatment was amputation of the leg.

Fig. 10.63 Benign neurilemmoma. F/41. These tumours are usually single and their cut surface has a variegated appearance, as this one has. It is usually not associated with neurofibromatosis.



Fig. 10.64

Fig. 10.64 Digital fibroma on the third finger. F/6 months. Microscopically, these tumours are characterized by the presence of spherical, eosinophilic inclusions in the cytoplasm of the proliferating fibroblasts.

Fig. 10.65 Keloid scar on the shoulder. F/31.

Fig. 10.66 Keloid scar. Ear piercing is popular in many parts of the world. This is a potent cause of keloid scars.



Fig. 10.65



Fig. 10.66

Fig. 10.67 Plantar fibromatosis. M/12. This mass of fibrous tissue was excised from the sole of the foot. Some plantar muscle is visible in the lower portion of the specimen. This tumour is locally aggressive, and will recur if it is not completely excised.

Fig. 10.68 Dupuytren's contracture of the hand. M/50. A hard lump develops in the palm and, as it contracts, the finger is flexed towards it. The fibrous tissue in this abnormality is exactly the same as that seen in plantar fibromatosis.

Fig. 10.69 Desmoid tumour removed from the abdominal wall. M/18. The fleshy, fibrous nature of the tumour can be seen in this cross-section. This is another example of a locally aggressive fibromatosis.



Fig. 10.67

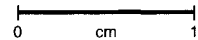
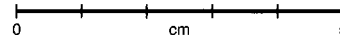


Fig. 10.68



Fig. 10.69



NERVOUS SYSTEM



Fig. 11.1

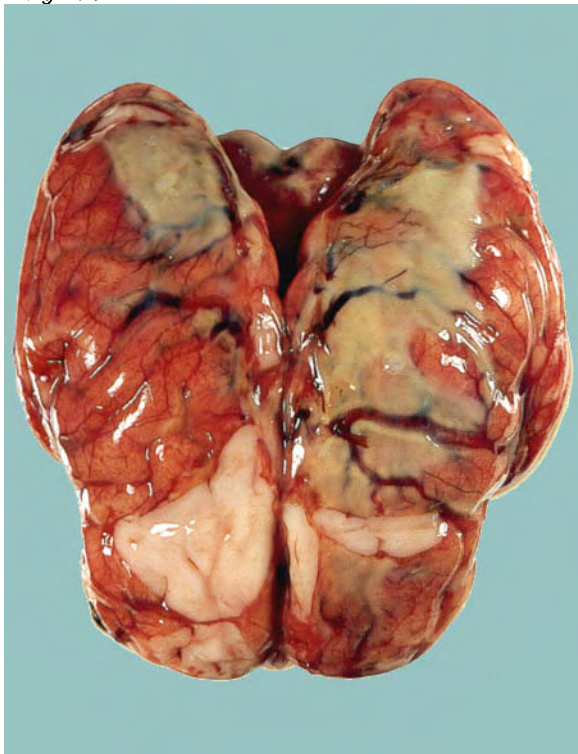


Fig. 11.2



Fig. 11.3



Fig. 11.4

Fig. 11.1 Acute meningitis. M/1. There are focal collections of pus in the subarachnoid space. This is the usual postmortem appearance of meningitis. *Haemophilus influenzae* was cultured from the CSF before death. *Neisseria meningitidis* and *Diplococcus pneumoniae* are the other common causes of bacterial meningitis.

Fig. 11.2 Neonatal meningitis. M/4 days. The meninges are reddened from vascular congestion. Thick, greenish pus fills the subarachnoid space. Most cases of neonatal meningitis are due to coliform organisms, as this one was. The leptomeninges over the frontal lobes have been torn and the surface of the brain is visible.

Fig. 11.3 Meningitis involving the spinal cord. M/3 months. The dura has been reflected and pus can be seen in the subarachnoid space. It is from this space that CSF is aspirated during lumbar puncture.

Fig. 11.4 Meningitis: bulging of the anterior fontanelle in a 2-month-old male infant. Meningitis causes raised intracranial pressure, and this can be easily seen in a baby because of tenseness or bulging of the fontanelle.

Fig. 11.5 Meningitis causing opisthotonos. M/1. Pus in the subarachnoid space causes spasm of neck muscles, giving the clinical sign of neck stiffness. In severe cases there is spasm of all the back muscles – opisthotonos.

Fig. 11.6 Meningitis: cerebrospinal fluid obtained at lumbar puncture. From left to right: (1) xanthochromic CSF; indicating the previous presence of blood; (2) clear CSF; and (3) cloudy CSF. Cloudy CSF is presumptive evidence of meningitis.



Fig. 11.5



Fig. 11.6



Fig. 11.7



Fig. 11.8

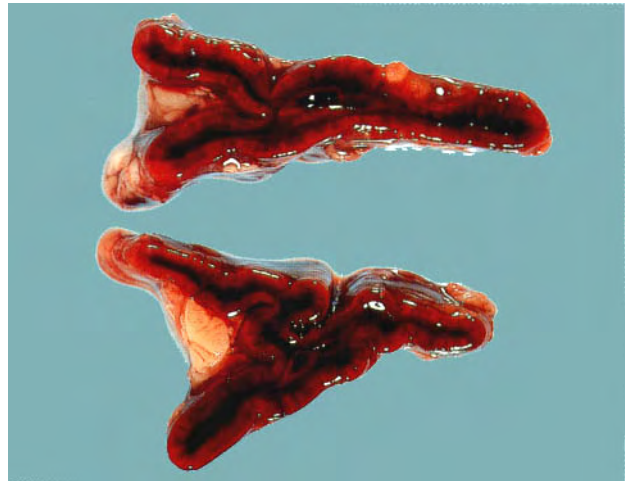


Fig. 11.9

Fig. 11.7 Waterhouse–Friderichsen syndrome. F/6 months. This child was well in the morning, became febrile and sick at midday, developed this red, haemorrhagic rash soon afterwards, and died in the late afternoon.

Figs. 11.8 & 11.9 Postmortem examination performed on the baby in Figure 11.7 revealed redness of the epiglottis (Figure 11.8) and bilateral adrenal haemorrhage (Figure 11.9). No other abnormality was found. These are the classic features of the Waterhouse–Friderichsen syndrome, which is caused most frequently by *Neisseria meningitidis*, but other organisms that cause meningitis may also produce the syndrome.

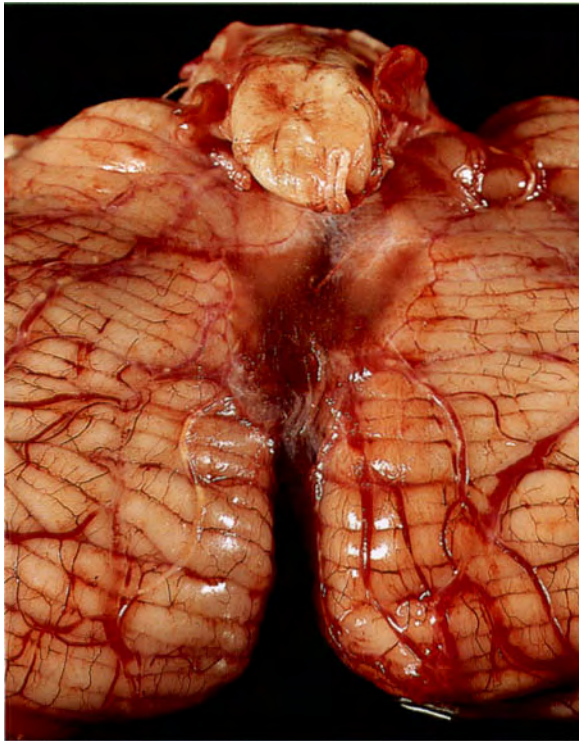


Fig. 11.10

Fig. 11.10 Normal cerebellum. The meninges over the cisterna magna are transparent.

Fig. 11.11 Meningitis cerebellum. F/3 months. The meninges over the cisterna magna are opaque owing to the presence of pus in the subarachnoid space. This has occluded the CSF outlets of the fourth ventricle, resulting in hydrocephalus – one of the complications of meningitis.

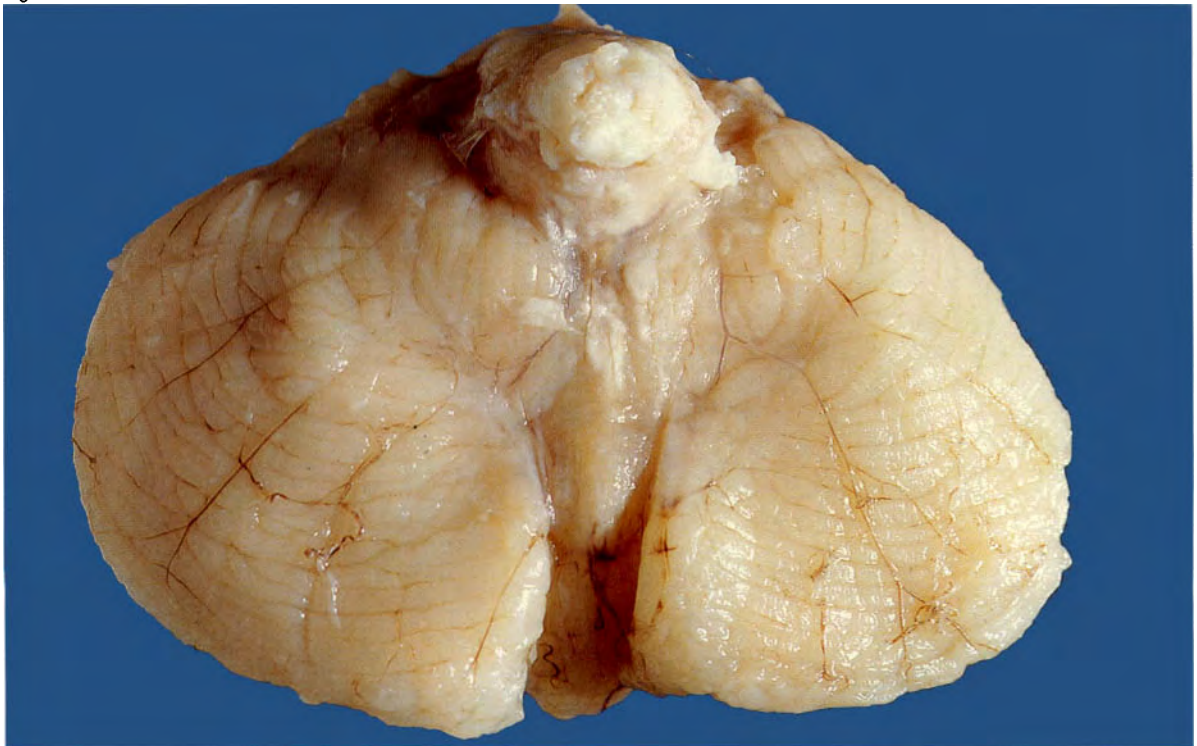


Fig. 11.11



Fig. 11.12



Fig. 11.13

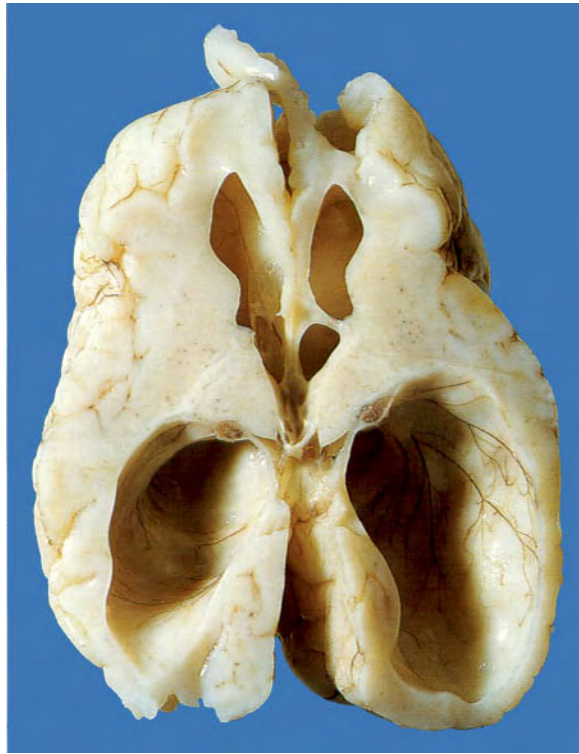


Fig. 11.14



Fig. 11.15



Fig. 11.16

Fig. 11.12 Meningitis hydrocephalus. Cross-section of the cerebellum shown in Figure 11.11, illustrating dilatation of the fourth ventricle with purulent exudate attached to its lining.

Fig. 11.13 Same case showing dilatation of the cerebral aqueduct.

Fig. 11.14 Same case showing dilatation of the third and both lateral ventricles.

Fig. 11.15 Meningitis complicated by osteomyelitis. M/2 $\frac{1}{2}$. Shortening of the right leg resulting from osteomyelitis of the head of the femur following meningitis.

Fig. 11.16 Meningitis: subdural collection of serosanguinous fluid. F/2. A common complication of meningitis.

Fig. 11.17 Meningitis complicated by a cortical infarct. Neonate. Note that neonatal brains do not have well defined grey and white matter.



Fig. 11.17

Fig. 11.18 Tuberculous meningitis. M/39. Note the opacity of the leptomeninges covering the interpeduncular cistern. The pus tends to accumulate along the base of the brain in TB meningitis.

Fig. 11.19 Tuberculoma. M/25. There is a well circumscribed mass in the right frontal lobe. Space-occupying lesions such as this are sometimes seen in patients with TB meningitis and may present with clinical features that mimic a neoplasm.

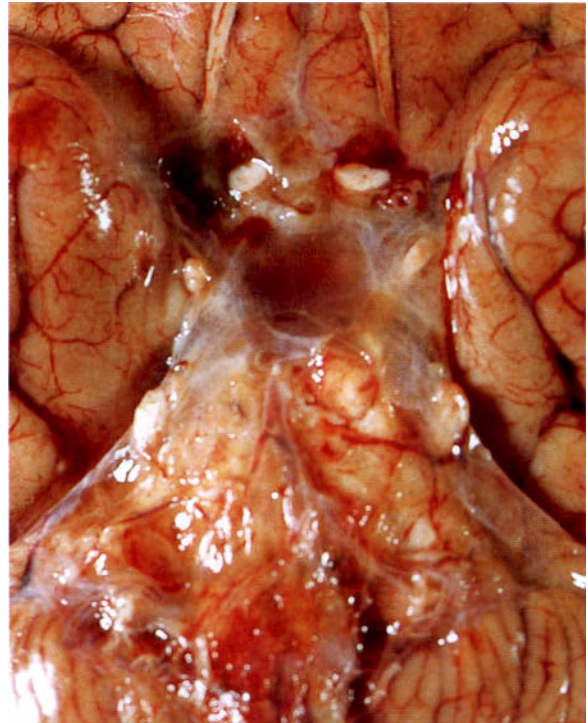


Fig. 11.18

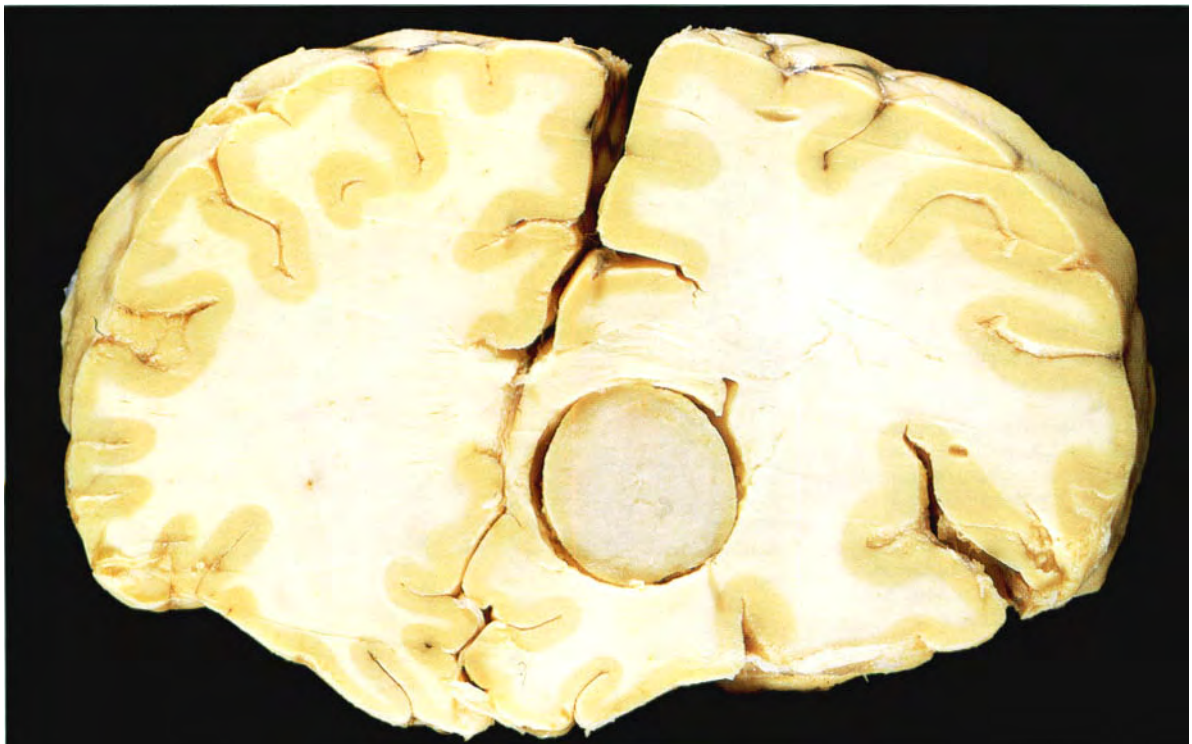


Fig. 11.19

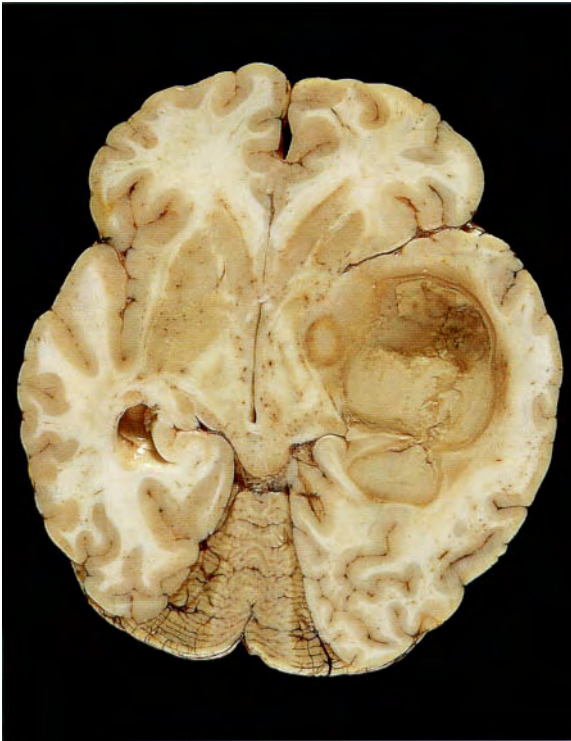
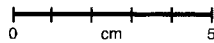


Fig. 11.20

**Fig. 11.20 Cerebral abscess in the right hemisphere.**

M/9. The abscess has been present for some time, as indicated by the presence of a partial capsule. Recent extension has occurred in two places through this capsule.

Fig. 11.21 Toruloma in the left frontotemporal region.

M/50. Toruloma is the name given to a tumour-like mass formed by an aggregation of *Cryptococcus neoformans*. The organisms produce a cryptococcal meningitis and then invade the brain parenchyma. The cut surface characteristically has a multiloculated mucoid appearance. The toruloma has extended into the basal ganglia. The space-occupying lesion on the left has caused compression of the third ventricle and has probably resulted in the haemorrhage noted in the right internal capsule, which in turn probably caused the patient's death.

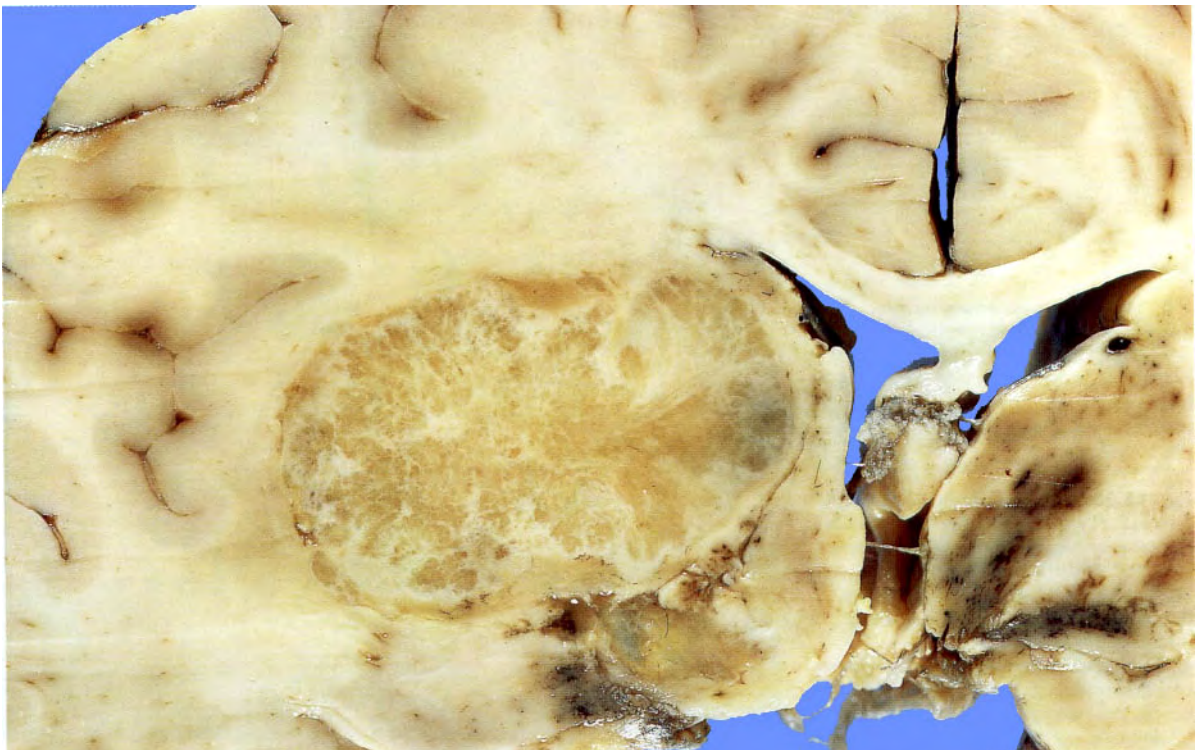


Fig. 11.21

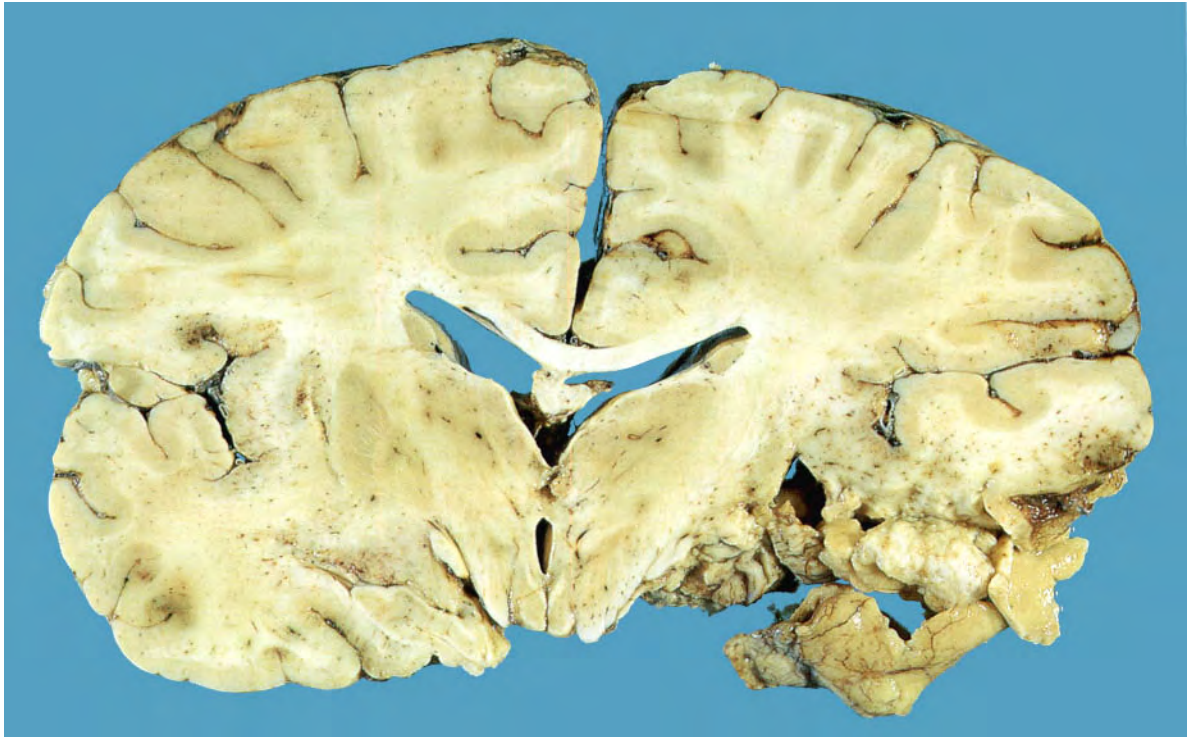


Fig. 11.22

Fig. 11.22 Herpes encephalitis. M/44. There is marked necrosis of the right temporal lobe, and petechial haemorrhages and early necrosis in the left temporal lobe. This distribution is characteristic of herpes simplex encephalitis.

Fig. 11.23 Cerebral malaria. M/67. The patient recently returned to Australia from Papua New Guinea, became febrile, and died before the correct diagnosis was made. There are multiple petechial haemorrhages throughout the white matter of the brain. This is the characteristic macroscopic appearance of this condition, but it is not present in all cases. The macroscopic appearance of fat embolus is identical to this (see Figure 11.46).

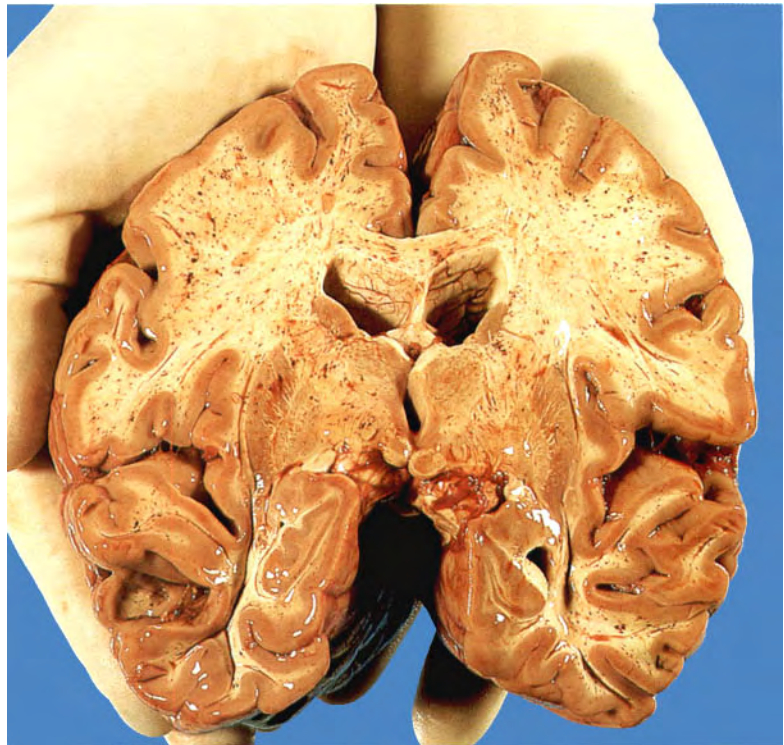


Fig. 11.23

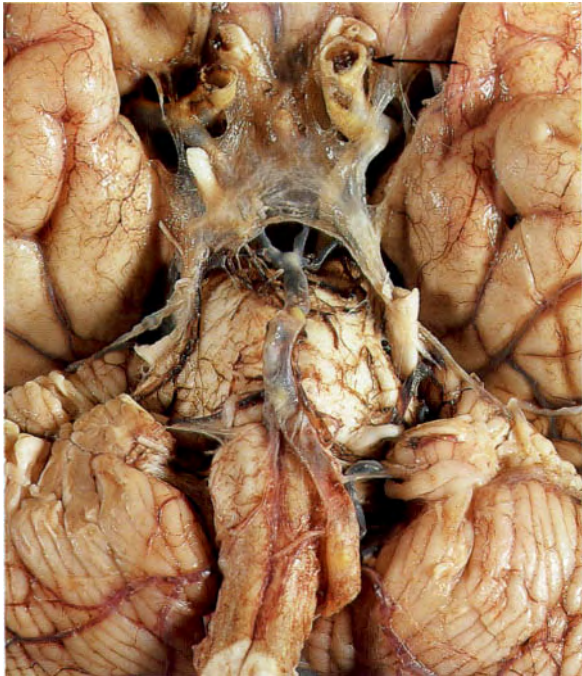


Fig. 11.24



Fig. 11.26



Fig. 11.25

The Pathology of cerebrovascular insufficiency

Cerebral infarction and cerebral haemorrhage

Figures 11.24 to 11.80 demonstrate many aspects of the arterial and venous systems of the brain, and the pathology resulting from thrombosis and haemorrhage involving these vessels.

Imaging techniques to identify the anatomy and pathology within the central nervous system have evolved since the introduction of X-rays in the early 1900s. Currently, the main techniques in use are CT (computed tomography) and MRI (magnetic resonance imaging).

Fig. 11.24 Cerebral infarction. F/85. Thrombosis of the left internal carotid artery (arrow) within the skull.

Fig. 11.25 Recent thrombosis of the right internal carotid artery at its origin in the neck. F/30. The thrombus has been removed from the artery.

Fig. 11.26 Recent thrombosis of the left middle cerebral artery. F/82.

Fig. 11.27 Cerebral infarction. M/60. Recent infarction in the distribution of the right middle cerebral artery which could have been caused by thrombosis at any of the sites illustrated in Figures 11.24 to 11.26. There is haemorrhage into the anterior portion of the infarct and the temporal lobe is soft and swollen, as can be seen by comparing it with the left temporal lobe.

Fig. 11.28 Vertical section of brain showing haemorrhagic infarction in the distribution of the right middle cerebral artery. M/48.

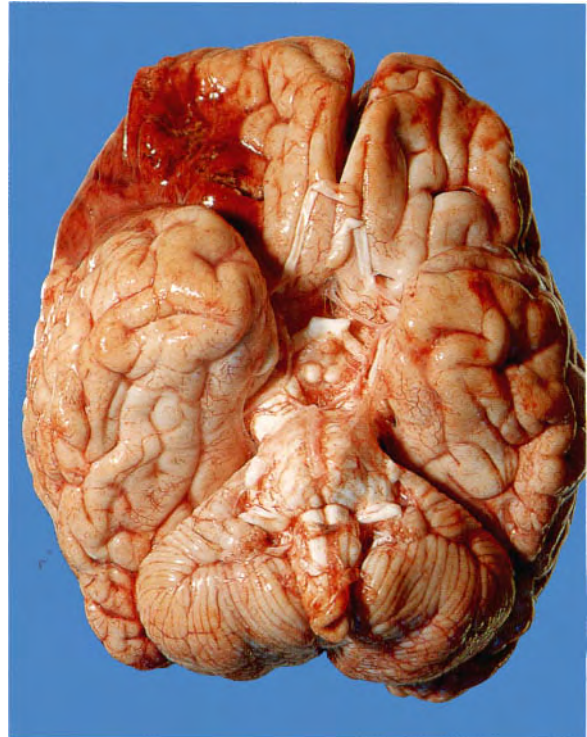


Fig. 11.27

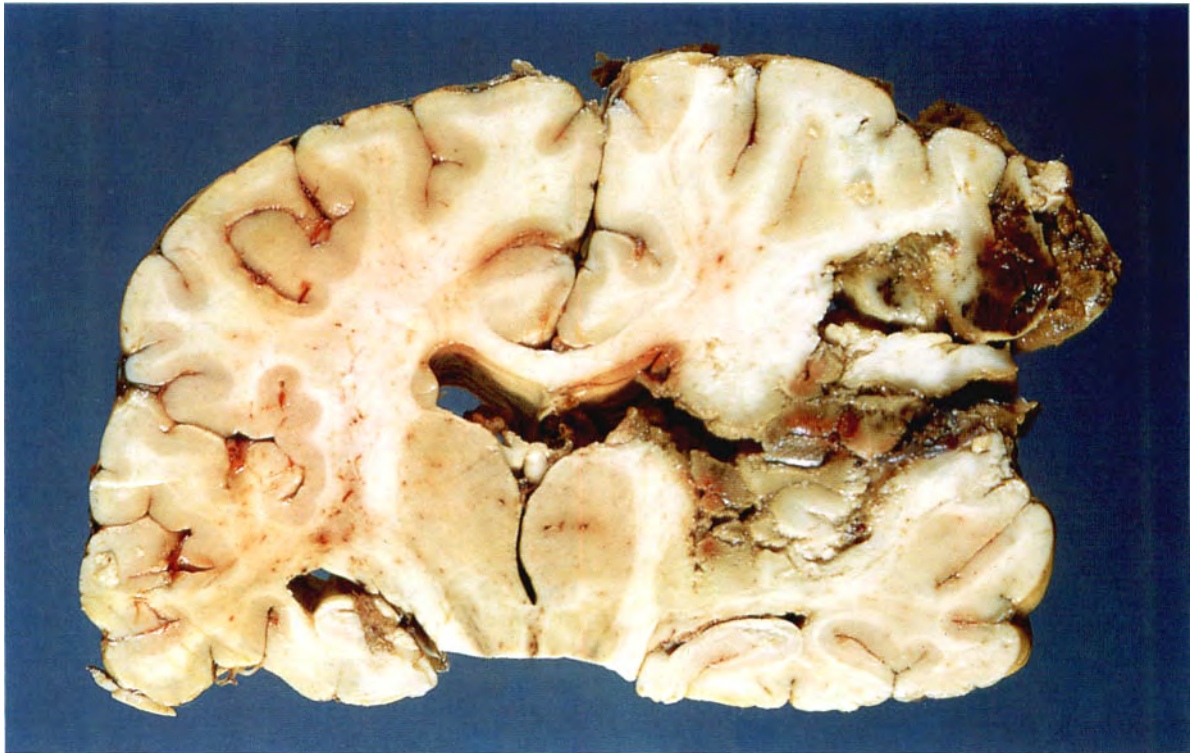


Fig. 11.28



Fig. 11.29



Fig. 11.30



Fig. 11.31

Fig. 11.29 Cerebral infarction. F/59. Old infarction in the distribution of the left middle cerebral artery. The necrotic brain substance has liquefied, leaving a cyst.

Fig. 11.30 Atrophy of the left cerebral peduncle from the brain in Figure 11.29.

Fig. 11.31 Atrophy of the right pyramidal tract from the brain in Figure 11.29.



Fig. 11.32

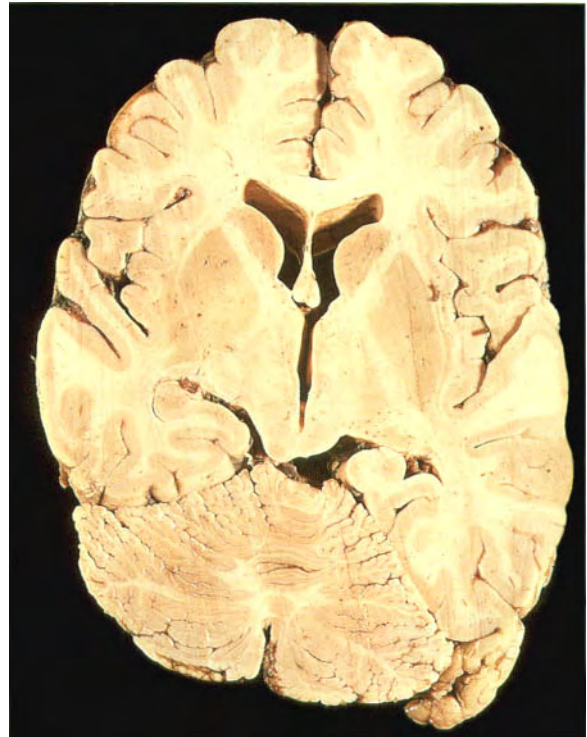


Fig. 11.33



Fig. 11.34

Fig. 11.32 CT brain scan showing a 'slice' through the lower third of the brain. It shows the hemispheres – frontal, temporal and occipital – the midbrain and the ventricles. The white opacities in the occipital horns of the lateral ventricles are calcifications in the choroid plexuses.

Fig. 11.33 This slice through a normal brain has been taken at a similar level to that of the CT and shows the accuracy of the anatomical correlation.

Fig. 11.34 An 'enhanced' CT scan (i.e. a CT scan performed after the injection of an iodine-based radio-opaque material) to 'enhance' the difference between the vascularity of the left temporal lobe (the territory supplied by the left middle cerebral artery) and the right one. This patient had suffered a 'stroke'. This investigation is performed in the early management of stroke patients to find out whether they have had a thrombotic episode or a haemorrhage. Cerebral artery thrombosis results in ischaemia with cerebral oedema and a variable degree of cellular necrosis. Such patients can be successfully treated with thrombolytic drugs. Cerebral haemorrhage, on the other hand, causes more cellular necrosis and is less amenable to treatment.



Fig. 11.35



Fig. 11.36

Fig. 11.35 This is a 'perfusion' CT scan on the patient illustrated in Figure 11.34. It shows more clearly the extent of the area of cerebral ischaemia. An estimation of the extent of ischaemia present in a 'stroke' patient allows an assessment to be made about prognosis. A 'perfusion' CT scan is a mathematical analysis derived from a timed sequence of contrast-enhanced images.

Fig. 11.36 Brain slice from another patient who died following infarction caused by occlusion of the left middle cerebral artery. Note that there has been haemorrhage into the softened, infarcted brain. The patient illustrated in Figures 11.34 and 11.35 had not advanced to the stage of bleeding into the infarct. This illustrates the usefulness of early investigation so that appropriate therapeutic measures can be instituted to prevent the condition progressing to an untreatable stage.

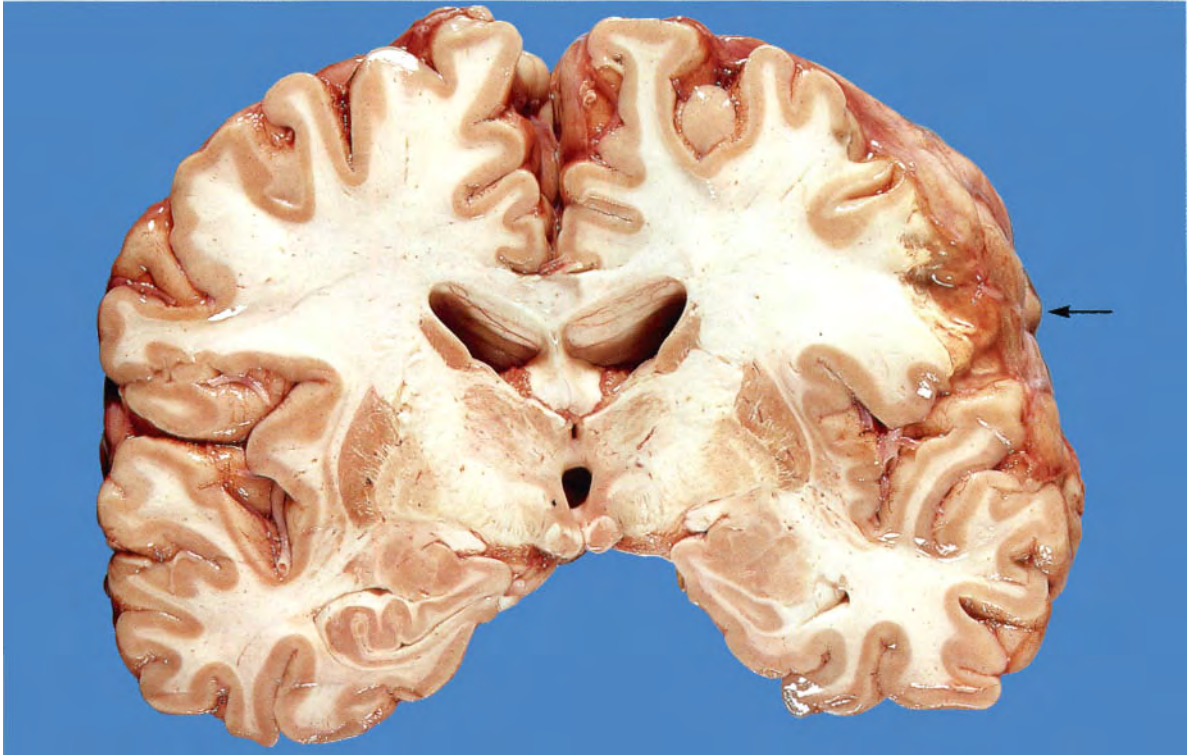


Fig. 11.37

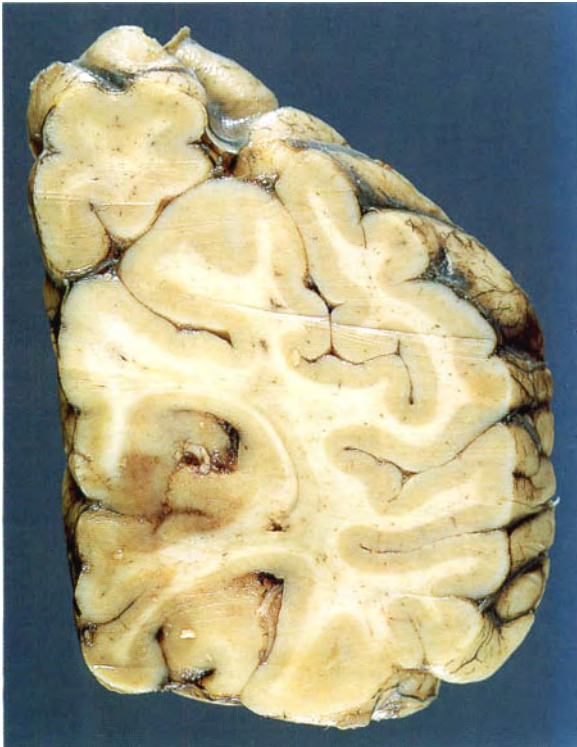


Fig. 11.38



Fig. 11.39

Infarction of specific areas of the brain – Figures 11.37 to 11.43

Fig. 11.37 Infarction of the motor speech area. F/78. The patient can hear and understand, but cannot speak properly. There is infarction of a localized area of cortex and underlying white matter at the posteroinferior end of the left frontal lobe. The abnormal area shows as a gap in the surface grey matter, with loss of some of the underlying white matter.

Fig. 11.38 Recent infarction of the inferomedial aspect of the right occipital lobe (the visual cortex) owing to occlusion of the right posterior cerebral artery. F/69. This caused blurring of her vision. The infarcted area is a darker colour than the adjacent normal cerebral cortex. It is oedematous, and softer than the adjacent normal brain. The junction between normal and infarcted brain is sometimes easier felt than seen.

Fig. 11.39 Cystic area in the distribution of the left posterior cerebral artery. M/80. The result of an old infarct.

Fig. 11.40 Vertebrobasilar insufficiency. M/55. There is thrombosis of the basilar artery extending into the terminal portions of the vertebral arteries. The branches of the vertebral arteries supply the brain stem, and the posterior inferior cerebellar artery arises from the vertebral artery. The basilar artery is formed by the junction of the two vertebral arteries on the inferior margin of the pons. It then runs for the whole length of the pons, ending in the posterior cerebral arteries. These in turn connect via the posterior communicating arteries with the internal carotid artery and the circle of Willis. Thrombosis of the basilar artery causes infarction in the pons, as shown here, with softening and loss of structure. The arrow points to a cystic area of old infarction in the distribution of the anterior inferior cerebellar artery, which arises from the basilar artery.

Fig. 11.41 Vertebrobasilar insufficiency. M/53. This shows an area of recent infarction of the posterior inferior portion of the right cerebellum. This is the area supplied by the posterior inferior cerebellar artery, which arises from the vertebral artery.

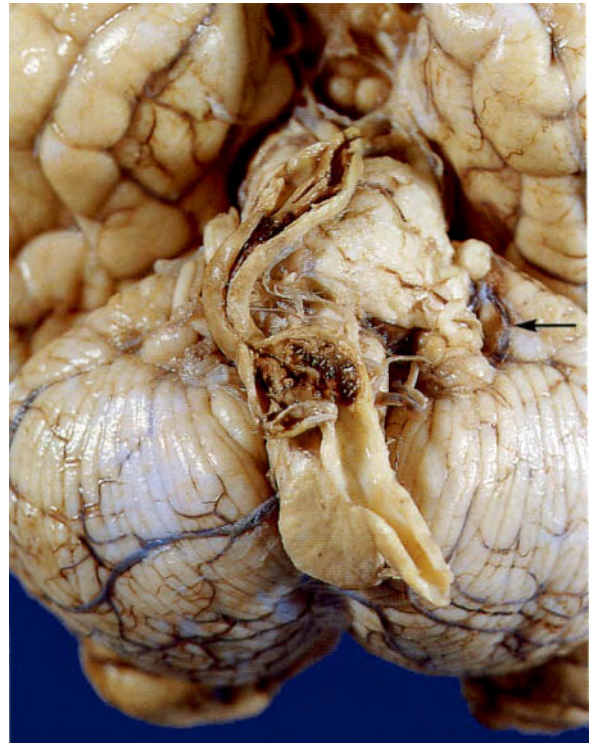


Fig. 11.40



Fig. 11.41



Fig. 11.42

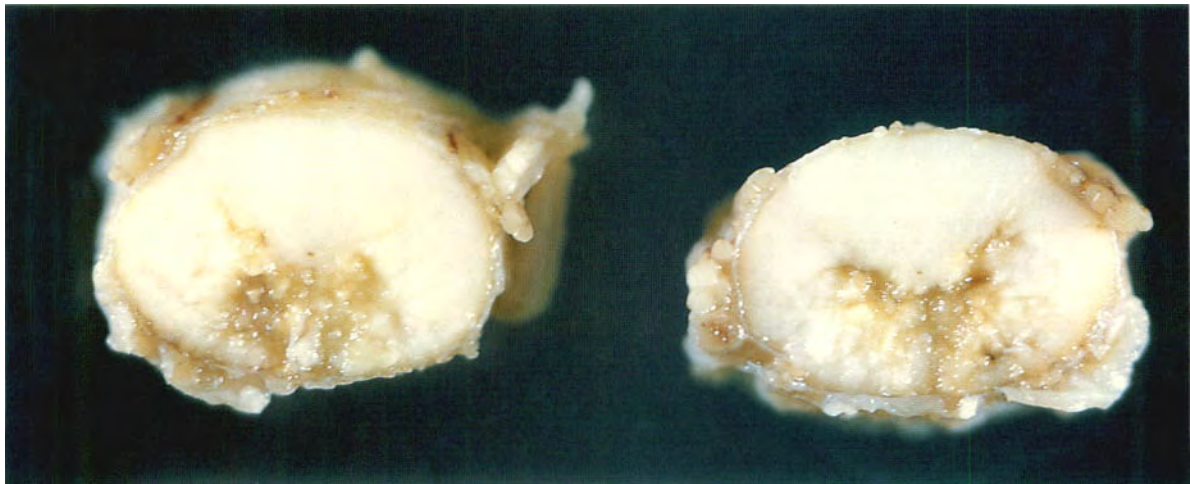


Fig. 11.43

Fig. 11.42 Vertebrobasilar insufficiency. F/54. The cerebellum shows a number of cystic areas of old infarction. There are old infarctions in the distribution of both posterior inferior cerebellar arteries, as well as in the left anterior inferior cerebellar artery. Thrombosis in the vertebrobasilar arteries results in the anatomical changes illustrated in these three figures. The clinical symptoms and signs produced by

thrombosis in this arterial system are reproducible and can be recognized by clinical examination.

Fig. 11.43 Recent infarction of the anterior portion of the spinal cord. M/83. This occurred as a result of thrombosis of the anterior spinal artery.

Fig. 11.44 Neonatal intracranial haemorrhage resulting from hypoxia. M/3 weeks. The brain shows an almost complete absence of development of the gyri, indicating marked prematurity.

Fig. 11.45 Tear in the tentorium cerebelli which resulted from traumatic delivery and caused death from haemorrhage.

Fig. 11.46 Fat embolus. F/25. The patient was in a motorcycle accident and sustained multiple fractures of both legs. The fat emboli caused petechial haemorrhages in the white matter throughout the brain, resulting in coma and death. The macroscopic appearance of cerebral malaria (see Figure 11.23) is identical to this.

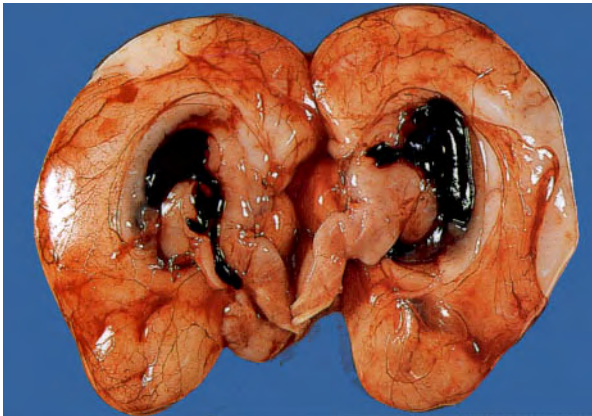


Fig. 11.44

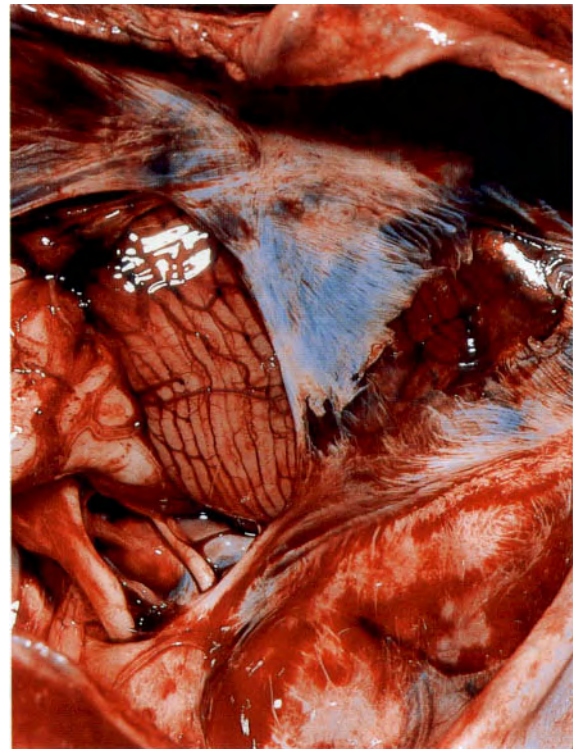
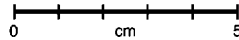


Fig. 11.45

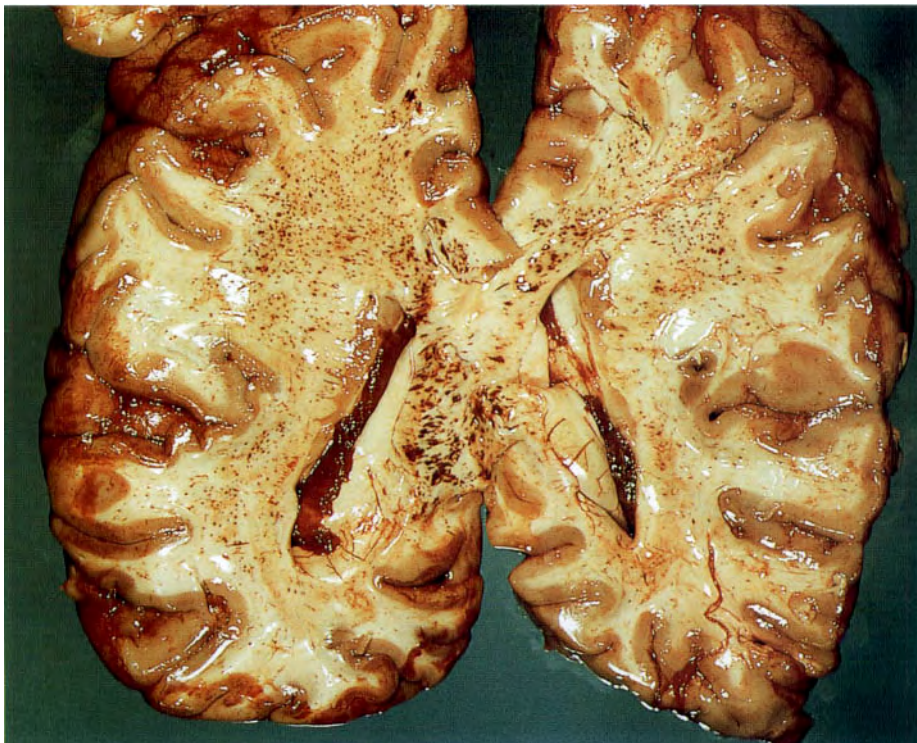


Fig. 11.46

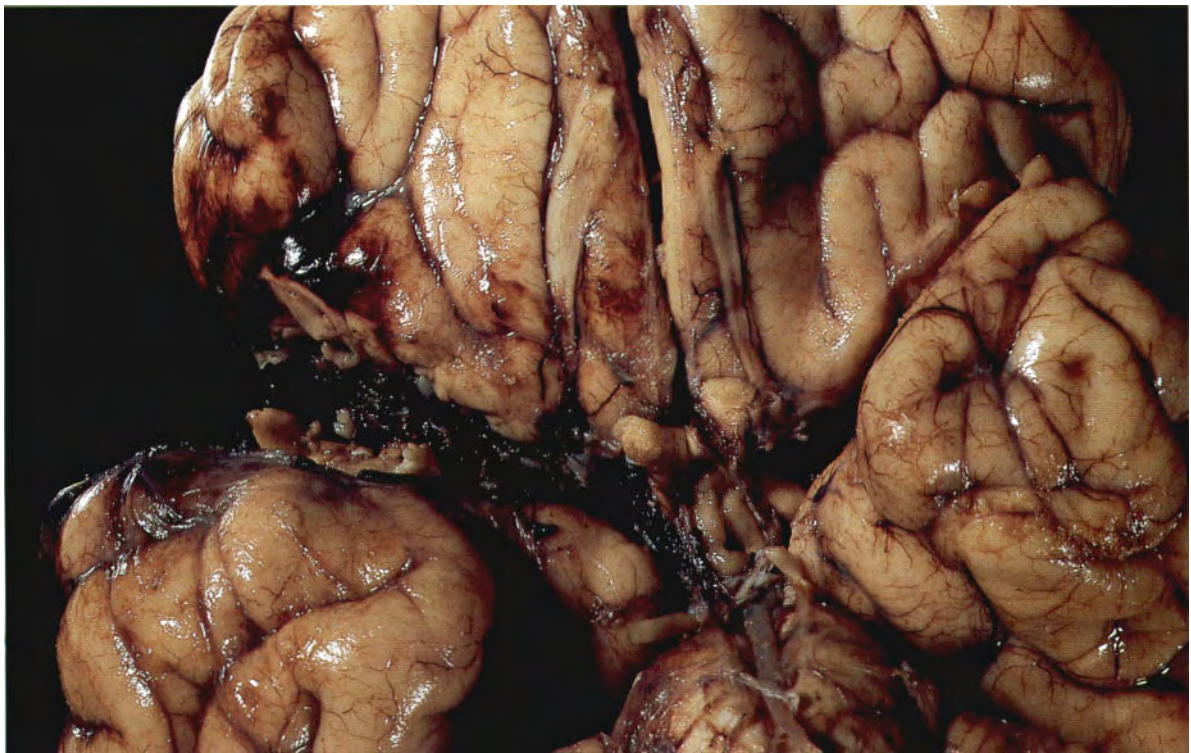


Fig. 11.47

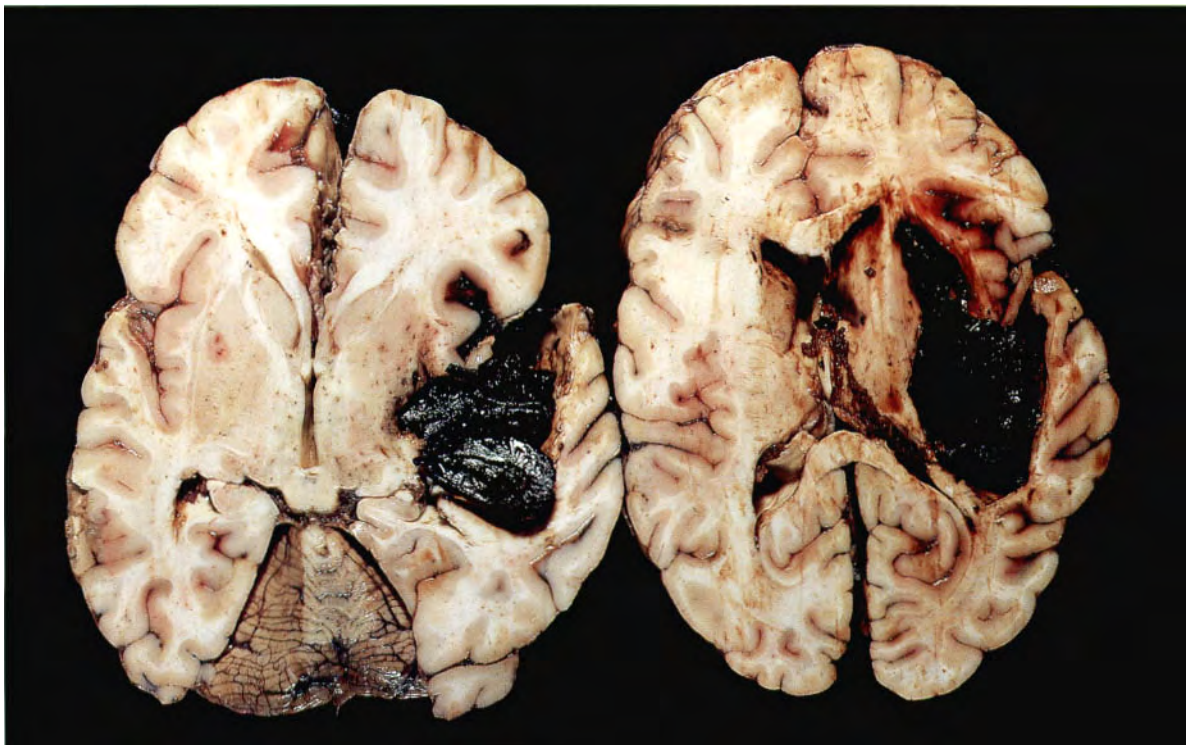


Fig. 11.48



Fig. 11.49

Fig. 11.47 Mycotic embolus occluding the right middle cerebral artery. M/13 with bacterial endocarditis.

Fig. 11.48 Cut slices of the brain in Figure 11.47 showing intracerebral haemorrhage resulting from rupture of the mycotic aneurysm that developed in the middle cerebral artery.

Fig. 11.49 Traumatic brain damage. M/60. The inferior surfaces of both frontal lobes and the anterior ends of both temporal lobes show loss of cortical substance and brown coloration of the meninges. This is more marked on the left than on the right. These areas of infarction resulted from injury caused by impact with the frontal plates and sphenoid bones during acceleration/deceleration trauma.

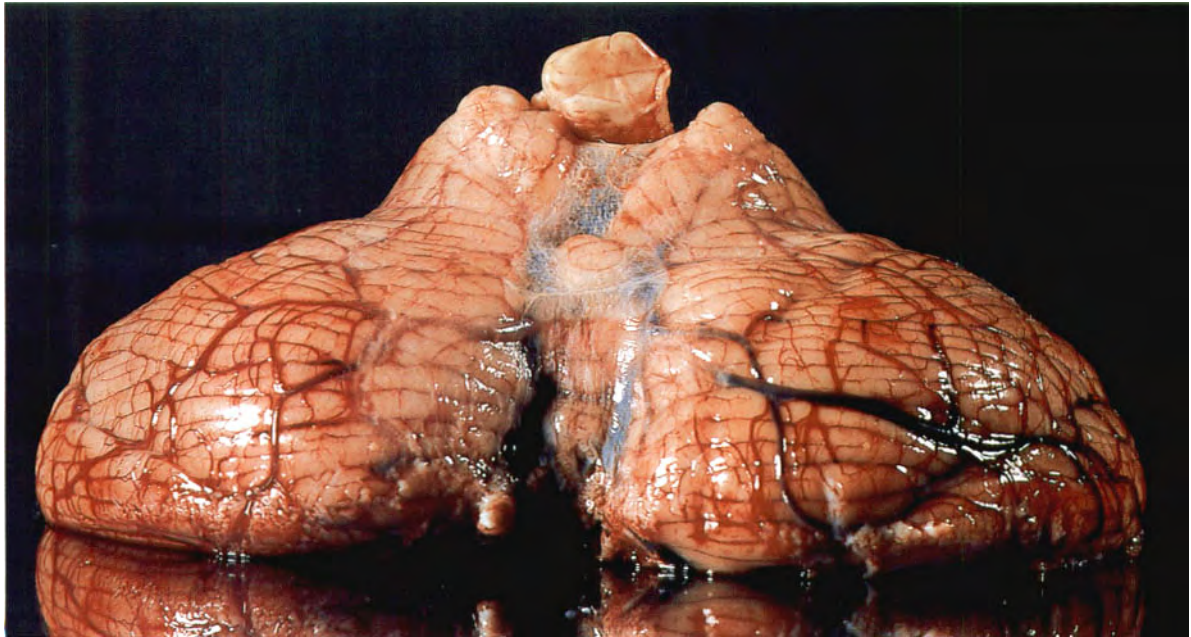


Fig. 11.50

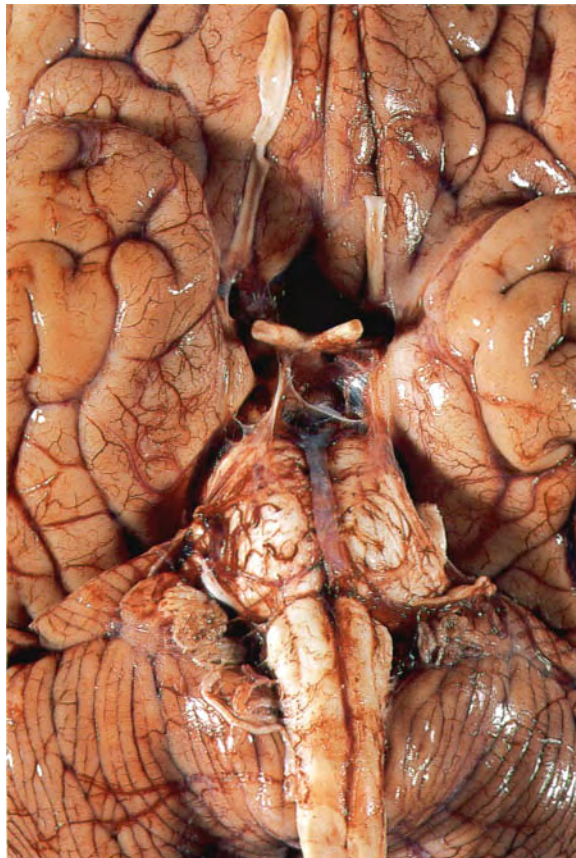


Fig. 11.51



Fig. 11.52

0 cm 1



Fig. 11.53

Effects of raised intracranial pressure – Figs 11.50–11.55

Fig. 11.50 Tonsillar herniation of the cerebellum. The groove made by the foramen magnum can be seen. There had been increased intracranial pressure, and this forced the cerebellar tonsils through the foramen magnum causing pressure on the brain stem – ‘coning’.

Fig. 11.51 Uncal herniation. The same brain as in Figure 11.50. The brain is viewed on its undersurface and the left uncus is more prominent than the right. It has herniated medially, causing stretching of the posterior communicating artery, and would have caused stretching of the sixth nerve as well. The tonsillar herniation of the cerebellum is also apparent.

Fig. 11.52 Multiple brain-stem haemorrhages. Another complication of raised intracranial pressure and frequently the final cause of death. (Brain-stem haemorrhage may also result from external trauma.)

Fig. 11.53 Recent infarction of both occipital lobes due to occlusion of both posterior cerebral arteries caused by compression of the arteries against the free edge of the tentorium cerebelli by raised intracranial pressure.

Fig. 11.54 Coronal section of the brain, showing the distribution of this infarction. Note the infarction of the posterior end of the thalamus because it is supplied by branches of the posterior cerebral artery.

Fig. 11.55 Infarction of the cerebral peduncles, which are also supplied by small branches of the posterior cerebral arteries. Many of the small branches of this artery, and of the other arteries forming the circle of Willis, can be seen in this photograph.

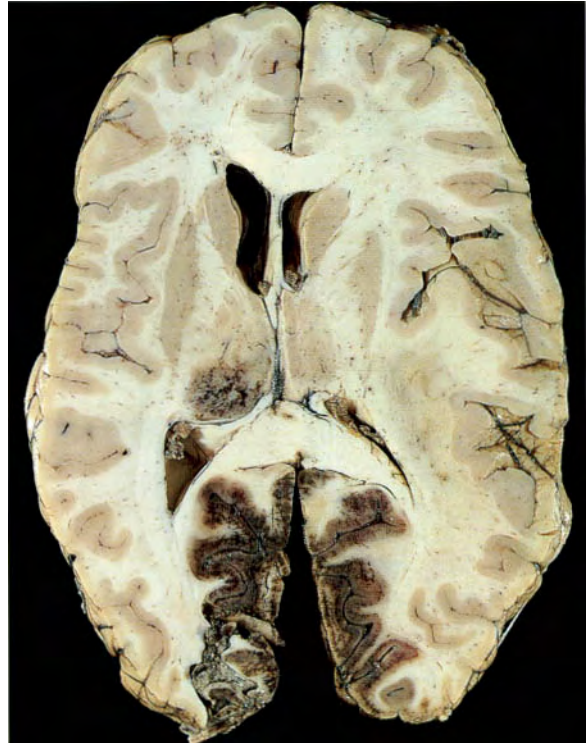


Fig. 11.54



Fig. 11.55

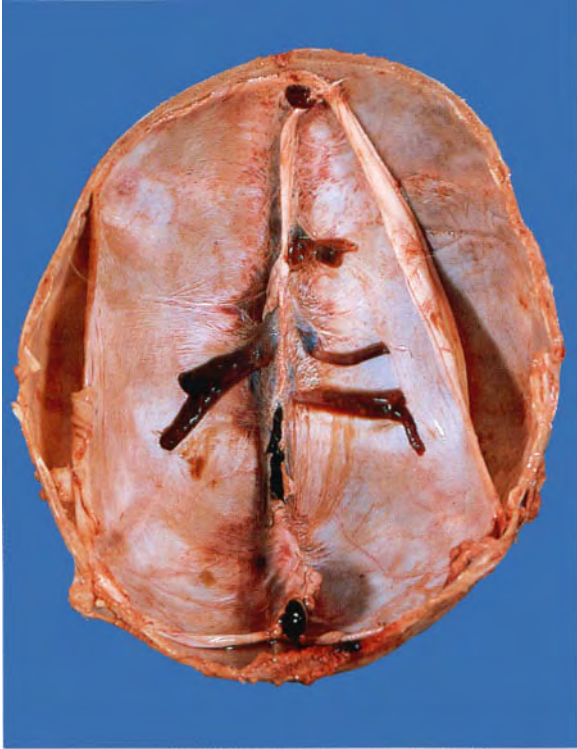


Fig. 11.56



Fig. 11.57

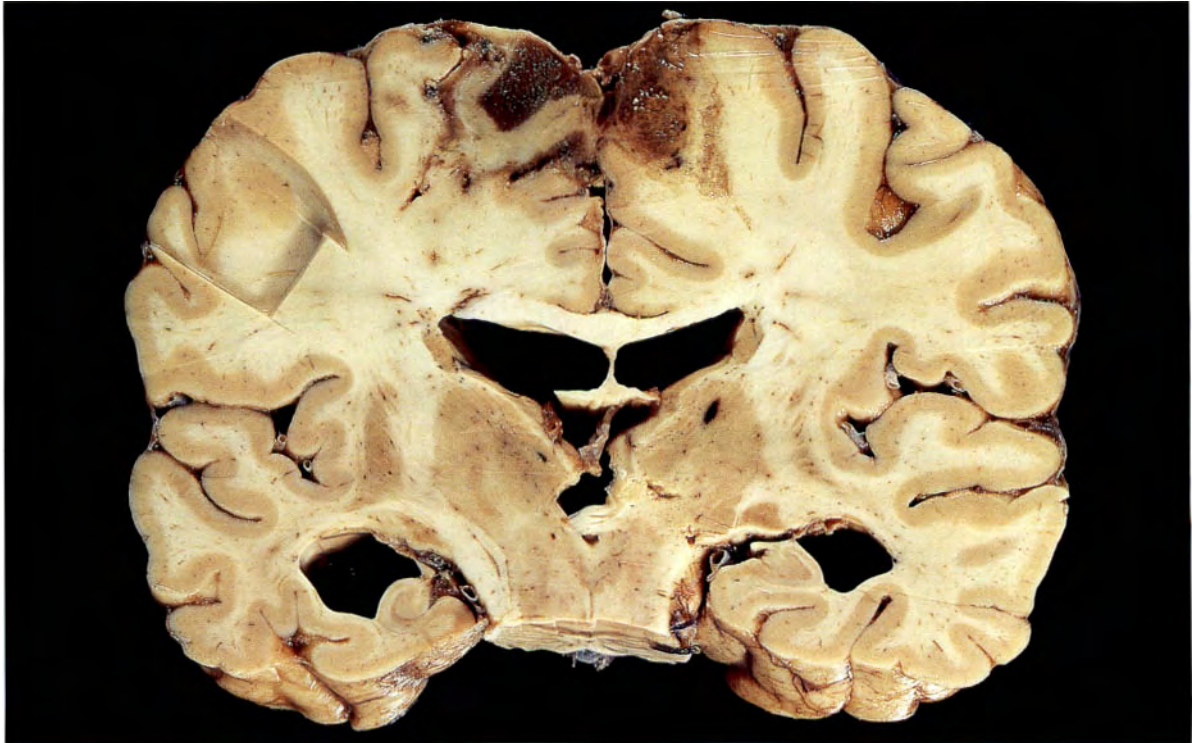


Fig. 11.58

Fig. 11.56 Sagittal sinus thrombosis. F/2. There is thrombus in the sagittal sinus and in the cortical veins that drain into it. In this case the thrombosis was a result of dehydration from diarrhoea.

Fig. 11.57 Cortical vein thrombosis. Thrombosis of the cortical veins draining into the sagittal sinus.

Fig. 11.58 Sagittal sinus and cortical vein thrombosis. Vertical slice through the brain, showing infarction and liquefaction of brain substance drained by the cortical veins. This infarction is in the region of the precentral gyrus.

Fig. 11.59 Right orbital cellulitis. M/41. This is a serious infection because the orbital veins drain directly through the orbital fissure into the cavernous sinus. This man recovered after treatment with antibiotics.

Fig. 11.60 Thrombosis of the right cavernous sinus. F/6. There is infarction of the adjacent brain due to occlusion of the veins that drain into the cavernous sinus. This followed unsuccessful treatment of orbital cellulitis.



Fig. 11.59

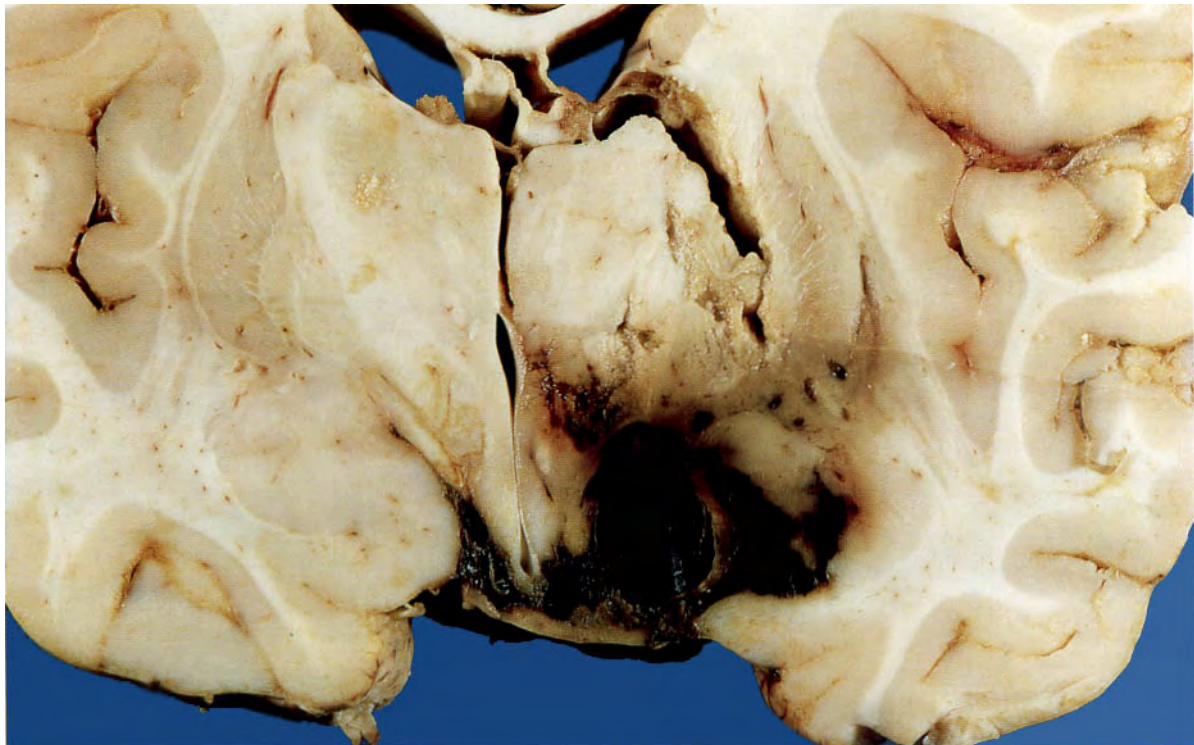


Fig. 11.60

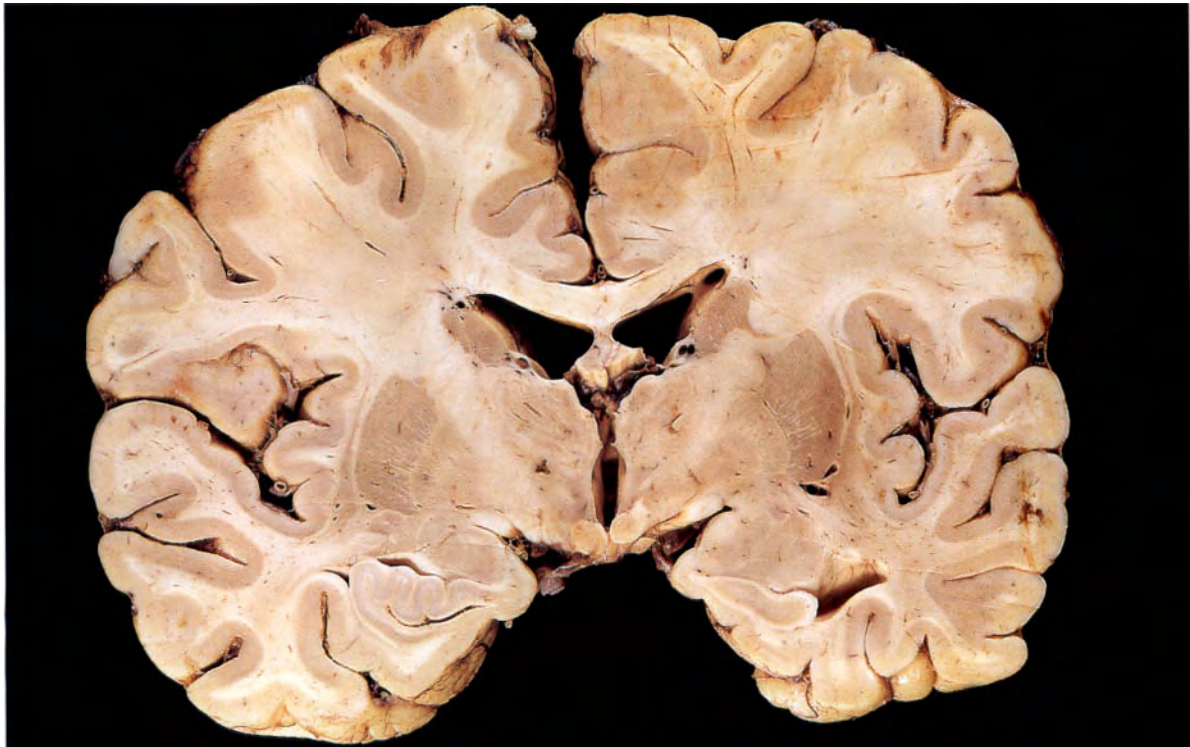


Fig. 11.61

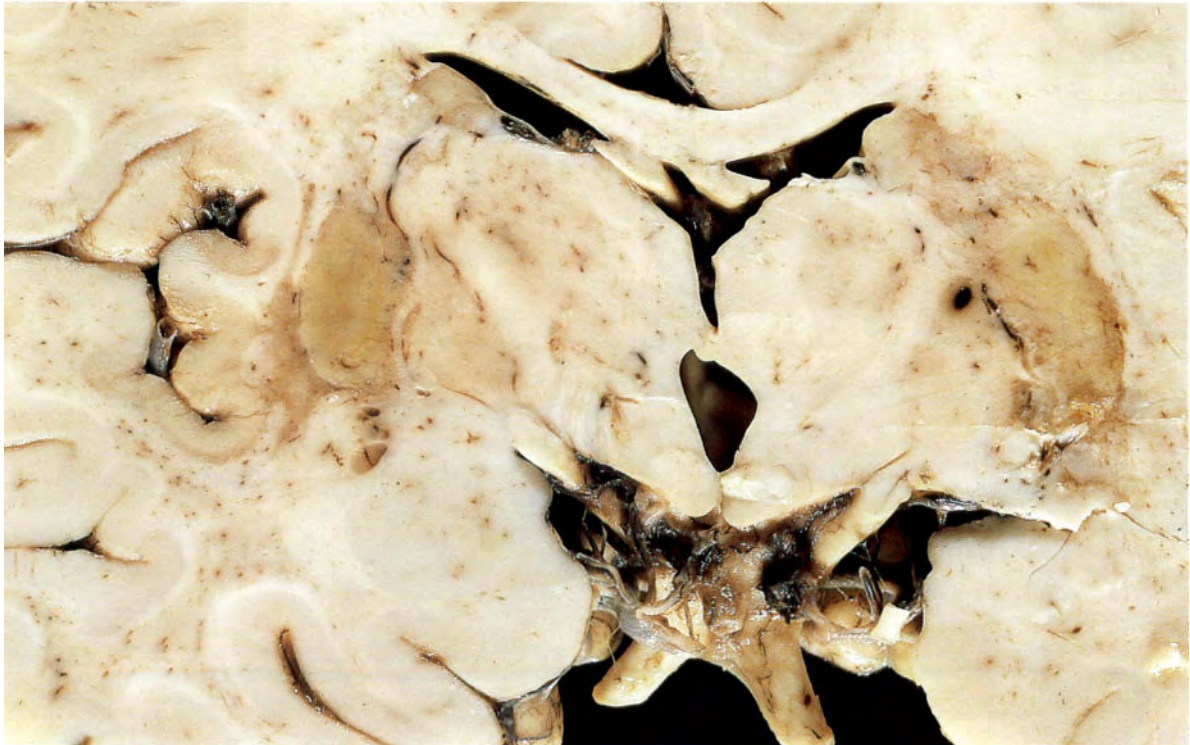


Fig. 11.62

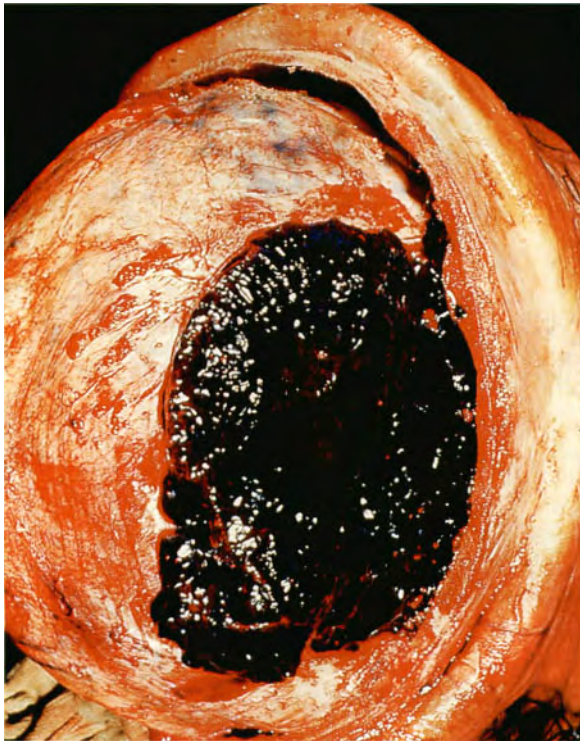


Fig. 11.63

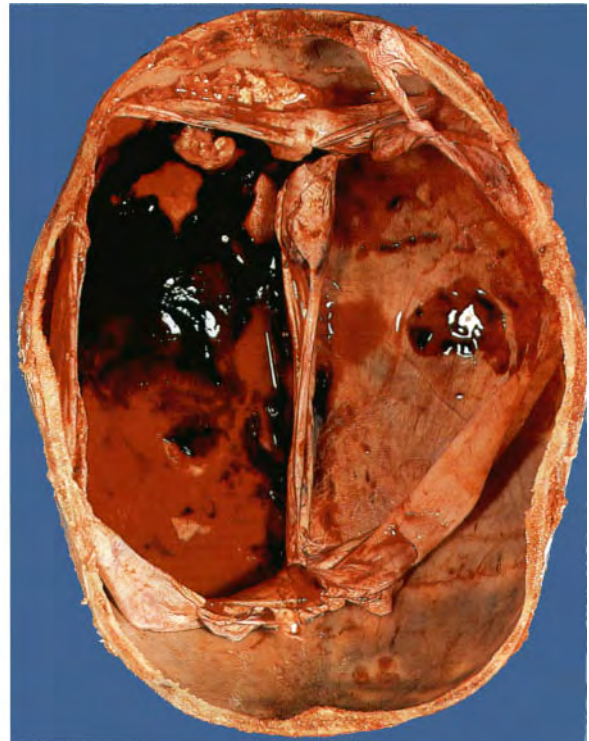


Fig. 11.64

Fig. 11.61 Normal brain. Slice of brain showing the normal internal deep cerebral veins running between the head of the caudate nucleus and the thalamus. Can you identify all the anatomical structures in this slice of brain?

Fig. 11.62 Deep cerebral vein thrombosis. F/3. Infarction of white matter in both hemispheres in the region of the internal capsules resulting from thrombosis of branches of the deep cerebral veins. This occurred during an episode of hypotension following open heart surgery.

Fig. 11.63 Extradural haemorrhage. M/16. This resulted from rupture of the right middle meningeal artery following a head injury. The classic history in such cases is: injury; quickly becomes unconscious; recovery (apparently normal) an hour or so later; unconscious again.

Fig. 11.64 Subdural haemorrhage resulting from rupture of veins following a head injury. M/3.

Fig. 11.65 Intracerebral haemorrhage. M/50. Hypertension. Death followed a few hours after the sudden onset of unconsciousness. Haemorrhage fills the third and both lateral ventricles. The insert is a CT scan of this patient taken on admission to hospital. It shows the haemorrhage.

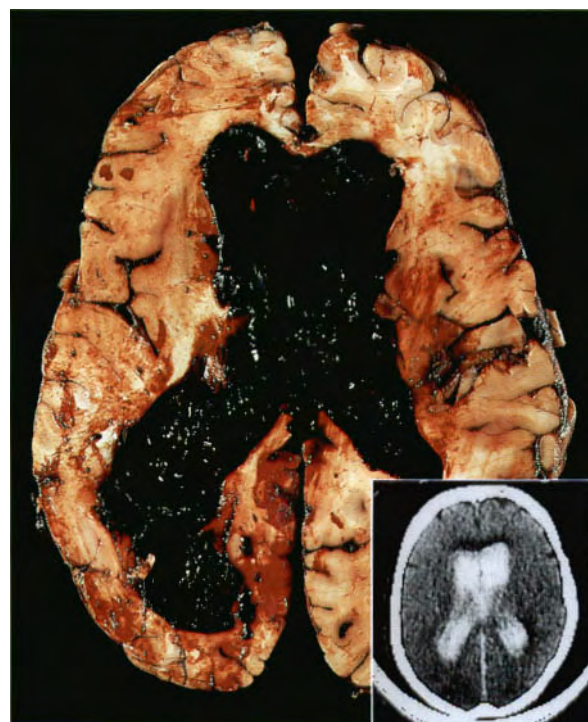


Fig. 11.65



Fig. 11.66



Fig. 11.68

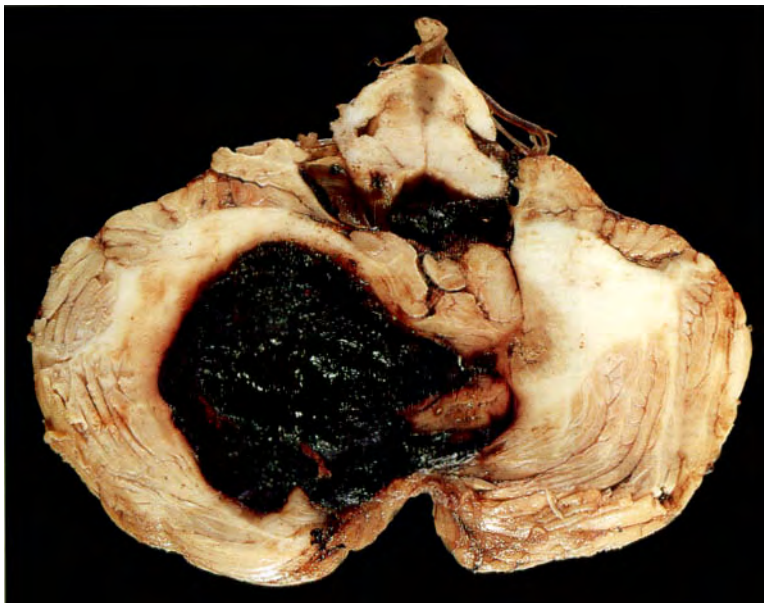


Fig. 11.67

Fig. 11.66 Pontine haemorrhage. F/42. Hypertension.

Fig. 11.67 Intracerebellar haemorrhage. M/82. Hypertension. This is the least common type of hypertensive haemorrhage.

Fig. 11.68 Acute gastric erosions. M/57. A well recognized complication of intracerebral haemorrhage.

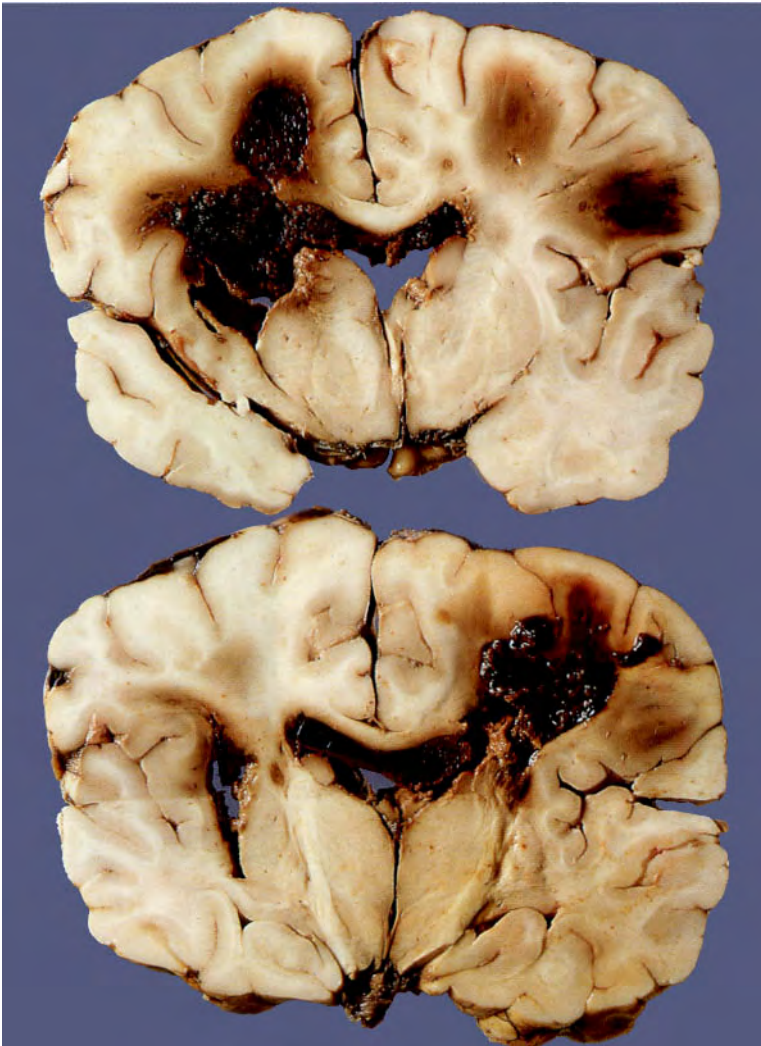


Fig. 11.69



Fig. 11.70

Fig. 11.69 Multiple haemorrhages through both hemispheres. F/16. The patient had acute myeloblastic leukemia and died as a result of a bleeding diathesis. The fact that the haemorrhages are multiple indicates a bleeding disorder rather than rupture of a major vessel. These two brain slices follow in sequence, the upper one first. They are both viewed from the anterior aspect.

Fig. 11.70 Haemorrhage into the spinal cord. M/61. This resulted from a road traffic accident.

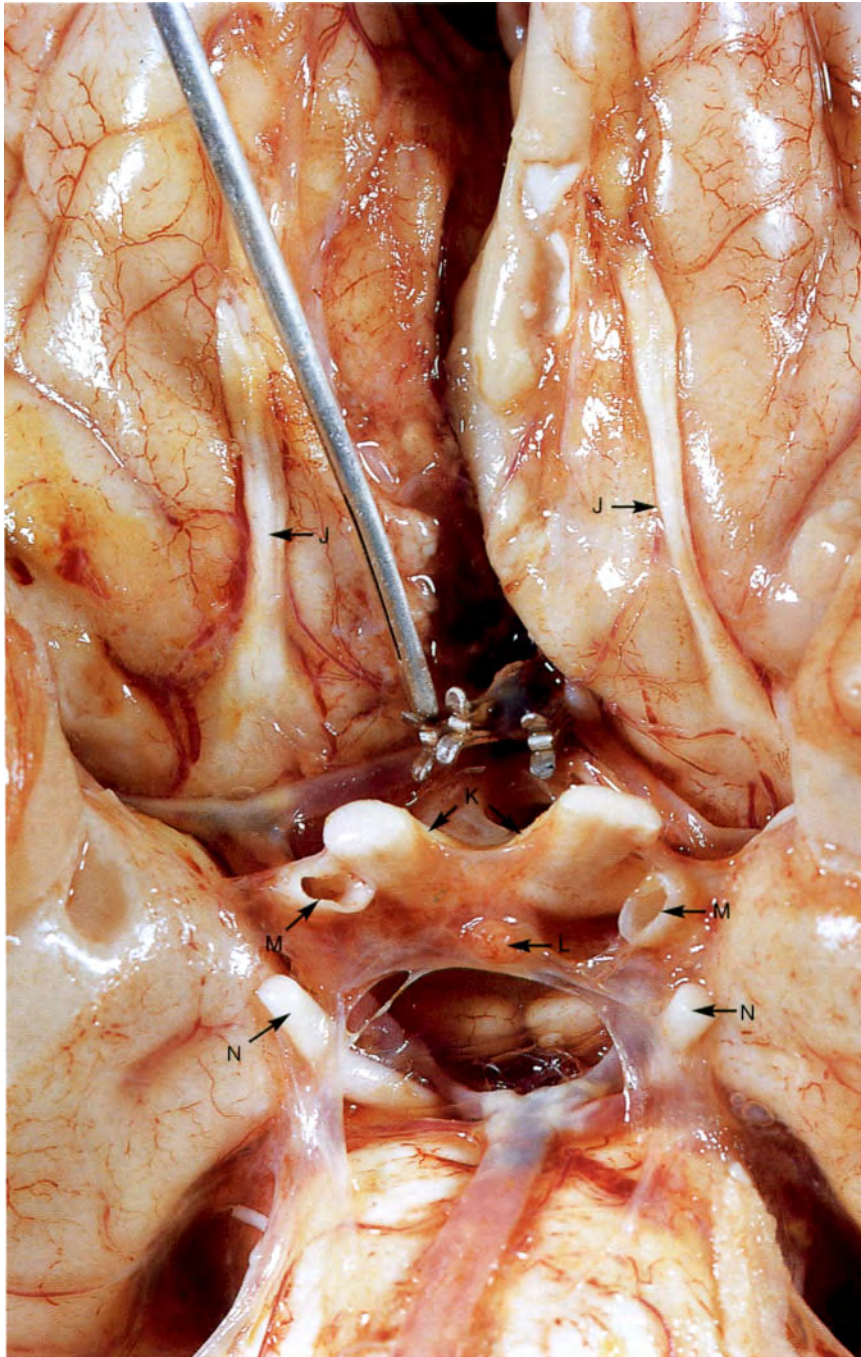


Fig. 11.71

Fig. 11.71 Berry aneurysm on the anterior communicating artery. M/48. The aneurysm bled, causing subarachnoid haemorrhage. Surgical clips were applied to the base of the aneurysm to control the bleeding. Note the arteries forming the circle of Willis. (The letters are explained in the legend to Figure 11.74.)



Fig. 11.72

0 cm 1

Fig. 11.72 Subarachnoid haemorrhage in the spinal cord following rupture of a berry aneurysm. F/33. The white spinal cord, seen at the upper end of the photograph, is encased by blood filling the subarachnoid space. The classic presentation is a sudden onset of severe headache, followed quickly by unconsciousness. Clinical examination shows marked neck stiffness.

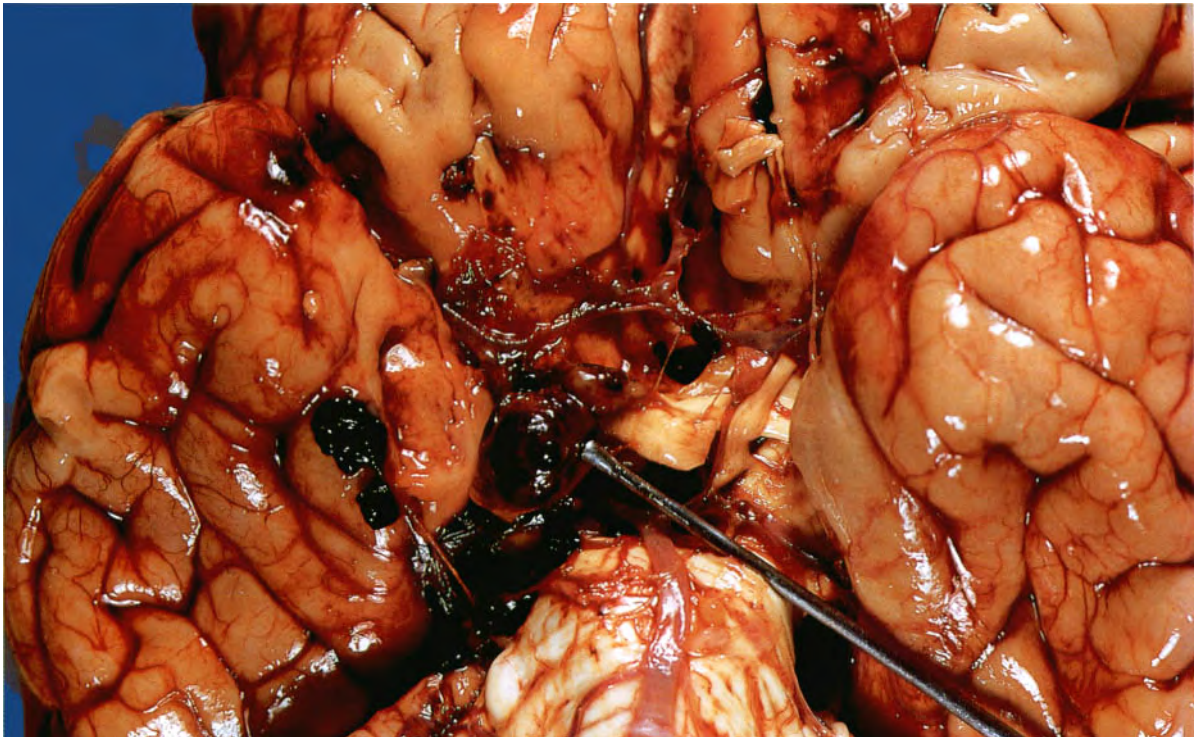


Fig. 11.73

Fig. 11.73 Ruptured aneurysm on the right internal carotid artery at the point where it becomes the middle cerebral artery. F/57. It had caused subarachnoid haemorrhage and had extended into the optic nerve. The aneurysms illustrated in Figures 11.71 and 11.73 are the commonest sites for intracerebral aneurysms.

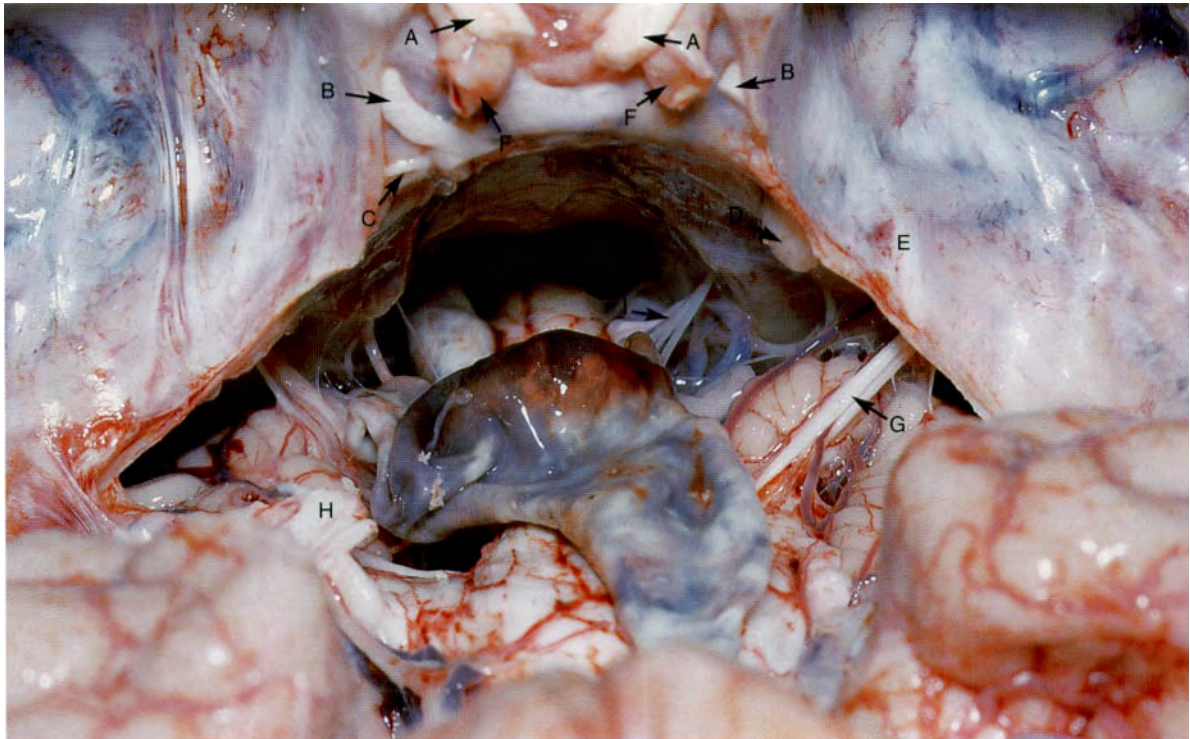


Fig. 11.74

Fig. 11.74 Large unruptured aneurysm of the basilar artery, an incidental finding. F/61. In this photograph the pons and brain stem (medulla oblongata) are viewed in situ as the brain was being removed during postmortem examination. At the top of the photograph one sees the optic nerves (A) anterior to the optic chiasm (which has been removed). The third nerves (B) are present lateral to the middle cerebral arteries. The thin fourth nerve (C) can be seen on the left side beneath the third nerve. The fifth nerve (D) can be seen on the right side beneath the dura mater on the surface of the petrous temporal bone (E). The middle cerebral arteries (F) are lateral to the pituitary fossa. The bone of the posterior surface of the pituitary fossa forms the clivus and extends downwards into the foramen magnum. The brain stem (medulla oblongata) extends into the foramen magnum and becomes the spinal cord. The aneurysm is in the basilar artery, which runs on the anterior surface of the pons. On the right side of the photograph the seventh (larger) and eighth (smaller) nerves (G) are passing into the petrous temporal bone. The origin of the thick fifth nerve from the middle of the pons (H) can be seen on the left side of the photograph. The ninth, tenth, eleventh and twelfth nerves (I) arise from the brain stem and can be seen in the foramen magnum on the right side of the photograph.

Refer to Figure 11.71. Here we see the first (olfactory) nerves (J) on the inferior surface of the medial portion of the frontal lobes. These nerves end in a bulb – the olfactory bulb. This is better seen in the nerve on the right of the photograph. The optic nerve and optic chiasm can be seen (K). Immediately behind the optic nerve is the stalk of the pituitary gland (L). Through the hole in the leptomeninges the two mamillary bodies can be seen. The beginnings of the two middle cerebral arteries from the terminations of the internal carotid arteries can be seen (M). The third nerves can be seen passing on the medial side of the cerebral peduncle (N). The thin fourth nerve can be seen passing on the lateral surface of the cerebral peduncle on the left side of the photograph. The right sixth nerve (O) can be seen arising from the lower border of the pons in Figure 11.83. The third, fourth and sixth nerves pass anteriorly in the lateral wall of the cavernous sinus, and thence to the orbit. It is easy to understand how the nerves can be stretched whenever there is raised intracranial pressure, and compressed by an aneurysm or a tumour in their course from the brain stem to the points where they exit the skull.



Fig. 11.75



Fig. 11.76



Fig. 11.77

The following clinical examples show how intracerebral lesions can be localized by the clinical effects caused by pressure on, or stretching of, cranial nerves.

Fig. 11.75 This elderly woman has been asked to look to her left. Both eyes move together.

Fig. 11.76 She has now been asked to look to her right. Only the left eye moves. This indicates the presence of a right sixth nerve palsy. Her right eyelid appears to be weak, which would indicate some involvement of the seventh nerve. This is more marked in Figure 11.77.

Fig. 11.77 Here she has been asked to put out her tongue. The tongue deviates to the right, indicating a right twelfth nerve lesion. The right side of the tongue is wasted, indicating that the lesion has been present for some time. Involvement of the sixth, seventh and twelfth nerves indicated to the neurologist that there was a lesion outside the brain at the position of the clivus, as illustrated in Figure 11.74 (between G and I).

This woman first presented in 1955, when imaging techniques were in their infancy and neurosurgery was a rather new specialty. The neurosurgeon operated and found a chordoma in the position predicted by the clinical examination. This lesion recurred 24 years later, when these photographs were taken.

Fig. 11.78 This young boy has a lesion of his right twelfth nerve. There is a bullet wound in his right cheek, caused by the accidental discharge of a .22 calibre rifle. X-ray showed that the bullet was lodged at the base of the skull near the right condyle, where the twelfth nerve leaves the skull through the condylar foramen.



Fig. 11.78

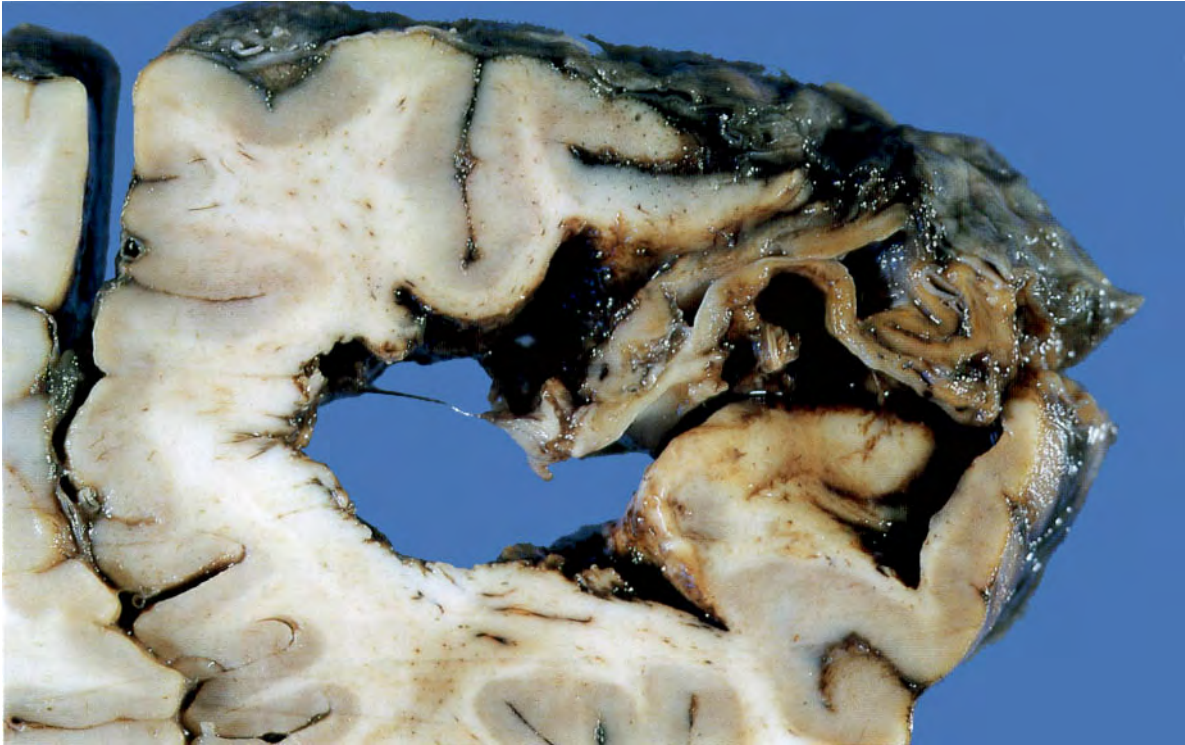


Fig. 11.79



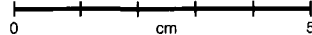
Fig. 11.80

Fig. 11.79 Large arteriovenous malformation. M/23. It involves the brain substance in the right temporal lobe and extends into the subarachnoid space. The bleeding caused subarachnoid and intracerebral haemorrhage and death.

Fig. 11.80 Large arteriovenous malformation in the spinal cord. M/31. Another cause of subarachnoid haemorrhage.

Fig. 11.81 Astrocytoma. M/53. Brain slice examined from its posterior aspect. The tumour has arisen in the right hemisphere and extends through the genu of the corpus callosum into the left hemisphere. There is haemorrhage and necrosis in the tumour, indicating that it is a high-grade malignancy. It has extended into the third ventricle, obstructing the interventricular foramina and resulting in hydrocephalus, as shown by the dilatation of the anterior horns of both lateral ventricles.

Fig. 11.82 Large haemorrhagic astrocytoma in the left hemisphere. F/2. The brain slice is viewed from its anterior aspect. The haemorrhage would have been the immediate cause of death.



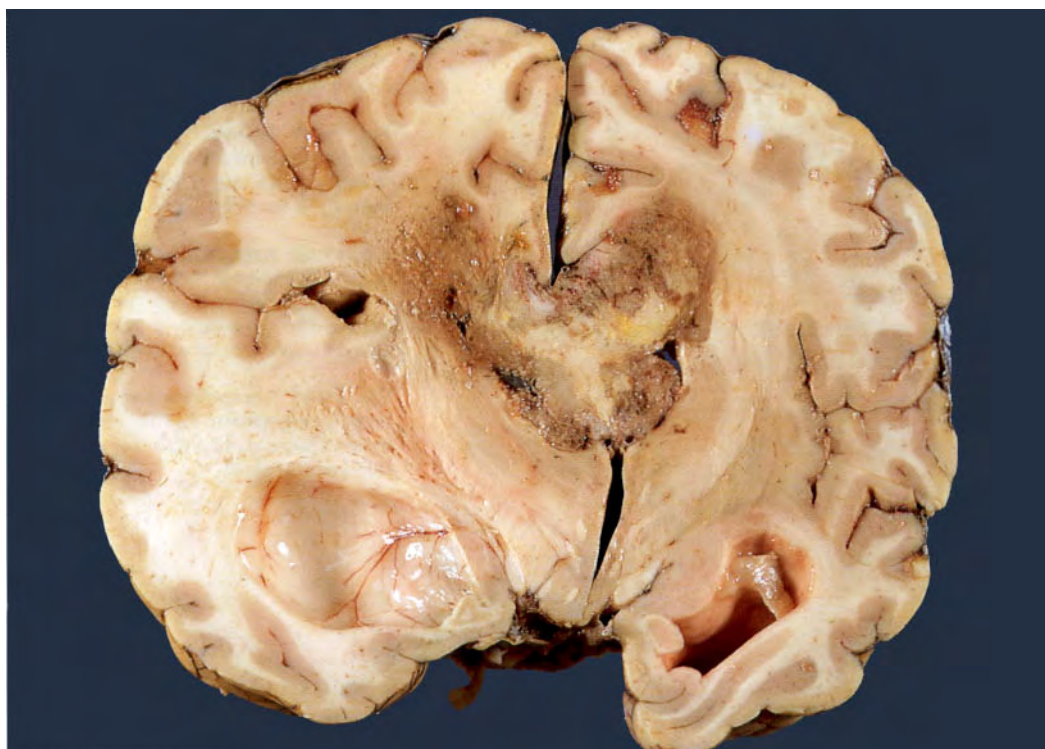


Fig. 11.81

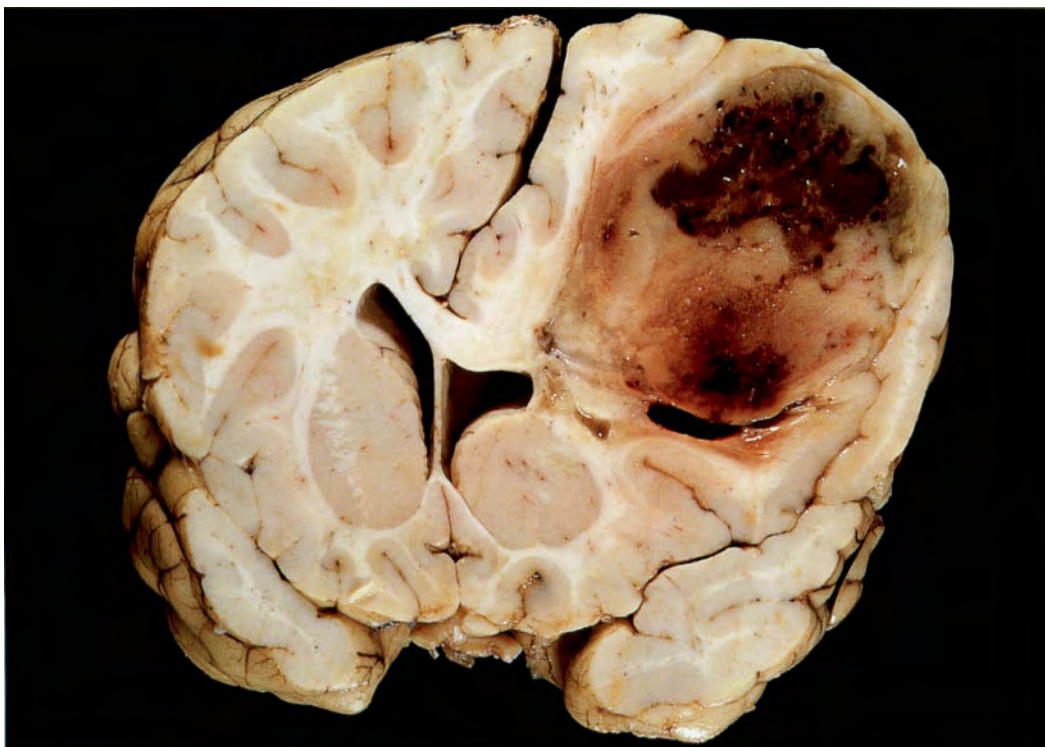


Fig. 11.82

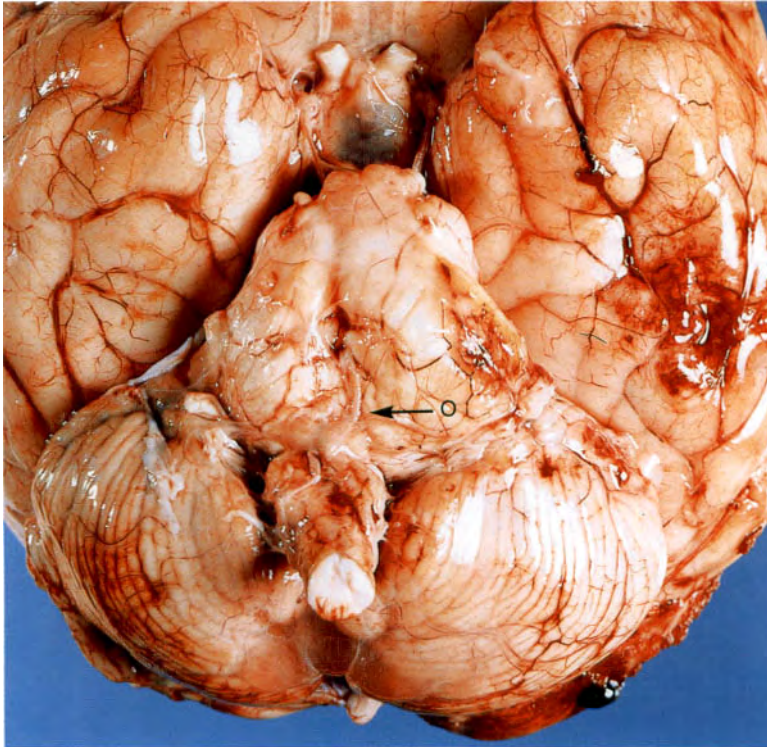


Fig. 11.83

Fig. 11.83 Astrocytoma in the brain stem. F/8. The pons is grossly enlarged. These tumours occur particularly in children and are relatively slow growing.

Fig. 11.84 Transverse section of pons and cerebellum showing haemorrhage into a pontine astrocytoma. M/15.

Fig. 11.85 Astrocytoma. F/3. The skull is irregularly thinned by raised intracranial pressure caused by the presence of the tumour. This appearance is sometimes called the 'beaten copper' skull.

Fig. 11.86 Cerebellum containing a large astrocytoma. F/6. The majority of brain tumours in children occur below the tentorium cerebelli.

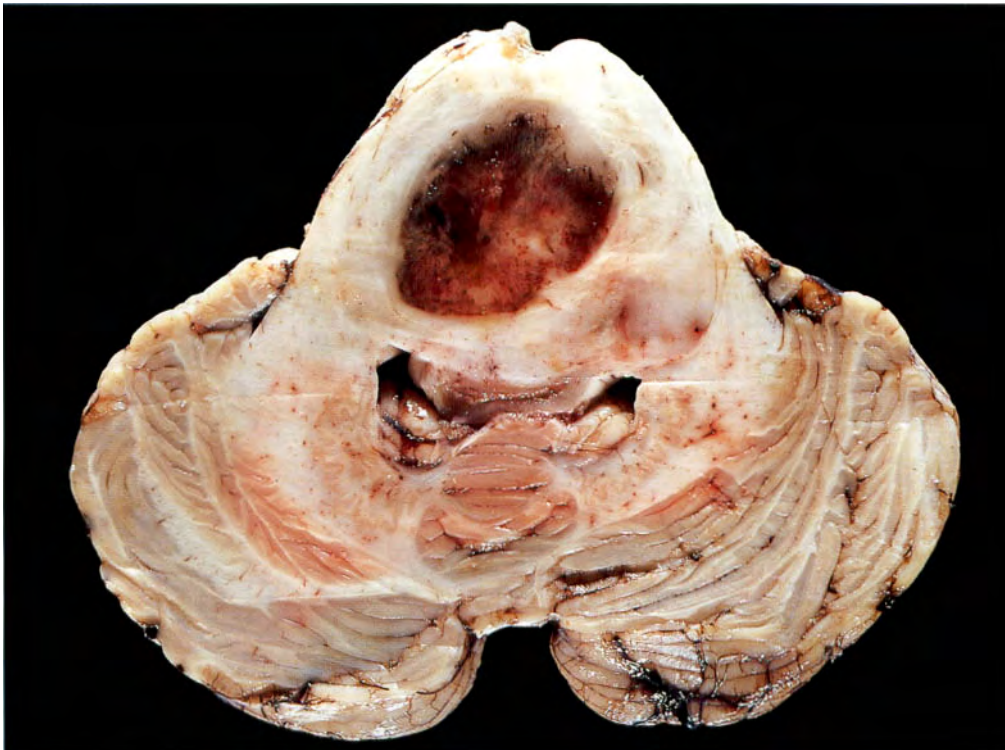


Fig. 11.84



Fig. 11.85



Fig. 11.86

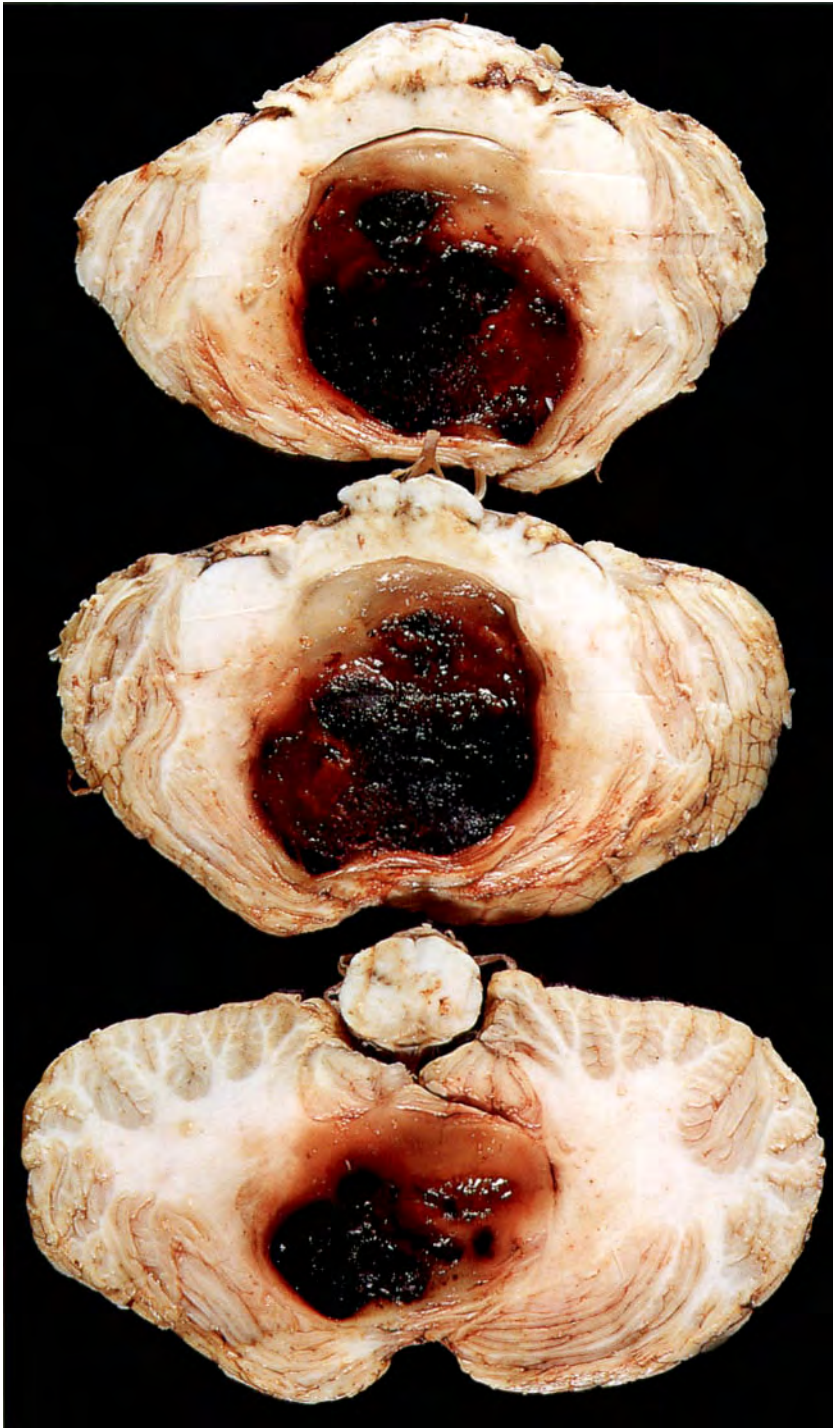


Fig. 11.87

Fig. 11.87 Medulloblastoma. F/10. Cross-sections of a cerebellum showing haemorrhage into a medulloblastoma. They typically arise in this midline site.



Fig. 11.88

Fig. 11.88 Transverse section of spinal cord showing tumour in the subarachnoid space around the cord. F/6. This mode of spread is characteristically seen in medulloblastoma.

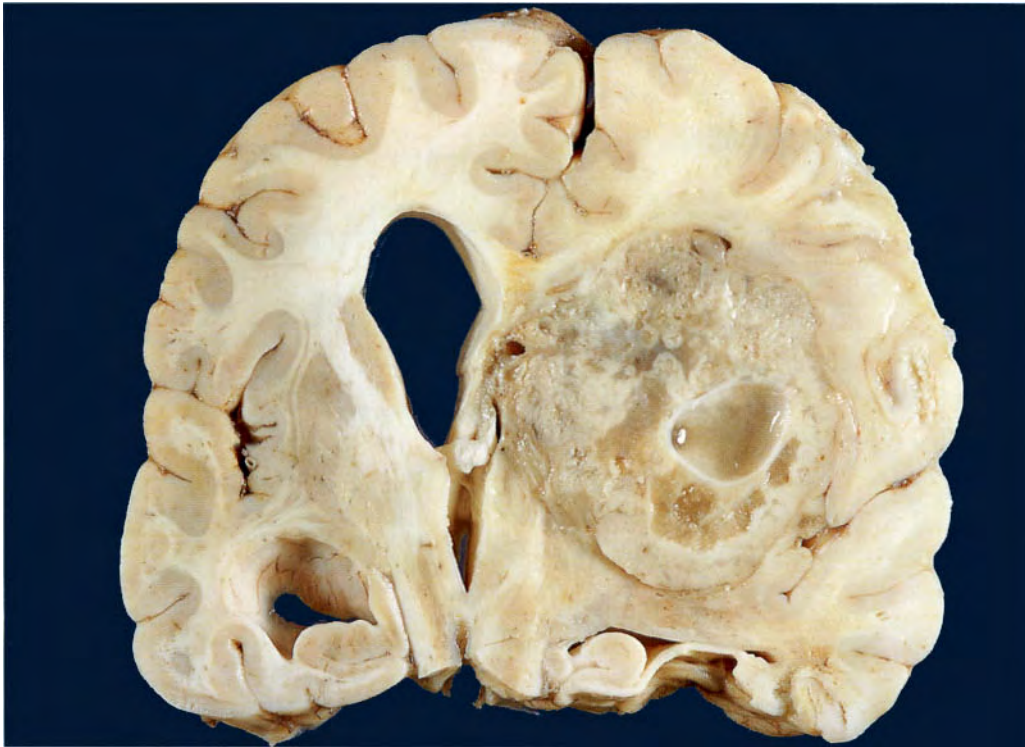


Fig. 11.89



Fig. 11.90

Fig. 11.89 Ependymoma in the right lateral ventricle. F/7. The tumour is well circumscribed and apparently confined to the ventricle. It has compressed the CSF pathways, causing dilatation of the third ventricle and the left lateral ventricle. The macroscopic appearance of this tumour suggests an ependymoma, but microscopic confirmation would be required.

Fig. 11.90 Secondary tumour in the brain. M/49. Secondary tumour deposits are usually multiple and well circumscribed. Pigmented secondaries indicate secondary melanoma or secondaries from a teratoma of the testis in a male, and in a female secondary melanoma or secondary choriocarcinoma. There is marked oedema in the right hemisphere, indicating the presence of raised intracranial pressure.

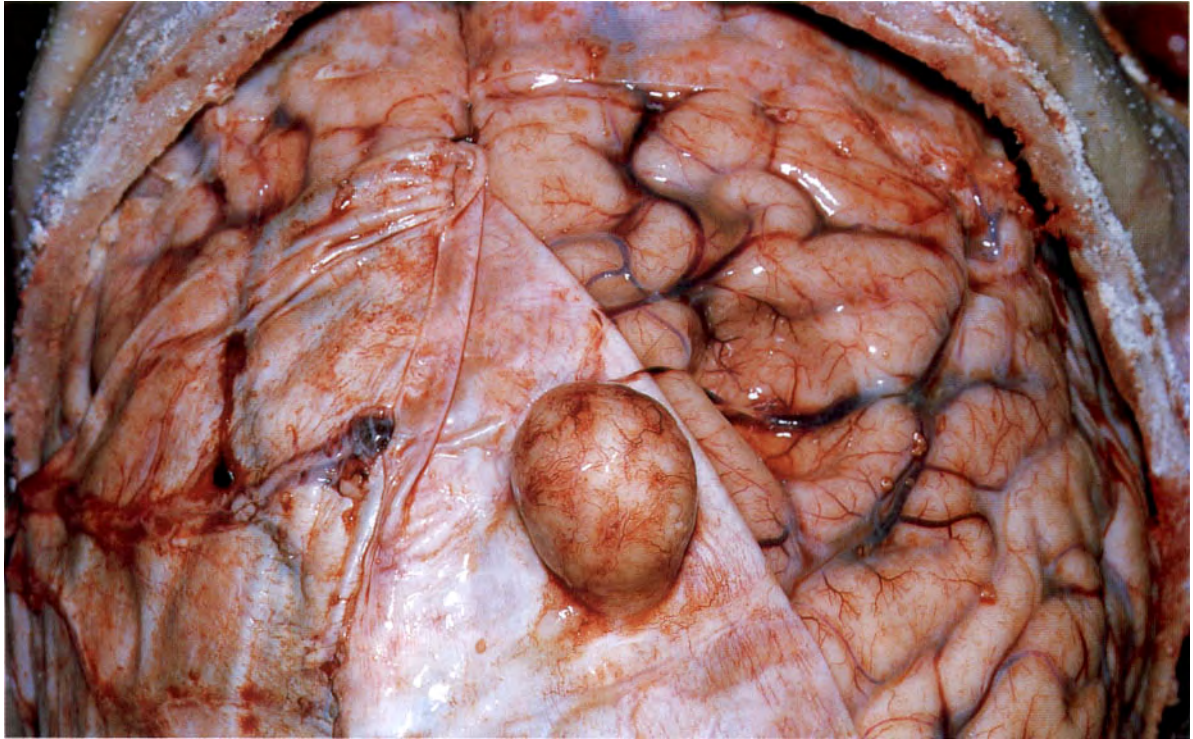


Fig. 11.91

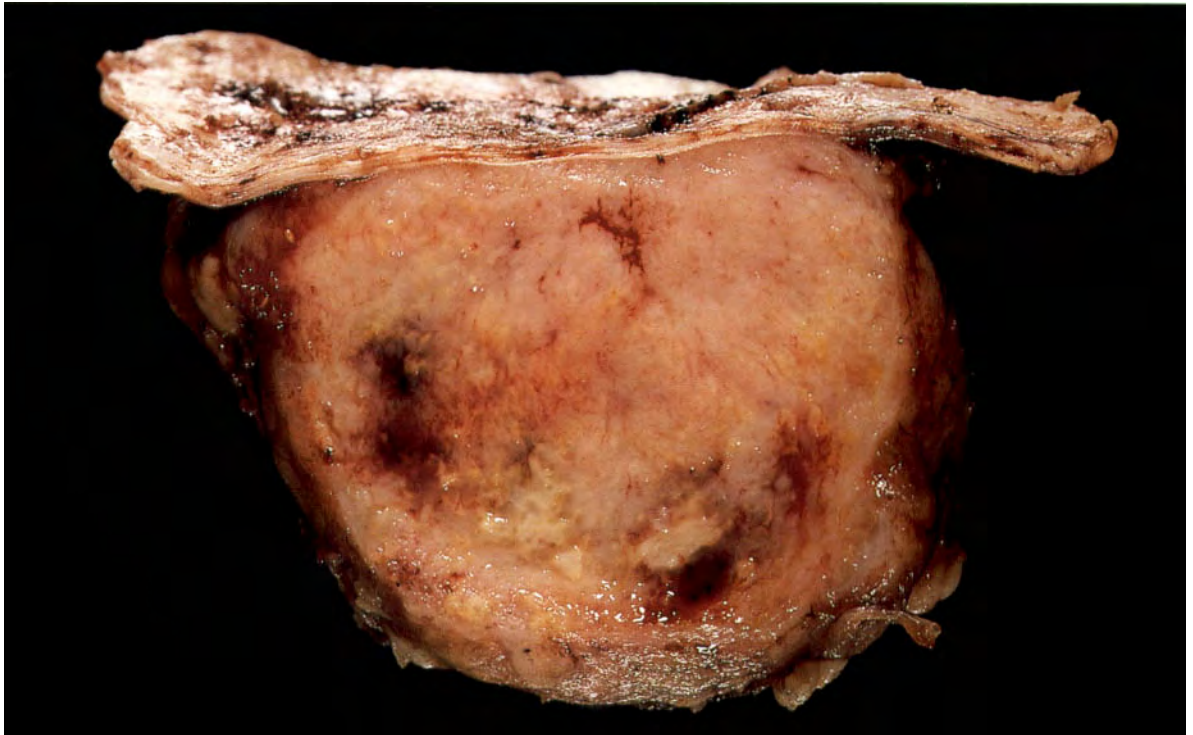


Fig. 11.92

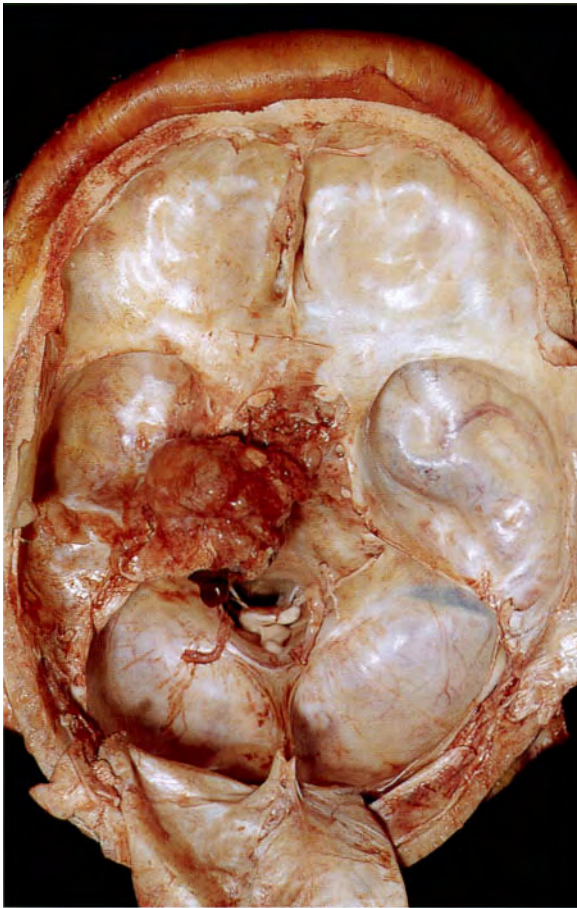


Fig. 11.93



Fig. 11.94

Fig. 11.91 Meningioma. F/46. Small, asymptomatic tumour attached to the dura.

Fig. 11.92 Transverse section of a meningioma removed surgically together with the attached dura. M/78.

Fig. 11.93 Meningioma. M/70. The brain has been removed to demonstrate the presence of a meningioma attached to the left petrous temporal bone and impinging on the pituitary fossa.

Fig. 11.94 Meningioma arising from the olfactory groove. M/89. Incidental postmortem finding.

Fig. 11.95 Meningioma arising from the left sphenoidal ridge. M/60. Incidental postmortem finding.

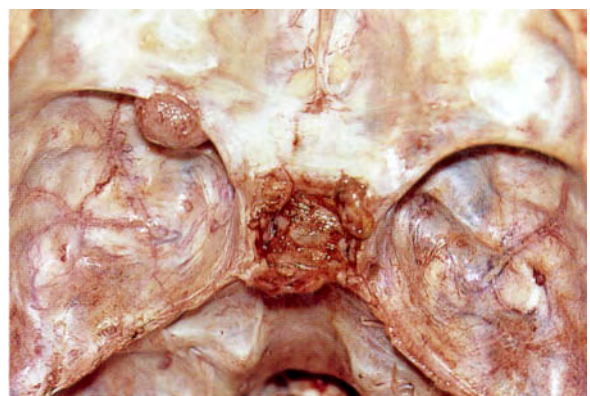


Fig. 11.95



Fig. 11.96

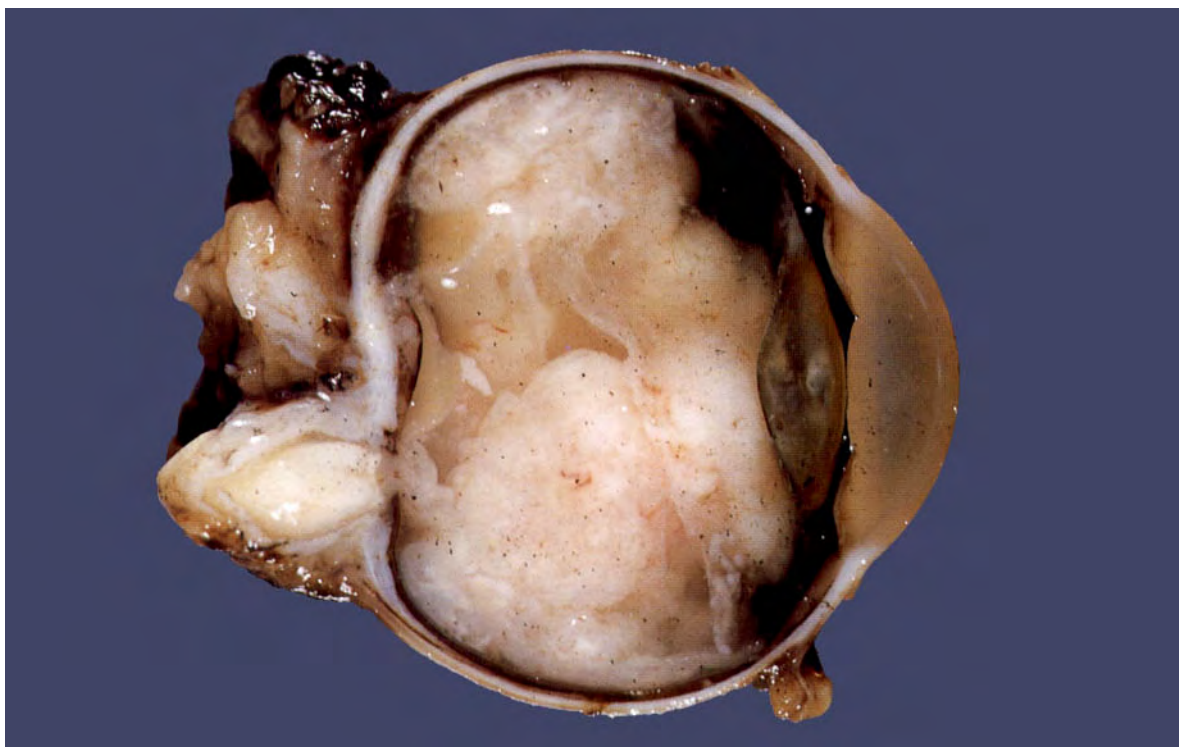


Fig. 11.97



Fig. 11.98

Fig. 11.96 Retinoblastoma. F/2. The mother was alerted to the condition by the white colour of the pupil. There was also some loss of vision.

Fig. 11.97 Retinoblastoma filling the posterior chamber of the eye removed surgically. There was no spread along the subdural space around the optic nerve, no tumour in the other eye, and no family history – features that are often present.

Fig. 11.98 Large pituitary adenoma. F/12. Microscopically this was a chromophobe adenoma, and clinically it was causing local pressure effects.

Fig. 11.99 Craniopharyngioma in the pituitary fossa. F/52. The main bulk of the tumour was situated above the sella turcica.

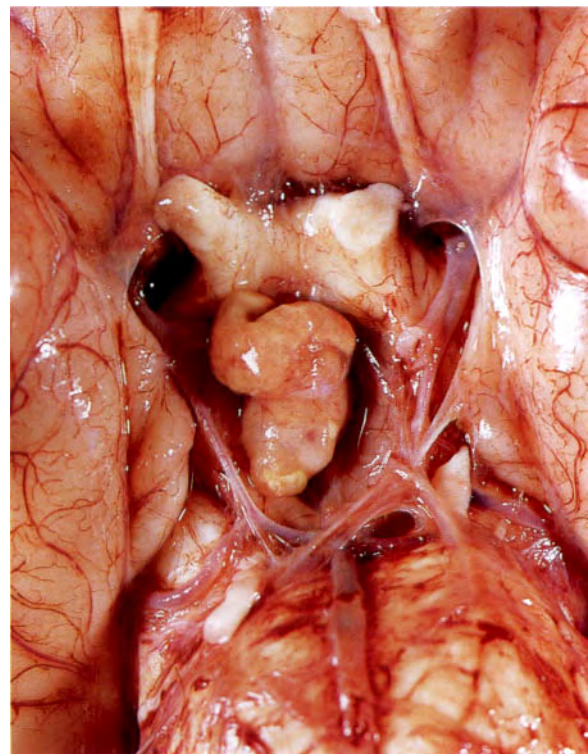


Fig. 11.99

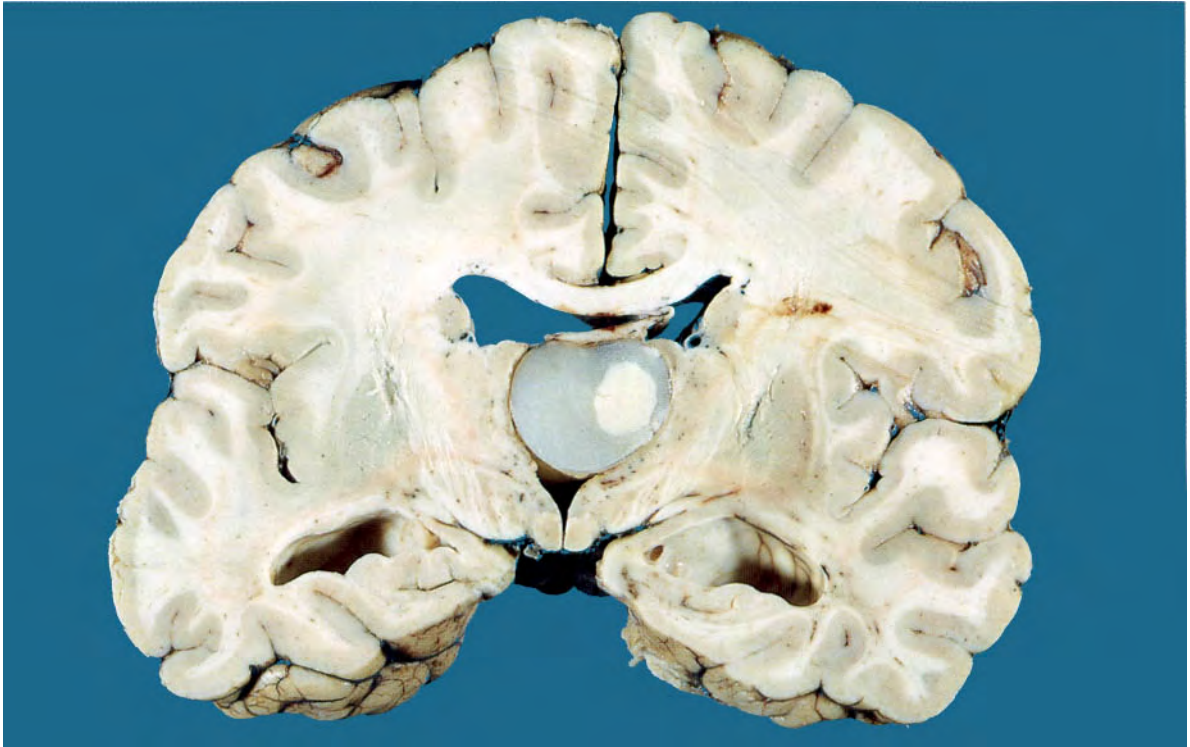


Fig. 11.100



Fig. 11.101



Fig. 11.102

0 cm 1

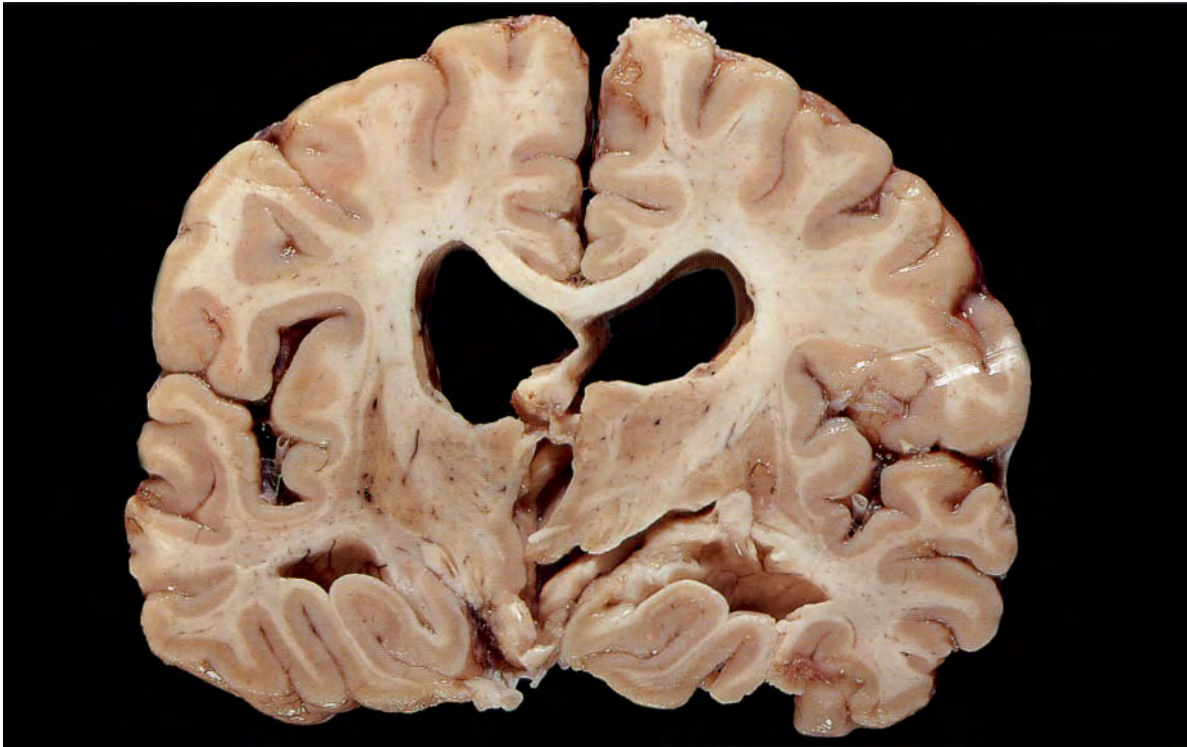


Fig. 11.103

Fig. 11.100 Colloid cyst of the third ventricle. M/16. The patient presented with intermittent headaches, particularly in the head-down position (a history which is characteristic of this lesion). Lumbar puncture was performed in a country hospital and the pressure shift resulted in herniation of the cerebellar tonsils (coning) and death.

Fig. 11.101 Neurilemmoma (acoustic neuroma) arising from the right eighth nerve. M/50. An incidental postmortem finding. It usually presents as deafness. This is a very large tumour. Since the introduction of CT and MRI scanning these tumours are identified at a very early stage, when they are small and easily amenable to surgical removal.

Fig. 11.102 Neurilemmoma arising on a peripheral nerve. M/20. Presented as a subcutaneous tumour which was excised.

Fig. 11.103 Huntington's chorea. F/54. Note the gross atrophy of both caudate nuclei and both basal ganglia. There is marked compensatory hydrocephalus resulting from the cortical and basal ganglia atrophy.



Fig. 11.104



Fig. 11.105



Fig. 11.106

Fig. 11.104 Alzheimer's disease. F/53. The atrophic brain on the left is compared with that of a normal 50-year-old on the right. Alzheimer's disease is the commonest form of presenile dementia.

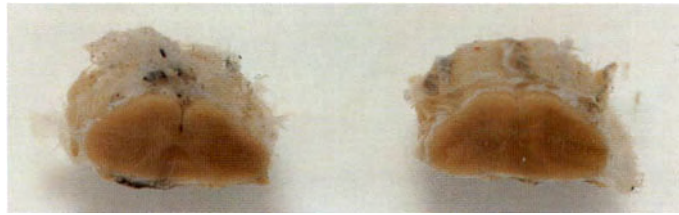


Fig. 11.107

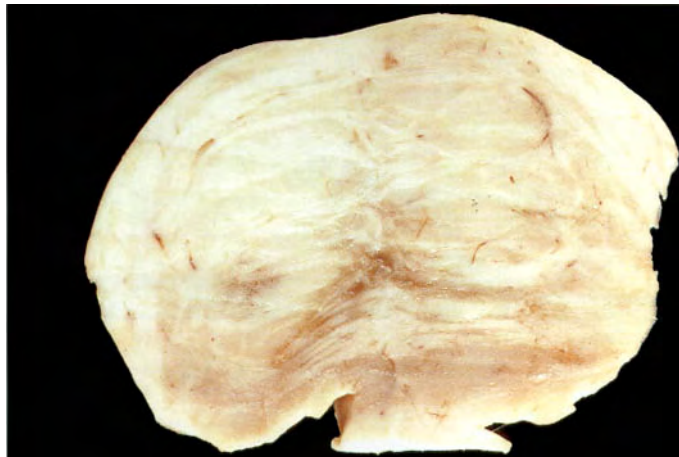


Fig. 11.108

Fig. 11.105 Alzheimer's disease. F/57. Note the gross atrophy of the cerebral gyri and widening of the sulci in all lobes, but particularly in the frontal lobe.

Fig. 11.106 Parkinson's disease. M/65. The transverse section of the cerebral peduncles in the upper specimen shows loss of pigment in the substantia nigra. The lower specimen for comparison shows normal substantia nigra.

Fig. 11.107 Atrophy of the posterior columns of the spinal cord. Three conditions cause this appearance: tabes dorsalis, vitamin B₁₂ deficiency (subacute combined degeneration) and Friedreich's ataxia.

Fig. 11.108 Central pontine myelinolysis. M/61. The area of demyelination is shown as a brownish discoloration. The patient was an alcoholic. This condition was first described in alcoholics, but it is now known to be associated with hypokalaemia, especially when this has been rapidly corrected.

Fig. 11.109 Multiple sclerosis. M/33. This diagnosis was made 6 years before death, when the patient first complained of ataxia. The ataxia was followed by increasing weakness of the legs and arms. For a few years before death from pneumonia he was confined to a wheelchair. This brain slice shows a large grey area of demyelination in the characteristic periventricular distribution (A). There is another large area of demyelination in the white matter of the temporal lobe (B).

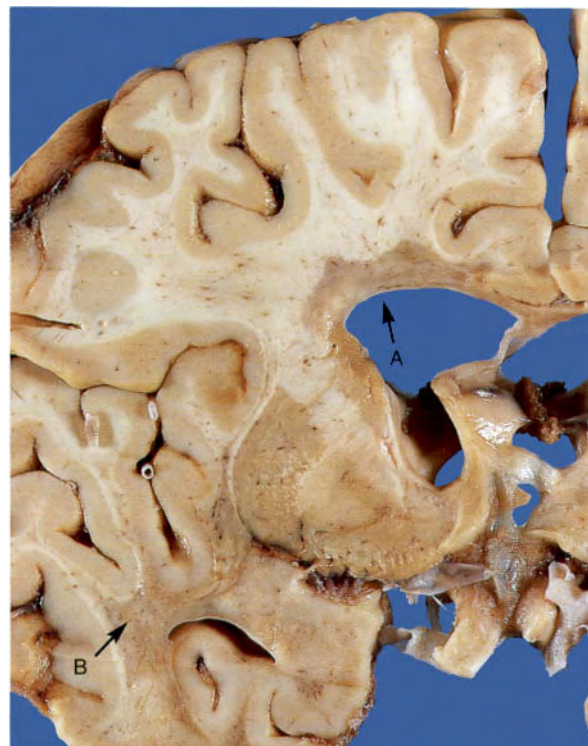


Fig. 11.109



Fig. 11.110

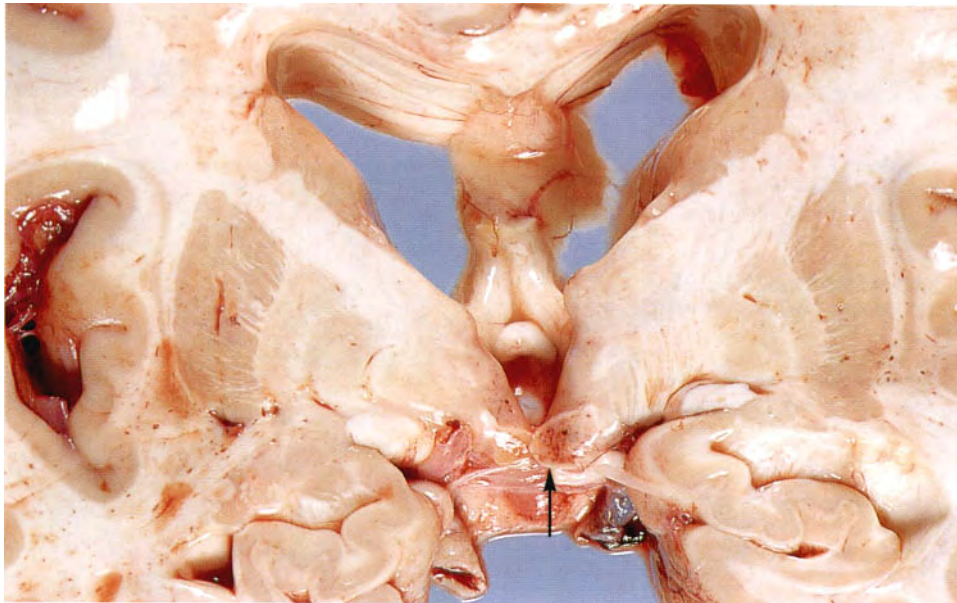


Fig. 11.111

Fig. 11.110 Kernicterus in a neonate with haemolytic disease of the newborn. There is yellow coloration in the subthalamic nuclei and the uncus hippocampi. With the early recognition and treatment of rhesus incompatibility, this condition is now rare.

Fig. 11.111 Wernicke's encephalopathy. M/67. Haemorrhages into the right mammillary body and beneath the ependyma of the third ventricle on the left. The patient was a known alcoholic.

Fig. 11.112 Microcephaly. F/19 months.

Fig. 11.113 Congenital hydrocephalus. F/8 months. Untreated.

Fig. 11.114 Anencephaly. Stillborn fetus.

Fig. 11.115 Hydranencephaly. The head was normal size. The child continued to breathe for 5 days. There were no cerebral hemispheres and the space was filled with fluid. The thalamus, cerebellum and brain stem were normal. The choroid plexus, which would normally be found in the lateral ventricles, can be seen attached to the thalamus.



Fig. 11.112



Fig. 11.113



Fig. 11.114

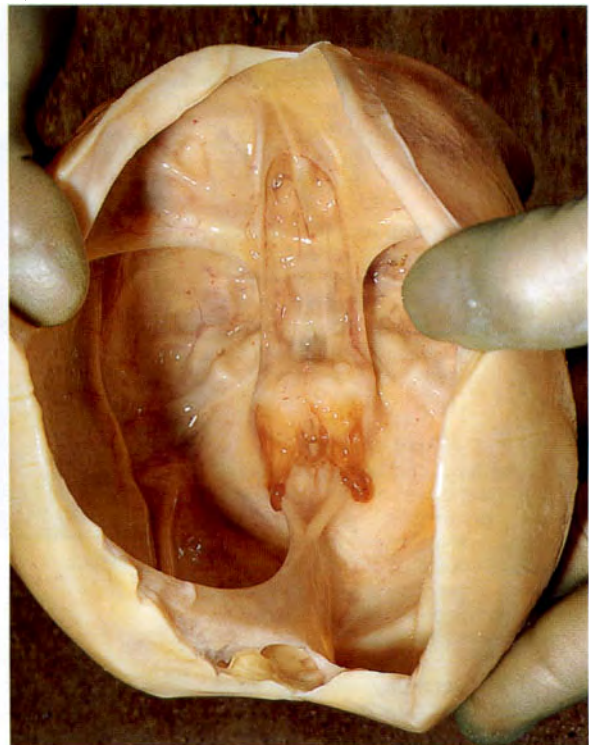


Fig. 11.115



Fig. 11.116



Fig. 11.117

Fig. 11.116 Meningomyelocele. F/1 day. This deformity results when leptomeninges and a variable amount of nervous tissue protrude through a defect in the posterior laminae of the lumbar vertebrae (spina bifida.) In this case there was very little nervous tissue in the herniation.

Fig. 11.117 Arnold–Chiari malformation. Longitudinal slice through the medulla and cerebellum showing this malformation, which is almost invariably associated with meningomyelocele. It consists of elongation of the medulla, herniation of the cerebellar tonsils through the foramen magnum, and a Z-shaped kink in the cervical spinal cord.



Fig. 11.118

Fig. 11.118 Hydromyelia. Dilatation of the central canal of the spinal cord, an abnormality often seen in Arnold–Chiari malformation.



Fig. 11.119

The commonest neural tube defect occurs in the lumbar region of the spine. Defects may also be seen in the thoracic and cervical regions, sometimes in the occiput, and sometimes in the frontal region at the base of the nose.

These defects may be identified in utero by ultrasound examination at about 12 weeks' gestation.

Fig. 11.119 Posterior encephalocele. Herniation of the brain through the occiput.

Fig. 11.120 Large frontonasal encephalocele. This abnormality appears to be more frequent in some racial groups than in others. There is a defect in the skull and usually only CSF-filled meninges protrude through the opening. It is therefore amenable to surgical repair.



Fig. 11.120



Fig. 11.121

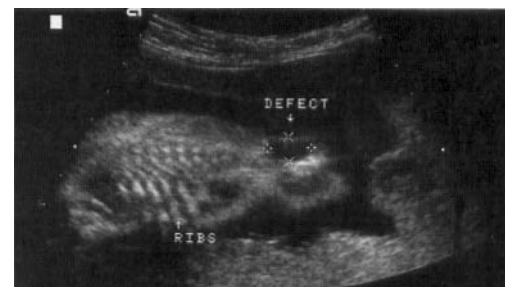


Fig. 11.122

Fig. 11.121 Anencephaly. Intrauterine ultrasound examination at 12 weeks' gestation. Note the relatively large eyes (frog's eye appearance).

Fig. 11.122 Intrauterine ultrasound examination at 12 weeks' gestation, showing the spina bifida malformation of neural tube defect.

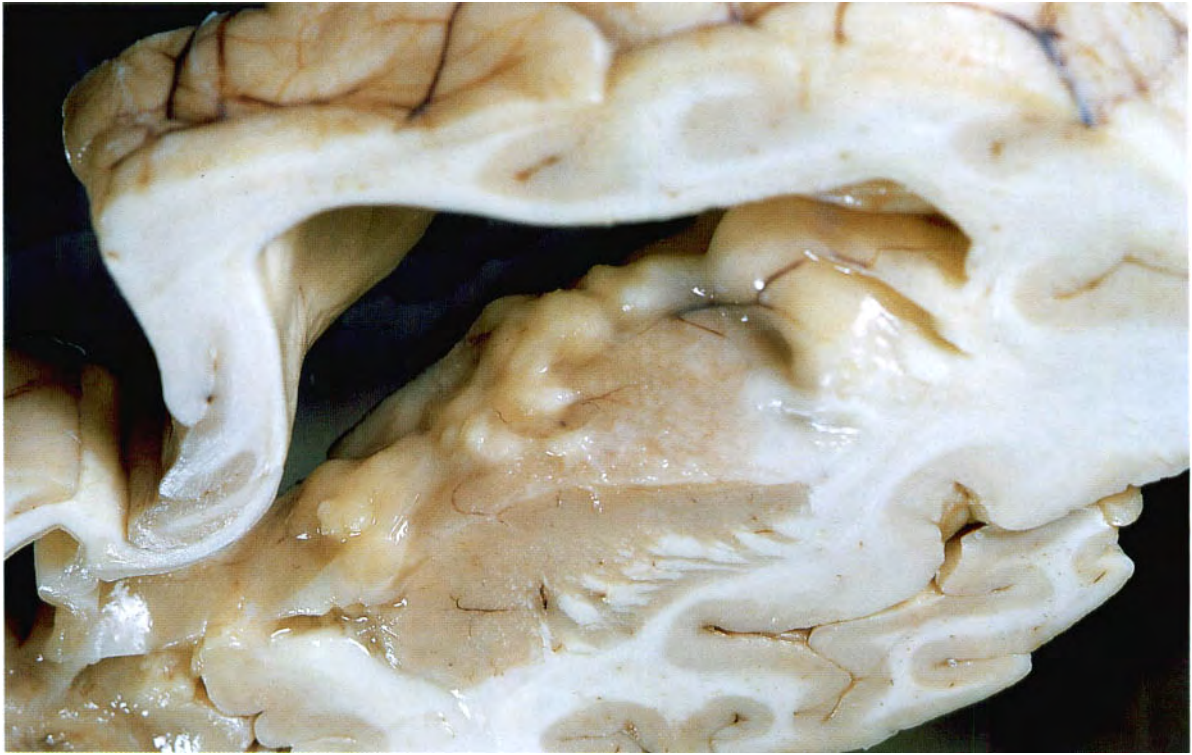


Fig. 11.123



Fig. 11.124



Fig. 11.125

Fig. 11.123 Tuberos sclerosis.

M/10. Brain slice showing dilated lateral ventricle with abnormal nodules of glial tissue attached to the ependymal lining. This appearance has been likened to the wax drippings on the side of a burning candle.

Fig. 11.124 The cortex of the brain shown in Figure 11.123. There is a large nodule of abnormal glial tissue on its surface. This is a tuber, and the presence of these hard nodules gave the condition its name. Microscopically, these lesions consist of atypical astrocytes. As a result, they can be misdiagnosed as astrocytomas if the histopathologist is not aware of the classic setting.

Fig. 11.125 Tuberos sclerosis.

M/15. This boy demonstrated the clinical hallmarks of this condition: mental retardation, epilepsy, and the presence of multiple nodular angiofibromatous lesions on the face. Tuberos sclerosis is inherited as an autosomal dominant trait.

Fig. 11.126 Kidney from a child with tuberous sclerosis. The multiple, creamy nodules are angioleiomyomas, which frequently occur in this condition.

Fig. 11.127 Cross-section of the heart of a neonate with tuberous sclerosis showing cardiac hamartomas – rhabdomyomas – which are another associated phenomenon.



Fig. 11.126

0 cm 5



Fig. 11.127

0 cm 5

Fig. 11.128 Poliomyelitis. Young adult male in Papua New Guinea with a withered left leg. This was a common sight throughout the world before the introduction of the polio vaccine.

Fig. 11.129 End stage of muscle disease. Transverse section from the atrophic muscle of a patient who had poliomyelitis as a child and died from other pathology. Most of the muscle has been replaced by fat, and only a small amount of red muscle remains. All chronic muscle diseases progress to grossly atrophic muscle such as this. The diagnosis of primary muscle disease depends on the clinical assessment, and microscopic examination of biopsies taken from muscles which are not completely atrophic.



Fig. 11.128

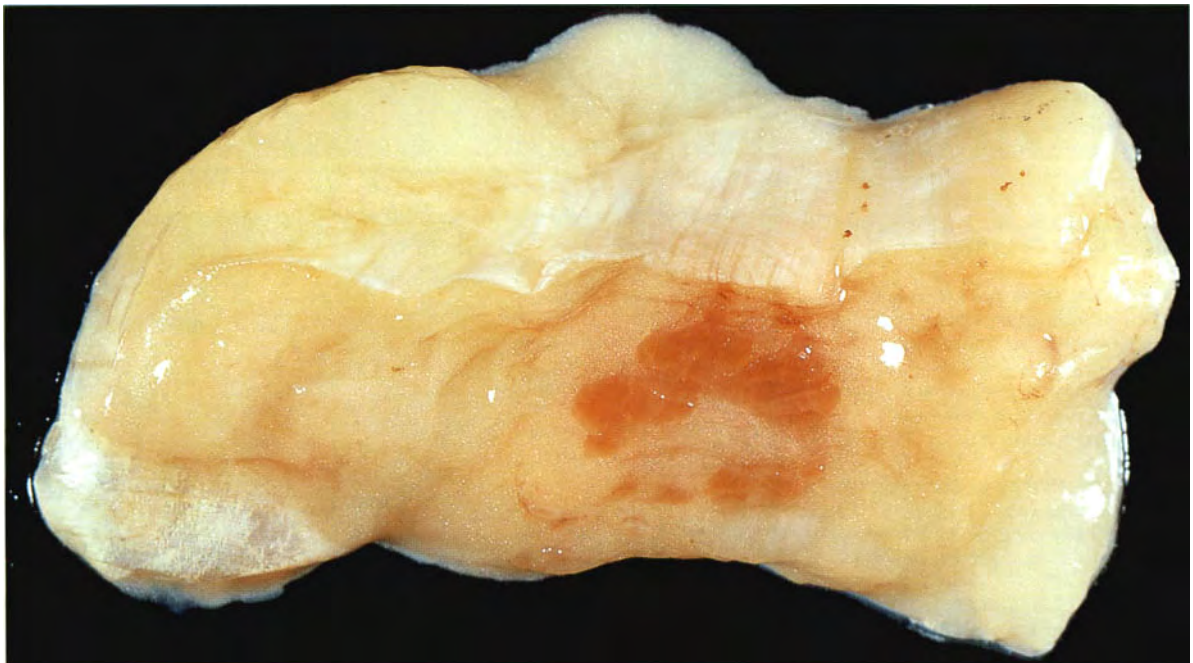


Fig. 11.129

0 cm 1

INDEX

- Abdominal striae, 187
Abscess
 acute pyelonephritis, 138, 139
 brain, 237
 epididymis, 150, 151
 liver, 122, 123
 amoebic, 126
 lung, 45, 46
 perianal, 106
 psoas, 209
 subdiaphragmatic, 125
Accessory nipple, 162
Achalasia, 69
Achondroplasia, 206
Acoustic neuroma (neurilemmoma), 272, 273
Acromegaly, 184, 185
Addison's disease, 192, 193
Adenocarcinoma
 bile ducts, 114, 115
 caecum, 104, 105
 colon, 104, 105
 endometrium, 169
 ileum, 92
 oesophagogastric junction, 76, 77
 ovary, 177
 rectum, 105
 stomach, 76, 77
 superficial (early gastric cancer), 78, 79
Adenochondroma, lung (benign hamartoma), 53
Adenoma
 adrenal cortex, 188, 190, 191
 parathyroid gland, 195
 pituitary, 184, 185, 188, 271
 thyroid gland, 198
Adenomatoid tumour, epididymis, 150, 151
Adenomatous polyps, colon, 101, 102
Adenomyoma
 gallbladder, 114
 uterus, 171
Adrenal gland
 atrophy in Addison's disease, 192
 Conn's syndrome, 191
 cortical adenoma, 188, 190, 191
 haemorrhage, 232
 hyperplasia, 189, 193
 focal nodular, 189
 medullary myelolipoma, 193
 neuroblastoma, 194
 secondary tumour, 193
Adrenogenital syndrome, 191
Air embolus, 20, 21
Alcoholic cirrhosis, 66, 125
Alkaptonuria, 221
Alveolar cell carcinoma (bronchoalveolar carcinoma), 58
Alzheimer's disease, 274, 275
Ameloblastoma, maxilla, 65
Amoebic colitis, 100, 101
Amoebic liver abscess, 126
Ampulla of Vater, calculi, 108
Amyloid goitre, 204
Amyloidosis, 204
Analgesic nephropathy, 141
Androgen-secreting adrenal tumour, 190, 191
Androgens, overproduction, 191
Anencephaly, 276, 277, 279
Aneurysm
 aortic
 abdominal, 3,
 dissecting, 6
 thoracic, 4, 5
 arteriovenous, 5
 intracerebral
 basilar artery, 260
 berry, 258
 internal carotid artery, 259
 long saphenous vein, 5
 syphilitic of aortic arch, 4, 5
 traumatic of superficial temporal artery, 5
 aneurysmal bone cyst, 219
 angioliomyomas, kidney, 281
 angiosarcoma
 breast, 160
 upper arm, 158, 159
 ankylosing spondylitis, 223
 annular pancreas, 70, 71
 anterior spinal artery thrombosis, 246
 anthracosis (coal miner's lung), 52
 anus
 fistula, 106
 imperforate, 94, 95
 squamous cell carcinoma, 105
 aortic aneurysm
 abdominal, 3, 5
 atheromatous plaques, 2
 dissecting, 6
 syphilitic, 4, 5
 thoracic, 4, 5
 aortic coarctation, 29
 aortic stenosis, 22
 hypertrophic cardiomyopathy, 18
 aortic valve
 acute rheumatic vegetations, 21
 Lambert's excrescence, 21
 rupture in bacterial endocarditis, 24
 appendicitis, acute, 92, 93
 acute peritonitis, 92, 93
 appendix
 carcinoid tumour, 94
 mucocoele, 94
 normal, 92, 93
 Arnold–Chiari malformation, 278
 arteriovenous aneurysm, 5
Arteriovenous malformation
 brain, 262
 spinal cord, 262
Arthritis
 gout, 222
 haemochromatosis, 118
 multiple haemarthroses, 222
 rheumatoid, 51, 222
Asbestos exposure, 52, 56
 pleural plaques, 57
Ascites, tuberculosis, 50
Aspergilloma, 46, 47
Aspergillus, 44, 46
 mucus plug, 44
Asthma, acute, 44
Astrocytoma, 262, 263
 brain stem, 264
 cerebellum, 264, 265
 haemorrhage, 262, 263, 264
 pons, 264
 skull thinning (beaten copper appearance), 264, 265
Atherosclerosis, 2
 coronary artery, 10
 endarterectomy specimen, 3
 renal artery, 136, 137
Atrial septal defect
 associated mitral valve defect, 28
 septum primum, 28
Atrium
 ball thrombus, 23
 myxoma, 30
Auricular appendage thrombus, 23
Auricular fibrillation, 23
Bacterial endocarditis
 aortic valve rupture, 24
 conjunctival petechial haemorrhages, 24
 mitral valve vegetations, 23
 mycotic embolism, 248, 249
 renal infarct, 24
Basilar artery
 aneurysm, 260
 thrombosis, 245
Benign prostatic hypertrophy, 146
Berry aneurysm, 258
Betel nut, 63
Bezoar, gastric, 75
Bile duct
 adenocarcinoma, 114, 115
 gallstones, 114, 115
 multiple hamartomas, 128
Biliary atresia, congenital, 116
Bladder
 bossellated calculus, 144
 outlet obstruction, 146
 transitional cell carcinoma, 144
Bleeding diathesis, multiple intracerebral haemorrhages, 257

- Bone
aneurysmal cyst, 219
fibrous dysplasia, 218, 219
giant cell tumour, 220, 221
hyperparathyroidism-related disease, 195
- Botryoid sarcoma, 167
- Brain,
abscess, 237
computed tomography (CT), 242, 243
cranial nerves, 260
normal, 242, 254, 255
secondary tumour, 267
third ventricle colloid cyst, 272, 273
toruloma, 237
traumatic damage, 249
tuberculoma, 236
- Brain stem,
astrocytoma, 264
coning, 251
cranial nerves, 260, 261
multiple haemorrhages, 250, 251
- Breast
angiosarcoma, 160
carcinoma, 156, 157
colloid, 158
male breast, 163
medullary, 158
congenital hypoplasia, 162
fat necrosis, 156
fibroadenoma, 154
fibrocystic disease, 154, 155
intraductal papilloma, 154, 155
juvenile hypertrophy, 162
lipogranuloma, 156
mammary duct ectasia, 154, 155
prosthesis leakage/rupture, 156
- Bronchiectasis
Aspergillus mucus plug impaction, 44
chronic, 44
- Bronchitis, chronic, 43
- Bronchoalveolar carcinoma (alveolar cell carcinoma), 58
- Bronchogenic carcinoma, 54, 55
secondary liver tumour, 130
see also Lung cancer
- Bronchogenic cyst, congenital, 41
- Bronchopneumonia
confluent, 45
mucoviscidosis, 111
- Buccal mucosa
haemangioma, 60
squamous cell carcinoma, 63
- Budd–Chiari syndrome, 120, 121
- Burkitt's lymphoma, 32
- Caecum
adenocarcinoma, 104, 105
carcinoma with ulcerative colitis, 98
- Café-au-lait spot, 226
- Calculus
ampulla of Vater, 108
bossellated vesical, 144
gallbladder, 113
nephrolithiasis, 140, 141
pancreatic duct obstruction, 108
renal, 144
ureteric, 144
- Candidiasis
epiglottis, 36
gastritis, 73
intrauterine, 182
oesophagitis, 66, 67
tongue, 61
- Carcinoid tumour
appendix, 94
lung, 53
small intestine, 91
- Cardiac failure
effects on liver, 120, 121, 125
prostatic vein thrombi, 42
- Cardiac tamponade, 11, 12
- Carotid artery
arteriovenous aneurysm, 5
endarterectomy, 3
ruptured aneurysm, 259
thrombosis, 239
Takayasu's arteritis, 4, 5
- Carotid body tumour, 194
- Cavernous sinus thrombosis, 253
- Central pontine myelinosis, 275
- Cerebellum,
astrocytoma, 264, 265
infarction, 245, 246
medulloblastoma, 266
meningitis, 233, 234, 235
tonsillar herniation, 250, 251
- Cerebral abscess, 237
- Cerebral artery thrombosis, 239, 242
- Cerebral infarction, 239, 240, 241, 242, 243
motor speech area, 244, 245
occipital lobe, 244, 245, 251
see also Stroke
- Cerebral malaria, 238
- Cerebral peduncle
atrophy, 241
infarction, 251
- Cerebral vein thrombosis, 254, 255
- Cerebrospinal fluid in meningitis, 231
- Cerebrovascular insufficiency, 239
- Cervical squamous cell carcinoma, 166
early invasive plus carcinoma in situ, 166
longstanding procidentia, 166
- Chemodectoma, 194
- Chest X-ray
miliary tuberculosis, 48, 49
staphylococcal pneumonia, 46
- Chocolate cyst, 174, 175
- Cholangitis, suppurative, 122, 123
- Cholecystitis
acute-on-chronic, 113
chronic, 113
- Choledochal cyst, 116
- Cholesterosis, 114
- Chondroma, 218, 219
- Chondrosarcoma, 220, 221
- Chorangioma (benign haemangioma of placenta), 180
- Chordoma, 220, 221, 261
- Choriocarcinoma, 169
- Circle of Willis, 258
- Clitoris hypertrophy, 191
- Clonorchis sinensis*, 126, 127
- Clostridium difficile*, 101
- Coal miner's lung (anthracosis), 52
- Coarctation of aorta, 29
- Coeliac disease, 79
- Colitis
acute, 100, 101
amoebic, 100, 101
ischaemic, 100, 101
pseudomembranous, 100, 101
- Colloid carcinoma, breast, 158
- Colon
adenocarcinoma
descending colon, 104, 105
polypoid, 104, 105
transverse colon, 104, 105
ascending, duplication, 88, 89
Crohn's disease, 99
diverticulosis, 96, 97
melanosis, 96, 97
mucosal dysplasia in ulcerative colitis, 98
polyps
juvenile, 102
multiple polyposis, 102
ubular adenomatous, 101, 102
- Common bile duct, gallstones, 114, 115
- Computed tomography (CT), 239
brain scan, 242
stroke, 242, 243
heart, 15
- Condylomata lata, 164
- Conjunctival petechial haemorrhages, bacterial endocarditis, 24
- Conn's syndrome, 191
- Coronary artery
bypass, 15
left, arising from pulmonary trunk, 30
occlusion with left ventricular hypertrophy, 19
thrombus, 10
- Cortical vein thrombosis, 252, 253
- Cranial nerves
anatomy and palsies, 260, 261
- Craniopharyngioma, 271
- Cretin, 198
- Crohn's disease
colon, 99
perianal abscess and fistulae, 106
terminal ileum, 84, 85
- Cryptococcus neoformans*, 237
lung infection (toruloma), 46, 47
- Cushing's syndrome, 187
adrenal cortical adenoma, 188
adrenal hyperplasia, 189
basophil pituitary adenoma, 188
clinical, 187
secondary adrenal hyperplasia, 193
secondary medullary thyroid carcinoma, 203
- Cutaneous haemangioma, 7

- Cyst
- aneurysmal bone, 219
 - choledochal, 116
 - dentigerous, 65
 - enterogenous, 88, 89
 - epididymis, 150, 151
 - kidney, 134, 135
 - lateral meniscus, 224
 - mucus retention, 60
 - ovary
 - chocolate, 174, 175
 - dermoid (benign teratoma), 177
 - endometriosis, 174, 175
 - simple follicular, 173
 - spleen, 34
 - synovial, 224
 - third ventricle colloid, 272, 273
 - thyroglossal, 204
 - thyroid gland, 197
- Cystadenocarcinoma, ovary, 176
- Cystadenoma
- ovary
 - mucinous, 175, 176
 - serous, 174, 175
 - pancreas, 112
- Cystic hygroma (lymphangioma), 7
- macroglossia, 61
- Cystic pituitary gland, 186, 187
- Cystitis, acute, 146
- Dacron graft, aortic aneurysm repair, 3
- Deep cerebral vein thrombosis, 254, 255
- Dentigerous cyst, 65
- Dermoid cyst, ovary (benign teratoma), 177
- torsion, 177
- Desmoid tumour, 228
- Diabetic kidneys, 138, 139
- Diaphragmatic hernia, congenital, 41, 70, 71
- Digital fibroma, 227
- Diplococcus pneumoniae*, 231
- Diverticulosis
- chronic, 96, 97
 - colon, 96, 97
 - sigmoid, 96, 97
- Double gallbladder, 113
- Double ureter, 132, 133
- Double uterus, 167
- Down's syndrome, 28
- Dubin–Johnson syndrome, 118
- Duodenal atresia, 70, 71
- Dupuytren's contracture, 228
- Dysgerminoma, 178
- Ear piercing, 227
- Ectopic pregnancy
- lithopaedion, 179
 - ovarian, 179
 - ruptured tubal, 179
- Electrocardiogram (ECG/EKG)
- anterior myocardial infarction, 8, 9
 - normal, 8, 9
 - posterior myocardial infarction, 10
- Elephantiasis, 16, 17
- Embryonal carcinoma, testis, 152
- Embryonal rhabdomyosarcoma, 167
- Emphysema
- centrilobular destructive (mild), 43
 - interstitial, 40, 41
 - pan-acinar destructive (severe), 43
- Empyema, 46
- Encephalocoele
- frontonasal, 279
 - posterior, 279
- Endolymphatic stromal myosis, 171
- Endometriosis
- extrapelvic, 174, 175
 - ileum, 88, 89
 - ovary, 174, 175
- Endometrium
- adenocarcinoma, 169
 - benign polyp, 168
 - hyperplasia, 169
- Enterocolitis, acute, 101
- Enterogenous cyst, 88, 89
- Ependymoma, 267
- Epididymis
- abscess, 150, 151
 - adenomatoid tumour, 150, 151
 - cyst, 150, 151
 - tuberculosis, 150, 151
- Epiglottitis, candidiasis, 36
- Epiglottitis, acute, 36
- Epispadias, 147
- Epstein–Barr virus, 32
- Epulis, congenital, 60
- Erythroblastosis fetalis, 180, 181
- Ewing's tumour, 220, 221
- Exomphalos, 82
- Exophthalmos, thyrotoxicosis, 198
- Extradural haemorrhage, 255
- Eye
- blue sclerotics, 206
 - ochronosis, 221
- Fallot's tetralogy, 26
- Fat embolism, 247
- Fat necrosis, breast, 156
- Fibrinous pericarditis, 20, 21
- Fibroadenoma, breast, 154
- Fibrocystic disease, breast, 154, 155
- Fibroelastosis, left ventricle, 30
- Fibroma
- digital, 227
 - ovary, 178
- Fibromatosis
- desmoid tumour, 228
 - plantar, 228
- Fibrous dysplasia, 218, 219
- Filariasis, 16, 17
- Fistula
- in ano, 106
 - perianal, 106
- Floor of mouth squamous cell carcinoma, 62
- Focal nodular hyperplasia
- adrenal gland, 189
 - liver, 128
 - lymphoid of ileum, 90, 91
- Follicular thyroid carcinoma, 200
- Foot ischaemia, severe, 3
- Fracture
- crush of vertebrae, 210, 211, 217
 - healed, 210, 211
- Friedreich's ataxia, 275
- Fundal petechial haemorrhages, bacterial endocarditis, 24
- Gallbladder
- adenomyoma, 114
 - calculi, 113
 - carcinoma, 114, 115
 - cholesterolosis, 114
 - double, 113
 - mucocoele, 114
- Gallstone ileus, 89
- Gallstones, 113
- common bile duct, 114, 115
- Ganglioneuromatosis, 202
- Gastric cancer, early (superficial adenocarcinoma), 78, 79
- Gastric diverticulum, 71
- Gastric erosions
- acute, 72, 73
 - complicating intracerebral haemorrhage, 256
- Gastric polyps, 74
- Gastritis, *Candida*, 73
- Giant cell tumour
- bone, 220, 221
 - tendon sheath (benign synovioma), 223
- Gigantism, 184, 185
- Goitre, 196
- amyloid, 204
 - multinodular colloid, 197
 - thyrotoxicosis, 198
- Gout, 222
- Granulomatous thyroiditis, 199
- Granulosa cell tumour, 178
- Gunshot wound
- rupture of heart, 16
 - twelfth nerve lesion, 261
- Gynaecomastia, 163, 190, 191
- Haemangioma
- buccal mucosa, 60
 - cutaneous, 7
 - liver, 128
 - placenta (chorangioma), 180
 - vertebrae, 219
- Haemarthrosis, 222
- Haematoma, liver, 121
- Haemochromatosis
- arthritis, 118
 - hepatocellular carcinoma, 117
 - liver, 117, 118
 - pancreas, 118
- Haemolytic disease of newborn, 276
- Haemopericardium, 11, 12
- Haemophilia, 222
- Haemophilus influenzae*, 231
- Hamartoma
- bile duct, 128
 - lung (adenochondroma), 53
- Hand, Dupuytren's contracture, 228

- Hashimoto's thyroiditis, 199
- Heart
- rhabdomyomas in tuberous sclerosis, 281
 - traumatic rupture, 16
- Hepar lobatum, 126, 127
- Hepatitis B, 119, 125
- Hepatoblastoma, 128, 129
- Hepatocellular carcinoma, 119, 128, 129
- clinical, 119
 - haemochromatosis, 117
 - lymph node secondary deposits, 119
- Hernia
- Richter's, 80
 - strangulated inguinal, 80
- Herpes encephalitis, 238
- Hiatus hernia, oesophagitis, 66
- Hirschsprung's disease, 94, 95
- Hirsutism, 187
- Hodgkin's disease, splenic deposits, 32, 33
- Honeycomb lung, 51
- Horseshoe kidney, 132, 133
- Human papilloma virus (HPV), 165
- Huntington's chorea, 273
- Hydatid cyst
- kidney, 135
 - liver, 126, 127
 - lung, 51
- Hydatidiform mole, 180
- Hydranencephaly, 276, 277
- Hydrocephalus
- complicating meningitis, 233, 234, 235
 - congenital, 276, 277
 - Huntington's chorea, 273
- Hydrocoele, 148, 149
- chronic, 148, 149
- Hydromyelia, 278
- Hydronephrosis, 136, 144
- nephrolithiasis, 140, 141
- Hydrops fetalis, 180, 181
- Hydrosalpinx, 172
- Hydroureter, 144
- Hymen, imperforate, 167
- Hypercalcaemia, 195
- Hyperparathyroidism
- bone disease, 195
 - parathyroid adenoma/hyperplasia, 195
 - secondary, 195, 196
- Hyperpituitarism, 184, 185
- Hypertension
- Conn's syndrome, 191
 - intracerebellar haemorrhage, 256
 - intracerebral haemorrhage, 255
 - left ventricular hypertrophy, 19
 - phaeochromocytoma, 194
 - polycystic kidney disease, 133
 - pontine haemorrhage, 256
- Hypertrophic cardiomyopathy, 18
- Hypogonadism, 185
- Hypokalaemia
- central pontine myelinosis, 275
 - Conn's syndrome, 191
- Hypopharynx, squamous cell carcinoma, 38
- Hypopituitarism
- cystic pituitary gland, 186, 187
 - empty pituitary fossa, 186, 187
 - hypogonadism, 185
- Hypoplastic lungs, 41, 70, 71
- Hypospadias, 147
- Ileum
- acute obstruction, 86, 87
 - adenocarcinoma, 92
 - carcinoid tumour, 91
 - Crohn's disease, 84, 85
 - endometriosis, 88, 89
 - enterogenous cyst, 88, 89
 - focal nodular lymphoid hyperplasia, 90, 91
- Ileus
- gallstone, 89
 - meconium, 83
- Iliac artery atherosclerosis, 2, 3
- Iliac vein thrombosis, 16, 17
- Imperforate anus, 94, 95
- Imperforate hymen, 167
- Infantile embryonal carcinoma, 152
- Inferior vena cava thrombosis, 16, 17
- Inguinal hernia, 80
- Inhaled foreign body, 39
- Inhaled vomitus, 39
- Insulin-secreting islet cell adenoma, 112
- Interstitial emphysema, 40, 41
- Interstitial pulmonary fibrosis, 51
- rheumatoid arthritis, 51
- Intracerebellar haemorrhage, 256
- Intracerebral aneurysm
- berry, 258
 - internal carotid artery, 259
 - subarachnoid haemorrhage, 258, 259
- Intracerebral haemorrhage, 255
- gastric erosions complicating, 256
 - multiple, 257
- Intracranial haemorrhage, neonate, 247
- Intracranial pressure elevation, 250, 251
- brain tumours, 264, 265, 267
- Intraductal papilloma, breast, 154, 155
- Intramedullary fibroma, kidney, 142
- Intramuscular myxoma, 224, 225
- Intrauterine ultrasound, neural tube defects, 279
- Intussusception, 86, 87
- Involucrum, 207
- Iodine deficiency, 196
- Islet cell adenoma, 112
- Jejunum
- atresia, 83
 - diverticula, 82
- Keloid scar, 227
- Kernicterus, 276
- Kidney
- acute lymphoblastic leukaemia, 142
 - analgesic nephropathy, 141
 - angioleiomyomas, 281
 - cystic dysplastic, 134, 135
 - diabetes mellitus, 138, 139
 - horseshoe, 132, 133
 - hydatid cyst, 135
 - infarction, 136, 137
 - multiple cortical infarcts, 136, 137 - multicystic, dialysis, 135
 - multiple simple cysts, 134, 135
 - polycystic disease, 133
 - sponge, 134, 135
 - tuberculosis, 140, 141
 - tuberous sclerosis, 281
 - uric acid infarcts, 136, 137
- Klebsiella rhinoscleromatis*, 37
- Knee joint
- arthritis from multiple haemarthroses, 222
 - cyst of lateral meniscus, 224
 - gout, 222
 - osteoarthritis, 221
 - rheumatoid arthritis, 222
- Krukenberg tumour, 177
- Kyphoscoliosis, 223
- Lambli's excrescence, 21
- Larynx
- pseudosarcoma, 38
 - squamous cell carcinoma, 38
- Lateral meniscus cyst, 224
- Left atrium
- ball thrombus, 23
 - myxoma, 30
- Left auricular appendage thrombus, 23
- Left ventricle
- fibroelastosis, 30
 - hypertrophy, 19
- Legs
- acute ischaemia, 3
 - elephantiasis, 16, 17
 - thrombotic oedema, 16, 17
- Leiomyoma
- oesophagus, 68, 69
 - pedunculated, 170
 - red degeneration, 170
 - stomach, 75
 - uterus, 170, 171
- Leiomyosarcoma, small intestine, 92
- Leukoplakia, 38
- Lichen sclerosis et atrophicus, 165
- Linitis plastica, 77
- Lip, squamous cell carcinoma, 62
- Lipogranuloma, breast, 156
- Lipoleiomyoma, uterus, 170
- Lipoma, 224, 225
- Liposarcoma, 224, 225
- spermatic cord, 148
- Lithopaedion, 179
- Liver
- abscess, 122, 123
 - amoebic, 126
 - subdiaphragmatic, 125
 - biopsies, different colours, 118
 - cardiac failure effects, 120, 121, 125
 - Clonorchis sinensis* infection, 126, 127

- congenital polycystic, 122
Dubin–Johnson syndrome, 118
focal nodular hyperplasia, 128
haemangioma, 128
haematoma, 121
haemochromatosis, 117, 118
hepar lobatum, 126, 127
hydatid cyst, 126, 127
infarction, 121
massive necrosis, 122
miliary tuberculosis, 50
secondary tumour, 130
 medullary thyroid carcinoma, 203
- Liver cirrhosis**
haemochromatosis, 117
hepatocellular carcinoma, 119
macronodular, 124, 125
micronodular, 125
- Lobar pneumonia, 45**
- Lumbar puncture, meningitis, 231**
- Lung**
abscess, 45, 46
acute asthma, 44
asbestosis and mesothelioma, 56, 57
aspergilloma, 46, 47
benign hamartoma
 (adenochondroma), 53
bronchoalveolar carcinoma (alveolar cell carcinoma), 58
bronchogenic carcinoma, 54, 55
carcinoid tumour, 53
coal miner's (anthracosis), 52
congenital lymphectasia, 41
empyema, 46
honeycomb, 51
hydatid cyst, 51
hypoplastic, 41, 70, 71
inhaled foreign body, 39
mixed pneumoconiosis, 52
mucoviscidosis, 111
paraffinoma, 51
pneumothorax, 46
progressive massive fibrosis, 52
silicosis, 52
subpleural rheumatoid nodule, 51
toruloma (cryptococcal infection), 46, 47
torulosis, miliary, 46, 47
tuberculosis,
 adult type, 49
 miliary, 48, 49
 old calcified lesion, 49
- Lung cancer**
bronchoalveolar carcinoma (alveolar cell carcinoma), 58
bronchogenic carcinoma, 54
hormone-secreting tumour, 193
malignant pericarditis, 55
pericardial invasion, 21
adrenal secondaries, 193
lung secondaries, 58
liver secondaries, 130
vertebral secondaries, 209
superior vena cava obstruction, 55
- Lymph nodes**
secondary tumour,
 hepatocellular carcinoma, 119
 melanoma, 32
 thyroid papillary carcinoma, 200
tuberculosis, 48, 49, 50
- Lymphangioma (cystic hygroma), 7**
macroglossia, 61
- Lymphectasia, congenital of lung, 41**
- Lymphoblastic leukaemia, acute**
kidneys, 142
testes, 152
- Lymphoid hyperplasia, ileum, 90, 91**
- Malignant Lymphoma**
Burkitt's, clinical, 32
diffuse, 32
Hodgkin's disease, 33
nodular, 32
small intestine, 90, 91
spleen, 32
stomach, 78, 79
- Macroglossia, 61**
- Magnetic resonance imaging,**
cerebral infarction, 239, 242, 243
myocardial infarction, 15
- Malaria, cerebral, 238**
- Mallory–Weiss tear, 73**
- Mammary duct ectasia, 154, 155**
- Mammogram, breast prosthesis, 156**
- Maxilla, ameloblastoma, 65**
- Meckel's diverticulum, 81**
- Meconium ileus, 83**
- Mediastinal widening, miliary tuberculosis, 48, 49**
- Medullary carcinoma**
breast, 158
thyroid, 201, 202
secondary liver tumour, 203
- Medulloblastoma, 266**
- Megacolon, acquired, 94, 95**
- Megaloureter, 132, 133**
- Megaesophagus, 69**
- Melanoma**
lymph node, 32
small intestine, 92
vagina, 165
- Melanosis coli, 96, 97**
- Meningioma, 268, 269**
- Meningitis**
acute, plus complications, 230–237
cryptococcal, 237
neonatal, 230, 231, 235
tuberculous, 236
- Meningomyelocoele, 278**
- Mesothelioma**
constrictive pericarditis, 56
pleural, 56, 57
- Microcephaly, 276, 277**
- Middle cerebral artery**
haemorrhagic infarction in its distribution, 240, 241, 242, 243
mycotic embolism, 248, 249
ruptured aneurysm, 259
thrombosis, 239
- Mitral valve**
defect, associated atrial septal defect, 28
stenosis, 22
subacute bacterial endocarditis, 23, 28
- Mitral valvotomy, 22**
- Motor speech area infarction, 244, 245**
- Mucinous cystadenoma, ovary, 175, 176**
Mucocoele,
 appendix, 94
 gall bladder, 114
- Mucoviscidosis,**
hepatic cirrhosis, 110, 111
lung, 111
meconium ileus, 83
pancreas (fibrocystic disease), 110, 111
- Mucus retention cyst, tongue, 60**
- Multiple enchondromata (Ollier's disease), 206**
- Multiple endocrine adenopathy syndrome type 2B, 203**
- Multiple myeloma**
long bones, 217
skull, 216, 217
spine, 217
- Multiple polyposis coli, 102**
- Multiple sclerosis, 275**
- Muscle atrophy, 282**
- Mycotic embolism, 248, 249**
- Myelolipoma, adrenal medulla, 193**
- Myocardial infarction**
anterior, 9, 15
 electrocardiogram, 8, 9
 coronary angiography, 11
 lateral, 14
left ventricle acute circumferential infarction, 14
magnetic resonance imaging, 15
mural thrombosis, 14
posterior, 11, 12, 13, 14
 electrocardiogram, 10
 rupture of interventricular septum, 13
 rupture of ventricle, 11
- Myxoma**
intramuscular, 224, 225
left atrium, 30
- Nasal polyp, 37**
- Neisseria meningitidis*, 231, 232**
- Neonatal intracranial haemorrhage, 247**
- Neonatal necrotizing enterocolitis, 86**
- Nephrolithiasis, 140, 141**
- Nephropathy, analgesic, 141**
- Nephrosclerosis, benign, 138**
- Neural tube defects, 279**
- Neurilemmoma, 226**
acoustic neuroma, 272, 273
- Neuroblastoma, 194**
- Neurofibroma**
plexiform of sciatic nerve, 226
subcutaneous, 226
tongue, 202

- Neurofibromatosis, 226
 Neurofibrosarcoma, sciatic nerve, 226
 Nipple
 accessory, 162
 Paget's disease, 161
- Obesity, Cushing's syndrome, 187
 Obstructive airways disease, chronic, 43
 Obstructive jaundice, 118
 Occipital lobe infarction, 244, 245, 251
 Ochronosis, 221
 osteoarthritis, 221
 Oesophagitis
 acute-on-chronic, 66
 Candida, 66
 Oesophago-gastric junction
 adenocarcinoma, 76, 77
 Mallory-Weiss tear, 73
 Oesophagus
 achalasia, 69
 ganglioneuromatosis, 202
 leiomyoma, 68, 69
 squamous cell carcinoma, 68, 69
 stricture, 69
 varices, 66, 67
 Oestrogen-secreting adrenal tumour, 190, 191
 Ollier's disease (multiple
 enchondromata), 206
 Oncocytoma (renal tubular adenoma), 142
 Opisthotonus, 231
 Oral cancer, 62
 Orbital cellulitis, 253
 Orchioblastoma, 152
 Osteoarthritis
 chronic, 221
 ochronosis, 221
 Osteochondroma, 218, 219
 Osteogenesis imperfecta, 206
 Osteogenic sarcoma, 219
 Paget's disease, 215
 Osteoid osteoma, 218, 219
 Osteomyelitis
 acute, 207
 chronic, 207
 complicating meningitis, 235
 Osteoporosis, 210, 211
 Osteosclerosis, 195
 Ovary
 benign mucinous cystadenoma, 175
 benign serous cystadenoma, 174, 175
 dermoid cyst (benign teratoma), 177
 torsion, 177
 dysgerminoma, 178
 ectopic pregnancy, 179
 endometriosis, 174, 175
 fibroma, 178
 granulosa cell tumour, 178
 Krukenberg tumour, 177
 papillary cystadenocarcinoma, 176
 polycystic, 173
 simple follicular cysts, 173
 thecoma, 178
- Paget's disease,
 bone (osteitis deformans), 211, 212, 213, 214, 215
 femur, 215
 osteogenic sarcoma, 215
 pelvis, 213
 skull, 212, 213, 214, 215
 tibia, 214
 extramammary of scrotum, 161
 nipple, 161
 Pancreas
 annular, 70, 71
 atrophy, 108
 benign cystadenoma, 112
 ectopic nodule, 108
 haemochromatosis, 118
 insulin-secreting islet cell adenoma, 112
 mucoviscidosis (fibrocystic disease), 110, 111
 pseudocyst, 109
 Pancreatic duct obstruction, 108
 Pancreatitis
 acute haemorrhagic, 109
 chronic, 109
 Papillary thyroid carcinoma
 multifocal, 201
 secondary lymph node tumour, 200
 solitary, 201
 Paraffinoma, lung, 51
 Parathyroid gland
 adenoma, 195
 hyperplasia, 195, 196
 Parkinson's disease, 275
 Parotid gland
 pleomorphic adenoma, 64
 Warthin's tumour (adenolymphoma), 64
 Partial mole, 180
 Patent ductus arteriosus, 25
 Patent foramen ovale, 28
 probe-patent, 27
 Pectoralis muscle absence, 162
 Pelviureteric obstruction, congenital, 136
 Penis, squamous cell carcinoma, 148
 Peptic ulcer
 chronic, 72, 73
 Meckel's diverticulum, 81
 Perianal abscess/fistulae, 106
 Pericarditis, 20, 21
 constrictive with mesothelioma, 56
 fibrinous, 20, 21
 malignant, 55
 Perisplenitis, 34
 Peritonitis, acute, 86
 appendicitis, 92, 93
 Petechial haemorrhages
 bacterial endocarditis, 24
 cerebral fat embolism, 247
 cerebral malaria, 238
 Phaeochromocytoma, 194, 203
 Pharyngeal diverticulum, 66, 67
 Phimosis, 147
 Pigmented villonodular synovitis, 223
 Pituitary adenoma, 184, 185, 188, 271
 Pituitary fossa craniopharyngioma, 271
 Pituitary infarction (Sheehan's syndrome), 186, 187
- Placenta
 accreta, 182
 chorangioma (benign haemangioma), 180
 infarcts, 180, 181
 quadruplets, 182
 retroplacental haemorrhage, 180, 181
 Plantar fibromatosis, 228
 Pleomorphic adenoma, 64
 Pleura
 mesothelioma, 56, 57
 plaques, 57
 Pleural effusion, 46
 Plexiform neurofibroma, 226
 Pneumatosis intestinalis, 103
 Pneumoconiosis, mixed, 52
 Pneumomediastinum, 40, 41
 Pneumonia
 chronic bronchiectasis, 44
 confluent bronchopneumonia, 45
 lobar, 45
 lung abscesses, 45, 46
 Pneumothorax, 46
 tension, 40, 41
 Poliomyelitis, 282
 Polycystic kidney disease, 133
 Polycystic liver, congenital, 122
 Polycystic ovaries, 173
 Pons
 astrocytoma, 264
 cranial nerves, 260
 haemorrhage, 256
 infarction, 245
 Popliteal artery occlusion, 3
 Portal vein thrombosis, 119
 Posterior cerebral artery
 cystic area in distribution, 244, 245
 occlusion, 244, 245, 251
 Posterior urethral valves, 146
 Pott's fracture of vertebrae, 208, 209
 Precocious puberty, 190, 191
 Prostatic vein thrombus, 42
 Pseudohermaphroditism, 191
 Pseudomembranous colitis, 100, 101
 Psoas abscess, 209
 Puberty, precocious, 190, 191
 Pulmonary artery atherosclerosis, 2
 Pulmonary embolus, 42
 Pulmonary hypertension
 pulmonary artery atheroma, 2
 right ventricular hypertrophy, 18
 Pulmonary infarction, 42
 Pulmonary oedema, acute, 37
 Pulmonary tuberculosis, 48, 49
 Pyelonephritis
 acute, 138, 139
 diabetic kidney, 138, 139
 xanthogranulomatous, 140, 141
 Pyometra, 168
 Pyonephrosis, 140, 141
 Pyosalpinx, 172
 Pyramidal tract atrophy, 241

- Quadruplets, placenta, 182
 Radiation enteritis, 86
 Rectum
 adenocarcinoma, 105
 hamartomatous polyp, 102
 solitary ulcer, 103
 villous papilloma, 101
 Renal artery thrombosis, 136, 137
 Renal calculus, 144
 Renal cell carcinoma, 142, 143
 Renal infarct
 bacterial endocarditis, 24
 cortical, 136, 137
 Renal intramedullary fibroma, 142
 Renal papillary necrosis, 138, 139
 Renal pelvis, transitional cell carcinoma, 142, 143
 Renal tuberculosis, 140, 141
 Renal tubular adenoma (oncocytoma), 142
 Renal tubular necrosis, 136, 137
 Renal vein thrombosis, 136, 137
 Retinoblastoma, 270, 271
 Rhabdomyoma, heart, 281
 Rhabdomyosarcoma, 224, 225
 Rhesus incompatibility, 180, 181
 Rheumatic fever, 22
 Rheumatic heart disease
 aortic valve vegetations, 21
 mitral valve stenosis, 22
 Rheumatoid arthritis
 knee joint, 222
 subpleural rheumatoid nodule, 51
 Rhinoscleroma, 37
 Richter's hernia, 80
 Riedel's thyroiditis, 200
 Right ventricular hypertrophy, 18
 Sagittal sinus thrombosis, 252, 253
 Salivary gland
 calculus, 63
 pleomorphic adenoma, 64
 Warthin's tumour (adenolymphoma), 64
 Salpingitis, chronic, 172
 Saphena varix, 5
 Scrotum, Paget's disease, 161
 Seminoma
 regressing, 151
 testis, 151
 Sequestrum, 207
 Serous cystadenoma, ovary, 174, 175
 Seventh nerve palsy, 261
 Sheehan's syndrome (pituitary infarction), 186, 187
Shigella, 101
 Silicosis, 52
 Situs inversus, 29
 Sixth nerve palsy, 261
 Skull
 astrocytoma-related thinning (beaten copper appearance), 264, 265
 multiple myeloma, 216, 217
 Paget's disease, 212, 213, 214, 215
 Small intestine
 chylous cyst of mesentery, 94
 Crohn's disease, 84, 85
 ganglioneuromatosis, 202
 intussusception, 86, 87
 ischaemic necrosis, 84, 85
 leiomyosarcoma, 92
 malignant lymphoma, 90, 91
 mucosa,
 'cobble stone', 84, 85
 flat (total villus atrophy), 79
 multiple carcinoids, 91
 obstruction, 88, 89, 92
 acute, 86, 87
 partial duplication, 88, 89
 secondary melanoma, 92
 tuberculosis, 85
 typhoid, 85
 volvulus, 83
 Spermatic cord, liposarcoma, 148
 Spina bifida, 279
 Spinal cord
 arteriovenous malformation, 262
 infarction, 246
 posterior column atrophy, 275
 subarachnoid haemorrhage, 258
 subarachnoid tumour, 266
 traumatic haemorrhage, 257
 Spinal X-ray
 hyperparathyroidism, 195
 osteoporosis, 210, 211
 tuberculosis, 208
 Spine
 ankylosing spondylitis, 223
 kyphoscoliosis, 223
 multiple myeloma, 217
 osteoporosis, 210, 211
 secondary carcinoma, 209
 tuberculosis, 207
 Pott's fracture of vertebrae, 208, 209
 psoas abscess, 209
 Spleen
 Hodgkin's disease, 32, 33
 malignant lymphoma, 32, 33
 multiple infarcts, 32, 33
 perisplenitis, 34
 simple cysts, 34
 traumatic rupture, 34
 Squamous cell carcinoma
 anus, 105
 buccal mucosa, 63
 cervix, 166
 early invasive plus carcinoma in situ, 166
 longstanding proclivencia, 166
 floor of mouth, 62
 hypopharynx, 38
 larynx, 38
 lip, 62
 oesophagus, 68, 69
 penis, 148
 tongue, 62
 vulva, 165
 Staphylococcal pneumonia, 46
 Stomach
 acute dilatation, 71
 acute erosions, 72, 73
 adenocarcinoma, 76, 77
 benign adenomatous polyps, 74
 bezoar, 75
 diverticulum, 71
 giant rugal hypertrophy, 74
 leiomyoma, 75
 linitis plastica, 77
 malignant lymphoma, 78, 79
 superficial adenocarcinoma (early gastric cancer), 78, 79
 Stroke
 computed tomography (CT), 242, 243
 see also Intracerebral haemorrhage
 Subacute combined degeneration of spinal cord, 275
 Subarachnoid haemorrhage, 258, 259, 262
 Subdiaphragmatic abscess, 125
 Subdural haemorrhage, 255
 Submandibular gland calculus, 63
 Superior mesenteric artery thrombosis, 84, 85
 Superior vena cava obstruction, 55
 Synovial cyst, 224
 Synovioma, 223
 Syphilis
 aortic arch aneurysm, 4, 5
 condylomata lata, 164
 hepar lobatum, 126, 127
 tabes dorsalis, 275
 Takayasu's arteritis, 4, 5
 Temporal artery aneurysm, 5
 Tendon sheath giant cell tumour (benign synovioma), 223
 Tension pneumothorax, 40, 41
 Tentorium cerebelli tear, 247
 Teratoma
 ovary (dermoid cyst), 177
 testis, 151
 Testis
 acute lymphoblastic leukaemic infiltration, 152
 infantile embryonal carcinoma, 152
 seminoma, 151
 regressing, 151
 teratoma, 151
 torsion, 148, 149
 tuberculosis, 150, 151
 Thalamic infarction, 251
 Thecoma, 178
 Third ventricle colloid cyst, 272, 273
 Thymoma, 53
 Thyroglossal cyst, 204
 Thyroid gland
 congenital absence, 198
 cyst, 197
 follicular adenoma, 198
 follicular carcinoma, 200
 goitre, 196, 197, 198
 medullary carcinoma, 201, 202
 secondary liver tumour, 203
 papillary carcinoma

- multifocal, 201
 - secondary, 200
 - solitary, 201
- Thyroiditis
 - granulomatous, 199
 - Hashimoto's, 199
 - Riedel's, 200
- Thyrotoxicosis, 198
- Tongue
 - candida infection, 61
 - lymphangioma, 61
 - macroglossia, 61
 - mucus retention cyst, 60
 - multiple neurofibromas, 202
 - squamous cell carcinoma, 62
- Tonsillar herniation of cerebellum, 250, 251
- Toruloma, 46, 47, 237
- Torulosis, miliary, 46, 47
- Tracheitis, acute, 36
- Tracheobronchitis, acute, 36
- Tracheo-oesophageal fistula, 66
- Tracheopathia osteoplastica, 37
- Tracheostomy, 36
- Transitional cell carcinoma
 - bladder, 144
 - renal pelvis, 142, 143
 - ureter, 142, 143
- Transposition of great vessels, 25
- Trauma
 - brain damage, 249
 - heart rupture, 16
 - spinal cord haemorrhage, 257
 - spleen rupture, 34
 - superficial temporal artery aneurysm, 5
- Triple ureter, 132, 133
- Truncal obesity, 187
- Tubal ectopic pregnancy, ruptured, 179
- Tuberculosis
 - ascites, 50
 - epididymis, 150, 151
- Ghon focus, 48, 49
- kidney, 140, 141
- lymph nodes, 48, 49, 50
- meningitis, 236
- miliary
 - liver, 50
 - lung, 48, 49
- pulmonary, 48, 49
- small intestine, 85
- spine,
 - Pott's fracture of vertebrae, 208, 209
 - psoas abscess, 209
 - testis, 150, 151
 - tuberculoma, brain, 236
- Tuberous sclerosis, 280, 281
- Twelfth nerve palsy, 261
- Typhoid, 85
- Ulcerative colitis
 - acute, 97
 - chronic, 97
 - caecal carcinoma, 98
 - hyperplastic polyps, 98
 - sigmoid colon mucosal dysplasia, 98
- Ultrasound, intrauterine neural tube defects, 279
- Umbilical cord
 - around neck of fetus, 182
 - candidiasis, 182
- Uncal herniation, 250, 251
- Upper arm angiosarcoma, 158, 159
- Ureter
 - calculus, 144
 - double, 132, 133
 - megaloureter, 132
 - transitional cell carcinoma, 142, 143
 - triple, 132, 133
 - ureteritis cystica, 135
- Uric acid infarcts, 136,
- Uterus
 - adenomyoma, 171
 - double, 167
 - endolymphatic stromal myosis, 171
 - leiomyoma, 171
 - intramural, 170
 - pedunculated, 170
 - red degeneration, 170
 - lipoleiomyoma, 170
- Vagina, malignant melanoma, 165
- Ventricle
 - fibroelastosis, 30
 - hypertrophy
 - left, 19
 - right, 18
 - septal defect, 27
- Vertebrae
 - crush fracture, 210, 211, 217, 219
 - multiple benign haemangiomas, 219
 - multiple myeloma, 217
 - osteoporosis, 210, 211
 - Pott's fracture, 208, 209
 - secondary carcinoma, 209
- Vertebrobasilar insufficiency, 245, 246
- Villous papilloma, rectum, 101
- Visual cortex (occipital lobe) infarction, 244, 245, 251
- Vitamin B₁₂ deficiency, 275
- Volvulus, 83
- Vulval squamous cell carcinoma, 165
- Vulvitis, acute, 164
- Warthin's tumour (adenolymphoma), 64
- Waterhouse-Friderichsen syndrome, 232
- Wernicke's encephalopathy, 276
- Wilms' tumour, 142, 143
- Wuchereria bancrofti*, 16, 17
- Xanthogranulomatous pyelonephritis, 140, 141